3.7 Molecular diatomic adsorbates on metals and semiconductors

3.7.1 CO and N_2 adsorption on metal surfaces

A. FÖHLISCH, H.P. BONZEL

List of symbols and abbreviations

ARUPS	angle resolved UPS
ARPEFS	angle resolved photoemission fine structure
ass	assumed
CDAD	circular dichroism in angular distribution of photoelectrons
CSOV	constrained space orbital variation
DLEED	diffuse (intensity) low energy electron diffraction
DOS	density of states
ESD	electron stimulated desorption
ESDIAD	electron stimulated desorption ion angular distribution
EELS	electron energy loss spectroscopy
fr. transl.	frustrated translational mode
FWHM	full width at half maximum
H	hollow adsorption site
HR-EELS	high resolution EELS
IETS	inelastic electron tunneling spectroscopy
IPS	inverse photoemission spectroscopy
IRAS	infrared reflection absorption spectroscopy
LEED	low energy electron diffraction
LITD	laser induced thermal desorption
MB	molecular beam (sticking coefficient)
MBS	molecular beam scattering
ML	monolayer
NEXAFS	near-edge X-ray absorption fine structure
PED	photoelectron diffraction (energy scanned mode; also: PhD [82Woo])
PES	potential energy surface
PFDMS	pulsed field desorption mass spectrometry [86Kru]
PJ-EELS	pressure jump EELS [89Whi]
PM-IRAS	polarization modulation infrared reflection absorption spectroscopy
RAIRS	reflection absorption infrared spectroscopy (IRAS)
RBS	Rutherford backscattering
REMPI	Resonance enhanced multi-phonon ionization [97Sch2]
S_0	initial sticking coefficient (at zero coverage)
SXD	soft X-ray diffraction
SFG	sum frequency generation
SHG	second harmonic generation
T	atop adsorption site
TDS	thermal desorption spectroscopy
TEAS	thermal energy atom scattering
T_g, T_s	gas temperature / surface temperature
T_p	temperature of maximum desorption rate (peak)
TPD	thermally programmed desorption
TP-EELS	temperature programmed EELS

TR-EELS	time resolved EELS
UPS	ultra-violet photoelectron spectroscopy
WFC	work function change
XAS	X-ray absorption spectroscopy
XES	X-ray emission spectroscopy
XPS	X-ray photoelectron spectroscopy
XPD	X-ray photoelectron diffraction (angle-scanned mode)
YXPS	XPS using Y Mζ radiation at 132.3 eV [89Düc]

3.7.1.1 Introduction

In this chapter the properties of adsorbed CO and N_2 on fcc, bcc and hcp metal surfaces of well-defined structure will be presented. All properties except surface diffusion coefficients [01See], work function changes [01Jac1] and surface core level shifts [01Den] due to adsorbed CO (or N_2) are listed in tables. The metals for which data have been collected are highlighted in the partial periodic table below. The larger portion of tabulated results concerns adsorbed CO. Data for adsorbed molecular N_2 are much less numerous. No relevant data have been found for elements in gray.

									Al	Si
Ti	V	**Cr**	Mn	**Fe**	**Co**	**Ni**	**Cu**	Zn	Ga	Ge
Zr	**Nb**	**Mo**	Tc	**Ru**	**Rh**	**Pd**	**Ag**	Cd	In	Sn
Hf	**Ta**	**W**	**Re**	**Os**	**Ir**	**Pt**	**Au**	Hg	Tl	Pb

Bold character: single crystal data reviewed in this section

Plain black character: thin film data reviewed (Ti, Mn, Zn, Sn)

Grey character: no data available (Si, V, Ga, Ge, Tc, Cd, In, Hf, Hg, Tl, Pb)

Single component elemental crystals of a single orientation have not been available in all cases. To provide some element-specific information regarding the adsorptive properties of rarely studied crystals, such as Ti, Zn, Mn, and Sn, we have also considered binary systems to a limited extent in section 3.7.1.6. The substrates consist of a small coverage (submonolayer to several monolayers) of the element of interest on a carrier single crystal of a different element. The modification of CO and N_2 adsorption behavior due to the added component may serve as a rough indicator of the chemical activity of that component. A list of such systems is given in section 3.7.1.6.

There have been a very large number of studies of CO adsorption on metal surfaces during the past 40 years. Many different aspects of CO adsorption have been discovered and described. It is impossible to cite all of those studies in this chapter and nearly equally impossible to present all published quantitative data in the respective tables. Although we have tried to cover all important and especially the recent publications, it is unavoidable that we have missed some. Therefore we admit at this point that our data collection is likely to be incomplete. We apologize to those whose work slipped through the search grid. What is true for the citations and data, is even more the case for the figures included in this chapter. Here the choice was rather subjective and arbitrary, motivated by our desire to present some outstanding examples.

Most refractory metals (bcc) surveyed in this chapter exhibit a high activity for CO adsorption and for breaking the C-O bond. fcc metals, on the other hand, are less reactive in general although most of them adsorb CO. The dissociation of CO, if it occurs, is in general structure sensitive. Several fcc metals, such as Ag, Au, Al, Sn and Pb, are fairly inactive or even inert to CO adsorption. It is therefore an important

issue in the context of surface reactivity to distinguish molecular and dissociated CO, once CO is adsorbed on the surface. Thermal desorption spectra (pressure versus temperature) have been used as an early and simple means to classify the adsorbed states.

A convention evolved to label thermal desorption peaks, beginning at low temperature, with Greek letters, e.g. α_1, α_2, . . , β_1, β_2, etc. which are often meant to indicate molecular (sometimes physisorbed) species and dissociated species, respectively. This designation of peaks has been adopted here as well, but the meaning of α and β has changed and does not necessarily stand for a molecular or dissociated adsorbed species. The nomenclature of adsorbed nitrogen is different than for adsorbed CO. At least four different states have been found, e.g. on Fe(111) [85Tsa, 86Whi1, 86Whi2, 87Fre, 87Gru1, 87Gru2], which are designated as follows (in order of increasing adsorption energy): δ-state: physisorbed N_2, γ-state: chemisorbed σ-bonded N_2 (oriented vertical to the surface), α-state: chemisorbed π-bonded N_2 (oriented nearly parallel to the surface), β-state: atomic nitrogen N. Depending on the availability of adsorption sites, several sub-states (e.g. of β and γ) may be distinguished. In the case of molecular N_2 these different states can be determined by thermal desorption or by vibrational and electron spectroscopies which have been summarized for transition metal surfaces in 1991 [91Rao].

Historically, the inability to make a clear distinction of adsorbed chemical states has led to quite a bit of confusion in the years prior to about 1960. Once electron and vibrational spectroscopies came into use, this was no longer an issue. Hence the data characterizing the adsorbed state in situ are primarily spectroscopic data, such as molecular vibrational frequencies and molecular valence orbital as well as atom- and chemistry-specific core level binding energies. Further important characteristics are the rates of adsorption and desorption, i.e. sticking coefficients and temperatures of desorption, but also measurements of energies of adsorption and desorption. Finally, structural data concerning the adsorption site on the surface and the bond parameters of the substrate atom – molecule configuration are desirable. Additional physical and chemical data, e.g. two-dimensional ordered CO structures, two-dimensional dispersion of CO molecular orbital states, coverage dependencies of various adsorption related quantities, or activation energies for CO dissociation, have been measured in some cases and will be reported in this section.

The adsorption of CO and the isoelectronic homonuclear N_2 on transition and noble metals are prototypes for molecular adsorption, mediated through the CO orbitals of σ and π symmetry, for example. The adsorption of CO on transition metal surfaces can also be dissociative, especially at elevated temperature. The dissociation to atomic carbon and oxygen, or alternatively the disproportionation of CO into adsorbed carbon and CO_2 is of considerable technological relevance, because this step is important for the catalytic hydrogenation of CO to methane (and higher hydrocarbons) which takes place on metals, notably Ni, Fe, Co, Rh and Ru [74Dal, 75Dal, 76Van, 77Pal, 78Dwy, 79Kre, 80Goo, 80Kre, 82Bon, 94Som].

3.7.1.1.1 Thermodynamic properties

For the molecular adsorption, the heat of adsorption determined via thermal desorption spectroscopy (TDS) and/or measurements of isosteres or isobars, gives us access to the total energy difference between the clean metal surface and the CO gas which is an important characteristic of CO molecules adsorbed to the metal surface. However, this quantity does not specify the adsorption path, eventually involving precursor states and special geometric effects, e.g. site selectivity and site blocking. The information on the dynamics of the adsorption process is contained in quantities, such as the coverage dependent sticking coefficient and the pre-exponential factors of adsorption. The heat of adsorption on fcc transition metals is relatively low but increases for bcc metals, such as seen in Fig. 1 [94Som]. Since no distinction between molecular and dissociative adsorption of CO is made, the latter increase may be related to a predominance of CO dissociation on these metals.

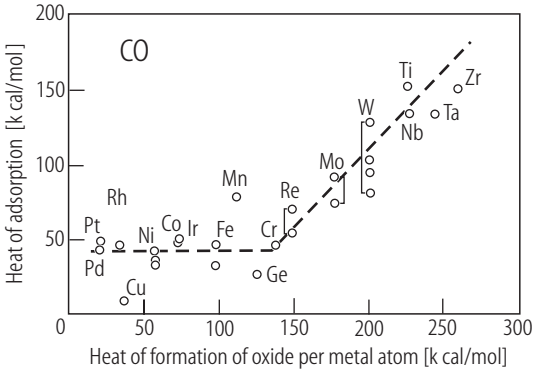

Fig. 1. Energy of adsorption of CO on transition metals as a function of the heat of formation of corresponding oxides [79Toy].

The heat of adsorption of CO and N_2 to metal surfaces is determined not only by the substrate material but also by the crystallographic orientation of the surface. It is highly sensitive to the coverage which is due to the interplay between the local interaction between the adsorbed species and the metal adsorbent, and the adsorbate-adsorbate interaction, both being direct and substrate-mediated. Although the molecules N_2 and CO are isoelectronic, there are important differences in their adsorption behavior on metals. In comparison, the heat of adsorption or the activation energy of desorption, respectively, of the isoelectronic N_2 is for the same metal surface always significantly lower than for CO. So is the activation energy of desorption for c(2×2)CO/Ni(100) 138.6 kJ/mol [83Koe1] and for the geometrically equivalent c(2×2)N_2/Ni(100) only 25 kJ/mol [84Gru3]. Thus N_2 is adsorbed in a much narrower range of temperatures (under vacuum conditions) than CO. One important aspect of CO adsorption is that its heat of adsorption is about one order of magnitude smaller than its gas phase dissociation energy (11.23 eV). The fraction is even less for the N_2 molecule. This observation has led to the longstanding assumption of a weak molecule surface interaction, where the chemisorption process causes only a small modification of the molecular orbital structure of the adsorbed relative to the free molecule. Consequently, the adsorbate electronic structure has been approximated by that of the free molecule, treated as a nearly unperturbed species weakly interacting with the substrate.

Based on recent X-ray emission spectroscopic observations, a different scenario has emerged in order to explain the relatively weak heat of adsorption: Here a a strong covalent interaction between the molecule and the substrate has been found, characterized by significant orbital mixing: This implies a modification of the internal molecular bond, which costs energy, and the formation of the surface chemical bond, where energy is gained. In this case, a low heat of adsorption is also expected, but it is the result of these relatively large, but almost equal opposing contributions.

3.7.1.1.2 Vibrational properties

Further properties of the adsorbate are accessible through vibrational spectroscopies, such as electron energy loss spectroscopy (EELS), infrared reflection absorption spectroscopy (IRAS), sum frequency spectroscopy (SFG) [94She, 96Klü, 01Ric], or atom and molecular beam scattering (TEAS, MBS). With these techniques the local bond strengths within the adsorbate-metal complex are determined through the excitation and observation of the moiety's vibrational modes [54Eis, 58Eis, 59Eis, 72Eis]. CO in the gas phase is characterized by a single vibrational mode, the C-O stretch at 2169.8 cm^{-1}. Upon adsorption the frequency of the C-O stretch decreases to values between 1700 cm^{-1} and 2050 cm^{-1}. This characteristic red shift of the C-O stretch indicates that in the adsorption process the internal C-O bond is weakened. The C-O stretch has also been instrumentalized to assign adsorption sites and substrate coordination [54Eis, 58Eis, 79Ric]. These assignments have been successful in many cases, but caution is advised, as several counter examples have surfaced [93Sch, 94Dav, 96Dav]. CO adsorption on well-defined stepped single crystal surfaces [78Bra1, 79Erl, 79Hop, 83Hof1, 85Hay1, 90Ben, 92Luo, 95Ram, 96Sve, 02Unt] as well as artifically roughened low-index surfaces [82Ort, 83Hof1, 90Tüs2, 02Unt] have been analyzed to correlate vibrational CO stretch frequencies with defect sites. Knowledge of this kind is important for

elucidating the adsorption of CO on small supported metal clusters, as they are used in heterogeneous catalysis [92Bad, 96Eva, 96Goy, 96Rai, 98Wol, 2002Unt, 02Yud]. These clusters may exhibit well-defined low-index facets and/or a multitude of defect sites, depending on their size and thermal history. Vibrational spectroscopies, especially SFG, have been used successfully to characterize defect sites on these small metallic clusters even for a wide range of CO pressures (10^{-7} mbar to 10^3 mbar).

There are also low energy frustrated translational and rotational modes of adsorbed CO. In particular, the frustrated translation normal to the surface (equivalent to a metal-carbon stretch) provides a qualitative indication of the CO-metal bond strength. Vibrational low energy modes of single adsorbed CO molecules have been detected by inelastic tunneling spectroscopy (IETS), either in a thin film diode geometry [81Kro] or by utilizing the scanning electron microscope in vacuum [99Lau, 99Lee, 00Lee, 01Hah, 03Wal]. Thermal energy He atom scattering (TEAS, HAS) of adsorbed CO on metals has also provided frequencies of the frustrated translational mode [96Hof, 03Gra]. The dispersion of low energy modes has been studied by this technique for the c(2×2)-CO layer on Cu(001) [95Ell, 96Hof] and the (4×2) structure of CO on Pt(111) [86Lah, 98Gra1]. The interaction within a molecularly adsorbed CO layer at higher coverage is substantial. This leads to a continuous shift in vibrational frequencies with coverage, observed for many systems, e.g. for CO on Ru(0001) [80Pfn]. Using high resolution XPS, the vibrational progressions of the core-ionized adsorbate species have been observed [98Föh, 99Föh1, 99Föh2]. The latter vary significantly with adsorption site [98Föh].

The intra-molecular bond of gas phase N_2 is stronger than that of CO with a N-N stretch at 2358 cm^{-1} [91Rao]. An adsorption induced weakening of this N-N bond is found to be small as long as the molecule is σ-bonded through one of its nitrogen atoms and more or less perpendicularly adsorbed at the surface. On the basis of the adsorption energy and the vibrational properties a chemisorbed N_2 species is not easily distinguished from a physisorbed species.

3.7.1.1.3 Geometric structure

To characterize the geometric structure of adsorbed CO molecules, i.e. bond distances and angles, techniques such as X-ray photoelectron diffraction (XPD, PED or ARPEFS) and, in case of long range order, low energy electron diffraction (LEED) have been utilized. Photoelectron diffraction is performed either in an angle-scanned mode at constant energy (XPD) or in an energy-scanned mode with variable photon energy (PED, ARPEFS). Whereas the first mode yields primarily bond directions (angles), the second yields bond distances and angles. CO adsorbs in general in an upright adsorption geometry, with the carbon atom pointing towards the metal surface. In the case of Ag surfaces there is some controversy whether the weakly chemisorbed CO is oriented parallel to the surface or in a random orientation [84Kra] [94San1, 94San2].

Upon adsorption the internal bond length of the gas phase CO molecule of 1.128 Å is typically extended towards 1.13-1.15 Å at a metal carbon distance between 1.26 Å and 1.9 Å. The adsorbed CO molecule can occupy both low coordination and high coordination sites, with both selective adsorption into a single site or simultaneous adsorption into differently coordinated sites. The adsorption of CO to most fcc metal single crystal surfaces leads to the formation of ordered superstructures, as determined by LEED. A particular metal surface of low-index orientation can support several different superstructures at certain coverages. Tilting of the molecular axis can be induced by the repulsive lateral interaction between the dipole moments of the adsorbed CO molecules.

The adsorption of N_2 takes place only in on top sites, where the N_2 molecular axis is oriented normal or nearly normal to the surface. This alignment causes the two N-atoms of the N_2 molecule to become chemically inequivalent. The determination of the adsorbate orientation in the chemisorbed state was helped significantly by XPS, where the chemisorbed N_2 phase exhibits a very distinct N 1s photoelectron spectrum, such as seen in Fig. 2 for N_2 adsorbed on Ru(001), W(110) [82Umb, 83Umb, 84Umb] and Ni(100) [78Fug, 84Gru4, 84Umb]. The spectra are quite similar and exhibit three peaks, aside from the fact that spectrum (b) for Ni(110) is less well resolved than the others [84Gru4, 84Umb]. The two N 1s peaks (1,2) at binding energies below 400 eV are so-called screened states while the broad peak (4) near 406 eV is due to shake up processes, originally called the unscreened state [78Sch, 82Umb, 83Men, 83Umb, 84Umb, 85Fre, 86Bre, 86Gol, 91Nil]. Weakly chemisorbed molecules generally exhibit shake-up photoemission features of considerable intensity [93Til].

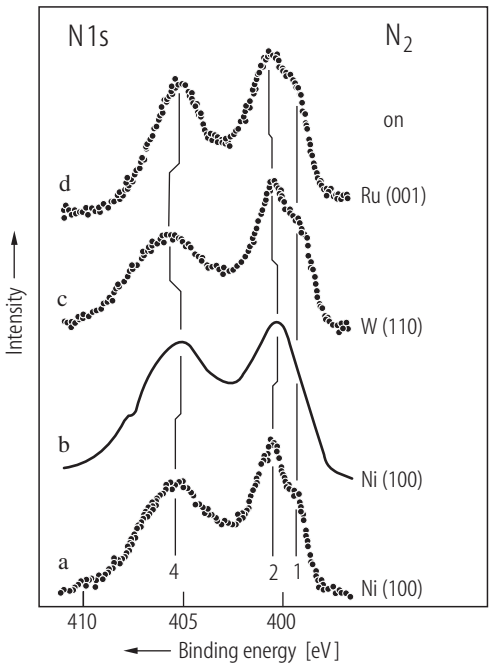

Fig. 2. N 1s core level spectra of chemisorbed molecular N_2 on three different single crystal surfaces as indicated. Spectrum (a) for Ni(100) was recorded at higher resolution than spectrum (b). The maximum near 400 eV is a double peak on all metals; [84Umb], [84Gru4].

In particular the investigations of the ordered c(2×2) layer of N_2 on Ni(100) have clarified the adsorbate configuration as well as the physics of photoemission from adsorbed N_2. It was shown that chemisorbed N_2 on this surface is oriented perpendicularly and that the two low binding energy peaks are representing the two chemically inequivalent N-atoms of N_2, one involved in bonding to the metal surface, the other pointing towards the vacuum [74Ege, 91Nil]. A representative set of high resolution N 1s spectra is given in Fig. 3 for several polar angles of emission [91Nil]. The screened state binding energies are 399.4 and 400.7 eV for the outer and inner N-atom, respectively. The assignment of peaks to individual N-atoms of N_2 is based on a study of the polar angle variation of N 1s intensity [74Ege]. The intensity ratio of the 400.7 eV peak to the 399.4 eV peak, shown in the inset of Fig. 3, reveals a maximum near normal emission, due to forward elastic scattering, which proves the perpendicular orientation of N_2 relative to the Ni surface, and furthermore, that the 400.7 eV peak corresponds to emission from the inner N-atom [91Nil].

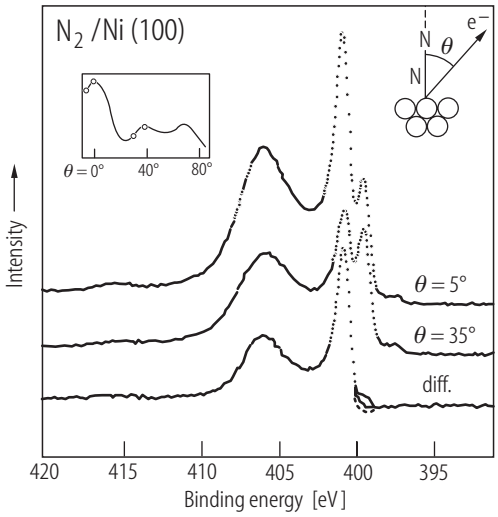

Fig. 3. N 1s core level photoemission spectra of N_2 adsorbed on Ni(100) in a c(2×2) structure. Spectra are recorded at two polar angles of 5 and 35° relative to the normal. The difference spectrum shows a large peak at 400.7 eV typical of electron forward scattering at the second (outer) nitrogen atom of a perpendicularly adsorbed N_2 molecule [91Nil]. The inset shows the polar angle dependence of the relative intensity at 400.7 eV to that at 399.4 eV.

The very intense N 1s shake-up peak was found to be different for the inner and outer N-atom. It consists of three contributions for the outer N-atom and is as such quite similar to the C 1s shake-up peak of adsorbed CO on Ni(100). The fully screened final states of adsorbed N_2 and CO are -NN* and -C*O which are in both cases equivalent to ground state -NO (* indicates core hole). Hence the similarity of the shake-up peaks is expected. The three contributions stem from excitations of bonding-to-antibonding states, excitations into Rydberg states, and intra-molecular excitations which are also known from the free molecule. For the inner N-atom, on the other hand, the fully screened final state of -N*N is equivalent to -ON which is a very weakly adsorbed species [74Ege]. Hence there is practically no split bonding-antibonding 2π orbital and no shake-up process involving related excitations [91Nil, 93Til]. It is important in this context that an ab initio calculation of the N 1s spectrum for a NiN_2 cluster, shown in Fig. 4, reproduces the experimental result of N_2 adsorbed on Ni(100) fairly well [85Fre].

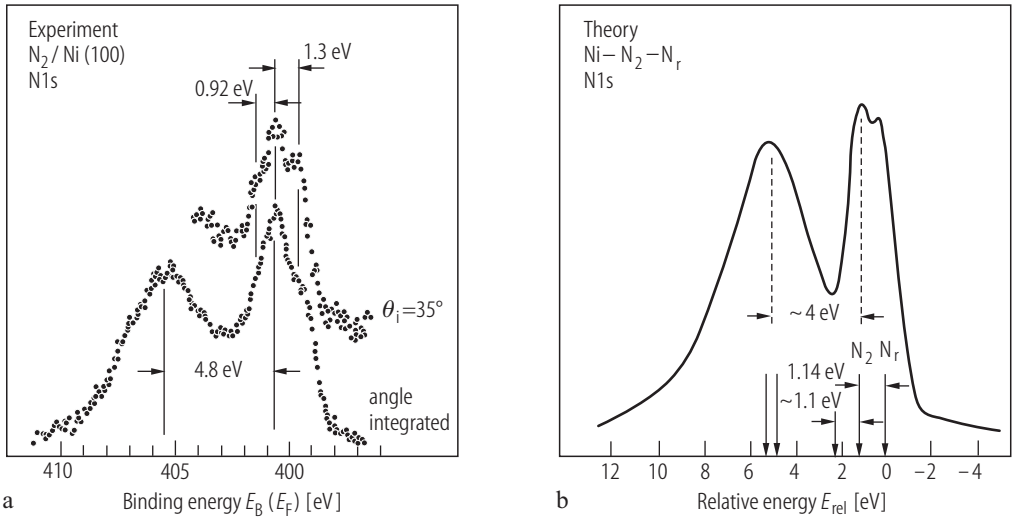

Fig. 4. Comparison of experimental [84Umb] (a) and theoretical N 1s spectrum (b) for N_2 adsorbed on Ni(100) and a NiN_2 cluster [85Fre]. The double peak near 400 eV is due to the two inequivalent N-atoms (initial state effect) while the broad peak near 405 eV is due to shake-up processes (final state effect).

3.7.1.1.4 Electronic structure and adsorption models

To understand why a particular structural arrangement of the adsorbed CO (or N_2) molecules on a metal surface yields the largest heat of adsorption, the valence electronic structure of the adsorbate needs to be studied in detail. The gas phase CO molecule has $C_{\infty v}$-symmetry and the ground state electron configuration $(1\sigma)^2(2\sigma)^2(3\sigma)^2(4\sigma)^2(1\pi)^4(5\sigma)^2$. The highest occupied molecular orbital (HOMO) is the 5σ, and the lowest unoccupied molecular orbital (LUMO) the $2\pi^*$. The gas phase N_2 molecule has $D_{\infty h}$-symmetry with the ground state valence electron configuration $(1\sigma_g)^2(1\sigma_u^*)^2(2\sigma_g)^2(2\sigma_u^*)^2(1\pi_u)^4(3\sigma_g)^2$, where the HOMO is the $3\sigma_g$ and the LUMO is the $1\pi_g^*$. Upon adsorption, the symmetry of the gas phase molecule is reduced to the lower symmetry of the surface. However, traditionally, the electronic states are still described in the framework of the gas phase symmetries.

There is an abundance of theoretical papers dealing with various aspects of CO and N_2 adsorption on metal surfaces. Different theoretical approaches make an assessment of accuracy difficult. Whenever theoretical data were reported that could be compared to experiment, they were included in the table section. However, quite often it was difficult or even impossible to locate theoretical data which are directly amenable to a comparison with experimental results. For this reason only a limited effort has been made to prepare a complete survey of such data. Instead we present results of more recent theoretical calculations for adsorbed CO on well defined metal surfaces. Hopefully these will serve as a starting point for locating additional studies.

Early work on CO adsorption on metals started with a molecular orbital approach. The starting point were infra-red spectra of CO adsorbed on supported metals (V, Cr, Mn, and Co) which showed a variation in the CO stretching region [64Bly, 69Bly, 87Bly]. Two main bands of CO for each metal were found, located at 1940 and 1890 cm^{-1} for V, at 1940 and 1880 cm^{-1} for Cr, at 1950 and 1890 cm^{-1} for Mn and at 2000 and 1880 cm^{-1} for Co. The two bands were suggested to correspond to two-fold and one-fold coordinated CO molecules [54Eis, 58Eis, 59Eis]. These data together with additional data for Fe, Ni, and Cu allowed a comparison across the first transition series from V to Cu. A molecular orbital model for the π-electron system of CO adsorbed on a cluster of metal atoms successfully accounted for the frequency shifts of the two principal bands, as the metal is varied across the series [64Bly, 69Bly, 87Bly]. Experimental observations like these were the basis of the well known Blyholder model of molecular CO adsorption [64Bly, 69Bly, 87Bly] which essentially calls for donation of electron charge from the carbon σ-orbital to the metal surface atom and backdonation of charge into the π bonding orbital of the C-O bond [64Bly, 69Bly, 87Bly].

Other theoretical studies of CO adsorption have been carried out in semi-empirical and *ab initio* frameworks of increasing complexity, see for example [77Doy, 80Ros, 83Bag, 84Bae, 84Bau, 84Her, 85Mes, 96Ham, 97Gro, 97Mor, 98Mor1, 00Kop]. Trends in chemisorption energy of CO for a number of fcc transition metal surfaces and metallic overlayer surfaces [92Rod] can be well described by a rather simple model taking into account the metal d states and the CO 2π* and 5σ states [96Ham]. Fig. 5 shows the correlation between the chemisorption energy and the d-band contribution, representative of the substrate. The local site structure on a surface can have a significant influence on the adsorption energy for the same metal. Calculations by DFT for a reconstructed Pt(110) (1×2) surface showed a variation of the CO adsorption energy from the weakest bonding site, a bridge site inside a one-dimensional trough, to the strongest bonding site, an atop site on an isolated Pt adatom, of about 1 eV [01Tho]. Thus CO adsorption on Pt adatoms is energetically preferred and may lead to considerable surface roughness or step formation.

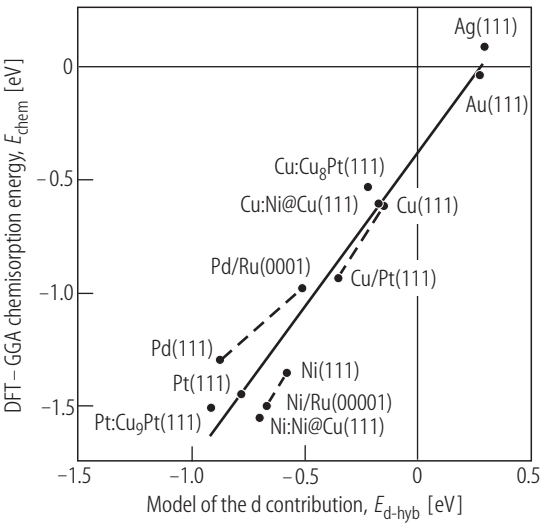

Fig. 5. Calculated energy of CO chemisorption versus a model dependent metal d-band contribution to the metal-CO bond. For a number of transition metal systems [96Ham]. Symbols: experimental values.

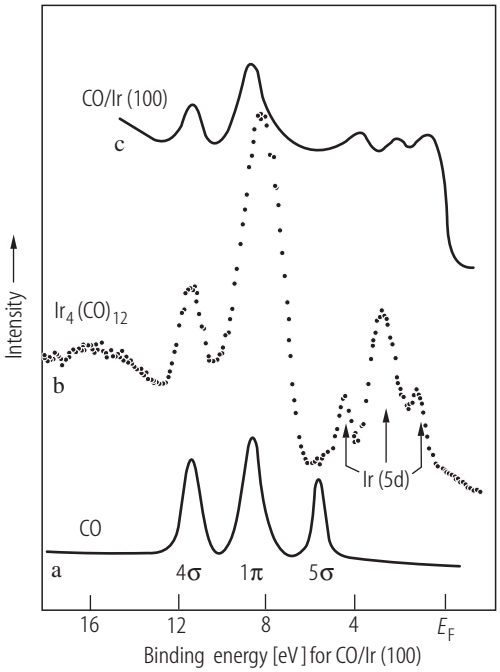

Fig. 6. UV photoelectron spectra of (a) gas phase CO, (b) $Ir_4(CO)_{12}$ carbonyl and (c) CO adsorbed on Ir(100) [78Plu].

Hückel molecular orbital theory was used to elucidate the π-orbital structure. Within this framework, the allylic configuration of the Ni-C-O trimer was derived [64Bly, 69Bly, 87Bly]. In analogy to bonding in transition metal carbonyls which have been described previously [51Dew] (historic overview by[01Mic]), a σ-bond between the carbon 2p and metal d_σ orbitals is formed, leading to additional charge on the central metal atom which is removed by a back-donation bond into the CO 2π* [64Bly, 69Bly, 87Bly]. The π-interaction was thought to be attractive while the σ orbitals were assumed unchanged for the free and adsorbed CO [64Bly, 69Bly, 87Bly].

With UPS the similarity between the adsorption bonds in a carbonyl and CO bonded to a metal surface was experimentally demonstrated for CO on Ir(100) and $Ir_4(CO)_{12}$ [78Plu] (Fig. 6). With the gas phase spectra included as a guideline, one can see that the 5σ level of adsorbed CO is shifted to higher binding energy in both cases (disregarding intensity changes). Details of carbonyl formation were also analyzed by IETS and STM for single Fe and Cu atoms deposited on a Ag(110) surface [99Lee, 00Lee]. Vibrational frequencies were shown to be quite similar to those for CO adsorbed on Fe and Cu surfaces [99Lau].

Angle-resolved ultra-violet photoelectron spectroscopy (ARUPS) as a band mapping technique has been particularly useful to determine the occupied valence states of adsorbed CO (or N_2) and their dispersion. By analogy, the unoccupied states have been determined by inverse photoemission spectroscopy (IPS). A thoroughly characterized system is the well ordered (2×1)p2mg CO layer on Ni(110) [89Kuh, 89Mem, 91Ran] which was analyzed by ARUPS and IPS. The resulting 2D band structure is summarized in Fig. 7. In general, the importance of the CO nearest neighbor distance as a parameter determining the band width is illustrated in Fig. 8 which shows a plot of the measured 4σ dispersion bandwidth versus CO nearest neighbor distance for hexagonally close-packed ordered structures. It can be seen that a logarithmic dependence is obtained, independent of the different substrate material [83Gre, 85Hof].

Many models concentrated solely on the frontier orbitals of the CO molecule, the 2π* and 5σ, where the 2π* was thought to interact with the metal d_π-states, forming a bonding $2\pi^*_b$ and antibonding $2\pi^*_a$ combination [81Fre, 82Mes, 83Fre]. The occupation of the bonding $2\pi^*_b$ was in this model equivalent to back bonding into the 2π*. Even though the two level orbital structure in this severely simplified model is not the three level structure derived by Blyholder [64Bly, 69Bly, 87Bly] this model has been and still is commonly called the "Blyholder model" of CO chemisorption. Another approach for the π interaction was taken by Gumhalter and coworkers, called the resonance model which is based on the Newns-Anderson model for a discrete electronic level interacting with a broad band. Here, the discrete CO 2π* level is broadened resonantly by the substrate interaction, leading to a partial occupation of the resulting broad band. This model implies a large occupied density of states near the Fermi level which could not be verified experimentally [89Kuh, 89Nil, 00Föh1]. In these models the molecule surface interaction is implied to be weak in comparison to the intra-molecular bond. The chemisorption process is expected to cause a small modification of the frontier orbitals HOMO and LUMO, leaving the electronic structure of the CO unit largely intact. A dative bond between the CO 5σ and metal states of σ symmetry is formed, leading to charge donation into the metal which is compensated by a back-donation into the CO 2π*. In this frontier orbital picture, a synergetic π and σ bond is achieved, where the internal C-O bond is weakened due to the increased population of the antibonding CO 2π* orbital in the back-donation.

An increase of CO π population through charge transfer into the CO 2π* has been repeatedly interpreted in support of the frontier orbital model and the resonance model. However, this is not conclusive. The calculations in [00Föh1] give a population of the 2π* by 22 % and a depopulation of the 1π by 12 % upon adsorption, thus yielding an increase of CO π population. However, this increase is not the result of a simple charge-transfer into the CO 2π*, leaving the 1π unaffected, but the result of orbital mixing within the CO π-system and with the metal band.

The importance of orbital mixing for the σ orbitals, notably between the CO 5σ and 4σ, has been pointed out both from theory and experiment [81Bru, 83Bag, 83Gre, 84Bag2, 85Sun, 86Bag, 87Her, 90Wur, 91Won, 95Hu]. In some studies, the σ interaction was considered attractive, [83Gre, 85Sun, 90Li, 90Wur, 91Won, 95Hu] based upon the finding that the 5σ state measured in UPS is shifted towards larger binding energies, relative to the 4σ. Bagus and coworkers found the σ interaction to be repulsive [81Bru,

83Bag, 84Bag2, 86Bag, 87Her]. They propose Pauli repulsion between the CO 5σ and the metal s-band which is partially compensated by a dative 5σ-d_σ bond. This mechanism explains the UPS binding energy shift of the 5σ, where the CO 5σ lone-pair penetrates the metal and its electrons are attracted to the not fully screened metal nucleus. Although 4σ-5σ orbital mixing is considered unimportant for adsorbed CO, [81Bru, 83Bag, 84Bag2, 86Bag, 87Her] they find for isoelectronic N_2 a substantial 4σ-5σ mixing [81Bru, 83Bag, 84Bag2, 86Bag, 87Her].

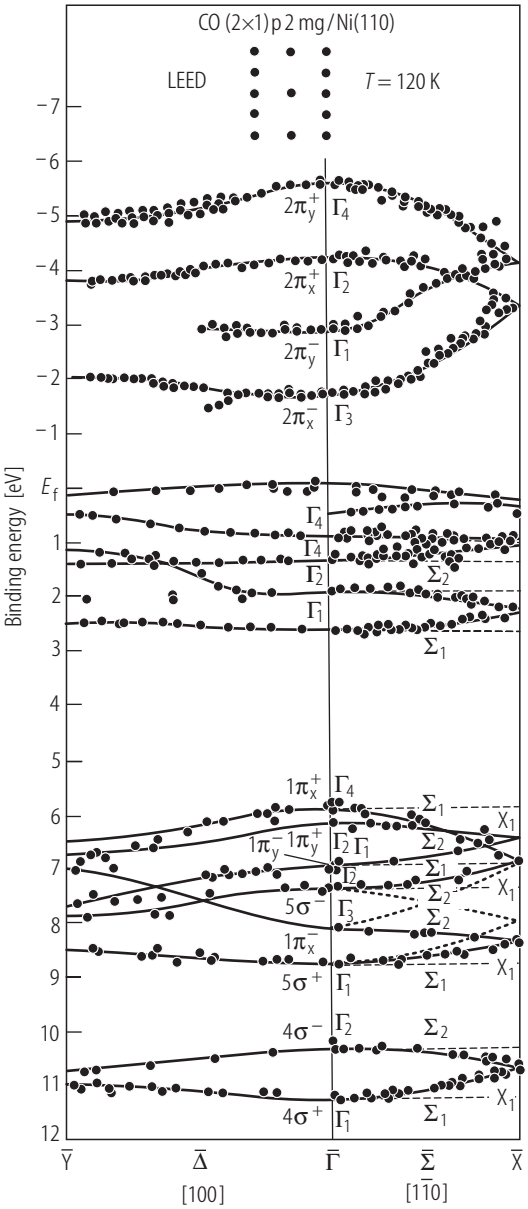

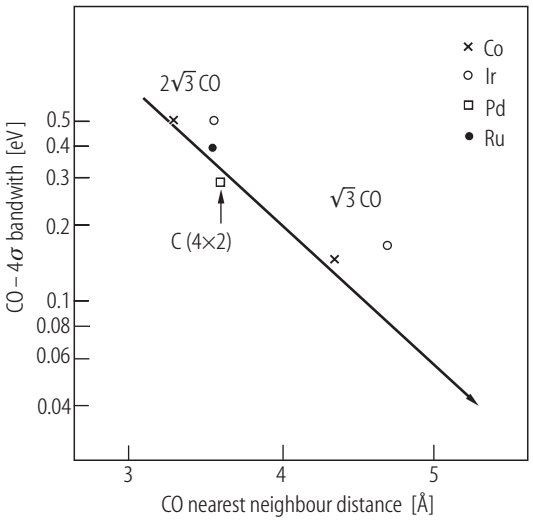

Fig. 8. Plot of 4σ bandwidth versus CO nearest neighbor distance in hexagonally close-packed ordered layers on Co(0001), [83Gre] Ir(111), [80Sea, 81Sea] Pd(111) [84Mir] and Ru(0001) [85Hof].

←

Fig. 7. Valence band dispersion of the (2×1)p2mg-CO structure on Ni(110) from ARUPS [86Kuh, 87Kuh, 89Kuh] and IPS [89Mem, 91Ran].

3.7.1.1.5 Atom specific electronic structure and the allylic model of CO adsorption

Resonant inelastic X-ray scattering or resonantly excited X-ray emission spectroscopy (XES) has the capability to resolve the valence electronic structure of an adsorbate in a local atom-specific and orbital symmetry selective way [92Was, 93Til3, 94Wie, 95Nil, 97Nil1, 97Nil2, 98Wei, 98Wie, 99Has, 99Sta2, 99Tri, 00Föh1, 00Föh2, 00Föh3, 00Kar, 00Nil, 00Nyb, 00Sti, 00Tri, 02Oga, 03Öst, 04Föh1, 04Föh2, 04Öst]. These properties make XES the experimental equivalent to a population analysis of the valence electronic structure. Thus, for adsorbed CO the valence contributions at the carbon atom and the oxygen can be distinguished and for adsorbed N_2 the inner and outer nitrogen atoms can be distinguished [98Ben]. Furthermore, XES allows to seperate and identify the adsorbate-specific valence states from the overlapping bulk metal valence band often dominating the valence region in UPS. In addition, Near edge x-ray absorption fine structure spectroscopy (NEXAFS) has been used to study the unoccupied adsorbate density of states [92Stö].

Using XES as an atom specific probe of the valence electronic structure, [00Föh1, 00Föh2, 00Föh3, 04Föh2] the relative distribution of the valence orbitals and their orbital symmetry at the carbon and oxygen atoms becomes accessible, shown in Fig. 9 for c(2×2)CO on Ni(100) and c(2×2)CO on Cu(100) in direct comparison to gas phase CO. In particular, the XES spectral distributions clearly discern adsorbate states which are energetically overlapping with the metal d-band, a result which was not visible in previous UPS spectra due to the strong photoemission signal from the metal substrate. Theoretical spectral distributions from *ab initio* DFT calculations of CO/Ni_{13} and CO/Cu_{26} clusters (Fig. 10) are in full agreement with the experimental results [00Föh1, 00Föh3]. We can thus visualize in Figs. 11 and 12 the adsorbate electronic structure with orbital contour plots from these calculations.

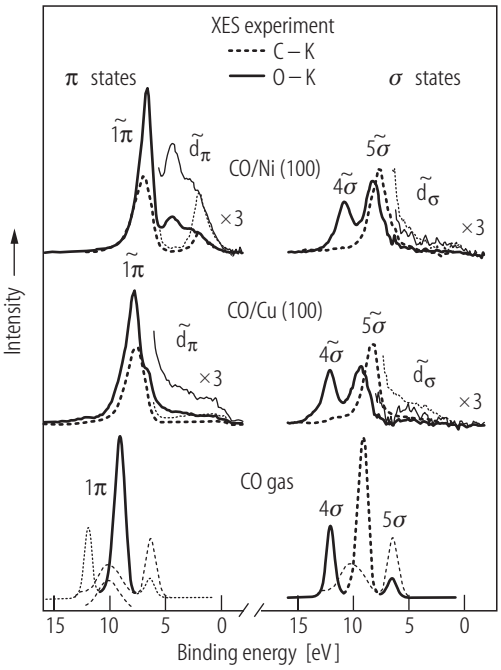

Fig. 9. X-ray emission spectra of CO gas [97Sky] adsorbed in on-top adsorption sites for c(2×2)CO/Cu(100) and c(2×2)CO/Ni(100) [00Föh1, 00Föh2, 00Föh3]. Note the atom specific and symmetry selective projection of the valence electronic structure.

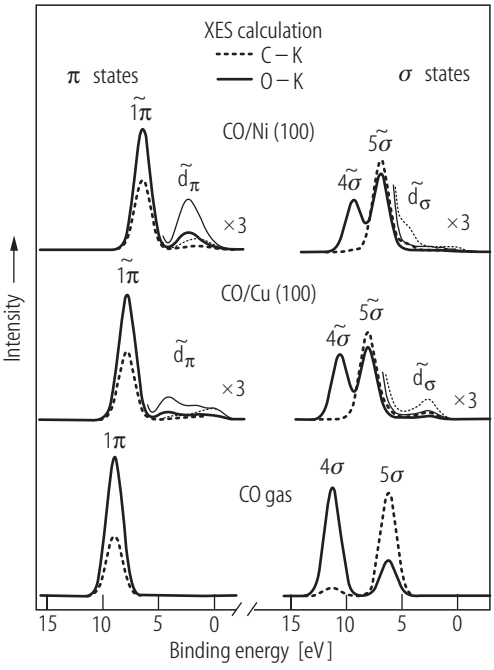

Fig. 10. Computed X-ray emission spectra of CO, CO/Cu_{26} and CO/Ni_{13} [00Föh1, 00Föh2, 00Föh3]. The experimental spectra in Fig. 9 are fully reproduced.

The π-system: Allylic configuration

In the free CO molecule there is only one occupied orbital of π-symmetry, the 1π. This is strongly polarized towards the oxygen atom of the molecule as seen in the experimental spectra of Fig. 9 and the calculated spectra in Fig. 10. Upon adsorption we note two important effects. In comparison to the 1π orbital of gas phase CO, the adsorbate 1π is less polarized towards the oxygen atom and new electronic states are found in the energy region between 5 eV and the Fermi-level. We denote this broad distribution of states as the d_π-band, since these states, as will be seen later, are largely derived from the metal *d*-band. Within this d_π-band an oxygen lone-pair state is observed with an orbital amplitude at the oxygen atom alone and none at the carbon atom. This finding gave rise to the allylic bonding model based on the covalent interaction in the CO-metal trimer moiety [00Föh1, 00Föh3].

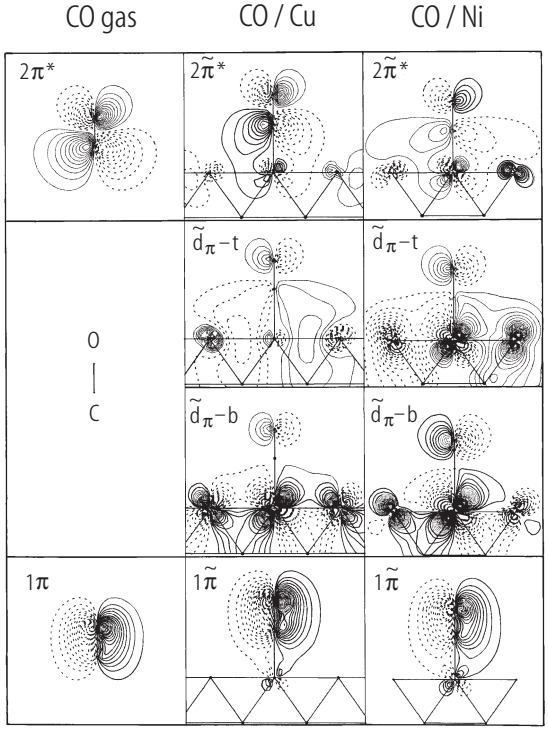

Fig. 11. Orbital contour plots of CO, CO/Cu_{26} and CO/Ni_{13} cluster corresponding to spectral features of π orbital symmetry in Figs. 9, 10 [00Föh1, 00Föh2, 00Föh3].

From the ground state orbital contour-plots in Fig. 11 which have been obtained from the same calculations that led to good agreement (Fig. 10) with the experimental XES in Fig. 9 the allylic configuration is directly accessible.

In the lower panel of Fig. 11, the gas phase 1π and the adsorbate 1π are shown. The 1π is polarized upon adsorption towards the carbon atom mixing with the d_π -orbital of the interacting metal atom. The amplitude of the 1π has the same phase between the O, C, and metal, constituting a bonding orbital between all atomic centers.

In the two middle panels of Fig. 11 orbital plots from two different energy regions within the d_π-band are shown. We have labeled the orbital representing the high-energy region at the 'bottom of the band' as the d_π-*b* and the orbital close to the Fermi-level at the 'top of the band' as d_π-*t*. The orbital plots of the d_π-*b* and d_π-*t* are characterized by one nodal plane at the central atom (carbon), opposite orbital amplitudes at the oxygen atom and the metal atoms. It is also evident that these represent a non-bonding oxygen lone-pair with strong metal *d*-character.

In the top panel of Fig. 11 the evolution of the 2π* orbital is shown. It has two nodal planes and is antibonding between all three atomic centers (metal, carbon and oxygen). In the free molecule the 2π* orbital is polarized towards the carbon atom, opposite to the polarization in the 1π orbital. Upon adsorption the orbital is polarized towards oxygen in comparison to the free molecule and shows some metal *d* contribution antibonding with respect to the molecule.

The observed π-electronic structure can be summarized into the conceptually simple allylic configuration of a covalent triatomic molecule modified by the varying electronegativity of the involved atoms. Thus, in a first step the adsorbate–substrate complex is reduced to the treatment of a covalent triatomic molecule consisting of the coordinating metal atoms (depending on on-top, bridge or hollow adsorption sites), the carbon atom and the oxygen atom [00Föh1, 00Föh3]. Such a molecular orbital view of CO chemisorption was first proposed by Blyholder [64Bly, 69Bly, 87Bly] using Hückel molecular orbital theory where independent of the chosen basis, the allylic configuration of the adsorbate π system is found, with the three characteristic hybrid orbitals. In a second step modifications from the three-atomic case are added due to the energetic width of the metal *d*-band and the delocalized *sp*-band [00Föh1, 00Föh3, 04Föh2]. However, an experimental verification of this theoretical model has not been possible prior to the application of XES to the adsorbate-electronic structure [00Föh1, 00Föh2, 00Föh3, 04Föh2] which allows an atom and symmetry projected analysis of the adsorbate valence states.

To deduce the various contributions to the adsorption energy and the local bond-properties, e.g. the C-O stretch frequency, the Constrained Space Orbital Variation (CSOV) method [84Bag1, 84Bag2] has been applied to the CO/Ni_{13} and CO/Cu_{26} clusters [00Föh1, 00Föh2, 00Föh3] and a weakening of the internal CO π-bond was found upon adsorption leading to a decreased C-O vibrational frequency.

The π-interaction stabilizes the adsorbate complex, since only the bonding 1π-orbital and the non-bonding d_π-band are occupied, whereas the antibonding 2π* remains unoccupied. Upon adsorption the internal C-O π-bond is partially broken which is compensated by the formation of a bonding metal-carbon interaction. For isoelectronic N_2 on Ni(100) the equivalent behavior was found [98Ben].

The σ-system

In the free CO molecule there are two occupied outer valence orbitals of σ-symmetry; the 4σ and the 5σ where the latter is the HOMO of the molecule. As seen experimentally in the lower part of Fig. 9 and in the calculations in Fig. 10 the 5σ orbital has a larger contribution on the carbon atom than on the oxygen atom while the 4σ orbital shows the reverse situation. Upon adsorption of the CO molecule, strong orbital mixing takes place in the σ-system, visible in the polarization of the 5σ orbital towards the oxygen atom and the 4σ towards the carbon atom (Figs. 9, 10). The 5σ and 4σ states show significant changes both in peak positions and in relative intensities. Additional states with low intensity in the XES spectra are found between the 5σ -state and the Fermi-level and are denoted d_σ band.

The computed adsorbate 5σ and 4σ orbital plots in Fig. 12, reveal in-phase (bonding) orbitals between the adsorbate and the metal, whereas the d_σ orbitals are antibonding between the metal and carbon atoms.

In general, the σ orbital structure is more complex than the π-orbital structure due to the involvement of more initial CO orbitals in contrast to the π-system with only the CO 1π and 2π* orbitals. In the σ-system, the occupied CO valence orbitals (3σ, 4σ and 5σ) and the unoccupied CO 6σ, with a large energy separation, mix with the metal states. This is seen in the XES spectra of adsorbed CO on the late transition metals Ni and Cu through the polarization of the 4σ and 5σ and the occurance of the d_σ band. As in the late transition metals the metal bands are highly occupied, anti-bonding adsorbate orbitals are occupied, making the adsorbate-substrate σ interaction repulsive. These qualitative arguments of a repulsive σ interaction have been investigated systematically with CSOV [84Bag1, 84Bag2] calculations on the CO/Ni_{13} and CO/Cu_{14}cluster model [00Föh1, 00Föh3], where the repulsive σ-interaction between the CO and the metal surface is accompanied by a strengthening of the internal C-O σ bond.

In summary, the adsorption of CO and N_2 is governed by a strong covalent adsorbate-substrate bond, characterized by significant orbital mixing of the initial molecular orbitals and the metal bands within each orbital symmetry. The orbital structure of the π system can be summarized as an allylic configuration and is, for the example of CO, the result of orbital mixing between the CO 1π, 2π* and the metal d_π-band. Experimentally, this is manifested in the observation of a characteristic oxygen lone-pair state. The π-interaction stabilizes the adsorbate-substrate complex, weakening the internal C-O π-bond upon adsorption. In the σ system equally strong orbital mixing takes place, leading to a strong polarization of the 5σ and the 4σ orbitals within the molecular unit. Depending on the filling of the metal

bands, antibonding σ orbitals become occupied and the σ-interaction for the late transition metals destabilizes the adsorbate-substrate complex, strengthening the internal C-O σ bond. In a valence bond model, the adsorption process can be described as the modification of the internal bonds in the CO gas molecule which is then compensated by the formation of the surface chemical bond to the metal substrate. The equilibrium properties of adsorbed CO are therefore the direct result of the balance between the σ - and π-interaction; both in terms of the total energy and the local bond properties, such as bond-distance and vibrational frequencies. This behaviour has been found for CO adsorbed in on-top sites and in higher coordinated sites, such as bridge and hollow sites [00Föh1, 00Föh3]. With increasing density of the adsorbate layers, direct and substrate mediated adsorbate-adsorbate interactions need to be taken into account in addition to the local contributions summarized in the allylic model of the metal-CO moiety [04Föh2].

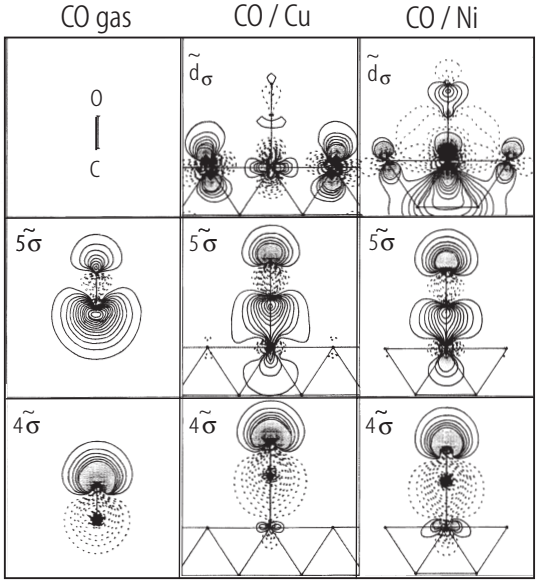

Fig. 12. Orbital contour plots of CO, CO/Cu_{26} and CO/Ni_{13} cluster corresponding to spectral features of σ orbital symmetry in Figs. 9, 10 [00Föh1, 00Föh2, 00Föh3].

3.7.1.2 CO adsorption on fcc metal surfaces

Al

The adsorption of CO on single crystal Al surfaces, possible only at low temperature of <40 K, has been studied under various aspects [79Pir, 80Chi, 82Flo, 83Sch, 86Pau1, 86Pau3, 88Ryb, 89Jac, 90Jac]. The C-O stretch vibration of adsorbed CO on Al(111) and Al(100) is with 2137 and 2135 cm^{-1} [88Ryb, 89Jac] nearly identical and close to the gas phase value, suggestive of rather weak physisorption. The adsorption energy is estimated as 20 kJ/mol [80Chi, 89Jac] and 33 kJ/mol [86Pau3]. Another study of CO/Al(100) reports 2060 cm^{-1} for the C-O stretch [86Pau3]. Also the influence of coadsorbed K was studied, showing a substantially modified adsorbed CO species with CO stretch frequencies as low as 1250 cm^{-1} and dissociation at elevated temperature [86Pau2, 87Pau]. UPS illustrates weak adsorption of CO on clean Al(111) by well separated 5σ and 1π molecular orbital peaks, in addition to the 4σ peak [80Chi, 89Jac]. Compared to the experimental heat of adsorption of CO on Al(111), theoretical values for atop bonded CO of 22.1 kJ/mol [83Bag] and 47.3 kJ/mol [96Ham] have been reported. A study of CO adsorption on a Cu-promoted Al(111) surface, where the coverage of Cu is less than half a monolayer, is interesting because EELS detects a C-O stretch at 1260 cm^{-1} and dissociation of CO at 348 K [93Col]. Although neither pure Al nor Cu are able to dissociate CO under such conditions, the Cu-modified Al surface is. Electron irradiation also leads to CO dissociation on Al(111) [82Flo].

Ni

The adsorption of CO on oriented Ni single crystal surfaces is one of the most intensely studied systems in the context of this chapter. Many examples of results were presented in the general introduction to this volume [01Bon]. Overall, CO adsorption is predominantly molecular on Ni surfaces. On the Ni(100) surface three ordered CO overlayers are formed: The c(2×2) at 0.5 coverage [72Tra2, 78All, 78Hor1, 79And2, 79Hei2, 79Pet, 80And, 80Ton, 81Kev, 82Bib, 88Uvd], the c(5√2×√2)R45° structure at 0.6 coverage [72Tra2, 82Bib, 88Uvd] and the (3√2×√2)R45° structure at 0.67 coverage [72Tra2, 82Bib, 88Uvd]. Both the thermodynamics of adsorption and desorption have been studied [72Tra2, 78Mad, 79Bor, 80Yat, 81Joh, 83Koe1, 93Stu, 93Tak, 95Vas]. The coverage dependent surface stress [94Gro], the thermodynamics of CO diffusion on the Ni(100) surface [87Roo] and the role of defects on dissociative adsorption [86Ste] have been determined.

The vibrational spectra have been measured with EELS and IRAS [82Bib, 87Ber, 88Uvd, 93Sin, 95Vas]. Based on the CO stretch frequencies, pure on top adsorption is assigned to the c(2×2) structure, whereas mixed on top and bridge adsorption takes place for the (3√2×√2)R45° and c(5√2×√2)R45° structures [82Bib, 87Ber, 88Uvd, 93Sin, 95Vas]. The valence electronic structure has been analyzed with photoemission spectroscopy [71Eas, 77All1, 78All, 78Hor1, 80Smi, 81Bru, 83Koe1, 94San3] and the atom specific and orbital symmetry resolved valence electronic structure has been determined with XES [00Föh1, 00Föh2, 00Föh3] (cf. previous section). The C1s and O1s core level binding energies of adsorbed CO have been determined with XPS [81Bru, 83Koe2, 88Uvd, 92Bjö, 98Föh, 99Föh1], where even the vibrational fine structure of the core-ionized species has been resolved [98Föh, 99Föh1]. The unoccupied density of the Ni-CO valence states has been investigated as well [87Joh, 88Zae, 92Bjö, 92Nil, 92Stö].

On the Ni(111) surface the following CO overlayer structures have been observed: (2×2) at 0.25 ML coverage [81Kev, 96Dav], (√3×√3)R30° between 0.30 and 0.42 ML coverage [74Chr, 76Con, 81Kev], c(2×4) at nominal 0.5 ML coverage [82Net, 93Bec, 93Sch, 94Dav, 94Map, 96Dav, 98Hel], (√7×√7)R19° at 0.56 ML coverage [76Con, 82Net, 98Hel] and c(2√3×4)rect at 0.62 ML coverage [98Hel]. The thermodynamic properties of the different phases have been studied by different techniques [74Chr, 76Con, 79Rub, 80Iba, 81Cam1, 82Net, 84Gij, 87Fro, 88Sur, 89Zhu, 93Stu, 98Hel]. Also the adsorbate induced surface stress [94Gro] and the surface diffusion activation energy of 29 kJ/mol with a pre-exponential factor of 1.2×10^{-5} cm^2s^{-1} [88Zhu] have been determined.

The assignment of local adsorption sites has evolved considerably. On the Ni(111) surface, the traditionally used assignment of local adsorption sites through the C-O stretch frequency has turned out to be questionable [93Sch, 94Dav]. Vibrational spectroscopy has been widely used for this purpose [77Ber, 79Cam, 80Erl, 85Per, 85Ryb, 87Fro, 88Sur, 91Ha, 94Dav, 97Smi]. CO bridge adsorption has been initially reported for the (√3×√3)R30° structure, based on PED data [81Kev] which later was reassigned to three-fold hollow sites [94Dav, 97Smi, 98Hel]. For the c(4×2) phase, the traditional assignment to bridge sites by vibrational spectroscopy [77Ber, 79Cam, 80Erl, 87Fro, 88Sur] has been replaced by three-fold hcp and fcc hollow sites based on LEED [94Map], XPS [98Hel], SEXAFS [93Bec], IRAS [97Smi] and PED [93Sch, 94Dav]. The same assignment was found for the (2×2) structure [96Dav]. Towards higher coverage in the (√7×√7)R19° phase, both on top and bridge sites are occupied [93Sch, 94Dav, 98Hel]. Using UPS the valence electronic structure has been determined [76Con, 76Wil, 88Gum, 90Sch]. Also the unoccupied states have been investigated [83Boz, 88Fra, 88Gum]. A detailed investigation of the CO core level binding energies has been used to support the assignment of local adsorption sites [84Jug, 98Hel].

Three ordered CO structures exist on the Ni(110) surface. The most frequently studied is the (2×1)p2mg at 1 ML coverage with the CO molecules occupying short-bridge sites and being tilted by about 20° relative to normal [73Mad2, 85Beh, 85Rie, 86Kuh, 88Han, 89Kuh, 92Kna, 93Hua, 93Pan, 94Zha, 95Rob, 95Spr, 98Emu, 01Pet]. At 0.75 ML a c(4×2) and at 0.62 ML a c(8×2) overlayer has been observed [85Beh]. In early work also other LEED patterns, e.g. a c(2×2) [73Tay, 80Mah], have been reported that could not be reproduced in later work. The thermodynamic adsorption and desorption

properties have been investigated [73Mad2, 73Mad3, 73Tay, 75Fal, 81Ber, 85Beh, 86Fro, 87Bau, 90Fei, 92DeA, 93Stu]. Also the CO surface diffusion parameters have been reported [91Xia, 92Xia, 96Ber].
The vibrational properties of CO on the Ni(110) surface have been analyzed with EELS [81Ber, 81Nis, 87Bau, 90Voi] and IRAS [92Lov]. Based on these investigations, a tilted short-bridge adsorption site for the (2×1)p2mg structure was supported. The valence electronic structure and dispersion has been been studied with ARUPS [82Hor, 84Rie, 86Kuh, 89Kuh] and the unoccupied states with inverse photoemission [86Fre2].

Vibrational studies of CO adsorption on stepped Ni(100) [93Sin, 96Sve] and Ni(111) [79Erl, 90Ben] surfaces have also been reported. The adsorption energy at step sites of Ni(510) is higher than on the (100) terrace sites although the energy difference is small. Ordering on the terrace is hindered by step adsorption [96Sve].

Cu

On the Cu(100) surface a disordered overlayer is found at 77 K below a coverage of 0.45 ML, but a well ordered c(2×2) structure exists at 0.5 ML coverage [72Tra1, 79Pri, 80And, 80Ton, 82Bib, 83Stö, 86McC, 88Uvd]. Further adsorption leads to a uniaxial compression and a c(7√2×√2)R45° structure at 0.57 ML [72Tra1, 79Pri, 82Bib, 88Uvd, 96McC, 97McC]. Furthermore it has been suggested that at even higher coverage of 0.6 ML even a c(5√2×√2)R45° structure exists [72Tra1, 82Bib]. On the Cu(100) surface the on-top adsorption site is preferred [72Tra1, 79Pri, 80And, 80Ton, 82Bib, 83Stö, 86McC, 88Uvd, 96McC, 97McC].

The thermodynamic properties have been investigated [72Tra1, 83Bur, 86Dub, 90Pet, 91Pet2, 92Tru]. Both the heat of adsorption and the activation energy of desorption follow the same trend of a rapid decrease from the zero coverage limit to a plateau between 0.1-0.5 ML coverage [72Tra1, 83Bur, 86Dub, 90Pet, 91Pet2, 92Tru], declining further with higher coverage. The pre-exponential sticking factor in the zero-coverage limit is found at $10^{-15.3\pm0.4}$ [91Pet2]. The sticking behaviour is described by the precursor-mediated adsorption model [81Cas], allowing for direct sticking into unoccupied chemisorption sites [96Dvo, 00Dvo]. The initial sticking coefficient at 110 K is 0.85, slowly decreasing until a rapid drop sets in reaching the compression phase beyond 0.5 ML coverage [96Dvo, 00Dvo]. The vibrational properties have been investigated with EELS [79And1, 88Uvd], IRAS [85Ryb, 90Hir, 92Tru, 94Hir, 95Hir, 96McC, 97McC, 98Gra2], SFG [90Har], Helium atom scattering [94Ber, 95Ell, 96Bra, 96Gra, 98Gra2, 03Gra] and STM-IETS [99Lau, 00Lee, 02Hei]. On the Cu(100) surface lateral adsorbate-adsorbate interactions and dephasing has been studied [90Har, 90Hir, 91Pet2, 92Bjö, 92Bor, 92Mor, 94Kam, 95Hir, 95Wei, 96Gra, 97McC, 98Gra2]. For example, the energy of lateral repulsion for the c(2×2) structure is at 4.2-8.3 kJ/mol [90Pet, 91Pet2]. CO adsorption at step and defect sites was characterized by low-energy vibrational modes [96Bra].

The binding energies of the valence states have been determined by UPS [75Bru, 76Dem, 77All2, 85Hes, 94San2, 94San3] and XES [00Föh1, 00Föh2]. The unoccupied states were studied by inverse photoemission [92Tsu] and NEXAFS [84McC, 86McC, 92Bjö]. The core-level binding energies have been determined with XPS [75Bru, 78Gun, 79Pri, 90Ant, 92Bjö] and resonant Auger investigations [87Wur, 94San3] and PSD [91Tre] were performed.

On the Cu(111) surface, adsorption above 90 K yields a (√3×√3)R30° structure at 0.33 coverage [77Kes, 79Pri, 80Hol, 96Mol, 99Bar], followed by a (1.5×1.5)R18° structure at 0.44 coverage [80Hol, 96Mol] and a (1.39×1.39) hexagonal overlayer at 0.52 saturation coverage [80Hol]. Tip-functionalized STM indicates that the saturation coverage exhibits a (4×4) supercell [99Bar]. Previously, the (1.5×1.5)R18° structure has also been assigned as a c(4×2) at 0.5 coverage [72Pri, 77Hor1] or as a (√7/3×√7/3)R49.1° [77Kes]. Likewise, the (1.39×1.39) hex. structure has been discussed as a (1.4×1.4) hex, (√2×√2) [79Pri] or (7×7) [79Pri]. For all phases, besides the saturation phase, CO occupies on-top adsorption sites [85Hay2]. In the saturation phase on-top and bridge sites are populated [80Hol, 85Hay2].

The thermodynamic properties of CO adsorption on Cu(111) have been studied extensively [75Con, 77Kes, 79Hol, 86Kir, 90Hin, 99Kne2]. The heat of adsorption and activation energy of desorption below 0.33 coverage are about 50 kJ/mol and above 0.33 coverage 38 kJ/mol [75Con, 77Kes, 79Hol, 86Kir,

90Hin]. The sticking coefficient remains more or less constant close to saturation coverage, indicative of precursor adsorption kinetics but also exhibits characteristic minima at the formation of the ordered overlayers [86Kir, 99Kne2]. The vibrational properties [79Hol, 79Pri, 85Hay2, 90Hir, 93Hir, 94Hir, 95Hir] and the valence electronic structure have both been determined [75Con, 86Kir]. Also two-photon photoemission has been performed of the CO covered Cu(111) surface [94Her, 95Her, 95Kno, 99Vel, 99Wol].

Two ordered CO overlayer structures have been observed on the Cu(110) surface below 215 K: a (2×1) structure between 0.25 and 0.5 coverage [77Hor2, 82Woo, 85Har, 86Hol, 95Hof, 96Ahn] and a compression structure at a CO coverage of 0.8, leading to a streaky (4/5×2) structure [96Ahn], also denoted as c(4/5×2) [85Har] or c(1.3×2) [77Hor2, 82Woo]. It is under debate, whether annealing to 170 K improves [85Har] the long range order in these two phases [96Ahn]. Next to them exist disordered phases both towards lower and higher coverage [77Hor2, 82Woo, 85Har, 95Hof, 96Ahn].

The thermodynamic properties of CO adsorption on Cu(110) have been studied with various techniques [73Wac, 77Hor2, 85Har, 91Pet2, 92Chr, 96Jin, 01Kun]. In particular the sticking coefficient [85Har, 91Pet2, 96Jin, 01Kun] is well described by a Kisliuk model with K=0.07±0.02 and S_0=0.95±0.05 [01Kun]. The vibrational modes of CO/Cu(110) have been determined, indicating on-top adsorption [79Wen, 82Woo, 84Hol, 92Mor, 94Hir, 98Bra, 99Lau]. In particular a clear anisotropy of the frustrated translation along and perpendicular to the atomic rows of the Cu(110) surface has been observed [97Ahn, 98Bra].

The valence electronic structure has been determined [78Kan, 82Mar, 85Che2] as well as the core-level binding energies [86Hol, 92Chr]. Also the unoccupied adsorbate states have been investigated [82Stö, 84Rog, 85Che2, 91Dav].

Rh

LEED studies have found three ordered overlayer structures on the Rh(100) surface. A c(2×2) structure is seen below 370 K for coverages between 0.2 and 0.6 ML, with an optimum coverage of 0.5 ML [78Cas, 82Kim, 87Gur, 90Leu, 94deJ, 96Bar, 97Wei, 98Str]. Above 0.5 ML CO coverage at 300 K, the structure coexists with the (4√2×√2)R45° structure, which saturates the surface at 300 K at 0.75 ML coverage [66Tuc, 82Kim, 87Gur, 90Leu, 94deJ, 96Bar, 97Wei, 98Str]. Heating to 350 K leads to the reapearance of the c(2×2) structure [98Str]. High CO exposure below 280 K results in a third structure, first denoted „split (2×1)“ [78Cas] but later designated as a c(6×2) with 0.83 ML saturation coverage [94deJ, 98Str].

The activation energy of desorption for CO/Rh(100) in the zero coverage limit has been determined with TPD as 131±4 kJ/mol, with a preexponential factor of $(4\pm3)\times10^{16}s^{-1}$ [94deJ], or 134 kJ/mol at $8.4\times10^{12}s^{-1}$ [82Kim]. Molecular beam studies yielded more reliable values of 149±10 kJ/mol and 135±8 kJ/mol at $10^{16.3\pm1.1}s^{-1}$ and $10^{14.5\pm0.9}s^{-1}$ [97Wei]. The coverage dependent sticking coefficient obeys the Kisliuk model with a zero coverage value of 0.75 and a Kisliuk parameter of K=0.7 [94deJ]. The CO molecules occupy up to 0.5 ML coverage (c(2×2) structure) on top sites, based on vibrational and XPS data [87Gur, 96Bar, 98Str]. However, with increasing coverage both on-top and bridge sites are occupied. The observation of a c(2×2) structure at 100 K with CO coverage as low as 0.2 ML implies island formation [87Gur]. The (4√2×√2)R45° and c(6×2) structures at coverages of 0.75 ML and 0.83 ML, respectively, exhibit both on-top and bridge site occupation in a coverage dependent way. For the (4√2×√2)R45° structure bridge/top occupation ratios of 2 [96Bar] and 2.3±0.5 [98Str] have been found. For the c(6×2) structure ratios of 1.2 [96Bar] and 0.8±0.2 [98Str] were reported. For the (4√2×√2)R45° superstructure IRAS indicates two on-top bound species and one bridge bound species, [87Gur] but another study claims one on-top bound and one bridge bound species [94deJ]. Bridge sites are occupied at elevated temperature for 0.4 ML coverage, whereas at 90 K CO favors on-top sites [87Gur]. Also surface contamination leads to increased bridge occupation [87Ric, 94deJ]. The numerical values of the difference in binding energy between on-top and bridge sites varies significantly: Gurney et al [87Gur] report for the (4√2×√2)R45° structure at 0.5 ML an energy difference of 4.60±0.25kJ/mol. Much lower values of 0.4 to 1.7 kJ/mol between 0.2 and 0.5 ML coverage were also reported [90Leu] but found to be influenced by contamination [94deJ]. The adsorption of CO on Rh(100) has also been investigated by UPS [83Koe1], XPS of the Rh surface core level shift [96Zac] and ion scattering spectroscopy [84Mol] and ESD [90Cra].

On the Rh(111) surface CO adsorbs in several different overlayer structures depending on sample temperature, CO coverage and the partial pressure of CO. At temperatures below 120 K a (2×2) CO structure at 0.25 ML coverage has been observed by LEED [79Thi2, 98Beu], followed at 0.33 ML by a (√3×√3)R30°-CO structure [97Gie, 97Ove, 98Beu] and a (4×4)-8CO structure at 0.5 ML [98Beu]. At a CO coverage above 0.5 ML, the LEED pattern exhibits continuously changing structures which early on have been termed „split (2×2)" [78Cas, 84deL] because the LEED spots coalesce with increasing coverage into the (2×2)-3CO pattern at the saturation coverage at 0.75 ML [97Gie, 97Ove, 98Beu]. At temperatures above 120 K, the low coverage (2×2)-CO and (4×4)-8CO patterns do not form, but a (1×1) LEED patterm has been found around 0.25 ML [98Beu]. At room temperature the (√3×√3)R30° CO structure at 0.33 ML and the (2×2)-3CO structure at 0.75 ML is found [78Cas, 79Thi2, 81Koe, 83vHo2, 84deL, 97Gie, 97Ove, 98Beu]. An investigation of the temperature dependence of the (√3×√3)R30°-CO and the (2×2)-3CO structures reported for the (√3×√3)R30°-CO structure an order-disorder transition at a temperature of 330±5 K [91Pet1, 97Ove]. Early LEED measurements, all performed above 120 K, have observed the (√3×√3)R30°-CO and (2×2)-3CO LEED patterns [78Cas, 79Thi2, 81Koe, 83vHo2, 84deL] but could not observe well the (2×2)-CO and (4×4)-8CO patterns. The earliest indication of a (2×2) pattern at 0.25 ML coverage was given by [79Thi1].

Structural analysis with LEED of the (√3×√3)R30°-CO [81Koe] and the (2×2)-3CO structures [97Gie] as well as surface X-ray diffraction of the (2×2)-3CO structure [99Lun] have led in combination with XPS work [97Beu, 98Beu, 01Sme] and He diffraction [97Ove] to a consistent determination of adsorbate geometry. In the (2×2)-3CO structure, one molecule sits in an on-top site while the other two molecules occupy three-fold fcc and hcp sites [97Beu, 97Gie, 97Ove, 98Beu, 99Lun, 01Sme]. Earlier work proposed erroneously a bridge site model, where two CO molecules were thought to occupy near-on-top sites and one CO molecule a bridge site [80Dub, 83vHo1, 83vHo2, 84deL].

XPS has been used extensively to determine the adsorption site [84deL, 97Beu, 98Beu, 01Sme]. It has been found, [97Beu, 98Beu, 01Sme] that up to 1/3 ML CO coverage, all molecules occupy on-top sites. At intermediate coverage up to 0.5 ML, a small number of threefold hollow sites becomes occupied, leading at saturation coverage to 1/3 in on-top and 2/3 in hollow sites. At coverage above 0.4 ML, the relative top/hollow occupation depends on the sample temperature. Up to 0.54 ML the relative amount of CO molecules in hollow sites increases with increasing temperature, wheras at coverages above 0.54 ML increasing temperature leads to a decreasing occupation of hollow sites [97Beu, 98Beu, 01Sme].

CO adlayers at variable CO background pressure have been studied at room temperature using scanning tunneling microscopy [00Cer]. Exposure of the Rh(111) surface to 5×10^{-8} torr leads to a (2×2) LEED pattern with three domains of (2×1) symmetry at 0.5 ML coverage [00Cer]. At 1×10^{-6} torr a STM image with (√7×√7)R19° periodicity has been observed with 3/7 ML coverage [00Cer]. For a CO pressure between 5 torr and 700 torr a STM image with (2×2) periodicity has been reported which has been proposed to represent the (2×2)-3CO structure [00Cer].

The thermodynamic properties of CO adsorption on the Rh(111) surface have been studied with TPD [78Cas, 79Thi2], laser desorption spectroscopy [88See] and molecular beam scattering [91Pet1, 97Wei, 99Beu]. TPD determined a first order adsorption via a mobile precursor. In particular, the coverage dependence of CO desorption [88See, 91Pet1] and the dependence of the initial sticking coefficient on the kinetic enery of impinging CO molecules [99Beu] have been investigated. Peterlinz et al. measured essentially the isothermal and isosteric rates of desorption by using CO molecular beams and in addition time-resolved specular Helium scattering from the adsorbed CO layer as a kinetic response amplifier [91Pet1]. The desorption rates of CO at coverages between 0 and 0.22 ML and at temperatures of 440-555 K, shown in Fig. 13, obey an Arrhenius behavior. The coverage dependence can be be fitted by either a constant desorption energy of 135 kJ/mol or a constant pre-exponential factor of 1.33×10^{14} s^{-1}. Neither can be quite correct because the repulsive interaction between adsorbed CO molecules calls for a decreasing adsorption energy with increasing coverage. However, the effect is small for this investigation (less than 10 %) because of the limited range of coverage.

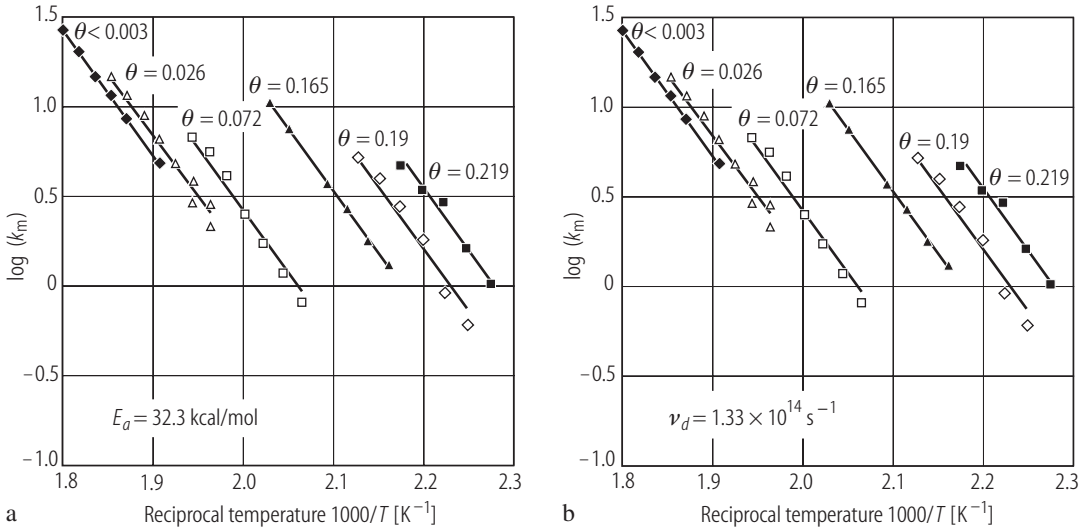

Fig. 13. Semi-log plots of isosteric CO desorption rates versus $1/T$ from Rh(111) at coverages of 0 to 0.22 ML and temperatures between 440 and 555 K [91Pet1]. Solid lines are best fits to the data assuming (a) a constant desorption energy and variable pre-exponential factor, and (b) a constant pre-exponential factor and a coverage dependent desorption energy of $E_d(\theta) = 135 - 6.77\ \theta - 160\ \theta^2$ [kJ/mol].

The binding enthalpy difference for hollow and on-top bound CO was determined as ~14.7 kJ/mol at an assumed pre-exponential factor of 10^{13} s^{-1} [80Dub]. The activation energy of the CO exchange reaction has been measured with TPD and isotope switch techniques as 35.6±2 kJ/mol [94Son], using supportive ESD work [94Cam]. Vibrational spectroscopy has played an important role in the determination of the registry of the CO on Rh(111) [80Dub, 81Koe, 84Koe, 84Tom, 93Wit, 01Wit]. Dubois et al. found in coverage dependent EELS investigations on-top adsorbed CO at a C-O stretch of 2070 cm^{-1} and bridge bonded CO at 1870 cm^{-1} with a coverage and temperature dependent ratio [80Dub]. The CO-metal frustrated translation was found at 420 cm^{-1} [80Dub]. However, based mostly on XPS, the correct assignment into fcc and hcp hollow sites in favor of the bridge sites was accomplished. In addition vibrationally resolved XPS, known to be highly sensitive to different adsorption states [98Föh], indicates next to on-top and hollow site adsorption also at 3L CO exposure a small population of bridge sites [01Sme]. The adsorption of CO on Rh(111) was also studied with UPS [78Bra2] and EDS [92Cra, 94Cam].

On the CO covered Rh(110) surface early LEED investigations showed at 300 K a c(2×2) pattern at 0.5 ML coverage and a (2×1)p1g1 pattern at 1 ML coverage [77Mar]. Subsequent structural work has uncovered a very complex adsorption behaviour illustrated in Fig. 14 [94Wei]. For all temperatures a disordered lattice gas has been found at CO coverages below about 0.08 ML. A highly intense pattern characterized by split c(2×2) spots appears at a CO coverage between 0.3 and 0.6 ML below 180 K. The "split" c(2×2) pattern converts to a pattern with diffuse, broad c(2×2) spots above 180 K. Overlapping diffraction features from "(3×2)", "(4×2)", and "(5×2)" symmetries are observed for CO coverage above about 0.62 ML and below 240 K. The "(5×2)" predominates at a coverage of 0.8 ML. With further increase in coverage, (2×1)p2mg LEED spots appear with the "(5×2)" features. A pure (2×1)p2mg pattern appears at 1 ML saturation coverage [94Wei].

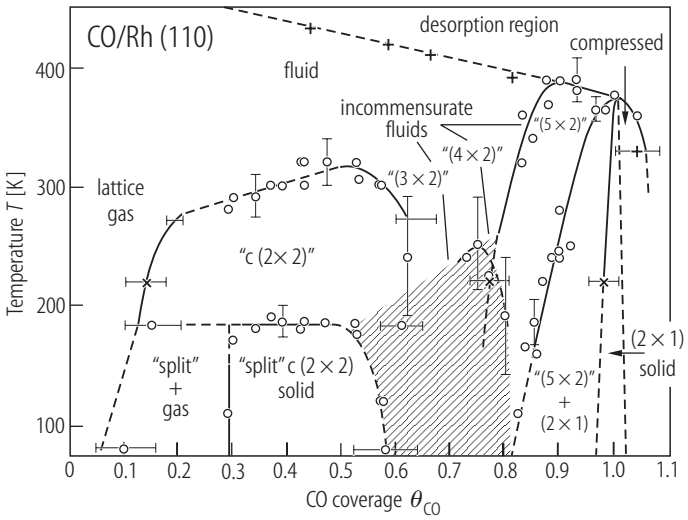

Fig. 14. Phase diagram of CO/Rh(110) according to [94Wei].

Next to the unreconstructed Rh(110)-(1×1) surface, also a clean (1×2) missing row reconstruction can be prepared [92Dha, 93Bel, 93Mur]. With increasing coverage the following LEED patterns are found: (1×2) at 0.24 ML, p(2×2) at 0.46 ML, diffuse c(2×4) at 0.52 ML, c(2×4) at 0.75 ML and (2×2)p2mg at 1 ML [92Dha]. On the unreconstructed Rh(110) surface, the zero coverage limit Arrhenius parameters for CO desorption have been determined [77Mar, 80Bai, 91Bow, 97Wei] with TPD to 130 kJ/mol [77Mar] and 132 kJ/mol [91Bow] at an assumed pre-exponential factor of 10^{13} s^{-1}. Modulated beam and single beam studies [97Wei] yielded 173.8±4 kJ/mol and 164.1±6 kJ/mol and pre-exponential factors of $10^{17.8\pm0.4}$ s^{-1} and $10^{16.8\pm0.6}.s^{-1}$, respectively. The coverage dependent sticking coefficient follows well the Kisliuk model, with an initial sticking coefficent of 0.68±0.01 and a Kisliuk parameter of K=0.3 [91Bow].

While the ordered superstructures are well recognized in the system, the registry of the CO molecules is debated. As TPD gives a single desorption peak at all coverages, a single adsorption site for any of the structures could be suggested. LEED suggests a short bridge adsorption site for the (2×1)p2mg structure at 1 ML [94Bat] and for the c(2×2) at 0.5 ML coverage [77Mar, 93Dha, 94Wei]. However, coverage dependent XPS [93Dha] shows a significant O1s binding energy shift with coverage and it was suggested, that below 0.54 ML on-top sites are occupied, whereas above 0.54 ML only bridge sites are occupied. Vibrational spectroscopy (EELS) yields CO stretch frequencies at 2008 cm^{-1} below 0.5 ML and at 1968 cm^{-1} above 0.5 ML [97Wei] which represents a rather small shift. To reconcile the experimenal findings, two different structural models, off-top and tilt models have been proposed for ordering in the overlayers, based on the symmetries of features in the LEED patterns. In off-top models, CO adsorbs perpendicular in short bridge sites along [110]. In tilt models, CO molecules occupy sites mainly on-top of Rh atoms, but tilted in [001] towards the troughs (long bridge). Based on the LEED investigation [94Wei] off-top models are favored for all overlayers except the (2×1)p2mg. The (2×1)p2mg phase is thought to consist of tilted CO molecules in on-top sites or to be due to a zig-zag reconstruction of the substrate [94Wei].

Pd

The adsorption of CO on the Pd(100) surface has been investigated with LEED [69Tra1, 78Bra1, 82Bib, 82Ort, 88Uvd, 91And, 92Ber2]. At half monolayer coverage a (2√2×√2)R45° is formed, followed at 0.67 ML coverage by a (3√2×√2)R45° phase and at 0.75 ML coverage by a (4√2×√2)R45° LEED pattern. The evolution of the LEED features above 0.5 ML coverage has attracted considerable attention, as they evolve in a rapid series of phases, or quasi-continuous [69Tra1, 79Bat]. In this coverage regime also a c(5√2×√2)R45° and a c(7√2×√2)R45° have been reported [82Bib]. This behaviour has been explained by the formation of domain superlattices above 0.5 ML coverage, where antiphase domains of the (2√2×√2)R45° structure, separated by domain walls with a higher density of CO molecules, are formed

leading to a continuous splitting of LEED spots including the (3√2×√2)R45° and (4√2×√2)R45° phases [92Ber2, 96Sch]. CO occupies bridge positions in an upright adsorption geometry in the (2√2×√2)R45° phase [78Bra1, 80Beh, 82Ort] which are also occupied at higher coverages where eventually some tilting occures [88Uvd].

The thermodynamics of adsorption have been investigated by several groups [69Tra1, 78Bra1, 80Beh, 97Yeo1] yielding the isosteric heat of adsorption at 161 kJ/mol from zero up to 0.45 ML coverage, decreasing rapidly to higher coverage, and a pre-exponental factor of $3\times10^{16}s^{-1}$, plus a sticking factor of 0.6 between 0 ML and 0.2 ML coverage, dropping rapidly thereafter indicating a precursor state [80Beh]. The vibrational properties have been investigated with EELS and IRAS [78Bra1, 79Beh, 82Ort, 83Hof1, 85Bro, 88Uvd] where the C-O stretch in all cases can be attributed to bridge bound species. The latter is even supported by IRAS on single crystal electrodes in aquaeous solution [90Yos]. Further studies of CO adsorption on Pd(100) and (111) were carried out by static SIMS [83Bro, 85Bro] where dominant $Pd_x(CO)_y$ ions were correlated with the coverage dependent site specificity of adsorption.

The valence electronic states have been determined by UPS [79Hor2, 80Beh, 94San1] and Auger resonant Raman scattering [94San1, 94San2, 94San3]. The core level binding energies of the C1s and O1s have been determined with XPS, [92Bjö, 94San1, 94San2, 94San3, 95Ped] as well as the adsorbate induced Pd core level shifts [91And].

On the Pd(111) surface CO forms a large number of ordered LEED structures [70Ert, 78Con, 83Hof1, 84Mir, 87Oht, 90Tüs1, 98Gie, 00Zas2]: θ=0.33 coverage (√3×√3)R30°, θ=0.5 c(4×2) or (√3×2) rect, θ=0.514 (√3×35) rect., θ=0.529 c(√3×17) rect., θ=0.545 (√3×11) rect., θ=0.556 c(√3×9) rect., θ=0.571 (√3×7) rect., θ=0.6 c(√3×5) rect., θ=0.63 (4√3×8) rect. and at θ=0.75 (2×2). It can not be excluded that a full sequence of (√3×n)rect. and c(√3×n)rect. (n odd) with coverage θ=0.5(n+1)/n exist [90Tüs1]. The adsorbate structures have also been investigated with STM [00Sau, 02Ros]. The preferred adsorption of CO into 3-fold hollow sites was experimentally found, supported by total energy calculations, whereby STM showed a height difference of 0.1 Å for CO in fcc and hcp hollow sites [00Sau]. A high-resolution two-photon UPS study of CO on Pd(111) illustrated significant changes in the image states of that surface [96Wal].

The thermodynamic properties, in particular as a function of coverage and temperature have been determined [70Ert, 74Con1, 89Guo, 93Sza2, 99Car, 01Sta, 02Bou], in addition to surface diffusion coefficients characterized by an activation barrier of 16.9 kJ/mol and a pre-exponential factor of 2.2×10^{-3} cm^2s^{-1} [97Sna]. Vibrational spectroscopy has established the initial adsorption in hollow sites up to 0.33 ML coverage, giving at intermediate coverages ~0.5 ML way to mixed bridge and hollow adsorption and towards saturation coverage mixed on-top and hollow adsorption [83Hof1, 90Tüs1, 92Kuh1, 93Sza2, 96Rai, 98Bou, 99Car, 00Sur, 02Bou, 02Unt]. The assignment of adsorption sites as a function of coverage via XPS has been reported [00Sur] and the valence electronic structure has been studied with photoemission [76Llo, 84Mir, 95Ban] und inverse photoemission [88Jen]. The adsorption of CO on stepped Pd surfaces was also studied by vibrational spectroscopies and ESDIAD which led to the identification of CO adsorbed at step and localized defect sites [95Ram, 96Sve]. Noteworthy is the rather different behavior on Pd(510) and Ni(510) surfaces: step-adsorbed CO is more weakly bound than CO on (100) terraces for Pd while the opposite is observed for Ni [96Sve]. It seems that CO on Pd(510) is adsorbed at the upper step edges while for Ni(510) it occupies initially sites at the bottom of the step edge.

The coverage and temperature dependent adsorption of CO on the Pd(110) surface has been investigated with LEED [74Con1, 75Lam, 86Gos, 88He, 90Rav2, 91Hu, 93Wan, 94Loc, 96Loc, 97Ram, 99Kat2, 00Yag], EELS [85Che1, 99Kat2 , 99Kat1], IRAS [85Che1, 89Rav, 90Rav1, 90Rav2], TPD [86Gos, 87Gos, 88He, 89Ehs, 99Jon, 00Yag], molecular beam scattering [98Jon, 99Jon, 01Hir], XPS [94Loc, 96Loc, 97Ram, 98Jon, 99Jon], UPS [78Weh], work funktion changes [88He] and field ion microscopy [92Gau1, 92Gau2].

The clean Pd(110) surface shows bulk truncation [85Die]. With increasing CO exposure the following LEED patterns have been observed below 140 K: a weak c(2×4) below 0.25 ML, a sharp (2×1) at around 0.4 ML, coexisting diffuse (3×1) and (2×1)p2mg around 0.6 ML and a sharp (2×1)p2mg pattern above 0.7 ML up to a full monolayer [99Kat2]. Below 0.4 ML CO adsorbs in an upright geometry, whereas nearest-neighbor repulsion tends to tilt the CO molecules alternatingly, [99Kat2] where the tilt angle for

the (2×1)p2mg has been determinded as 24±3° [94Loc, 96Loc] and for the (2×1) as 11±4° [93Wan]. The previously named studies conclude bridge adsorption sites except for one [93Wan]. Adsorption of CO in the coverage range between 0.3 ML and 0.75 ML leads at elevated temperature above 250 K to an adsorbate induced missing row Pd(110)-(1×2) surface reconstruction [90Rav2, 91Hu]. Saturation coverage at 300 K or annealing of the low temperature (2×1)p2mg phase between 330 K and 250 K leads to a (4×2) LEED pattern at 0.75 ML coverage. Annealing to higher temperature leads to a (1×1) pattern [88He, 90Rav2, 91Hu]. Also the adsorbate induced surface core-level shifts have been determined [91Com].

TPD measurements after CO exposure at 130 K report five desorption peaks α_1, α_2, α_3, β_1, β_2 , where the α_3, β_2 peaks at 318 K and 393 K have been associated with the surface structure reconstruction of (2×1)p2mg→(4×2) and (4×2)→(1×1), respectively, at an activation energy of 55.5 kJ/mol for T >393 K, 24.3 kJ/mol for 393 K >T >318 K and 10.1 kJ/mol for 318 K>T [00Yag]. The zero coverage desorption activation energy lies in the range of 126-149 kJ/mol [99Jon, 00Yag, 01Hir], [74Con1]. The overall sticking probability has been described by a Kisliuk model with S_0≈1 [87Gos, 90Rav1, 90Rav2, 00Yag] and a low K parameter [00Yag]. Only one investigation reported a significant lower S_0≈0.5 [98Jon, 99Jon]. Vibrational spectroscopy finds at 135 K the C-O internal stretching mode above 1895 cm^{-1} to blueshift continuously with increasing coverage, whereas the external Pd-CO vibrational modes, i.e. the stretching mode at 363 cm^{-1} change drastically and simultaneously with the LEED patterns, a feature that has been attributed to a switching of the tilting direction of the adsorbed CO molecules during the phase change [99Kat2]. For the (2×1)p2mg structure six vibrational modes have been found [99Kat1, 99Kat2, 02Kat]. It has been pointed out, that the CO stretch frequency at 2003 cm^{-1} makes it difficult to directly assign the bonding site solely from vibrational data [93Wan]. At 300 K the CO coverage dependent adsorbate induced surface reconstruction has been monitored with IRAS [85Che1, 89Rav, 90Rav1, 90Rav2].

Ag

On Ag(111) reversible CO adsorption above 77 K was found by measuring the surface potential changes between 77-123 K and 10^{-1}-10^{-8} torr where the isosteric heat of adsorption varies from 26.7 kJ/mol to 16.7 kJ/mol linear with the surface potential [76McE1]. This was interpreted as weak chemisorption or rather physisorption without long range order (no LEED pattern). Schmeisser et al. find for physisorbed CO on Ag(111) an orientationally ordered phase with two molecules per unit cell and with the CO oriented parallel to the surface, in analogy to the previously reported ordered herringbone structure of N_2 on graphite [85Sch].

The bonding of CO to the Ag(110) surface has been discussed controversially as physisorption [84Kra] or chemisorption [94San2]. Physisorption has been concluded from photoelectron spectra of the core and valence region of CO adsorbed on Ag(110) at low temperature [84Kra]. The valence spectra show that the large bonding shift of the 5σ level observed for CO adsorbed on transition metals as well as the large relaxation shifts are absent for CO/Ag(110). This proves that the CO molecule is physisorbed on Ag(110). Polarisation-dependent spectra indicate that CO is not bound to the surface in an upright geometry but rather with its molecular axis parallel to the surface, or in a random orientation. The C 1s and O 1s core levels exhibit pronounced satellite structure. By comparison with the spectra from the CO/Ni and CO/Cu it is shown that the satellite structure and the differences in extra-atomic relaxation shifts can be well understood by invoking a model in which both core and valence photoelectron spectra are governed by the degree of screening of the photon-induced hole through metal-adsorbate charge transfer.

On the other hand, a chemisorptive bond is concluded from studies of CO adsorption on Cu, Ag and Au using core and valence photoemission, X-ray absorption and autoionization of core excited states [94San2, 94San3]. The purpose was to investigate the nature of the adsorption bond of CO on Ag(110) and Au(110) by starting out from the well-established chemisorption system CO/Cu(100)-c(2×2). The photoemission spectra of CO on Ag(110) and Au(110) showed strong shake-up satellites both for the

valence and core levels. The separation of the satellite closest to the main line is observed to follow the position of the substrate d-band relative to the Fermi level. The CO adsorption strength for the noble metals is deduced to decrease in the order Cu-Au-Ag. This estimate is based on the widths of the XAS resonances, which are related to the adsorbate-substrate interaction strength of the core excited states, and the relative shake-up intensities, which are expected to increase with a decreasing adsorption strength in the ground state [94San2, 94San3]. The same trends regarding the shake-up intensities are observed both for the valence and core levels. Further support for the formation of a chemisorption bond comes from the study of single Ag-CO and Au-CO complexes on a NiAl(110) surface because IETS indicates a hindered frustrated rotational mode at 209.7 cm^{-1} and a C-O stretch of 2145 cm^{-1} for the AgCO complex [03Wal].

EELS measurements have been performed [93Hom] on a physisorbed disordered bilayer of CO on Ag(110) as a function of electron incidence angle and scattering angle as well as primary electron energy. It has been found that in the submonolayer regime the a3π and a1π electronic excitations are quenched because of adsorbate-substrate interactions, whereas strong losses with a clearly resolved vibrational splitting are observed at coverages above a monolayer. The intensities of these excitations behave differently as a function of the experimental geometry which can be explained by the different characters of excitations, i.e. one is optically allowed whereas the other is optically forbidden. Also the electron trajectories play an important role for the ratio of the cross-sections of these two excitations due to electron-image charge interaction and diffraction effects.

Ir

Clean Ir(100) and Ir(110) surfaces show stable surface reconstructions [73Chr, 76Hag, 78Nie, 91Koc, 92Avr] whereas Ir(111) is unreconstructed [78Tay2]. Stable and clean surfaces of both Ir(100)-(1×1) and Ir(100)-(5×1) can be obtained. Adsorption of CO on the Ir(100)-(1×1) surface leads to the formation of a c(2×2) [69Gra, 91Kis] and, depending on the speed of dosing, an unstable (1×1) LEED pattern [91Kis]. On the Ir(100)-(5×1) surface the exposure to CO has led to the formation of a (2×2) LEED pattern [69Gra] which has not been verified in later investigations, reporting (1×1) LEED patterns [76Bro, 91Kis]. It was further found, that there is no difference in reactivity towards CO between the Ir(100)-(1×1) and Ir(100)-(5×1) surfaces [76Rho].

To elucidate the subtle differences for the adsorption of CO on both the (1×1) and the (5×1) reconstructed Ir(100) surface at room temperature, EELS and LEED experiments have been conducted [91Kis]. CO is adsorbed on both surfaces at all coverages in on-top sites. All four vibrational modes of the adsorbate have been detected. Adsorption of CO on the (5×1) surface lifts the reconstruction locally giving rise to a (1×1) LEED pattern. The vibrational frequencies of the CO-molecules on both surfaces differ only slightly. At saturation the iridium-CO and the C-O stretching frequencies are 485 and 2075 cm^{-1} on the (5×1) and 497 and 2068 cm^{-1} on the (1×1) surface, respectively. The frequency of the rotational mode of the CO molecule is found to be at 425 cm^{-1} and the frustrated translation at 53 cm^{-1}, both showing no dispersion along the ΓM direction. The C-O stretching vibration shows dispersion due to dipole-dipole interaction, even when the overlayer is not ordered. An IRAS and LEED investigation [93Mar] of CO adsorbed on the reconstructed (5×1) and unreconstructed (1×1) surfaces of Ir(100) at 300 K report a single C-O stretch initially at 2026 cm^{-1} on the (1×1) surface and a more complex adsorption behavior on the (5×1) surface. For the latter at least five distinct C-O stretching bands have been observed sequentially between 2025 cm^{-1} and 2097 cm^{-1} as a function of exposure. In contrast to previous studies, LEED results suggest that the (5×1) reconstruction is not fully lifted, even after exposure to relatively high CO pressures [93Mar].

The adsorption of CO on the Ir(111) surface with three-fold rotational symmetry leads to the typical (√3×√3)R30° [69Edm, 71Gra, 73Wei, 74Doy, 76Com1, 76Com2, 76Hag, 76Küp, 77Iva, 78Com, 81Sea, 89Mar, 96Lau] and (2√3×2√3)R30° [76Com1, 76Com2, 76Hag, 76Küp, 77Iva, 78Com, 81Sea, 89Mar, 96Lau] superstructures with 1/3 and 7/12 coverage, respectively. Analogous to Ru(100), the question has been raised whether the CO binding state at coverages exceeding 1/3 for the (√3×√3)R30° superstructure differs from the low coverage adsorbed CO [74Mad] or are merely governed by the repulsive adsorbate-

adsorbate interaction, increasing with the continuing compression of the original (√3×√3)R30° layer to a (2√3×2√3)R30° layer [76Com2]. In earlier LEED investigations highly coordinated bridge and hollow adsorption sites were favored [74Doy, 76Com1, 76Com2, 76Hag, 76Küp, 77Iva, 78Com]. However, more recent investigations based on EELS and IRAS have clearly established bonding in on-top sites for the (√3×√3)R30° and for the (2√3×2√3)R30° structures. Similar to the geometrically equivalent Ru(001) surface [80Pfn], all the CO molecules feel a similar substrate potential, leading to the (2√3×2√3)R30° structure with equivalent terminal adsorption sites.

TPD indicates the existence of three sequentially populated CO bonding states [96Lau]. The first peak at ~550 K fills in until the maximum intensity of the (√3×√3)R30° LEED pattern is observed. At this point a second state, desorbing at lower temperatures appears leading to the (2√3×2√3)R30° structure. At even higher coverage a third low temperature shoulder appears around 300 K, indicating that some mobility of the CO molecules is required for its formation [97Sus1]. The adsorption and desorption kinetics of CO on Ir(111) has been extensively studied [76Com1, 76Com2, 76Küp, 76Zhd, 78Tay2, 78Zhd]. [96Lau, 97Sus1, 97Sus2]. The vibrational properties have been investigated as a function of coverage with EELS [89Mar] where with increasing CO coverage an Ir-CO frequency between 475 and 490 cm^{-1} and a C-O stretch between 2025 and 2050 cm^{-1} has been found. Using Fourier transform IRAS, TPD and LEED at sample temperatures between 90 and 350 K, only a single absorption band, between 2030-2090 cm^{-1} has been observed with increasing CO coverage up to 0.7 ML [96Lau]. The coverage-dependent frequency shift of the IR band can be described quantitatively using an improved dipole coupling model. The contribution of the dipole shift and the chemical shift to the total frequency shift were separated using isotopic mixtures of CO. The chemical shift is positive with a constant value of approximately 12 cm^{-1} for all coverages, whereas the dipole shift increases with coverage up to a value of 36 cm^{-1} at a coverage of 0.5 ML [96Lau].

The Ir(110) surface shows a clean surface reconstruction, which has been initially interpreted as a missing row (1×2) surface reconstruction but subsequent investigations STM [91Koc], ion-scattering [92Avr] and LEED [95Lyo] have determined a grooved, microfaceted (331) reonstruction, consisting of (111) terraces two atoms wide, which has a LEED pattern similar to a (1×2) missing row surface reconstruction [91Koc]. Early work on CO adsorption led to the observation of a (2×2) structure [73Chr, 78Nie, 78Tay1, 78Tay2, 78Tay3]. This is to be understood as relative to the (1×1) structure of the unreconstructed surface, equivalent to a (2×1) with respect to the (1×2) reconstructed surface. In addition a (4×2) structure was found [78Tay1, 78Tay2, 78Tay3]. In the early literature a (2×1)p1g1 was proposed, which turned out to be due to coadsorbed oxygen [78Tay1, 78Tay2, 78Tay3]. Also the observation of c(2×2) surface structures appears to be due to dissociation of CO and the subsequent CO adsorption onto carbon and oxygen contaminated Ir(110) surfaces [78Nie].

A combined LEED, IRAS and TPD study at 300 K [95Lyo] has come to the conclusion, that CO adsorbs on the reconstructed Ir(110) surface in on-top sites at all coverages, presumably oriented near the (110) surface normal. IRAS shows a single band for the C-O stretch that shifts from a low-coverage value of 2001 cm^{-1} to a saturation-coverage limit of 2086 cm^{-1}. This frequency shift was separated into two contributions by using isotopic substitution, one being due to dipole-dipole interactions and a smaller one due to chemical effects (d-electron competition). TPD spectra yield in agreement with previous work three adsorption states at 380 K, 490 K and 610 K [73Chr, 78Tay1, 78Tay2, 78Tay3, 94Kan, 94Men]. To reconcile the three adsorption states observed in TPD with the single C-O stretch frequency, continuously changing with coverage from a low-coverage value of 2001 cm^{-1} to a saturation-coverage limit of 2086 cm^{-1}, indicative of a single adsorption site, a model of discontinuous binding energy decrease as a function of CO-CO next neighbor coordination has been proposed. Starting from the clean surface, the first state consists of CO molecules of approximately the same binding energy in an ordered structure with short range or poor long range order up to a coverage of 0.33. Increasing the coverage further leads to the filling of the second TPD state up to a coverage of 0.8, where the CO molecules are having up to two direct CO neighbours causing a IRAS dipole shift. At 0.8 coverage also some ordering was observed. The ordered structures at 0.33 and 0.8 coverage seem to correspond to the previously observed (2×2) amd (4×2) structures [78Tay1, 78Tay2, 78Tay3]. Towards even higher coverage, up to maximum coverage 1 ML, the number of next neighbours increases even more [94Kan, 94Men].

For the (2×2) structure a desorption energy of 154.9 kJ/mol [73Chr] was found. Coverage dependent measurements yielded $(146.5 - 67 \times \theta)$ kJ/mol [78Tay1, 78Tay2, 78Tay3], with a pre exponential factor falling from 3×10^{12} s^{-1} to 1×10^{9} s^{-1} at saturation coverage. Initial sticking coefficients of 0.8 [87Ste], 0.9 [78Tay1] and 1.0 [78Nie] have been reported which are initially independent of coverage but decreasing to small values at high coverages. A detailed investigation of the sticking coefficient and the formation of an extrinsic precursor state (weakly bound state above occupied sites) has been performed using a supersonic molecular beam [87Ste]. The sticking coefficient drops with increasing molecular beam energy (0.8 at 8.4 kJ/mol to 0.35 at 142.3 kJ/mol beam energy) because inelastic scattering occurs with increasing beam energy, in contrast to a trapping/desorption scattering into an extrinsic precursor state at low beam enegies [87Ste]. These findings were later reproduced [97Bur].

Pt

The clean Pt(100) surface exhibits a (5×20) reconstruction at room temperature, with the outermost layer showing a quasi-hexagonal arrangement, normally referred to as the hex-phase [79Hei1, 86Beh, 92Guo]. Depending on the annealing temperature, the hexagonal layer undergoes for above 1070 K a rotation of 0.7° denoted as hex-R phase [78Bon, 95Mar]. Next to the stable reconstructed surfaces, there exists also a metastable (1×1) bulk terminated surface [78Bon, 78Bro] which transforms above 400 K [81Dav, 81Nor] through an intermediate (1×5) structure [82Hei] to the stable hex-phase. A conversion of the hex-phases to the metastable (1×1) surface can be carried out by adsorption, lifting the hex reconstruction and subsequent removal of the adsorbate by a low temperature catalytic reaction [75Bon2, 78Bon, 81Bar2]. The surface free energy difference between the clean hex and (1×1) phases has been derived as 20 kJ/(mol Pt_s) [95Yeo]. It has been suggested that the adsorbate induced hex to (1×1) transition plays an important role for oscillatory reactions on Pt(100) [86Imb, 88Sch, 93Imb].

The calorimetric heat of CO adsorption on Pt(100), measured by a supersonic molecular beam in normal incidence, has been determined as a function of coverage at 300 K [96Yeo]. On the (1×1) surface, the differential heat is 225 kJ/mol near zero coverage, stays constant at 215 kJ/mol between 0.1 and 0.25 ML, then decreases to a second plateau at 179 kJ/mol between 0.25 and 0.5 ML coverage, finally decreasing abruptly to a value of 85 kJ/mol. The sticking coefficient on the (1×1) surface decreases linearly between 0 and 0.5 ML coverage from S=0.6 to S=0.26, then falling to a steady state value S=0.04. Earlier results quoted a constant sticking coefficient of 0.6 [78Bro] and 0.75 [83Beh] below 0.4 ML coverage followed by a rapid decrease in the range up to 0.5 ML. On the hex surface, the differential heat is initially 180 kJ/mol and decreases to a plateau at 170 kJ/mol between 0.15 and 0.5 ML coverage. Towards higher coverage an abrupt decrease to the steady state value of the (1×1) surface is observed [96Yeo]. The sticking coefficient on the hex surface is S=0.73 at low coverage, decreasing almost linearly [83Beh, 93Hop, 96Yeo] to S=0.26 at coverage 0.5 ML, then approaching the steady state value S=0.04. For coverage larger than 0.5 ML, the sticking coefficient is the same for the hex and (1×1) surfaces [96Yeo]. Some earlier measurements [77McC, 83Beh] show the same trend, whereas others show an almost constant value up to 0.3 ML coverage and a subsequent decrease [80Cros].

The mechanism of the CO induced hex to (1×1) phase transition has been proposed to involve a lifting of the hex reconstruction by the initial adsorption, followed by migration and trapping of CO into (1×1)-CO islands with a local coverage of 0.5 ML, starting at a critical coverage of 0.05 ML [82Thi, 83Beh, 83Thi] or 0.08 (± 0.05) ML at 300 K [83Jac2]. The resulting island formation has been investigated by various methods, especially STM [83Beh, 87Rit, 94Bor]. With increasing coverage, the area of the surface covered by the (1×1) islands increases but the islands themselves remain constant in size [94Bor].

On the (1×1) surface, combined IRAS and LEED investigations have reported at both 90 and 300 K a single linear band of an on-top species, shifting from 2065 to 2090 cm^{-1} with increasing coverage, and at least three different bands in the bridge region at frequencies between 1867 and 1910 cm^{-1}, depending on coverage [95Mar]. The ratio of bridge to on-top varies with coverage and temperature. On the hex surface and at low exposure the CO stretch is observed at 2083 cm^{-1} and assigned to an on-top adsorption site on this surface [91Gar, 95Mar]. At a coverage exceeding 0.13 ML the hex surface reconstruction appears to

start by converting into the (1×1) structure, indicated by the observation of an on-top band at 2089 cm^{-1} and a band at 1873 cm^{-1} due to a bridge species [95Mar]. However, the assignment of the feature at 2083 cm^{-1} as an on-top species on the hex-reconstructed Pt(100) surface at 0.13 ML coverage is challenged by the observation that the hex to (1×1) conversion starts at 0.01 to 0.03 ML at 400 K and independent of temperature above 200 K [93Hop]. Then, at low coverages, the small frequency shifts on the hex and (1×1) surface are likely to be due to a small change in the local coverage within the (1×1) islands [95Yeo]. These investigations clarify in particular for the c(2×2) overlayer at 0.5 ML coverage the previously controversial discussion of bonding sites, bridge [82Bib] or on-top [83Beh, 84Ban]. The adsorption of CO to the Pt(100) surface has also been studied with UPS [82Bro].

The adsorption of CO on Pt(111) leads to a series of ordered superstructures identified by LEED [77Ert, 82Ste, 87Ogl, 87Tüs, 88Bla, 90Ryb, 91Won, 94Vil, 98Jen, 98Ma, 00Zas1]. Up to 0.33 ML, a (√3×√3)R30° superstructure is formed with CO occupying on-top sites. At 0.5 ML, CO forms a c(4×2) structure containing 0.25 ML on-top and 0.25 ML bridge-bonded CO. At higher CO coverages, the c(4×2) structure is compressed along the $[1\bar{1}0]$ direction, leading to the observation of a (√3/2×√3/2)R15° at 0.58 ML [82Ste] and a 2/3(√3×3)rect at 0.67 ML [98Ma]. Additional phases have been reported, such as (4×4) at 0.18 - 0.19 ML [90Ryb] and (8×8) at 0.3 ML [87Tüs, 90Ryb]. The use of high pressure STM has led to the observation of ordered structures of CO at pressures of 200 Torr and above [94Vil, 98Jen].

The adsorption and desorption energies have been studied in great detail. A very sensitive measurement of CO adsorption at low coverage was developed on the basis of thermal energy He atom scattering [82Poe1, 82Poe3, 82Poe4, 84Poe, 87Ver]. The high scattering cross section of 125 $Å^2$ of adsorbed CO, measured for He atoms of 63 meV energy at 40° incidence, is responsible for this sensitivity [82Poe1, 82Poe2, 83Poe2, 84Poe, 88Yin]. The coverage dependent desorption energy of CO has been found to decrease from 134 kJ/mol to 105 - 84 kJ/mol between zero and 0.5 ML, then a further decrease to around 41 kJ/mol at 0.67 ML coverage [77Ert, 84Poe, 86See]. Calorimetric measurements [97Yeo2] find a similar trend, but higher values, where the heat of adsorption at 300 K is initially 183±8 kJ/mol, declining to 118±19 kJ/mol at 0.5 ML coverage. At higher coverage up to 0.75 ML a constant value of 65±3 kJ/mol is found. CO adsorption on vicinal Pt(111) surfaces is characterized by higher binding energy sites, such as step and kink sites [82Poe4]. The coverage dependent sticking probability of CO on Pt(111) shows a precursor mediated behavior [82Poe] which is up to 0.5 ML described by the Kisliuk expression [77Kis] with $K = 0.55$ and an initial sticking coefficient of 0.8 [97Yeo2]. Above 0.5 ML, the sticking probability falls to the steady state value ~0.05. Similar low temperature adsorption kinetics have been found [93Cud]. This general trend is reported in a large number of studies [74Lam1, 76Chr, 77Col, 77Ert, 77McC, 79Hor1, 79Nor, 81Cam2, 81Lin, 82Ste, 86See, 93Cud, 96Zae, 97Yeo2]. Since CO adsorption on step edges with an adsorption energy of 146 kJ/mol and a pre-exponential factor of 1.25×10^{15} s^{-1} plays an important role [81Cam2], there is quite a variation of the numerical values of the adsorption energy in the literature due to non-flat (111) surfaces.

The diffusion parameters of CO on Pt(111) have been investigated in great detail by various methods [67Lew, 82Poe2, 88Reu, 92 Kwa, 94Fro, 98Ma] and depend significantly on the presence of step edges. Using flat and stepped Pt(111) surfaces and a linear optical diffraction method [98Ma] CO diffusion on Pt(111) between 133 and 313 K and 0.1 to 0.67 ML coverage has been found to follow an Arrhenius law with a diffusion activation energy of 12.5 - 19.7 kJ/mol and 30.6 - 33.0 kJ/mol for flat and stepped surfaces, respectively [98Ma]. The desorption process has also been investigated with REMPI [97Sch2] and ESD [93Sza1, 95Sza].

The vibrational spectra of CO on Pt(111) have indicated bridge and on-top bound species. In particular the c(4×2) phase at 0.5 ML coverage, with half the molecules in on-top and bridge sites, has been studied extensively [77Iba, 79Hop, 82Ste, 86Lah, 89Mal, 89Per, 90Per, 90Ryb, 96Klü, 97Eng, 99Eng]. The CO stretch mode for on-top and bridge adsorbed CO is established at 2081 - 2104 and 1850 - 1855 cm^{-1}, respectively, and the CO metal stretch for on-top and bridge at 468 - 480 and 363 - 380 cm^{-1}, respectively. Also the low energy vibrational modes have been determined by He scattering [86Lah, 98Gra1, 03Gra] and EELS [82Ste]. The vibrational dynamics have been studied as well [86Lah, 89Mal, 89Per, 90Bec, 91Bec, 97Eng]. For low coverage only on-top occupation has been found, whereas at

higher coverage the ratio of bridge to on-top varies [82Ste, 88Ols, 89Mal]. As a function of coverage, the evolution of the core level binding energies [95Bar] and resonant core level excitation and decay [89Mur, 92Wur, 94Bjö] have been studied. Integrated O1s and C1s intensities yield relative coverages (which may be calibrated) while binding energy shifts indicate relative site occupancies, such as seen in Fig. 15 [94Bjö]. The use of SFG has allowed to study CO adsorption up to 700 Torr pressure. Here the on-top and bridge modes gradually disappear and a broad band at 2045 cm^{-1} prevails [96Su]. Vibrational spectra of CO adsorbed on stepped Pt surfaces show stretch frequencies in the range 2065 - 2081 cm^{-1} which are associated with CO bonded to step sites [85Gre, 85Hay1].

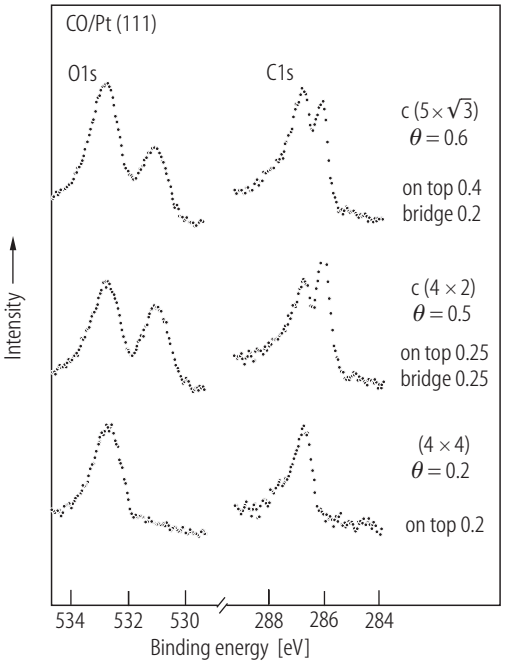

Fig. 15. C1s and O1s core level spectra of three ordered CO layers on Pt(111) at coverages of 0.2, 0.5 and 0.6 ML. Note changes in ratio of on-top to bridge adsorbed CO. Data were obtained with monochromatized Al K_α radiation at 1487 eV [94Bjö].

The clean Pt(110) surface exhibits a (1×2) reconstruction [72Bon2] where every alternate atomic row in the [100] direction is missing [82Jac1, 88Fer]. The exposure to CO at temperatures above 250 K lifts the reconstruction, and a (1×1) LEED pattern of a surface with residual disorder is observed for coverages above 0.5 [76Com3, 82Fer, 82Hof1, 82Jac1]. Annealing of the Pt(110) surface at 500 K and exposure to CO leads to an ordered (2×1) superstructure with coverage 1 on an unreconstructed substrate [76Com3]. Models with (2×1)p1g1 [74Lam2, 76Com3, 81Bar1, 82Bar, 82Hof1, 82Hof2, 84Bar, 87Wes] and (2×1)p2mg [84Rie, 92Win, 01Now] symmetry have been proposed. Angle-resolved XPD results seem to provide solid evidence for the (2×1)p2mg-CO structure [01Now]. The CO-induced conversion of the Pt(110) reconstruction to a non-reconstructed surface proceeds via defect formation [89Gri]. The reason is most likely the high adsorption energy of CO on Pt adatoms compared to regular surface sites, illustrated in Fig. 16 [01Tho]. The lower the coordination of a Pt atom, the higher the adsorption energy. The energy scales also with the center of the local d-band which is related to band narrowing [01Tho]. Below 250 K a metastable c(8×4) phase has been observed [82Fer, 82Jac2, 86Fre1, 01Now] where during adsorption the equivalent of an entire monolayer of Pt atoms is displaced [82Jac1]. Here CO effectively adsorbs well ordered on a (1×2) reconstructed Pt(110) surface [82Fer]. A structure model was proposed for this layer [01Now]. The clean non-reconstructed Pt(110) surface was also prepared [82Fer]. The structural transformation has been studied with STM [89Gri], RHEED [95Sch] and surface core level shifts [87Düc].

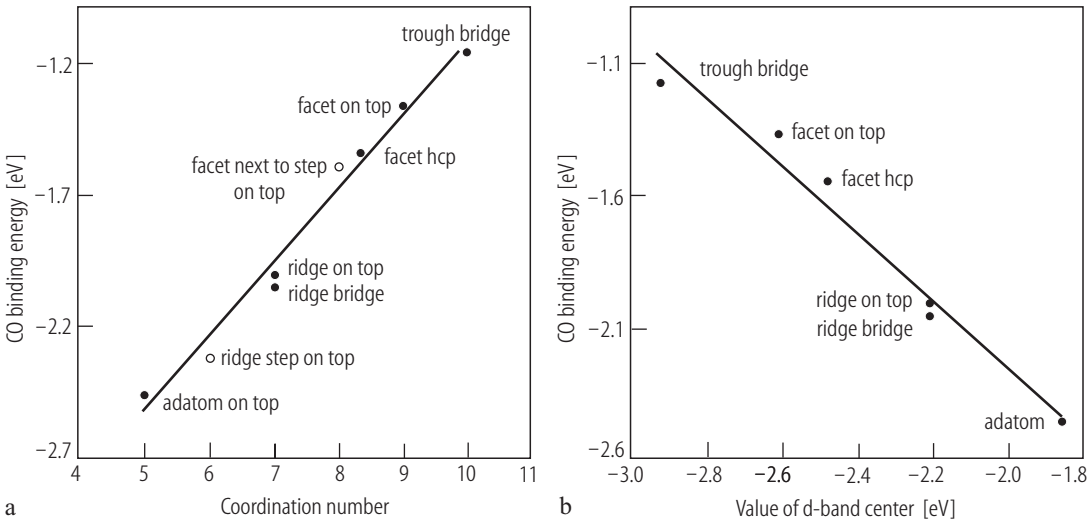

Fig. 16. Chemisorption energy of CO on different sites of a Pt(110) surface versus (a) local coordination of the bonding Pt, (b) the value of the d-band center [01Tho].

On the Pt(110)-(1×2) surface at 300 K, using the temperature modulation technique, the activation energy of CO desorption has been determined in the zero coverage limit to 150.7 ± 6 kJ/mol at a pre-exponential factor of 3×10^{14} s^{-1}, decreasing linearly up to a coverage of 0.15 ML to 134.0 ± 6 kJ/mol at a pre-exponential factor of 3×10^{14} s^{-1} [88Eng]. Below 0.5 ML coverage a constant sticking coefficient 0.8 has been observed, indicating adsorption via a precursor state [76Com3, 82Hof1]. Towards higher coverage a molecular beam study reports at 0.1 ML and 0.6 ML coverage 148 and 140 ± 15 kJ/mol [80Fai]. Isosteric heats of adsorption have been reported up to saturation coverage [76Com3, 77McC, 80Fai, 82Hof1, 82Jac1].

Vibrational spectroscopy (IRAS, EELS) has shown, that adsorption of CO on Pt(110) at 300 K is exclusively in on-top sites at all coverages [82Hof1, 84Bar, 87Hay, 96Klü, 98Sha2]. The C-O stretch frequency shift with coverage of 50 cm^{-1} has been found to be due to dipole coupling. Bridge bonded species, which do not occur at 300 K, have been reported after partial desorption [84Hof, 86Fre1] and for adsorption at lower temperatures [83Hof2, 86Fre1, 01Now] but an IRAS investigation between 90 and 300 K could not observe any bridge species at any coverage [98Sha1, 98Sha2]. No C-O frequency change has been observed when the (1×2) reconstructed surface phase converts to the (1×1) surface. At 90 K, the observed saturation coverage on the frozen (1×2) surface is the same [98Sha2] or about 10 % higher [01Now] than at 300 K. In the latter case nearly 20 % bridge adsorbed CO is detected by a binding energy shift of the O1s XPS core level. Hence on-top and bridge sites on second layer Pt atoms must also be occupied. Heating the saturated adlayer formed at 90 K to 140 - 160 K leads to a marked intensity increase in the CO band which is assigned to the creation of the c(8×4) surface phase [98Sha2]. Further heating above 250 K completely converts the Pt surface to a disordered (1×1) phase with adsorbed CO. The driving force for the restructuring process has been attributed to a small increase in the heat of adsorption for CO, located in on-top sites on Pt atoms along the (1×2) ridges compared with CO in on-top sites on Pt atoms in the (1×2) troughs [98Sha2]. The situation is different again below 30 K, where the clean surface reconstruction is not lifted and hence CO adsorption on the missing row reconstructed Pt(110)-(1×2) has been observed [98Sha1]. Here, two C-O stretch bands are observed. Warming to 40 K starts surface diffusion, leading to chain condensation, limited towards higher temperature at 60 K by further thermodynamic transition. A complex structure model for the c(8×4)-CO has been proposed [01Now]. Further studies of adsorption of CO on the Pt(110)-(1×2) surface have been carried out with UPS [77Shi1, 81Bar1, 82Bar, 82Hof2, 89Düc], IPE [91Ber] and XPS [86Fre1, 87Düc, 01Now].

Au

For the adsorption of CO on Au surfaces, the formation of a chemisorptive bond has been difficult to establish experimentally. Whereas for the Au(111) and Au(100) surface only physisorption occures, the most reactive Au(110) surface shows indications of weak chemisorption. Based on the similarity between UPS data on CO/Cu(100) and CO/Au(110), the formation of a chemisorptive bond on the Au(110) surface is derived in analogy to the weak chemisorption on the Cu(100) surface [89Düc]. The chemisorption of CO on Au(110) is further supported by the analysis of XPS shake-up intensities, XAS line shapes and the comparison of autoionization spectra for the weak CO chemisorption on Cu(100), Ag(110) and Au(110) [94San2, 94San3]. In He scattering studies of the CO/Au(111) system the angular dependence of the cross sections has been found to be very sensitive to the adatom potential. It was found that a hard bump representation of the adatom is inadequate for the differential scattering [85Ell]. Reflection-absorption infrared spectra of CO adsorbed on Au(332) show a single band which first appears above 2120 cm^{-1} [97Rug] and shifts to lower wavenumber with increasing coverage. The band is broad and consists of at least three poorly resolved components. The study of single Au-CO complexes on a NiAl(110) surface is of interest in this context because IETS indicates a hindered frustrated rotational mode at 282 cm^{-1} [03Wal].

3.7.1.3 CO adsorption on bcc metal surfaces

Cr

The study of CO adsorption on Cr(110) by a number of different techniques, e.g. LEED, EELS, UPS, XPS, ESDIAD and Auger electron spectroscopy, has shown this metal surface to be highly reactive towards CO adsorption and dissociation [84Shi, 85Shi2, 85Shi3, 86Meh, 86Shi]. Vibrational spectra provided clear evidence for the sequential adsorption of CO into two different molecular states at 120 K. The first, called α_1-state, is characterized by very low C-O stretch frequencies at 1150 and 1330 cm^{-1} and a complete lack of ion emission in ESDIAD. This α_1-state was atributed to a π-bonded CO molecule oriented nearly parallel to the Cr(110) surface. An ordered c(4×2) structure was formed at 120 K and a coverage of about 0.25. The second CO species, called α_2-state, observed at higher coverage and at the same temperature was characterized by three vibrational frequencies at 495, 1865 and 1975 cm^{-1}. ESDIAD showed O^+ ion emission in nearly perpendicular direction. Hence this state was identified as CO bonded through the carbon atom in atop and bridge sites, respectively, both oriented perpendicular to the surface. The α_1-state was also identified as a precursor to CO dissociation [85Shi2]. Pre-adsorbed oxygen inhibits the formation of the α_1-state CO but not the α_2-state CO. Even the c(4×2)-CO layer is disordered and converted to α_2-state CO by adding adsorbed oxygen [85Shi3]. Cr(110) exposed to CO at 300 K leads to only dissociated C and O. Overall there must be a low barrier for the dissociation of adsorbed CO on Cr. A related theoretical molecular orbital study of adsorbed CO on Cr(110) shows that a high coordinate lying down configuration is favored at low coverage [86Meh]. This is mainly due to a destabilization and emptying of the antibonding counterparts to σ and π donation bonds. Backbonding to the CO $2\pi^*$ orbital is enhanced which stabilizes a nearly horizontal orientation of CO.

Of interest is also the effect of Cr thin films deposited on the Ru(001) surface on CO adsorption [02Eng]. Adsorption and dissociation of CO is considerably enhanced compared to clean Ru(001).

Fe

The combined use of TDS and vibrational spectroscopy (EELS) has been demonstrated to great advantage in the study of CO/Fe(100) [87Moo1, 87Moo2]. Figure 17 illustrates the procedure and some of the results. A TDS trace on the right shows the different desorption states due to molecular and dissociated CO, α- and β-states, respectively. Heating a saturated CO layer from 120 K to temperatures,

where one or several states have desorbed, and taking EELS spectra of the residual layer, yields information on the various states still adsorbed on the surface. It is clear from the data in Fig. 17 that α_1 and α_2 are molecular CO states, because of the C-O stretch frequencies at 2020 and 2070 cm^{-1}, respectively. The most interesting case is the α_3 species, characterized by a very low frequency of 1210 cm^{-1} which is attributed to a tilted CO molecule. This particular α_3 CO partly desorbs and partly dissociates in the temperature range 343-483 K leaving C and O on the surface which give rise to the β desorption peak at 830 K. The tilt angle of the adsorbed α_3 CO has been studied by three different techniques, NEXAFS [87Moo3], XPD [89Sai] and CDAD [94Wes]. It was found to be about 55° relative to normal [89Sai]. The most recent result of the angular dependence of the circular dichroism of the CO 4σ orbital is displayed in Fig. 18 and compared to calculated angular dependencies assuming a range of tilt angles. From the comparison of experiment and theory a tilt angle of 40°±10° is concluded [94Wes].
The conversion of adsorbed CO among different adsorption states on an Fe(100) surface was investigated through the coadsorption of labelled $^{13}C^{16}O$ and unlabelled $^{12}C^{16}O$ [88Lu]. In these experiments selected adsorption states were initially populated by one type of CO and the surface was then exposed to the other type. While no conversion occurred between the β-CO states and the α-states, or between α_2 and α_1 states, significant conversion was observed between the α_2 and the (tilted) α_3 states. A relative energy profile of the adsorption state conversions was proposed, based on these observations [88Lu].

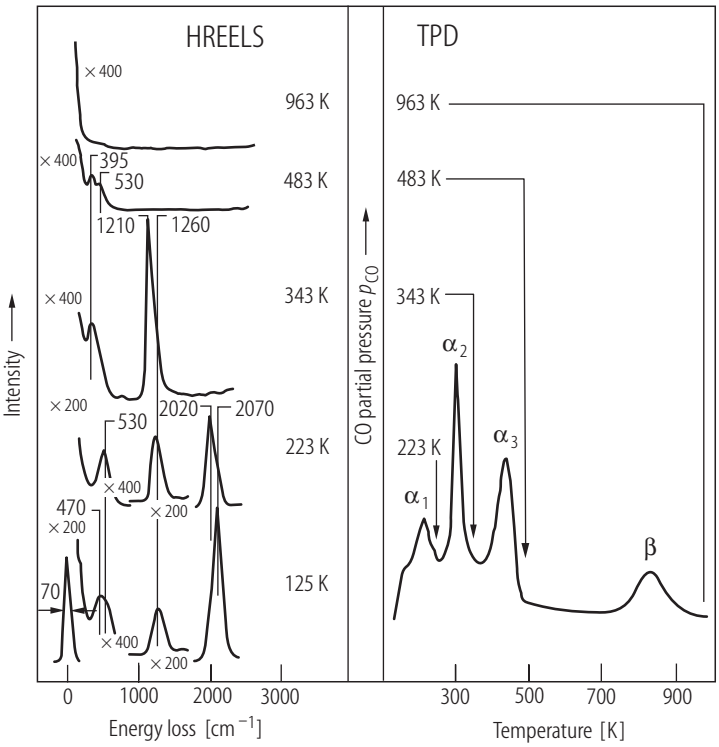

Fig. 17. CO on Fe(100), correlation between vibrational spectra (left) and thermal desorption data (right) for conditions where several α and β-states have been separated [87Moo2].

Thermal energy atom scattering (TEAS) has been used to study CO adsorption on Fe(111) [92Ber1]. The He specular intensity drops rapidly and smoothly with CO exposure on the Fe(111) surface. In contrast to CO/Pt(111) [83Poe1] the diffuse scattering of He from CO on Fe(111) is not a negligible fraction of the intensity. The surface exhibits a finite reflectivity even at high CO coverages. An effective scattering cross section for molecular adsorbed CO of 56 $Å^2$ was derived from a fit of the reflectivity data to a model taking this diffuse scattering into account. The He atom scattering cross section of dissociated C,O was determined to be 93 $Å^2$ [92Ber1].

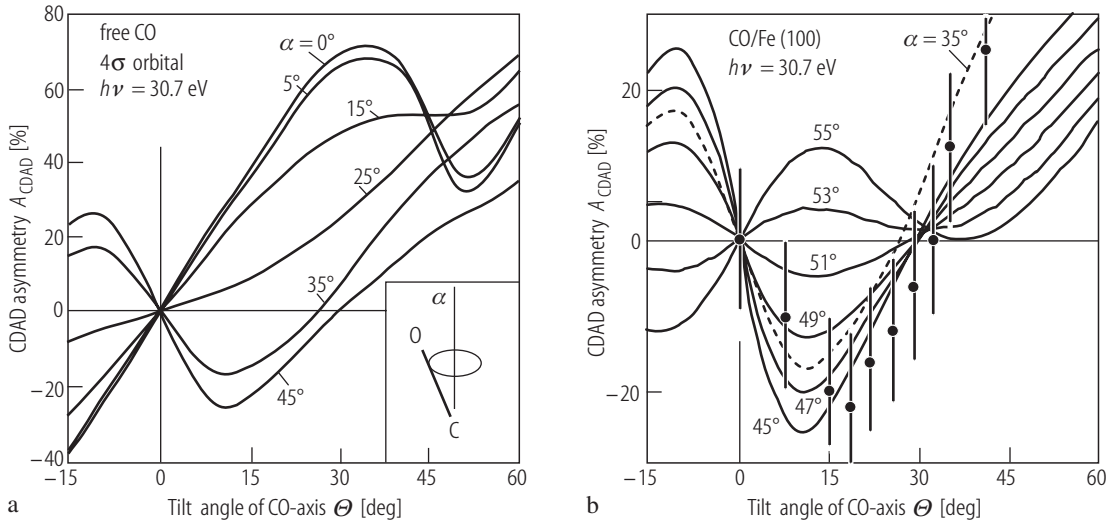

Fig. 18. Measured CDAD asymmetry of CO 4σ orbital and calculated values for several tilt angles Θ of the CO axis relative to the surface. (a) free CO molecule at $h\nu$ = 30.7 eV. (b) For CO adsorbed on Fe(100) [94Wes].

Nb

An early study of CO adsorption on a Nb field emitter (FEM) tip showed evidence of desorption of CO at 150 K [64Kle]. Changes in the FEM emission pattern at about 600 K were interpreted to indicate CO dissociation. No direct evidence of adsorbed molecular or dissociated CO on Nb surfaces has been presented. In general, the behavior of CO on Nb is thought to be similar to CO on Ta, Mo and W surfaces [70For]. Although clean surfaces of Nb(110) crystals have been prepared [66Haa], no studies of CO adsorption on (110) oriented single crystals of Nb are known. The sticking probability of CO on Nb(111) at 300 K was determined as 0.06 and a maximum work function change of 0.25 eV has been reported [64Oma].

Mo

We briefly discuss the adsorption of CO on Mo(110). Molecular and dissociative adsorption of CO occur [81Kel]. The rate of dissociative CO adsorption was analyzed in detail for clean and pre-covered Mo(110) surfaces by utilizing XPS and UPS as an indicator of molecular and dissociated CO [81Sem, 86Eri]. The thermally induced conversion of adsorbed CO to carbon and oxygen was measured at several coverages and temperatures. The rate of CO dissociation in the adsorbed state is described by an Arrhenius expression, according to $r_{dis}(T) = A\exp(-E_{dis}/kT)$, with E_{dis} as the activation energy of dissociation and A as the pre-exponential factor. Isothermal as well as thermal conversion spectra (applying a linear temperature ramp) were used to extract A and E_{dis} separately [86Eri]. Results were obtained for clean Mo(110) and surfaces modified with coadsorbed S, C, O and K. The results are listed in Table 3. Pre-exponential factors and activation energies show a pronounced compensation effect, as seen in Fig. 19, which means that high activation energies are associated with high pre-exponential factors, and vice versa.

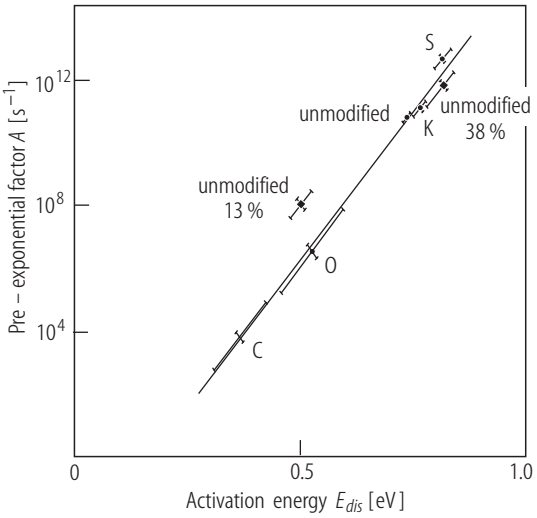

Fig. 19. Plot of pre-exponential factor versus activation energy for CO dissociation on modified Mo(110) surfaces. The rate parameters for all surfaces fall on a single line in this plot of log(A) versus E_{dis}. At 300 K dissociation rates are nearly the same, however, for all surfaces. [86Eri].

Vibrational spectra (IRAS) of CO adsorbed on Mo(110) at 95 K are shown in Fig. 20 [91He1]. At low exposure (2 L = 2.6 mbar·s of CO) no evidence of a C-O stretching frequency is seen in the range of 1800-2100 cm^{-1}. Three separate peaks at 1885 - 2010 cm^{-1} are observed at higher CO exposures, with the one near 2040 cm^{-1} rising to high intensity at 13 mbar·s. Although CO sticking is expected to be high at this low temperature, no evidence of molecular CO is seen at low coverage by IRAS. A plot of the total amount of carbon, measured by Auger electron spectroscopy, versus CO exposure confirms the presence of CO at low exposures but the integrated IRAS intensity of all CO peaks in Fig. 21 versus CO exposure reveals a range of zero intensity up to 3 L = 4 mbar·s. The solution to this apparent problem is given by Fig. 22 which shows vibrational spectra (EELS) of CO/Mo(110) at 120 K over a larger range of frequencies [91Che]. At low to intermediate coverages a C-O stretch frequency at 1345 cm^{-1} is detected and interpreted as a molecular tilted CO species whose intramolecular bond is weakened due to its adsorption geometry. This species is easily dissociated at higher temperature via an intermediate species characterized by an even lower frequency at 1130 cm^{-1} [91Che]. He et al. could not see the low-frequency CO species by IRAS but they produced indirect evidence for its presence by a titration experiment with vapor deposited Cu [91He1]. A small amount of Cu was added (about 0.9 ML) to a low coverage of CO adsorbed at 95 K. A peak at 2101 cm^{-1} was then detected. Heating this surface to 145 - 225 K and recording IRAS spectra showed this peak to be stable. The peak was attributed to CO that had migrated from Mo surface sites to Cu sites where it assumes an upright configuration. The disappearance of the tilted CO species with high CO coverage [91Che], Fig. 22, is most likely due to crowding on the surface, leaving no room for a tilted molecule.

The orientation and bonding of adsorbed CO on Mo(100) was studied by EELS, angle-resolved UPS and near-edge X-ray absorption fine structure (NEXAFS) [87Ful]. Two different CO species can be clearly distinguished by their C-O stretch frequencies measured by EELS. At low coverage CO exhibits a very low stretching frequency of about 1200 cm^{-1} [85Zae]. Both NEXAFS and ARUPS unequivocally indicate that at this coverage CO is tilted at approximately 40° to the surface normal. This CO tilting at low coverages cannot be ascribed to adatom-adatom interactions. Measurements of the positions of the photoelectron peaks of the tilted molecule indicate that both the 1π and the 5σ orbitals participate in surface bonding. Based on these observations, a bonding model is proposed in which the tilted CO molecule is chemisorbed in a fourfold hollow site [87Ful]. At high coverage CO exhibits a stretch frequency near 2100 cm^{-1} which is compatible with an on-top bonded species. ARUPS indicates that this CO chemisorbs with its axis perpendicular to the surface in an analogous manner to that observed on other transition metal surfaces. Overall, a similarity to CO adsorbed on Fe(100) is obvious [85Ben, 89Dwy, 89Sai].

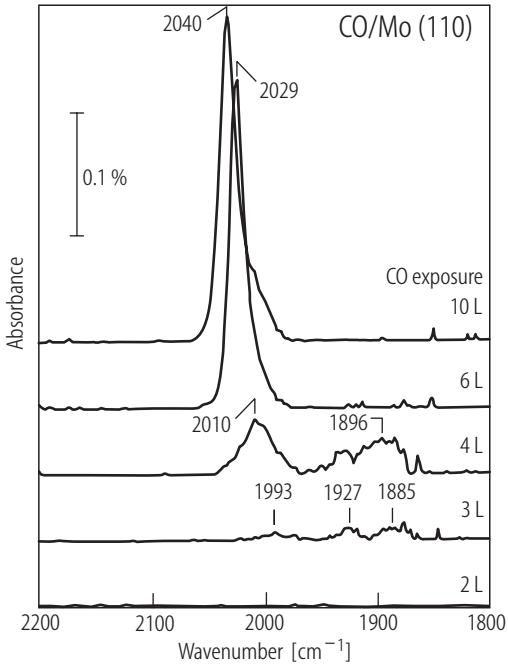

Fig. 20. Vibrational (IRAS) spectra of CO on Mo(110) at 95 K; [91He1].

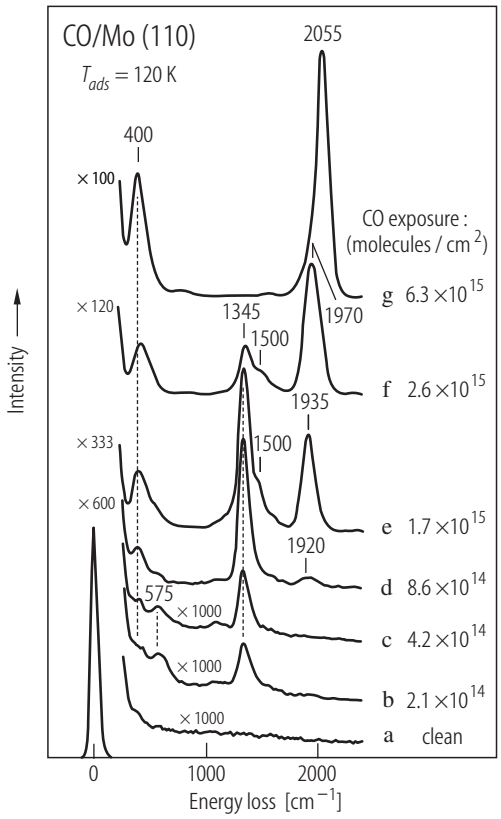

Fig. 22. EELS spectra of CO on Mo(110) at 120 K taken for increasing coverage; [91Che].

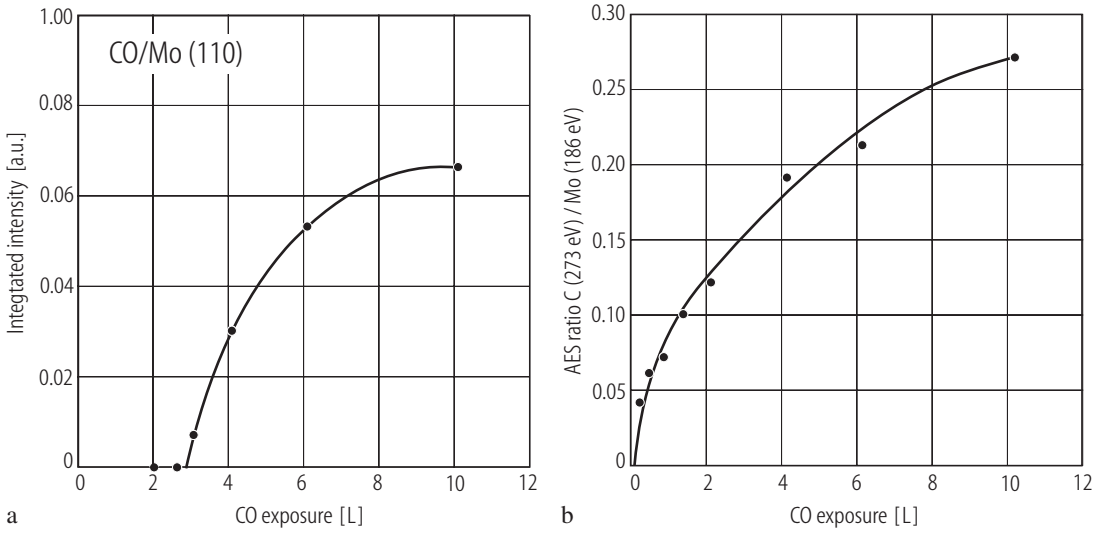

Fig. 21. (a). Integrated intensity of IRAS peaks versus CO exposure at 90 K. **(b).** AES peak ratio C(273eV)/ Mo(196eV) versus CO exposure at 95 K; [91He1].

Ta

A study of CO adsorption on a (110) oriented FEM tip was analyzed by changes in the emission pattern [63Kle]. Annealing to 125 K produced some CO desorption but no direct diagnostic of the adsorbed layer was possible in this work. In another study of adsorbed CO on a single crystal of Ta(100) at 300 K showed evidence of dissociative adsorption and dissolution of C into the bulk at elevated temperatures [74Che]. Ordered surface structures appear being due to atomic oxygen. No desorption takes place at temperatures below about 2000 K. Further information on reactions of CO with Ta are given by Horz [78Hor2]. Several studies of CO adsorption on Ta(110) surfaces modified by added Cu or Pd have appeared more recently [93Kuh1, 93Sel, 95Pic1].

W

For CO adsorption on W surfaces the initial rate of adsorption is high for a range of surface (T_s) as well as gas (T_g) temperatures, such as shown in Fig. 23 and Fig. 24 for the coverage dependent sticking coefficient of CO on W(110) and W(100) surfaces [71Koh, 79Wan]. Thermal desorption spectra from W(110) exhibit multiple states, seen in Fig. 25, which may be grouped into two regions, at 200 - 400 K and at 900 - 1200 K. These states were designated α- and β-states, respectively, with the special notion that the α-state of a primary CO layer ("virgin"), prepared on the clean W(110) surface, produced a single peak at 375 K. This peak was attributed to the "virgin" state of CO. Adsorbing CO on surfaces that had been flashed to 500 - 600 K after primary CO adsorption, exhibited a broad range of several α-states, distinctly different from virgin CO, Fig. 25. These α-states seemed to be more weakly bound than "virgin" CO [71Koh]. Is CO initially adsorbed molecularly or dissociatively, i.e. breaking into separately adsorbed C and O species? A clue to answering this question comes from Fig. 26 which is a plot of the amount of CO desorbed at T <500 K versus the total amount adsorbed at 100 K [71Koh]. No CO desorbs below 500 K for coverages up to 0.25 which means that all of the initially adsorbed CO must either be strongly bound to the surface or be converted into such a species during heating, so that all surface species desorb at T >900 K. The initially adsorbed CO may be all molecular or a mixture of molecular and dissociatively adsorbed CO - situations which can not be resolved by thermal desorption spectra alone. Most likely only dissociated CO is present after heating to 500 K.

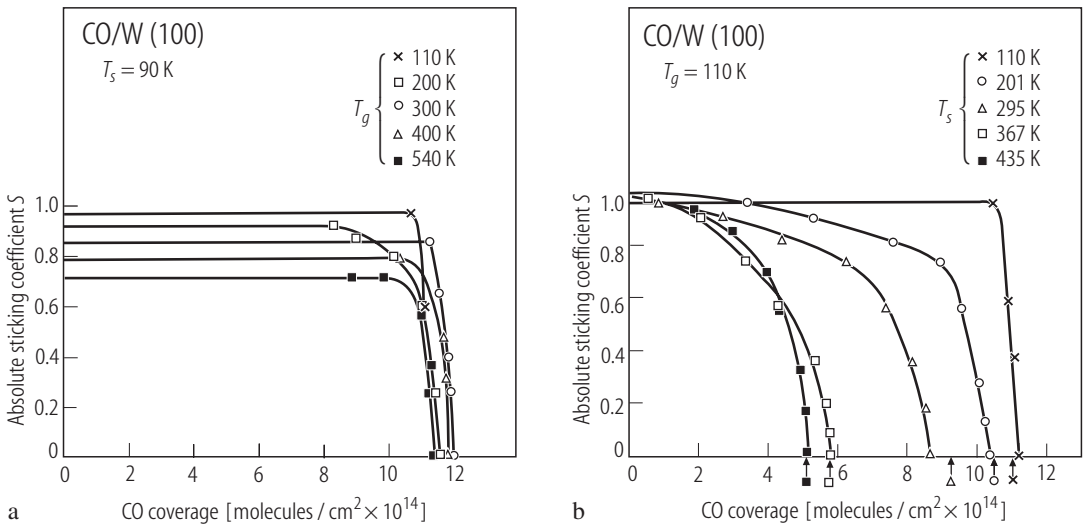

Fig. 23. Coverage dependence of absolute sticking coefficients for CO on W(100) at **(a)** 90 K and **(b)** 110 K [79Wan].

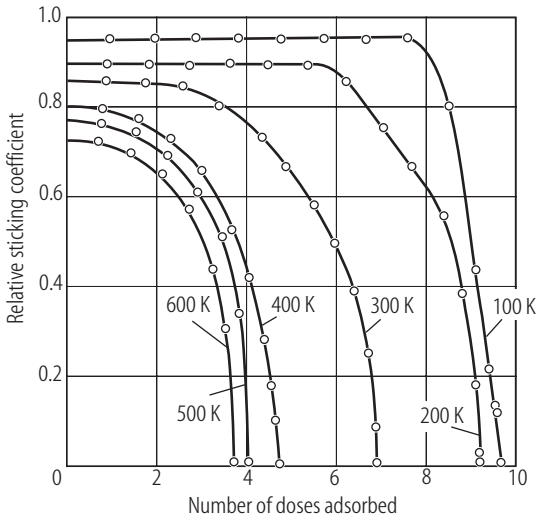

Fig. 24. Coverage dependence of relative sticking coefficient of CO on W(110) at 30 K [73Koh].

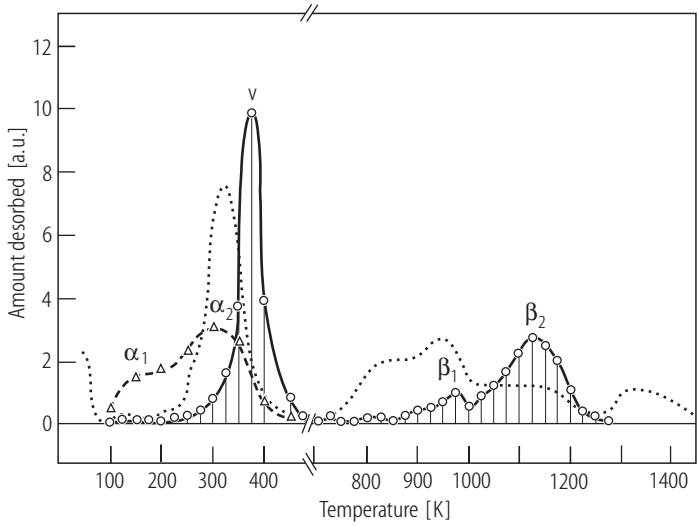

Fig. 25. (O) Thermal desorption spectrum of saturated CO ("virgin") layer on clean W(110) adsorbed at 77 K. (Δ) Desorption of layer saturated at 77 K after heating virgin layer to 600 K. Dotted line: desorption from polycrystalline W surface [71Koh].

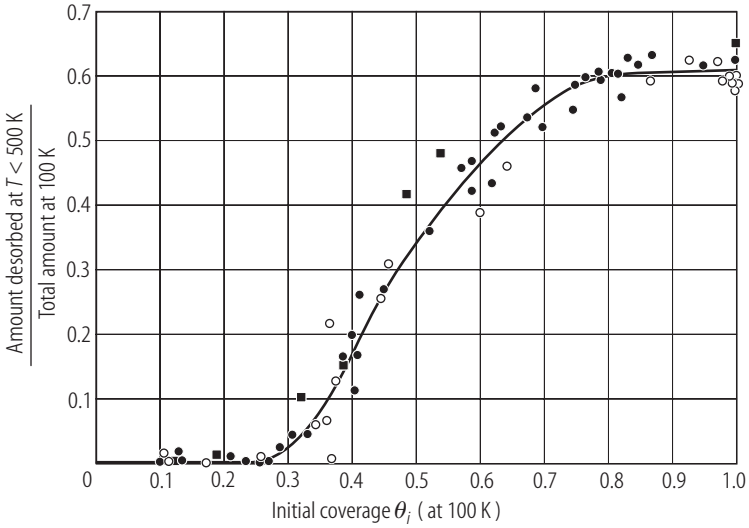

Fig. 26. Amount of CO desorbed at T <500 K relative to total amount of CO (adsorbed at 100 K) versus initial CO coverage (adsorbed at 100 K) [71Koh].

Early spectroscopic work by UPS of adsorbed CO on W(100) and W(110) concentrated on detecting CO molecular orbital related emission peaks for various conditions where α and β desorption states may be predominant [76Plu]. The β_3 state on W(100) was identified as dissociated CO, giving rise to a c(2×2) LEED pattern, and tentatively attributed to C and O in 4-fold hollow sites. Low coverage adsorption of CO into this state even at room temperature seemed likely. Other β states consist also of C and O strongly bound to the surface, with the CO bond considerably weakened or fully dissociated. Virgin and α CO are molecular and bonded through the C atom to the surface ("carbonyl-type bond"), with some remaining uncertainty, whether CO is linearly or bridge bonded. On W(110) the virgin state is molecular, it both desorbs and converts to β-CO on heating to 500 K. Readsorption on a saturated layer heated to 700 K forms α-CO which is not identical to the initial virgin state CO [76Plu].

A further clarification of CO adsorption on W came from various sources, quantitative X-ray photoemission spectra being one of them [83Umb]. Molecular and dissociated CO in the adsorbed state can be well distinguished by their O 1s and C 1s core level binding energies (Table 7), and the intensities of the respective lines can be taken as a reliable measure of relative CO coverages [73Mad1, 74Yat3]. Hence the amounts of molecular and dissociated CO, here virgin and β-states, respectively, were measured for a CO layer, initially adsorbed up to saturation at 100 K, and then heated successively to a temperature T [83Umb]. It is concluded from Fig. 27 that only molecular CO is present up to about 270 K where it begins to partially desorb and mostly convert into dissociated C and O, the latter being equivalent to the sum of β-states. Note that at >400 K all of the adsorbed CO is dissociated.

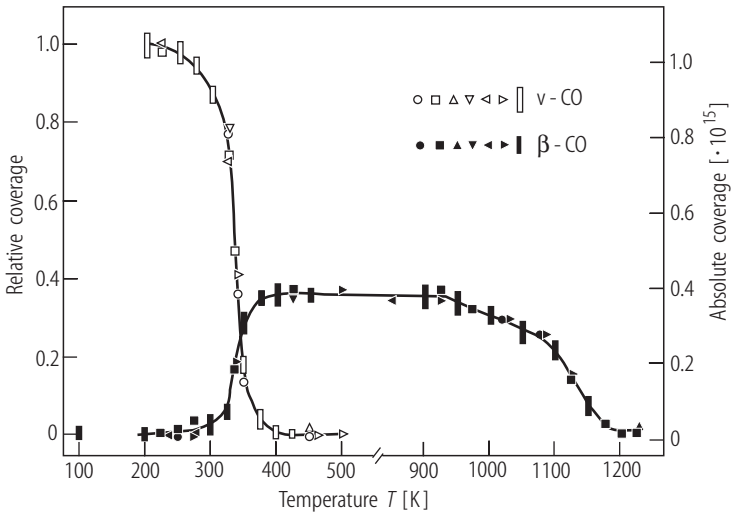

Fig. 27. Evolution of adsorbed CO layer on W(110) separated into virgin (v) and β CO at 100 K, based on quantitative O 1s photoemission spectra [83Umb].

Further insight into the nature of CO/W(110) was gained by vibrational spectra of virgin CO adsorbed at 90 K [91Hou]. The spectra were taken at several CO coverages in the range 0.23 - 0.67 and show two peaks in the C-O stretching region, Fig. 28. The growth of the two peaks with coverage suggests that the species at 1360 cm^{-1} is adsorbed first, followed by the second species at 2020 cm^{-1}. A maximum coverage of the low frequency state is found near 0.4 total CO coverage. As the total CO coverage increases, the amount of the 1360 cm^{-1} state decreases and becomes undetectable at >0.7 . Separate annealing experiments demonstrated that the 1360 cm^{-1} CO state converts to dissociated CO below 250 K. All of this behavior, together with measured work function changes due to adsorbed CO, are consistent with a molecular CO species whose axis is strongly inclined, estimated at about 70° relative to normal [91Hou]. Although CO adsorption characteristics seem to be similar for W(110) and W(100), a low frequency CO state has so far not been verified for the W(100) surface.

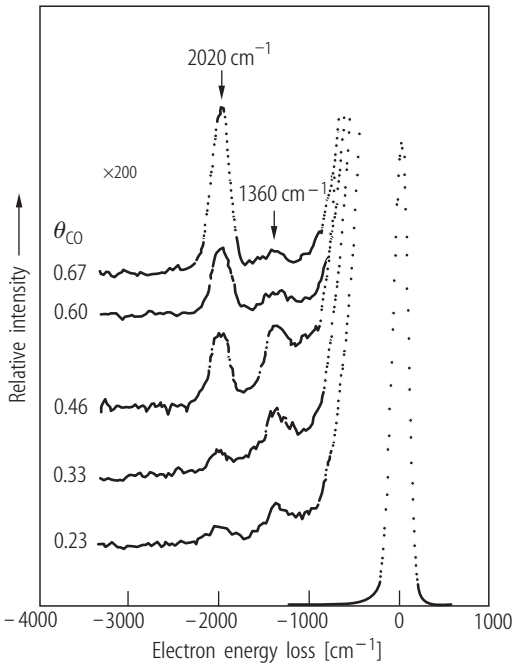

Fig. 28. Coverage dependent EELS spectra of CO adsorbed at 90 K on W(110). Note transient appearance of 1360 cm^{-1} frequency indicative of a tilted CO species [91Hou].

3.7.1.4 CO adsorption on hcp metal surfaces

Ti

Several studies of CO adsorption on Ti($10\bar{1}1$) and Ti(0001) are known [78Fuk, 80Fuk3, 98Kuz]. UPS and XPS were used to study the valence band DOS and the effect of adsorbates on individual photoionization cross sections [80Fuk3]. Dissociation of CO leads to the formation of oxides and carbides at the surface, characterized by O1s and C1s spectra at 529.8 ± 0.2 eV and 281.8 ± 0.2 eV, respectively [78Fuk]. The kinetics and mechanism of dissociative chemisorption of CO on Ti(0001) at T = 300 K and exposures of 0 - 300 Langmuir were investigated by X-ray photoelectron spectroscopy and X-ray photoelectron diffraction [98Kuz]. The results were used to characterize the initial elementary stages of chemisorption, to determine the positions of adsorbed atoms and to distinguish between the different types of kinetics of filling in the non-equivalent adsorption centers with carbon or oxygen atoms. A series of possible variants of the CO chemisorption on the Ti(0001) surface was calculated by the first-principle linear method of muffin-tin orbitals in the full-potential version (LMTO-FP) [98Kuz].

Co

CO adsorption on the basal plane of Co(0001) has been studied in fair detail by several groups [77Bri, 79Fre, 83Gre, 83Pap, 96Bei, 00Cab, 00Lah]. Three ordered CO structures at coverages between 0.33 and 0.58 were detected by LEED. The coverage dependent energy of desorption was determined as 96 - 128 kJ/mol [83Pap]. The dispersion of the electronic valence orbital derived states at 0.33 and 0.58 coverage, illustrated in Fig. 29 and Fig. 30, was measured by ARUPS [83Gre]. The local structure of adsorbed CO at 160 L was determined by LEED, yielding a C-O bond length of 1.17 ± 0.06 Å and a Co-C bond length of 1.78 ± 0.06 Å [00Lah]. Beitel et al. studied adsorbed CO at pressures between 10^{-10} and 600 mbar at 300 - 550 K by polarisation modulated RAIRS [96Bei]. Linearly and bridge-bonded CO could be distinguished. Annealing in high pressure CO at 100 mbar and 450 - 490 K produces defect sites at the Co(0001) surface which are possibly related to the formation of Co carbide due to dissociation of CO

[96Bei]. Cabeza et al. compared CO adsorption on clean Co(0001) and Pt modified Co(0001) using LEED and photoemission spectroscopy [00Cab]. CO adsorbs molecularly on both Pt and Co surfaces. The coverage of CO on Co(0001) is higher than on the modified Pt/Co surface. Pt causes also a lowering of the adsorption energy which is in agreement with theory.

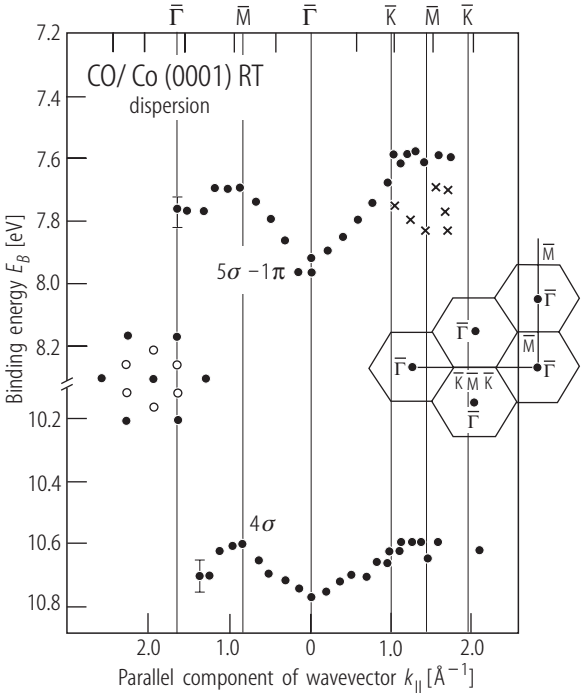

Fig. 29. Dispersion of CO molecular orbital states for the ordered (√3×√3)R30° CO layer on Co(0001) at room temperature. Inserts show LEED pattern and measured directions in reciprocal space [83Gre].

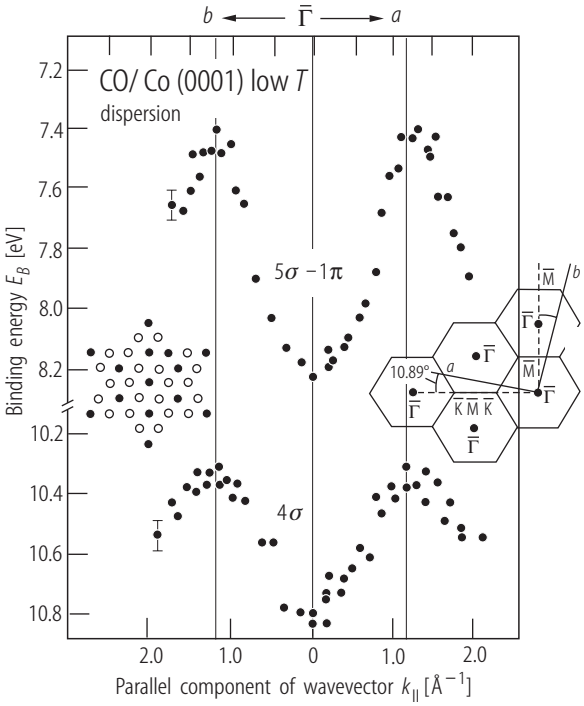

Fig. 30. Dispersion of CO molecular orbital states for the ordered (2√3×2√3)R30° CO layer on Co(0001) at room temperature. Inserts show LEED pattern and measured directions in reciprocal space [83Gre].

The behavior of CO adsorption on higher index surfaces of Co, such as Co($10\bar{1}2$) and Co($11\bar{2}0$) was also investigated [78Pri, 82Pap, 84Hab, 85Pap, 96Too]. CO is molecularly adsorbed on Co($11\bar{2}0$) below 300 K, with a coverage independent isosteric heat of adsorption of 143 kJ/mol [85Pap]. Molecular and dissociative adsorption occur above 300 K. Molecular adsorption of CO is found at 100 - 420 K on Co($10\bar{1}0$) with an isosteric heat of adsorption of 143 kJ/mol, dropping to 120 kJ/mol with increasing coverage [82Pap]. Two ordered structures, p(2×1) and c(2×1), are observed at 300 K by LEED. CO adsorption on Co($10\bar{1}2$) is molecular at 300 K and leads to a (3×1) structure [78Pri]. Heating the adlayer causes both desorption and dissociation of CO. Recently, the formation of the CO-induced (3×1) structure on Co($11\bar{2}0$) has been investigated by scanning tunnelling microscopy [98Ven]. The molecular adsorption of CO is found to create a trough-and-ridge structure running along the (0001) direction and comprising a (3×1) periodicity in well-ordered regions. STM measurements conducted during CO exposure show that the adsorption induces migration of Co atoms along the surface. A "missing row-added row" model for the formation of the (3×1) structure is proposed, in which every third zig-zag row of atoms in the clean Co($11\bar{2}0$) surface is absent [98Ven].

Zn

Studies of CO adsorption on Zn crystals are not known. We briefly consider CO adsorption on thin films of deposited Zn. CO was reported to not adsorb on thick Zn films at 80 K under ultra-high vacuum conditions [90Car, 93Rod]. In contrast, adsorption is observed on Zn atoms bonded to Ru(0001). Bimetallic bonding induces a reduction of approximately 0.5 eV in the binding energy of the core and valence levels of Zn. This shift probably increases the strength of the Zn-CO bond. CO molecules adsorbed on Zn adatoms show an O(1s) binding energy close to 535.2 eV and a desorption temperature of approximately 125 K. Both properties indicate a very low energy of adsorption and a very weak contribution of π-backbonding to the ZnC-O bond. By comparison, CO adsorption on polar ZnO surfaces, either Zn or oxygen terminated, is relatively weak, with adsorption energies between 29 [00Bec]. and 52 kJ/mol [80Gay] for both surfaces.

Zr

CO readily dissociates on adsorption on a ploycrystalline Zr surface [80Foo]. Quantitative studies of CO behavior are complicated because of dissolution of C and O into the bulk of the material. Studies of CO adsorption on single crystal surfaces are not known.

Ru

An extensively studied example of molecular adsorption is CO on Ru(0001). The dependence of the sticking coefficient of CO on coverage at surface temperatures between 100 and 400 K is shown in Fig. 31 [83Pfn1]. There is a slow nearly temperature independent decrease with coverage up to about 0.3 where a well ordered (√3×√3)R30°-CO structure forms. This result, corroberated by a measurement of the intial sticking coefficient as a function of translational kinetic energy of incident CO in Fig. 32, [00Rie] indicates non-activated adsorption. Thermal desorption spectra of CO in Fig. 33, measured by the change of electron work function, reveal two adsorption states and first order desorption kinetics [83Pfn2]. When the heating rate for thermal desorption, $\beta_H = dT/dt$, is varied over about three decades, the energy of desorption and the pre-exponential factor for a certain coverage can be determined from a plot of β_H/T_p^2 versus $1/T_p$ as shown in Fig. 34 [83Pfn2]. Alternatively, desorption isotherms can be constructed from the desorption data of Fig. 33. A set of isotherms for the temperature range 432 - 513 K is given in Fig. 35 for the same system [83Pfn2]. Evaluation of this large amount of data leads to the coverage dependent isosteric adsorption energy of CO on Ru(0001) and the associated pre-exponential factor in Fig. 36 [83Pfn2]. The discontinuity in both quantities at the CO coverage of 0.33 is related to a structural transition from the (√3×√3)R30° to a more compressed CO layer.

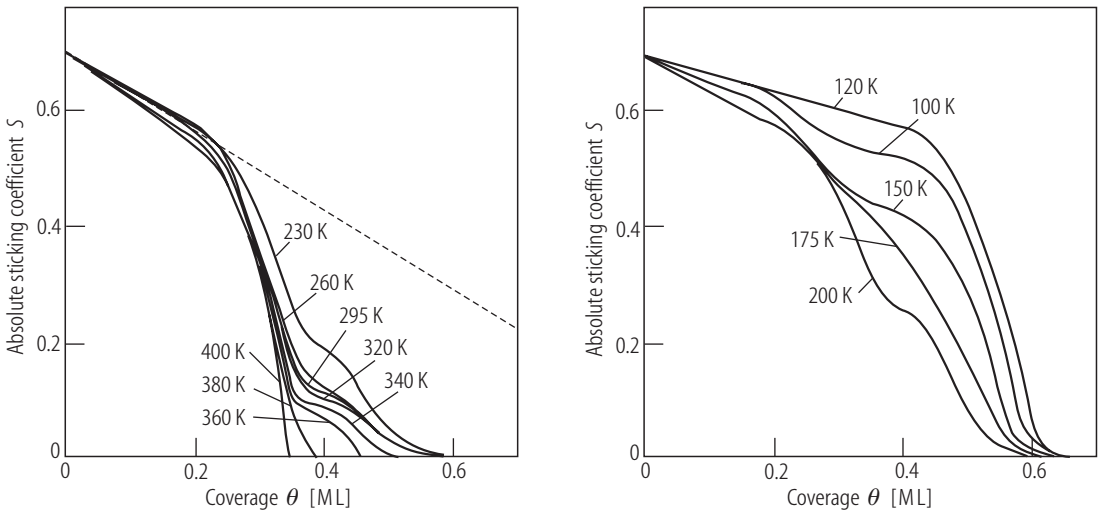

Fig. 31. Coverage dependence of absolute sticking coefficients S for CO on Ru(0001) at adsorption temperatures between 100 and 400 K; [83Pfn1].

Fig. 33, see next page

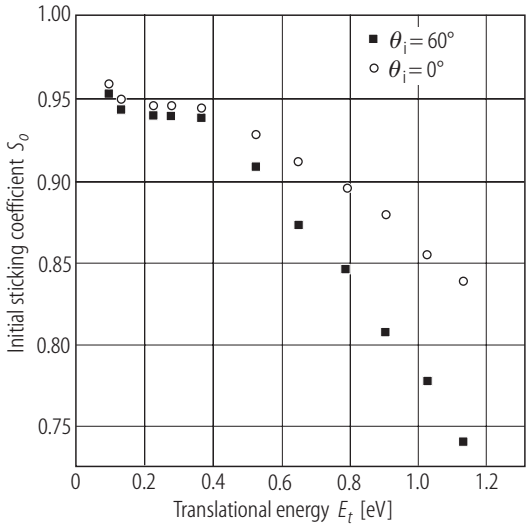

Fig. 32. Dependence of the initial sticking coefficient S_0 on translational (kinetic) energy for CO on Ru(0001) at 0° and 60° incidence angle at T_s = 273 K; [00Rie].

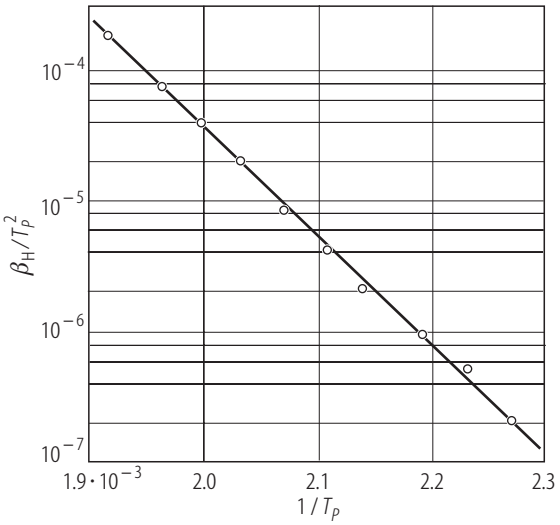

Fig. 34. Evaluation of peak temperatures from thermal desorption data of CO/Ru(0001), according to Falconer and Madix [75Fal], to obtain the effective desortion energy; [83Pfn2].

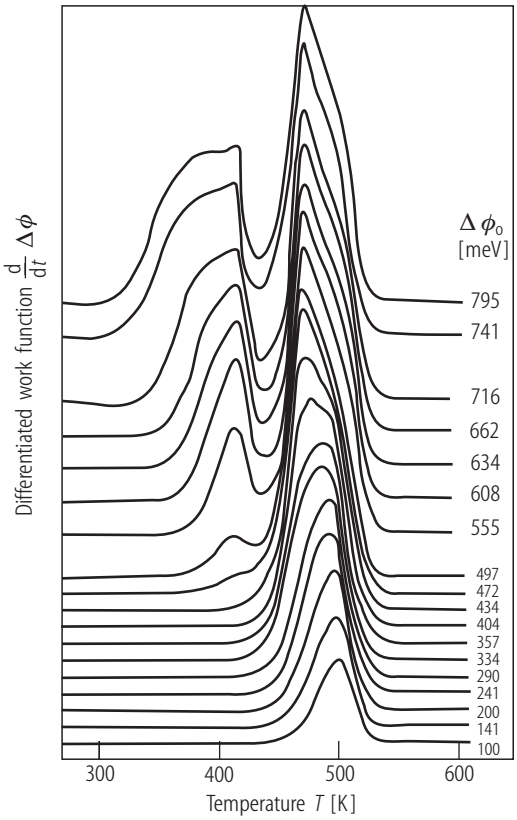

Fig. 33. Differentiated work function versus temperature curves for CO on Ru(0001), illustrating the coverage dependent thermal desorption of CO; [83Pfn2].

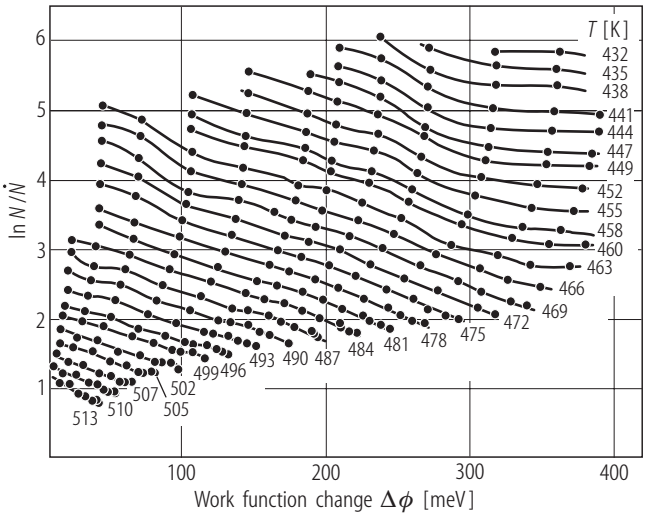

Fig. 35. Desorption isotherms obtained from the data of Fig. 33 for CO on Ru(0001) according to the procedure by Bauer et al. [75Bau] [83Pfn1]. Temperatures in K are given for each isotherm.

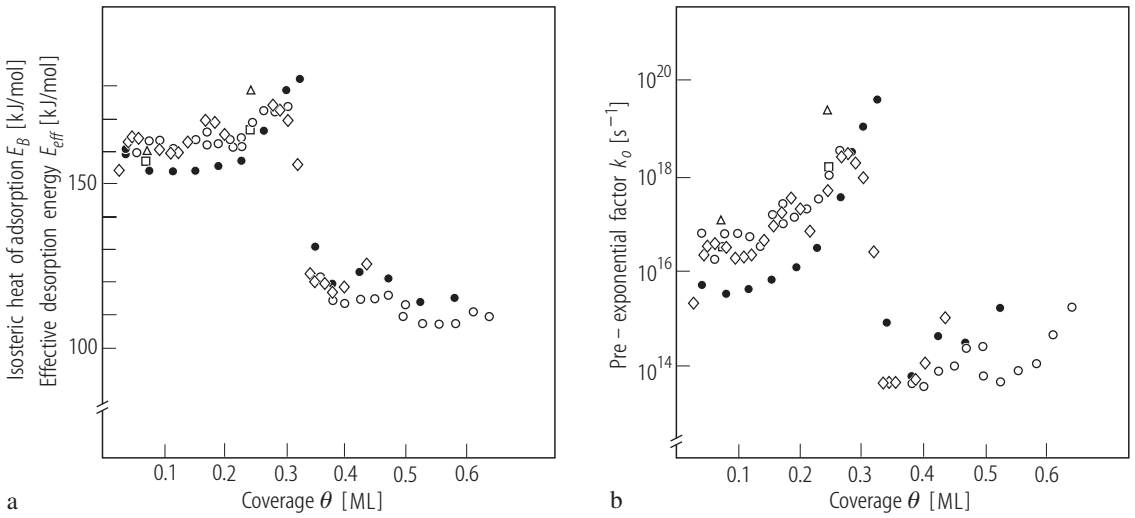

Fig. 36. Coverage dependence of **(a)** isosteric heat of adsorption as well as effective desorption energy and **(b)** pre-exponential factor of desorption for CO on Ru(0001); [83Pfn2].

The dynamics of CO scattering from a Ru(0001) surface has also been investigated. Fig. 37 shows the angle-resolved flux distribution of scattered CO molecules at surface temperatures of 273 and 550 K from the clean and for 273 K also from the CO-covered surface, at an incident kinetic energy of 0.8 eV [00Rie]. The maximum of the distribution at 68° is shifted relative to the angle of incidence (60°), indicative of parallel momentum increase or refraction due to the deep molecular adsorption well for CO. Surface phonon - molecule interaction is responsible for broadening and asymmetry of the distribution in Fig. 37.

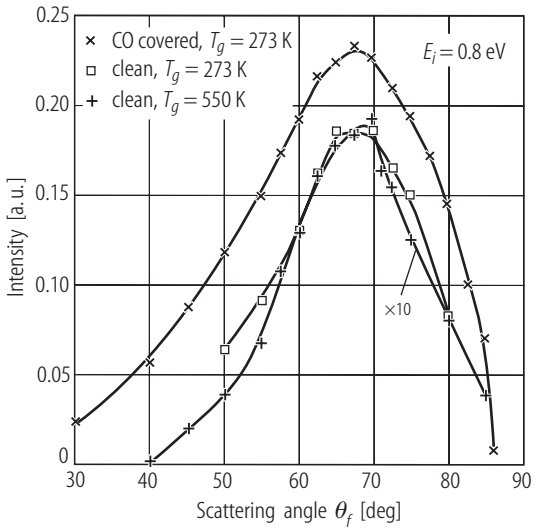

Fig. 37. Angle-resolved flux distribution of CO molecules scattered from Ru(0001) at 60° incidence angle. Surface temperature as indicated; [00Rie].

A comparison of CO adsorption on differently structured surfaces of the same material is of interest from the point of view of structure sensitivity of adsorption. Thermal desorption spectra for CO from Ru($10\bar{1}0$) are seen in Fig. 38 [75Bon1, 89Lau]. Peaks at about 370 and 500 K are representing molecular CO adsorption and the similarity to the spectra in Fig. 33 suggest that structure sensitivity is not very significant. This observation is supported by the coverage dependent activation energy of desorption evaluated from a line shape analysis of the desorption traces [89Lau]. The energy data in Fig. 39 for Ru($10\bar{1}0$) are in the same range as those for the Ru(0001) surface in Fig. 36a.

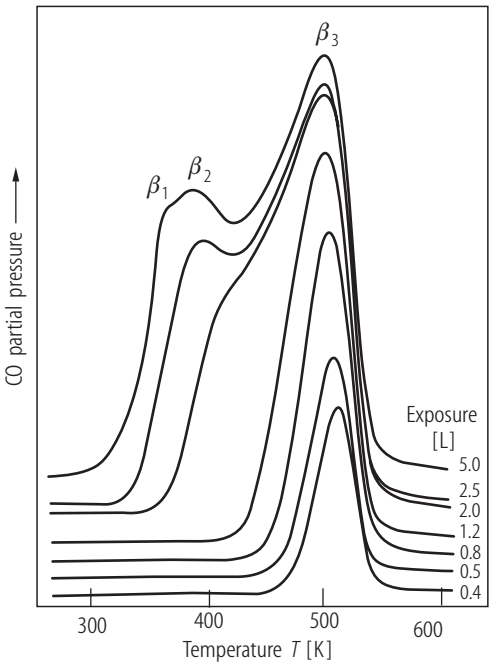

Fig. 38. Thermal desorption spectra of CO from Ru($10\bar{1}0$) showing three desorption states; [89Lau].

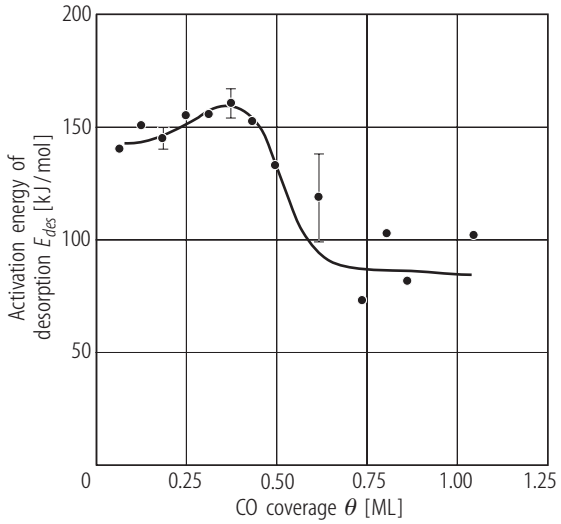

Fig. 39. Activation energy of desorption versus CO coverage, derived from line shape analysis of TDS traces; [89Lau].

The interaction within a molecularly adsorbed CO layer at higher coverage is substantial. This leads to a continuous shift in vibrational frequencies with coverage, such as seen for CO on Ru(0001) in Fig. 40 [80Pfn]. The C-O stretch vibration frequency increases with increasing CO coverage from 1984 to about 2060 cm^{-1} at saturation of 0.67. The actual saturation density is here 1.11×10^{15} CO/cm^2. The density for the well ordered (√3×√3)R30°-CO structure is 5.45×10^{14} CO/cm^2. By comparison, measured frequencies of CO on the more open Ru($10\bar{1}0$) surface also show a similar shift in stretch frequency with coverage, Fig. 41 [89Lau]. There are at least four well ordered structures of CO in this case, and if we calculate the absolute CO coverage for the (3×1) structure, for example, it is 5.2×10^{14} CO/cm^2 and the C-O stretch frequency is 2019 cm^{-1}. This compares very well with the absolute CO density of the (√3×√3)R30° structure on Ru(0001) and its frequency of 2021 cm^{-1}. Similarly at saturation: the density on Ru($10\bar{1}0$) is 1.06×10^{15} CO/cm^2 at a frequency of 2062 cm^{-1} and on Ru(0001) it is 1.11×10^{15} CO/cm^2 at a frequency of 2060 cm^{-1}. Hence the registry of CO with the substrate surface seems to be only of secondary importance for CO-CO interactions.

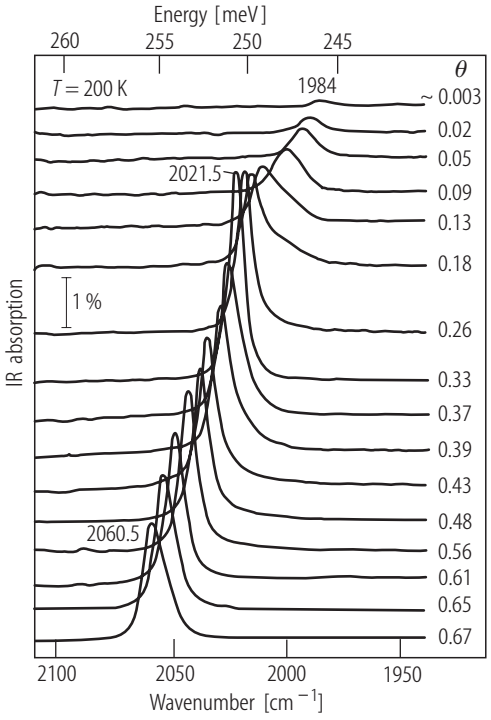

Fig. 40. Coverage dependence of the C-O stretch vibrational frequency of CO adsorbed on Ru(0001) at 200 K, measured by IRAS; [80Pfn].

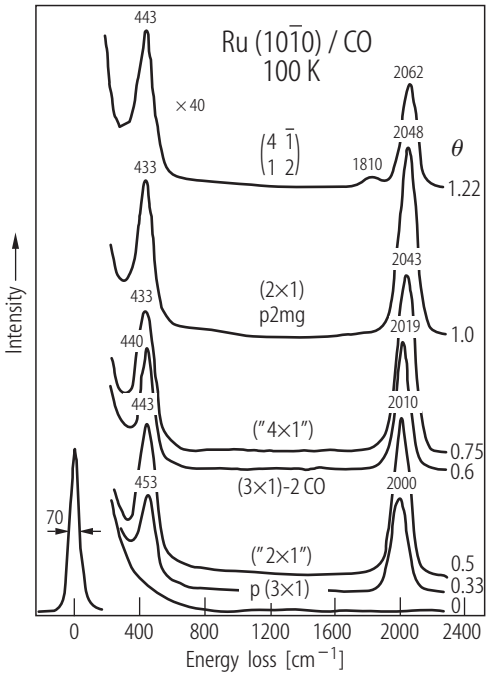

Fig. 41. Correlation of vibrational spectra (EELS) and CO overlayer structure on Ru(10$\bar{1}$0) at 100 K. Note coverages of CO on the right; [89Lau].

CO on Ru(0001) at the highest coverage forms the ordered structure designated (2√3×2√3)R30° [83Pfn1]. Orientation of CO and lateral intermolecular interactions were studied for this structure by ARUPS [85Hof]. Using p-polarized light at 35 eV energy and measuring the polar angle dependence of the intensity of the 4σ molecular orbital, not involved in the adsorption bond, yields the distribution shown in Fig. 42. Compared to theory, the experimental data are consistent with perpendicularly adsorbed CO. Recording the variation of molecular orbital peak positions with emission angle, using both p- and s-polarized light, the two-dimensional band structure of the (2√3×2√3)R30° CO layer could be determined [85Hof]. The result is presented in Fig. 43 as a plot of binding energy versus parallel component of the electron wave vector (which is conserved in photoemission). There is a substantial dispersion in all orbitals but strongest in the 5σ orbital of CO which is involved in Ru-CO bonding. The dispersion gap is about 0.7 eV at the $\bar{\Gamma}$-point. Corresponding energies for the 4σ and 1π orbitals are 0.4 eV and 0.5 eV, respectively. The dispersion indicates a large lateral interaction between CO molecules in this compact layer. Similar results for ordered CO layers of high density have been obtained for both the (√3×√3)R30° and the (2√3×2√3)R30° structures on Co(0001) [83Gre], shown in Fig. 29 and Fig. 30, respectively, and for CO/Ir(111) [80Sea, 81Sea], CO/Pd(111) [84Mir] and CO/Ni(110) [86Kuh]. The comparison of these data shows that the amount of dispersion is lower for the lower coverage structure. A more general correlation is given in Fig. 8 which shows a plot of the measured 4σ dispersion bandwidth versus CO nearest neighbor distance for all of these hexagonally close-packed ordered structures. It can be seen that a logarithmic dependence is obtained regardless of the substrate material [83Gre, 85Hof]. Hence the dispersion is greatly governed by CO-CO repulsive lateral interactions.

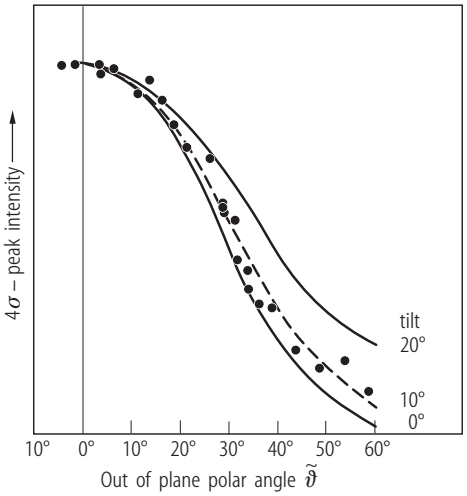

Fig. 42. Intensity of CO 4σ peak as a function of polar angle for the (2√3×2√3)R30° structure on Ru(0001). The angle of incidence is 45°, p-polarized light at $h\nu$ = 35 eV [85Hof]. The full and dashed lines are theoretical dependencies according to Davenport theory taken from [82Bar].

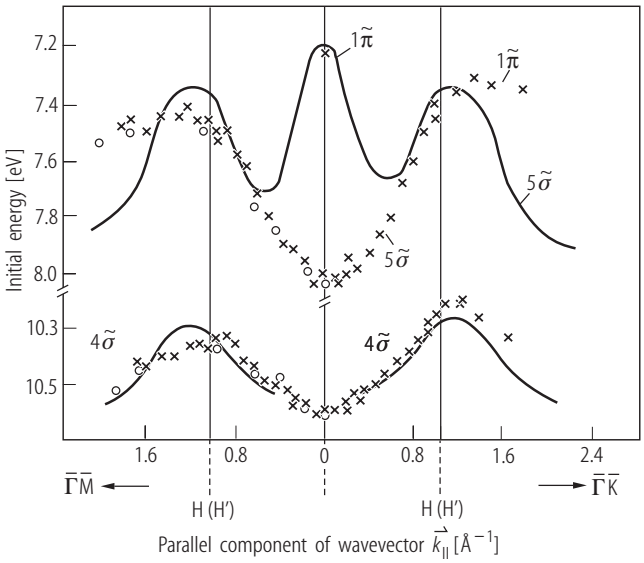

Fig. 43. Two-dimensional band structure of CO-related molecular orbitals along the substrate $\overline{\Gamma}\overline{K}$ and $\overline{\Gamma}\overline{M}$ directions of the (2√3×2√3)R30° structure on Ru(0001); [85Hof].

The interaction of CO with Ru field emitter surfaces has been studied by pulsed field desorption mass spectrometry (PFDMS) at a pressure of 1.3×10^{-6} mbar CO and temperatures of 328 K and 458 K. Probing the stepped region in the vicinity of the (0001) pole of the Ru field emitter, various ionic species have been detected, including singly and doubly charged subcarbonyls $Ru(CO)_x^{n+}$ (x=1 - 4). The intensities of these species as well as their relative abundances depended on the field strength, the repetition rate of the field pulses (field free reaction time) and the surface temperature. A consecutive reaction is considered involving chemisorbed Ru subcarbonyl molecules. These $Ru(CO)_x$ species reach steady surface concentrations at different relaxation times which depend on temperature. $Ru(CO)_2$ is formed by an activated process. A reaction model is presented which describes the removal of Ru lattice atoms and their diffusion into the adsorbed layer via $Ru(CO)_2$ formation as part of a process inducing morphological changes of the Ru emitter apex [86Kru].

Irradiation of a Ru(0001) surface covered with CO using intense femtosecond laser pulses (800 nm, 130 fs) leads to desorption of CO with a nonlinear dependence of the yield on the absorbed fluence (100 - 380 J/m^2). Two-pulse correlation measurements reveal a response time of 20 ps (FWHM). The lack of an isotope effect together with the strong rise of the phonon temperature (2500 K) and the specific electronic structure of the adsorbate-substrate system strongly indicate that coupling to phonons is dominant. The experimental findings can be well reproduced with a friction-coupled heat bath model [00Fun]. Broad-band IR sum frequency generated radiation (SFG) was also used to excite the fundamental and higher order stretch vibration of low-coverage adsorbed CO on Ru(0001) [00Hes1]. Due to the high intensity of the incident IR radiation the vibrational transitions $\upsilon = 0\rightarrow1$ at 1989 cm^{-1}, $1\rightarrow2$ at 1962 cm^{-1} and even the $2\rightarrow3$ at 1936 cm^{-1} were excited at a CO coverage of 0.004 ML. The anharmonicity constant was determined to be 13.6±0.6 cm^{-1} from fitting the experimental spectra, in good agreemnet with the analysis of overtone spectra [98Jak1]. The dissociation energy of the adsorbed C-O bond was evaluated in the framework of a Morse potential as 9.18±0.03 eV (compared to 11.09 eV for gaseous CO) [00Hes1]. The excitation of the $\upsilon = 1\rightarrow2$ hot band depends on the CO coverage. As the coverage increases to 0.33, this band is no longer observed and the fundamental $0\rightarrow1$ transition shifts to lower frequencies. A single broadened band is detected at coverages above 0.025. This phenomenon is interpreted in terms of a local oscillator to delocalized phonon transition [00Hes2]. High-resolution infrared reflection absorption spectroscopy of CO on Ru(001) utilizing a continuously tunable infrared laser has been carried out at 85 - 300 K [86Hof]. A small shift in the CO stretch of 2.5 cm^{-1} was reported with increasing temperature.

Investigations of CO adsorption on structurally more diverse surfaces, such as Ru($10\bar{1}0$) [89Lau], Ru($11\bar{2}0$) [80Car, 01Wan1, 01Wan2], Ru($11\bar{2}1$) [03Fan] and stepped Ru(1,1,10) [85Shi1] showed a larger variety of adsorbed CO states but also CO dissociation at 300 K and elevated temperatures. CO adsorbed on Ru($11\bar{2}0$) gives rise to two ordered structures, a p(1×2) and a (1×2)p2mg with increasing coverage [01Wan1]. The latter is characterized by a glide plane related to the zig-zag rows of Ru surface atoms and on-top bonded CO molecules on them. Whether the CO coverage of the (1×2)p2mg is 0.5 or 1.0 is not quite clear [01Wan1, 03Fan]. The C-O stretch of >1994 cm^{-1} supports an upright configuration of CO. A tilted CO species exhibiting a low stretch frequency of 1552 cm^{-1} and a bending mode at 690 cm^{-1} is observed at low coverage and temperatures up to about 240 K [01Wan2]. Dissociation of this adsorbed CO species is observed around 300 K by EELS [01Wan2]. A four-fold hollow adsorption site is suggested for this tilted CO species.

The Ru($11\bar{2}1$) with its multi-site surface is particularly interesting [03Fan]. Three molecular species, α_1-CO, α_2-CO and β-CO can be distinguished by EELS as well as TDS. β-CO is observable only at low coverage and characterized by a low stretch frequency of 1335 cm^{-1}, thus typical for a molecule inclined towards the surface. This state dissociates at about 300 K. The weakly bound α-states have stretch frequencies in the range 1770 - 2050 cm^{-1} and are perpendicularly adsorbed. The α_1-state converts to β-CO at moderate total coverage and T >360 K, increasing the amount of dissociated CO [03Fan]. On the other hand, β-CO is destabilized at low temperature and increasing CO coverage by converting to α_1-CO.

Self-consistent density functional calculations have been carried out for the adsorption of O and CO as well as the dissociation of CO on Ru(001) [98Mav]. The effect of straining the surface on its chemical properties have been studied in particular. It was found that the surface reactivity increases with lattice expansion (up to 3 %), coupled to an upshift of the metal d-states. As a consequence, the energy of adsorption and the activation barrier for dissociation of CO decreases, thus increasing the amount of total dissociated CO [98Mav]. The underlying reason for the strain-induced effect is the shift in the center of the relatively narrow d-band. A more general relationship between the interaction strength of adsorbed species and the position of the center of the d-band is demonstrated for several transition metals and simple adsorbed species [98Mav].

Re

CO adsorption on Re surfaces has been much less studied than on W or Mo surfaces [77Hou, 80Duc, 80Fuk2, 83Tat, 85Tat, 88Kel]. The adsorption on Re(0001) and a stepped basal plane by TPD, LEED and AES showed two α-states and one β-state. The coverage of the latter is dependent on surface structure and presumably dissociated [77Hou]. Molecular and dissociated CO states are also observed in TDS, as seen in Fig. 44 for a clean Re($10\bar{1}0$) surface [88Kel]. This figure also demonstrates how adsorbed sulfur blocks efficiently adsorption sites for CO. The ability of Re to dissociate CO is particularly perturbed since β-states are eliminated faster than α-states, Fig. 44b. Spectroscopic data are not available in this case. CO adsorption on stepped Re surfaces has also been studied, with emphasis on the question of step-induced dissociation of CO [81Duc]. The results turned out to be complicated and difficult to reproduce. The study of CO adsorption on the thin film system Re/Pt(111) is also of interest in this context because it demonstrates an increase in adsorption energy relative to clean Pt(111) and Re(0001) [99Ram]. Furthermore, the modification of a Re(0001) surface by metallic adsorbates and ist effect on CO adsorption has been studied [90He].

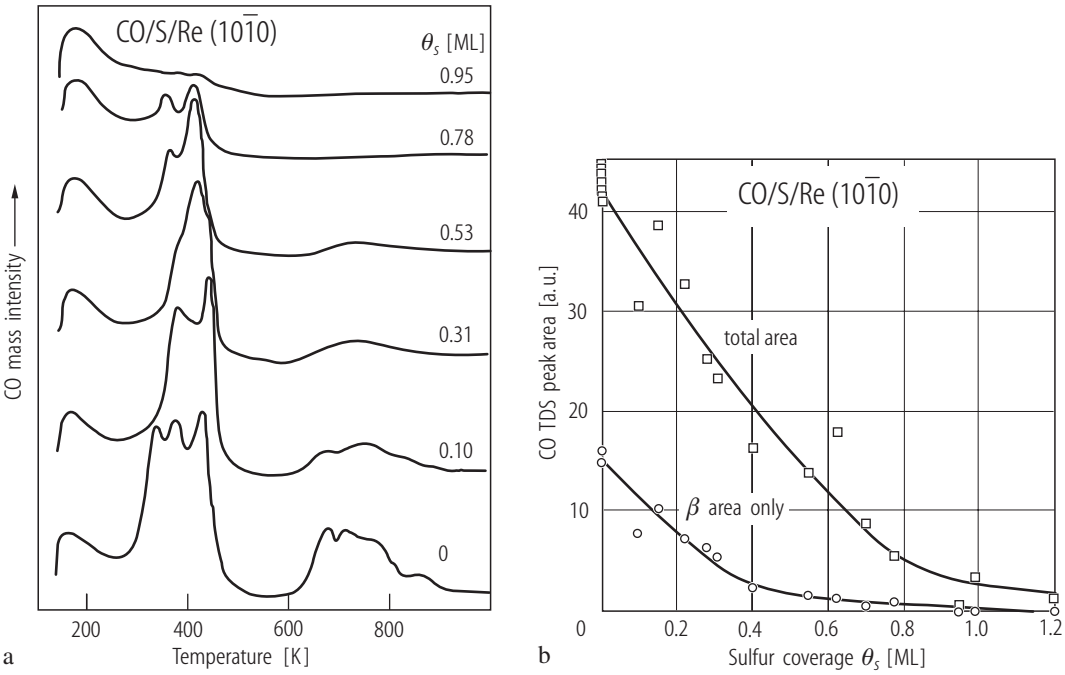

Fig. 44 (a). Thermal desorption spectra of CO for clean and sulfur covered Re(10$\bar{1}$0) surfaces. Initial CO exposure was constant for all traces. **(b).** Relative CO coverage versus sulfur coverage on Re(10$\bar{1}$0) illustrating a "poisoning" effect of S; [88Kel].

Os

A single study of CO adsorption on polycrystalline Os is known [80Fuk1]. Photoemission and desorption studies indicate that CO is molecularly adsorbed on clean Os. A desorption peak at 550 K is recorded. Adsorption of CO on a carbonized Os surface produces a desorption peak at 440 K and different CO photoemission peaks. Spectral data for the latter structure are consistent with molecular adsorption in which the CO axis is nearly parallel to the surface and both C and O are involved in bonding.

3.7.1.5 CO adsorption on simple cubic metal surfaces

Mn

No studies of CO adsorption on well defined poly- or single crystalline Mn surfaces are known. The reactivity of Mn for adsorbed CO can only be estimated from a few studies of CO adsorption on thin films of Mn deposited on carrier crystal surface, such as Fe(110) [93Sie], Ru(001) [87Hrb1, 87Hrb2, 90Hrb, 96Sha], Pd(100) [95Wu], and Cu(100) [99Grü]. At room temperature, Mn grows layer by layer on Ru(001). The first three layers are pseudomorphic with respect to the Ru substrate. At higher coverages, manganese layers adopt a commensurate structure with a ($\sqrt{3}\times\sqrt{3}$)R30° LEED pattern. At coverages of more than 10 layers, the growing layer of manganese becomes disordered. These structures are thermally unstable, and annealing to 700 K transforms them to a 1×1 pseudomorphic structure. A new, higher temperature CO desorption state at 650 - 800 K appears at submonolayer coverages. The indications are that added Mn increases significantly the propensity of CO to dissociate [90Hrb]. Details are briefly reported in the next section on binary systems.

3.7.1.6 CO adsorbed on relevant binary systems, modelled by ultra-thin metal overlayers

The properties of adsorbed CO on some of the binary systems listed in Table 1 are included in the data tables section. Much of the experimental work has been reviewed in several papers [91Rod3, 91Rod4, 92Cam, 92Rod, 93Kuh2]. CO adsorption on compound or alloy systems has also been investigated, such as on surfaces of NbC(111) [92Eda], Pd_3Mn [99Del] and Pt_3Me where Me stands for Ti, Co or Sn [86Pau1, 92Ros]. Because the investigations on thin film bimetallic surfaces are of interest in connection with CO adsorbed on clean metal surfaces, additional results will be briefly presented below.

HREELS and Auger electron spectroscopy (AES) have been utilized to study CO adsorption and dissociation on copper deposited on an Al(111) single crystal [93Col]. Exposing Cu/Al(111), possessing approximately one-half monolayer of copper, to CO produces a species which exhibits a weak vibrational mode with an unusually low CO stretching frequency of 1260 cm^{-1}. The low-frequency CO mode indicates that this species possesses a severely weakened C-O bond. This is verified by thermal CO dissociation upon heating to 348 K indicated by the formation of adsorbed carbon and oxygen on the surface. The thermal instability and the vibrational spectra of the low frequency CO species suggest that the CO is bound in a di-sigma structure, where both the C and O atoms are chemically bonded to metal atoms [93Col].

The vibrational properties of CO adsorbed on fcc Fe(100) thin films, grown at 300 K on Cu(100), were studied using IR reflection absorption spectroscopy [99Tan]. At low exposure only a single C-O stretch band appears at 1920 cm^{-1} which shifts to 1998 cm^{-1} with increasing coverage. At higher exposure a second C-O stretch band is observed at 2020 cm^{-1} which increases in intensity and shifts to 2048 cm^{-1} at high coverage. The initially observed band can be ascribed to the bridging CO and the second band to atop CO. Although the bridging CO was stable up to about 380 K, the atop CO band was less stable and disappeared above 313 K [99Tan].

The adsorption of CO on Fe monolayers on W(110) was studied by thermal desorption, XPS, UPS, work-function and electron-impact measurements [97Nah]. The clean Fe layers deposited/annealed at 90 K and 600 K show very different work functions, but they behave similarly in CO adsorption. The latter is qualitatively similar to clean W(110). CO is molecularly adsorbed at 90 K to a coverage of CO/W = 0.8 - 0.85. Heating leads to desorption of part of the CO with peaks at 320 K for the 600 K Fe layer and 250 and 340 K for the 90 K layer. Also an amount of CO/W = 0.27 converted to dissociated CO, indicated by a shift in the O 1s binding energy from 531.8 eV for virgin CO to 530.1 eV for dissociated CO. UPS spectra of CO for the two Fe layers are very similar and do not differ appreciably from those of CO on W(110). All results indicate that the properties of adsorbed CO on these Fe films are quite similar to CO on W(110) [97Nah].

Adsorption of carbon monoxide on the c(8×2) phase of Mn/Cu(100) at 100 K was studied by means of UPS, work function change measurements, and LEED. Two stages of adsorption can be separated. The first type of molecularly adsorbed CO does not change the substrate structure. No adsorbate-induced superstructure can be observed, and the work function is increased by 0.9 eV. Further adsorption leads to a loss of long range order of the Mn film, and the CO-metal interaction as revealed by UPS is changed, accompanied by a decrease of the work function by 0.16 eV. It is not possible to re-establish the ordered film structure by annealing. No dissociation of CO occurs below 200 K [99Grü].

The interaction of vapor-deposited Mn with the Ru(0001) surface and its effect on CO chemisorption were studied by Auger electron spectroscopy, thermal desorption spectroscopy, isotopic exchange, and LEED [87Hrb2, 90Hrb]. Layer by layer growth of Mn is observed at room temperature. The first three layers are pseudomorphic with respect to the Ru substrate [96Sha]. At higher coverages, Mn layers adopt a commensurate structure with a (√3×√3)R30° LEED pattern. At coverages of more than 10 ML, the growing Mn layer becomes disordered. Disordered and (√3×√3)R30° structures are thermally unstable, since annealing to 700 K transforms them to a pseudomorphic (1×1) structure, together with a large decrease in the Mn/Ru AES ratio. A new, higher temperature CO desorption state at 650 - 800 K appears at Mn coverages of 0.3 - 1 ML. Coadsorbed CO isotopes show random mixing on Mn/Ru which together with the high temperature desorption state is indicative of CO dissociation [90Hrb].

Table 1. CO adsorption studied on model binary metal systems, prepared as a thin film of metal A on an oriented single crystal of metal B. Metal A or B belong to the category of metals reviewed here in context of CO adsorption properties.

Binary system overlayer/ substrate	Maximum coverage of overlayer [ML]	Data in tables (T) or detailed (D) below	References
Co/Mo(110)	1.0 - 5		91He2, 91He3
Cr/Ru(001)	0.1 - 0.5		02Eng
Cu/Al(111)	0.5	D, T	93Col
Cu/Mo(110)			92Kuh2
Cu/Re(0001)	~ 5		91Rod1
Cu/Ru(0001)	~ 40	T	91Rod2, 99Kne1
Cu/Ta(110)			93Kuh1
Fe/Cu(100)	8	D, T	99Tan
Fe/Mo(110)	1.5		90He
Fe/Ru(0001)	2	T	88Ega
Fe/W(110)	1	T	90Ber
Fe/W(110)	1	D, T	97Nah
Fe/W(100)	1		90Ber
Fe/Re(0001)			90He
K/Fe(110)	<0.4	T	79Bro, 92Zhu
Mn/Cu(100)	0.9	D, T	99Grü
Mn/Fe(110)	<2	T	93Sie
Mn/Pd(100)			95Wu
Mn/Ru(0001)	3.5	T, D	90Hrb
Ni/Mo(110)	1.5-6		91Cam, 91He3, 93He
Ni/Ru(0001)	Theory		96Ham
Ni/W(110)			90Rod
Pd/Co(0001)	Theory		98Pic
Pd/Re(0001)	3.1		92Cam
Pd/Ru(0001)	~ 8		92Cam
	Theory		96Ham
Pd/Ta(110)	3	D	90Koe, 93Sel, 95Pic1
Pd/W(110)			90Kuh, 92Kuh2
	Theory		95Pic2
Pt/Co(0001)	0.6	T	00Cab
Pt/Ti(111)	Theory		97Pic
Pt/W(110)	Theory		95Pic2
Re/Pt(111)	3	T	88God
	1.85	T	99Ram
Sn/Ni(111)	~ 1	D	95Xu
Sn/Pt(111)	0.4	D	94Xu
Ti/Nb (poly)	alloy	T	98Yos
Zn/Ru(0001)	1.0	D	93Rod

A study of CO adsorption on Mn/Fe(110) using XPS as a means to distinguish molecular and dissociated CO on the surface provided evidence for the promotion of CO dissociation by Mn [93Sie]. This effect was seen at several Mn coverages. The onset of dissociation could be located at 200 - 300 K, depending on Mn coverage, and was considerably lower than about 380 K observed for clean Fe(110) [79Bro]. The total amount of dissociated CO at 523 K was 14 and 80 % of the initial coverage for clean Fe(110) and Mn/Fe(110), respectively [93Sie].

CO chemisorption properties of Pd monolayers and ultrathin Pd films of various thicknesses on Ta(110) have been investigated using TDS, HREELS and LEED [93Sel]. Using Arrhenius plots constructed from CO desorption data, the activation energies of CO desorption on these films were determined. On the pseudomorphic Pd monolayers with coverages of 0.6 - 1.0, CO desorbs with an activation energy of approximately 63 kJ/mol. This value is in contrast to 150 kJ/mol measured on the bulk Pd(111) surface and indicates a strong alteration in the CO chemisorption properties at low Pd coverage. For Pd films annealed to 550 K, the CO desorption energy increases with the size of the Pd clusters, which form on top of the Pd monolayer. HREELS, used to probe the CO adsorption site on these Pd films, shows that CO adsorbs predominantly in atop sites on the pseudomorphic and the fcc(111) Pd monolayers. A small amount of bridge adsorbed CO is detected which corresponds to CO molecules adsorbed on small Pd clusters. This is consistent with LEED observations which indicate that the fcc(111) structure is reconstructed to the pseudomorphic structure upon exposure to CO [93Sel].

The chemisorption of CO on a Sn-covered Ni(111) surface (Sn coverage 0.33) has been studied with reflection-absorption infrared spectroscopy (RAIRS) and temperature programmed desorption. Formation of the (√3×√3)R30°-Sn/Ni(111) surface strongly suppresses CO adsorption. Only 0.04 ML CO can be chemisorbed on this surface at 110 K, exclusively at atop sites. The binding energy of this adsorbed CO is reduced to only about 43 kJ/mol. Additionally, no significant effect of subsurface Sn on CO chemisorption was observed. These results are in sharp contrast to a previous study of CO chemisorption on the (√3×√3)R30°-Sn/Pt(111) surface [94Xu], where the chemisorbed CO saturation coverage, adsorption site distribution and desorption temperature were quite similar to those of the Pt(111) surface. The kinetics is strongly influenced by Sn, indicative of a modified (physisorbed) precursor state for chemisorbed CO. Whereas the sticking coefficient of CO on clean Pt(111) is about 0.9 at 100 - 300 K, it decreases to 0.2 at 250 K with 0.33 Sn coverage [94Xu]. The influence of Sn on CO chemisorption is ascribed to repulsive Sn-CO interactions. The differences in the chemisorption properties of Pt-Sn and Ni-Sn surface alloys are rationalized by considering the different sizes of the surface unit cells and the location of Sn with respect to the surface plane [95Xu].

The adsorption of CO on Zn/Ru(0001) surfaces has been studied using thermal desorption mass spectroscopy, core and valence level photoemission and Auger spectroscopy. At 80 K, CO does not adsorb on thick Zn films under ultra-high vacuum conditions [90Car, 93Rod]. In contrast, adsorption is observed on Zn atoms bonded to Ru(0001). Bimetallic bonding induces a reduction of approximately 0.5 eV in the binding energy of the core and valence levels of Zn. This shift probably increases the strength of the Zn-CO bond. CO molecules adsorbed on Zn adatoms show an O(1s) binding energy close to 535.2 eV and a desorption temperature of approximately 125 K. Both properties indicate a very low energy of adsorption and a very weak contribution of π-backbonding to the ZnC-O bond. For CO chemisorption on Zn/Ru(0001) surfaces, Zn blocks Ru sites approximately on a one-to-one basis and induces a weakening of the Ru-CO bond [93Rod]. By comparison, CO adsorption on polar ZnO surfaces, either Zn or oxygen terminated, is relatively weak, with adsorption energies between 29 [00Bec] and 52 kJ/mol [80Gay] for both surfaces.

3.7.1.7 Adsorption of N_2 on metals

The nomenclature of adsorbed nitrogen states is traditionally different from that of adsorbed CO. At least four different states have been found, e.g. on Fe(111) [85Tsa, 86Whi1, 86Whi2, 87Fre, 87Gru1, 87Gru2], which are designated as follows (in order of increasing adsorption energy):

δ-state: physisorbed N_2

γ-state: chemisorbed σ-bonded N_2 (oriented vertical to the surface)

α-state: chemisorbed π-bonded N_2 (oriented nearly parallel to the surface)

β-state: atomic nitrogen N.

Depending on the availability of adsorption sites, several sub-states (e.g. of β and γ) may be distinguished. The PES should therefore exhibit at least four different minima, one for each state, with corresponding barriers between them [87Gru2].

Ni

On the Ni(100) surface N_2 adsorbs with the molecular axis normal to the surface (γ state), which leads to two inequivalent N atoms, which have been separated by XPS [90Mar]. Earlier XPS studies mostly focussed on the significant shake-up intensity accompanying the XPS main lines [81Bru, 84Umb, 90Rao]. The valence electronic structure of chemisorbed N_2 has been determined with UPS [81Bru], in particular the c(2×2) structure with UPS [84Dow], and XES [98Ben]. The c(2×2) structure at 0.5 ML coverage has been established by LEED [84Dow, 84Gru3] and the thermodynamic properties as a function of coverage have been determined [84Gru3].

Desorption spectra of N_2 from Ni(111) are shown in Fig. 45, starting at about 22 K, with increasing coverage [86Bre]. At low coverage a chemisorbed N_2 state is occupied first, recognized by the desorption peak at 88 K. This peak shifts to lower temperature with increasing coverage and a second peak at $T = 45$ K indicates a physisorbed N_2 state. Further exposure leads to even another group of peaks at 28 - 30 K which are attributed to a second and third layer of physisorbed N_2 molecules (condensed solid phase) [86Bre]. The peak temperatures of 45 and 85 K correspond to adsorption energies of about 10 and 20 kJ/mol, respectively, based on a first order desorption process and a pre-exponential factor of 1×10^{13} s^{-1}. Heating the N_2 covered surface to 60 - 70 K allows to form a pure chemisorbed phase and thus a separate spectroscopic characterization of both phases.

Vibrational spectra of adsorbed N_2 support the general assignment of physisorbed and chemisorbed attributes to these adsorbed molecular states because the N-N stretch vibrational frequency is almost identical to that of gaseous N_2 for physisorbed N_2 while it is about 130 cm^{-1} lower for the chemisorbed species [92Shi]. On the Ni(111) surface two LEED patterns have been observed. At 0.33 ML coverage a (√3×√3)R30° structure [91Yos] and at 0.5 ML coverage a (2×2) structure [89Qui]. The thermodynamic properties have been determined as a function of coverage [86Bre, 91Yos] as well as the vibrational evolution [89Qui, 91Yos]. The valence electronic structure has been determined with UPS [86Bre, 88Umb, 90Rao] and the N1s core levels with XPS [86Bre, 88Umb].

N_2 adsorption on the Ni(110) surface forms a (1×1) structure between 0 - 0.3 ML coverage above 140 K [83Gru1, 84Gru3], a (2×1) structure at 0.5 ML coverage, a fluid phase between 0.4 and 0.72 ML coverage and a c(1.4×2) at 0.72 ML saturation coverage [80Gol, 83Gru1, 83Jac1, 84Gru3, 88Kuw]. Their thermodynamic properties [80Gol, 83Gru2, 83Jac1, 84Gru3, 88Kuw] and their vibrational behaviour [82Ban, 82Hor, 86Bru, 86Str, 87Bru, 88Kuw, 89Sch] have been determined. The XPS data of adsorbed N_2 on Ni(100) have already been discussed in section 3.7.1.1.3 in context with Figs. 2 - 4 which show N1s core level spectra in detail. These spectra support the perpendicular orientation of N_2 on Ni as well as its relative weak chemisorption. Furthermore, the system at saturation coverage has been investigated with UPS [82Hor, 90Rao] and XPS [80Gol, 90Rao].

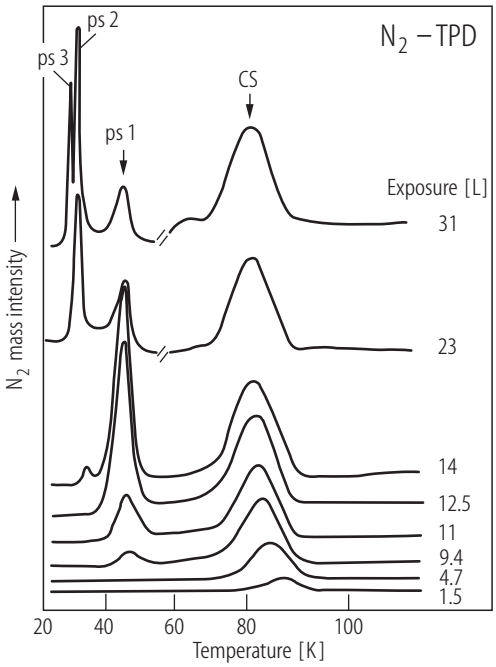

Fig. 45. Thermal desorption spectra of N_2 adsorbed on Ni(111) for different exposures (equivalent to coverages) at 20 K. All peaks shown are due to molecular N_2 labelled ps1-ps3 = physisorbed N_2 , cs = chemisorbed N_2 . Exposures are given in 1×10^{14} molecules/cm^2; [86Bre].

Rh

On Rh surfaces TDS has identified three desorption features [83Hen]. Field emission microscopy indicates structure sensitive adsorption and the activation energies of adsorption have been determined [83Hen].

Pd

Adsorption of N_2 on Pd films [68Kin] and on the Pd(110) surface [87Kuw] has been reported and characterized with TDS. On the Pd(110) surface a (2×1) LEED structure has been observed and vibrational spectroscopy indicates a perpendicular (γ state) orientation [87Kuw]. On the Pd(111) surface, photoemission spectroscopy indicates only physisorption [82Hor].

Ir

Early work using field emission microscopy showed indications of crystal-face specific adsorption of N_2 [83Hen]. On the Ir(100)-(1×1) and the Ir(100)-(5×1) surfaces N_2 adsorption has been studied with IRAS, TDS and LEED [93Gar]. N_2 appears to adsorb in on-top sites without lifting the clean surface reconstruction [93Gar]. On the Ir(111) surface reversible adsorption has been observed with EELS and TDS [90Cor]. The Ir(110)-(1×2) surface has been investigated by XPS, UPS, AES, LEED and TDS [81Ibb]. In particular a p1g1(2×2) LEED pattern has been observed [81Ibb].

Pt

The adsorption of N_2 on the Pt(111) surface originally reported [77Shi2, 79Ris] based on EELS and TDS was in subsequent investigations found to be due to defect sites [96Aru]. Nevertheless, condensed layers of N_2 form ordered structures [00Zep].

Fe

The adsorption of N_2 on Fe surfaces has been studied intensely because of its relevance to the technical catalytic production of NH_3 [80Ert, 81Ert, 85Sto]. The rate of dissociative chemisorption on low-index Fe surfaces is very slow, with the fastest rate reported for the Fe(111) plane [77Boz1, 77Boz2]. This surface behaves differently from other well studied metal surfaces, such as Ru(0001), Re(0001), Ni(100), Ni(111) and W(110). The bcc Fe(111) surface has three differently located surface atoms (A, B and C with 4, 6 and 7 nearest neighbors) and hence there is a variety of adsorption sites. Two different types of chemisorbed N_2 have been detected on this surface, the γ-state being an upright species and the α-state being a π-bonded or at least severely tilted species [82Ert2, 84Gru1, 85Tsa, 86Whi2, 87Fre]. Their desorption temperatures are 110 and 145 - 160 K, respectively, and signify rather different energies of adsorption. The γ-state tends to convert to the α-state of N_2 at 110 K while the latter is known to dissociate to atomic N at T >150 K. Fig. 46 shows a set of adsorption isotherms for the equilibrium between α-state and gaseous N_2 which is evaluated to yield the isosteric heat of adsorption of 31.4 kJ/mol [82Ert2].

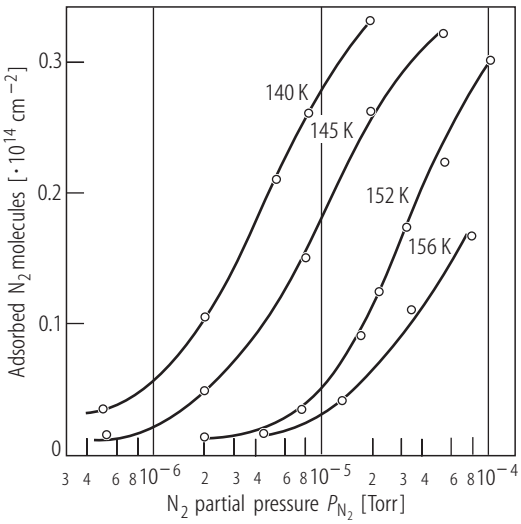

Fig. 46. Adsorption isotherms (N_2 coverage versus pressure) for the equilibrium $N_{2,gas} \Leftrightarrow N_{2,ad}$ (α-state) on Fe(111) [82Ert2]. The isosteric heat of adsorption evaluated from this data is 31.4 kJ/mol.

A theoretical 2D potential energy diagram for N_2 on Fe(111) has been calculated using a LCAO formalism [85Tom]. An interesting result is the region illustrating the transition between γ- and α-states, Fig. 47, with an activation energy of about 20 kJ/mol [84Gru2]. The same figure gives also the N-N stretch vibrational frequencies [84Gru1, 85Tsa, 86Whi2] and heats of adsorption of the two states [87Fre]. Detailed descriptions of molecular and dissociative N_2 adsorption on Fe(111) and the conversion from δ to γ and from γ to α to β state are given in [87Gru1, 87Gru2]. The well depths (heats of adsorption) of the molecular N_2 states are 20.7, 24.5 and 31.4 kJ/mol for δ, γ and α states, respectively. The activation energies for the conversion from δ to γ, from γ to α and from α to β are about 16.6, 18.5 and 28 kJ/mol, respectively [87Gru2]. These are approximate numbers since the actual PES is quite complex because of the additional degrees of freedom of the N_2 molecule.

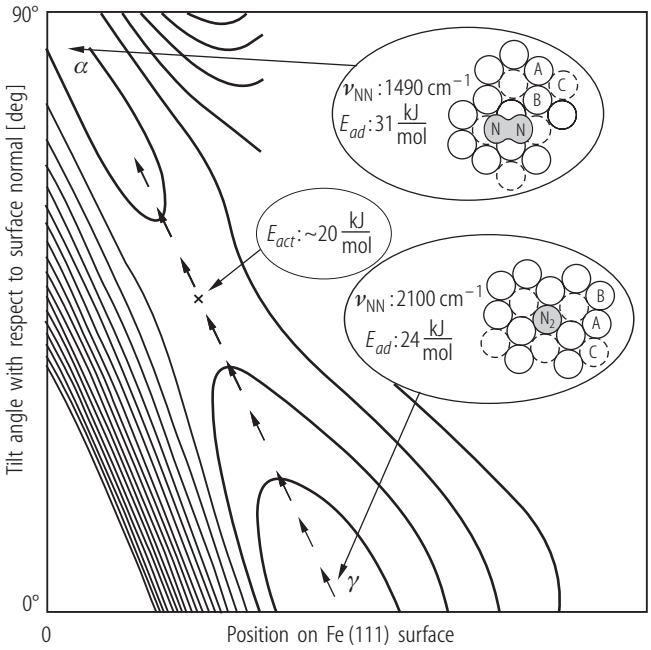

Fig. 47. Schematic two-dimensional potential energy surface for N_2 on Fe(111) [85Tom] illustrating the transition between molecular γ and α states. The insets show the adsorption energies [84Gru2] and vibrational stretch frequencies [85Tsa, 86Whi2] as well as the activation energy of conversion [84Gru2, 87Fre].

Despite the existence of two well defined molecular N_2 chemisorbed states (γ and α), the initial sticking coefficients of dissociative adsorption on Fe(111), Fe(110) and Fe(100) are lower than 10^{-6} at 300 K and above [77Boz1, 77Boz2]. However, the initial rates of adsorption are not equal and were reported as 60:3:1 in the sequence of (111), (100) and (110) [77Boz2]. Increasing the crystal temperature leads to a decrease of the sticking probability, Fig. 48 [87Ret2]. Such a behavior suggests the existence of a molecular precursor state and an activation barrier for the dissociative adsorption of N_2. Increasing the kinetic energy of the incident N_2 molecules greatly enhances sticking, as seen in Fig. 49 for Fe(111) at a surface temperature of 520 K [87Ret1, 87Ret2]. At 100 kJ/mol and above the sticking coefficient is about 0.1, an increase of five orders of magnitude. There is evidence that dissociative adsorption of N_2 on this surface goes via the α-state as precursor since population of this state increases also with increasing kinetic energy of N_2. This behavior is in contrast to N_2 adsorption on W(110) where no precursor seems to be involved [87Ret2]. Additional studies with the adsorption of vibrationally excited N_2 molecules (nozzle heated to 2000 K, 15 % $v = 1$ and 3 % $v = 2$) at higher kinetic energy showed that only a small increase in sticking was observed due to the additional vibrational energy [87Ret1].

The interaction between adsorbed N atoms on Fe(100) has been studied by high resolution STM at 298 K [99Öst]. There is a tendency to form small islands of c(2×2)-N order due to nearest neighbor repulsion and next-nearest neighbor attraction. These interactions are quantitatively assessed by the technique of configuration distribution analysis [99Öst]. The effect of coadsorbed alkali metals on N_2 adsorption on Fe surfaces has also been studied [82Ert1, 85Tsa, 86Whi2, 88Rao]. Altered adsorption sites and enhanced dissociative adsorption rates, coupled with changes of the adsorbed molecular precursor state, have been observed. In this context, the rate of ammonia synthesis by promoted Fe, for which the dissociative adsorption of N_2 was found to be most important, is also increased considerably [86Bar1, 88Str]. In this context it is of interest to draw attention to a study of N_2 adsorption on Cr-Fe alloys of (110) orientation [88Dow]. The initial sticking coefficient of N_2 on Cr(110) is very high compared to that on Fe(110). On the $Fe_{72}Cr_{28}$(110) alloy N_2 sticking is considerably impeded whereas surface Cr forms some nitride phase.

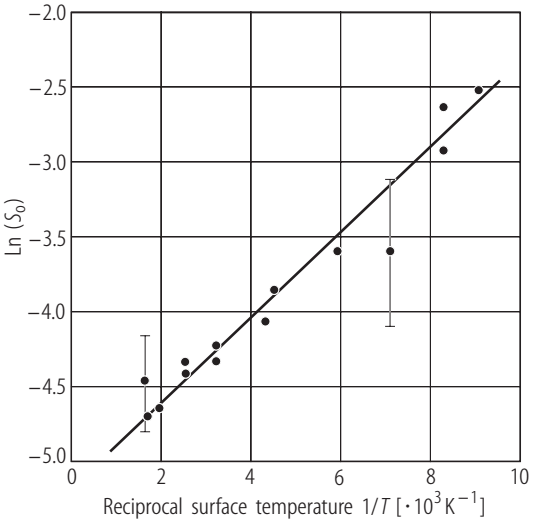

Fig. 48. Log-plot of initial sticking coefficient S_0 of dissociative N_2 adsorption on Fe(111) versus reciprocal surface temperature, at normal incidence and a kinetic energy of N_2 of 1.05 eV; [87Ret2].

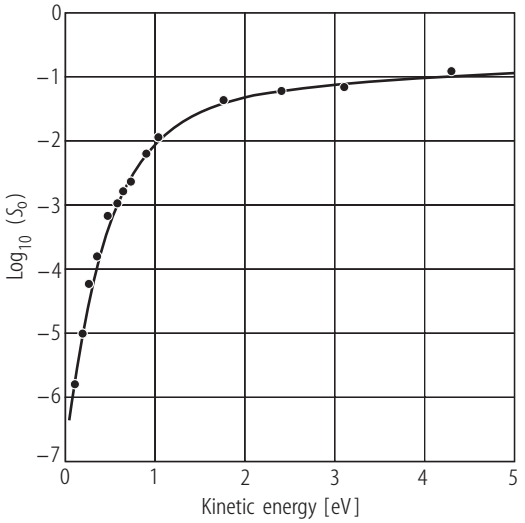

Fig. 49. Initial sticking coefficient S_0 of dissociative N_2 chemisorption on Fe(111) versus kinetic energy of incident molecules at normal incidence and a surface temperature of 520 K; [87Ret2].

W

Historically, one of the first extensive investigations of N_2 adsorption on well defined surfaces was carried out on (110), (100) and (111) planes of tungsten [61Ehr1, 61Ehr2, 62Ehr1, 65Del, 88Ehr]. This work was also the first clear demonstration of structure sensitivity in adsorption. Adsorption at 300 K was mostly dissociative on W(100) and W(111) (β-state, heat of adsorption about 315 kJ/mol) [65Del] but no sticking was observed on W(110) [79Bes, 79Pol, 82Liu]. A unique quantitative demonstration of the structure sensitivity of N_2 adsorption in the vicinity of the W(110) orientation was carried out by Besocke et al. who studied a W(110) single crystal which exhibited a central region of ideal (110) and four vicinal regions, Fig. 50, two tilted toward the (100) face having steps running in [001] direction, and two tilted towards the (112) face having steps running in $[\bar{1}10]$ direction [79Bes]. Tilt angles were 10° and 5° in each case. The step densities of the vicinal orientations varied between 8×10^6 cm^{-1} and 4×10^6 cm^{-1}. Exposing this crystal to N_2 at 300 K showed that no adsorption could be detected on the (110) surface (step density $<2\times10^5$ cm^{-1}) but significant amounts on the vicinal surfaces. On the latter the amount was proportional to the step density (or the number of step sites), see Fig. 50 [79Bes]. Once the step sites were filled, adsorption came to a halt. At elevated temperature of 920 K, filling of the terrace sites occurred by diffusion of atomic N from the step sites.

A weakly bound γ-state on W(110) and W(100) was found at lower temperatures of 100 - 130 K, with an estimated heat of adsorption of 38 kJ/mol [65Del]. This γ-state was thought to be atomic. It was later identified as a molecular state [79Fug]. The situation for the W(111) plane was more complicated because adsorption/desorption at 110 - 220 K provided evidence for three nitrogen states: γ, α and β (in the sequence of increasing desorption temperatures). The α-state was suggested to be molecular N_2 based on its dipole moment [65Del]. The heats of desorption were 38, 67 and 314 kJ/mol for γ, α and β-states from W(111), respectively. The α-state, typical for the (111) orientation, has also been found on polycrystalline tungsten [62Ehr2]. This early work proved to be pace-setting for all later studies of N_2 adsorption on metal surfaces. Spectroscopic investigations of N_2 adsorption on tungsten single crystal surfaces clarified to a large extent the nature of the various adsorbed states (see Tables).

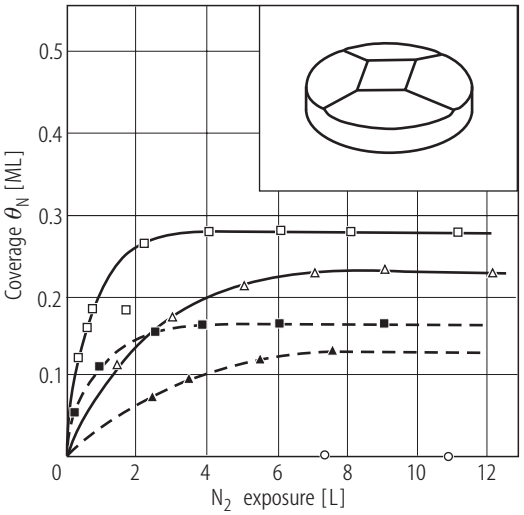

Fig. 50. Plot of nitrogen coverage versus exposure for dissociative adsorption of N_2 on W(110) (**O**) and four vicinal W surfaces at room temperature [79Bes]. Symbols for the vicinal surfaces: □ steps parallel to [001], 10° miscut; ■ steps parallel to [001], 5° miscut; Δ steps parallel to $[\bar{1}10]$, 10° miscut; ▲ steps parallel to $[\bar{1}10]$, 5° miscut.

Ru

A comprehensive study of the coverage dependence of the heat of adsorption/desorption, pre-exponential factor and sticking coefficient of N_2 on Ru(0001), analogous to CO on the same surface [83Pfn1, 83Pfn2], has been carried out by Menzel et al. [83Men]. The results are summarized in Fig. 51. There are essentially three coverage regimes to be noted: in the first regime up to $\theta = 0.16$, the heat of adsorption is 38 - 42 kJ/mol, with a pre-exponential factor of 2×10^{14} s^{-1}, and the sticking coefficient at 0.38; the second regime is characterized by an increase in the adsorption energy, pre-exponential factor and sticking coefficient; in the third regime all quantities are observed to drop to much lower values. Regime 1 is a pure phase of chemisorbed N_2 (γ-state), regime 2 a mixture of chemisorbed and physisorbed N_2 (δ-state), and the adorption/desorption data in regime 3 are dominated by the physisorbed N_2 which has a significantly lower heat of adsorption. The sticking coefficient data are separated into γ and δ parts. A pure physisorbed phase can not be obtained.

The dissociative adsorption of N_2 on Ru(0001) has been widely studied [00Jac]. Initial reports of low sticking at 300 K were confirmed by more recent investigations [96Die, 99Dah]. The presence of an activation barrier to dissociative adsorption, suspected on the basis of low sticking coefficients, was confirmed by checking the kinetic energy dependence of sticking [97Rom]. An increase in kinetic energy up to 4 eV caused an increase in the sticking coefficient of more than four orders of magnitude. Dahl et al. measured the sticking coefficient of N_2 dissociative adsorption on Ru(0001) as a function of substrate temperature, Fig. 52, and found an increase with rising temperature, equivalent to an activation energy of 39 kJ/mol [99Dah]. The sticking coefficient at room temperature was about 2×10^{-12}, in good agreement with Dietrich et al. [96Die]. To find out whether residual steps on the surface were more active than the perfect terrace, they deposited a small amount of Au onto this crystal. Au is known to diffuse to and bind at the step sites, making these sites inactive for N_2 dissociation. As a result, the measured sticking coefficient of N_2 dropped by more than seven orders of magnitude (at 500 K), suggesting the clean Ru(0001) terraces to be even more inert towards N_2 dissociation than hitherto believed [99Dah]. A density functional calculation of the activation barriers for N_2 dissociation at terrace and step sites, shown in Fig. 53, supports the experimental results. The dynamics of collision-induced desorption (CID) of molecular N_2 from Ru(0001), exposed to hyperthermal rare gas colliders generated in a supersonic atomic beam source, have been studied [98Rom]. As a non-thermal desorption process, however, it will not be discussed here.

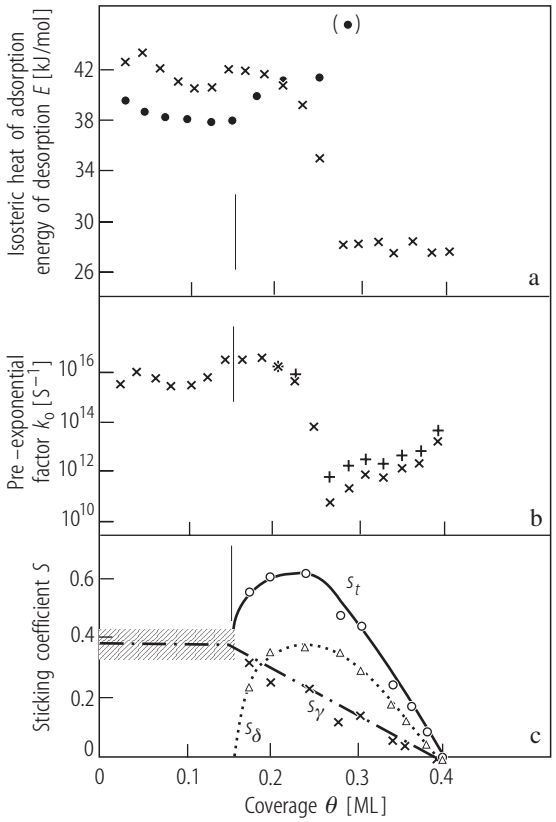

Fig. 51. Low temperature adsorption of N_2 on Ru(0001): Coverage dependence of (a) isosteric heat of adsorption (x) and energy of desorption (•), (b) pre-exponential factor of desorption, (c) sticking coefficients into physisorbed δ and chemisorbed γ molecular N_2 states. s_t is the total sticking coefficient; [83Men].

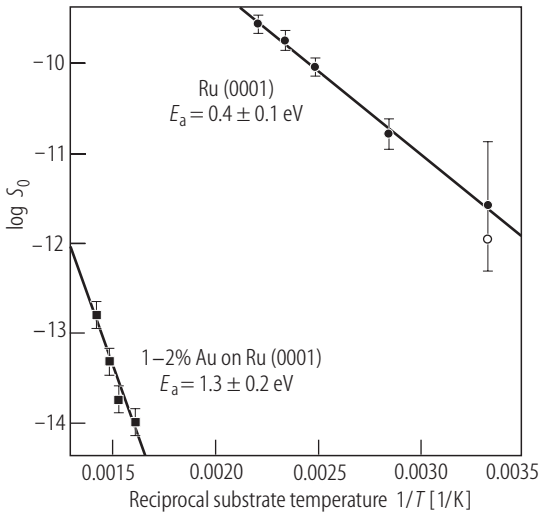

Fig. 52. Initial sticking coefficient of dissociative adsorption of N_2 on clean and Au-covered Ru(0001) as a function of reciprocal substrate temperature [99Dah]. The Au coverage of 1 - 2 % is so low that only residual step sites are believed to be occupied. Activation energies of adsorption are obtained from the slopes. The open cicle is a separately measured point at room temperature; [96Die].

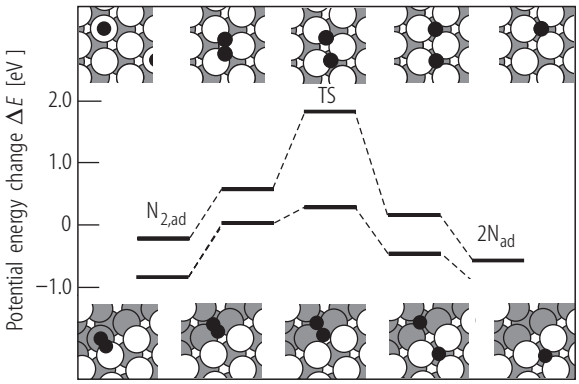

Fig. 53. Results of a density functional calculation of potential energies of adsorbed N_2 on Ru(0001) in its molecular state, transition state (TS) and dissociated state, 2N. The upper curve represents the dissociation on a flat terrace, while the lower curve is the result of a similar calculation for a step site. Configurations are shown in each case. Note the large differences in activation barrier of dissociation; [99Dah].

Re

Similar to iron, rhenium is a very active catalyst for ammonia synthesis [82Spe1, 82Spe2, 84Ass, 87Haa1, 87Haa2]. Adsorption of N_2 on various Re surfaces was shown to be structure sensitive [87Haa1] and a corresponding striking structure sensitivity was demonstrated for ammonia synthesis at 870 K where a ratio of 1:50:1700 was found for the (0001), $(10\bar{1}0)$ and $(11\bar{2}0)$ orientations of Re, respectively [84Ass]. The small activity of Re(0001) was even attributed to the edges of the crystal. Indeed, a very low sticking coefficient of about 10^{-5} for N_2 has been reported at 300 K on Re(0001) [76Liu, 91Por]. A strong increase in the dissociation probability was found with increasing kinetic energy of incident N_2 molecules, such as shown in Fig. 54 [91Por]. This behavior could be well reproduced by a quantum mechanical calculation assuming an activation barrier for N_2 dissociation [90Hen, 91Por].

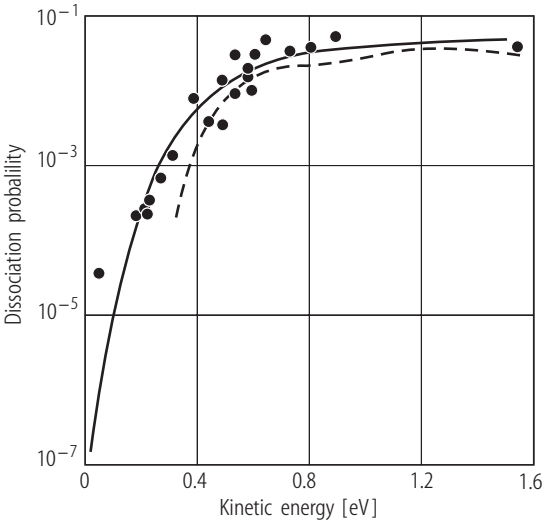

Fig. 54. Plot of dissociation probability (sticking coefficient) versus translational kinetic energy of incident N_2 on Re(0001) at a surface temperature of 300 K [91Por]. The points are experimental data and the solid line is obtained theoretically for the v=0 state. The dashed line represents a calculation for the v=1 state, at a fixed total energy.

Activated dissociative adsorption

Many investigations show that there is substantial evidence for activated dissociative chemisorption of N_2 on close-packed surfaces of metals, e.g. on Fe(110) [77Boz1, 77Boz2], Ru(0001), [96Die, 97Rom, 99Dah], Re(0001) [76Liu, 82Liu, 90Hen, 91Por], W(110) [65Del, 71Tam, 75Sin, 76Yat2, 81Cos, 84Lee, 86Pfn] and possibly Mo(110) [72Mah, 88Ehr]. These systems are characterized by low initial sticking coefficients, such as shown in Table 2, but also by a strong dependence of the adsorption rate on incident kinetic energy and even incident angle of N_2 molecules. Low sticking coefficients can only be measured reliably, if the presence of pre-dissociated N_2 in the gas phase, e.g. due to interaction of N_2 with hot tungsten filaments in a vaccum chamber [93Shi, 96Die], can be ruled out. In the particular case of Ru(0001), this effect caused a difference in the initial sticking coefficient of six orders of magnitude [96Die]. Experiments on Ru(0001) have demonstrated [99Dah] that a relatively higher rate of adsorption at step sites can be sufficient to cause an overall measurable rate of adsorption, even if the ideal step-free surface may possibly not be able to dissociate any N_2. Similar effects had been noted on a Re field emitter tip of (0001) orientation where no adsorption of N_2 took place on the perfect (0001) terrace as long as the temperature stayed between 300 and 550 K [68vOs, 76Liu]. At higher temperature the terrace was filled with atomic N via surface diffusion from the vicinal range.

Table 2. Activated dissociative adsorption of N_2 on densely packed surfaces.

Substrate	Crystal structure	Initial sticking coefficient	Temperature [K]	Activation energy of dissociation [kJ/mol]	References
Fe(110)	bcc	$<1 \times 10^{-7}$	508	~ 29	77Boz2
Mo(110)	bcc	0.09	300		72Mah, 82Liu
Re(0001)	hcp	$<1 \times 10^{-5}$	300		76Liu, 82Liu
		9×10^{-6}	218	14±2	87Haa1
		4×10^{-5}	830	58±14	91Por
Re(0001)			theory	73	88Ass
Re(0001)			theory	55-167 site dependent	90Hen
Ru(0001)	hcp	1×10^{-12}	300	39	96Die, 99Dah
Ru(0001)/Au		1×10^{-17}	500	126	97Jac, 99Dah
Ru(0001)	hcp		theory	135-183	98Mor2, 99Dah
				212	97Rom
W(110)	bcc	0.004	300		71Tam
		0.003	800	41-92	84Lee, 86Pfn

Angle-resolved desorption of N_2 from W(110) showed a non-cosine distribution, Fig. 55, indicative of an activation barrier for dissociative adsorption [81Cos]. Molecular beam studies with variable translational energy of impinging N_2 molecules on W(110) have shown that the coverage and hence the sticking coefficient for dissociative adsorption rises with increasing kinetic energy [84Lee, 86Pfn]. A series of uptake curves of nitrogen taken for several kinetic energies up to about 100 kJ/mol are presented in Fig. 56 [84Lee]. Different binding states of nitrogen are being populated as the incident kinetic energy rises. This is best seen by the TDS traces of nitrogen with increasing coverage, Fig. 57, one set at low (4.2 kJ/mol) and one at high kinetic energy (104 kJ/mol). The corresponding dependence of the initial sticking coefficient versus the incident N_2 energy is given in Fig. 58 [84Lee]. A second investigation of this kind also measured the adsorption rate at various incident angles relative to normal; the results are summarized in Fig. 59 [86Pfn]. In all of these studies the initial sticking coefficient of N_2 for nearly thermal beams is 0.003. A rapid increase in sticking coefficient (note logarithmic scales) sets in at kinetic energies above 40 kJ/mol. The maximum activation barrier for dissociative adsorption was derived from the data at normal incidence, Fig. 60, and is found to be 92 kJ/mol [86Pfn]. Realistically, one expects a distribution of activation barriers of a width of about 50 kJ/mol. Hence the maximum activation energy is higher than the values given before [81Cos, 84Lee]. The finding of activated N_2 adsorption on the close-packed W(110) surface is an example for the structure sensitivity of adsorption, because the variation of the sticking coefficient with coverage for various other tungsten single crystal surfaces, summarized in Fig. 61, illustrates the rather unique behavior of the (110) plane [75Sin].

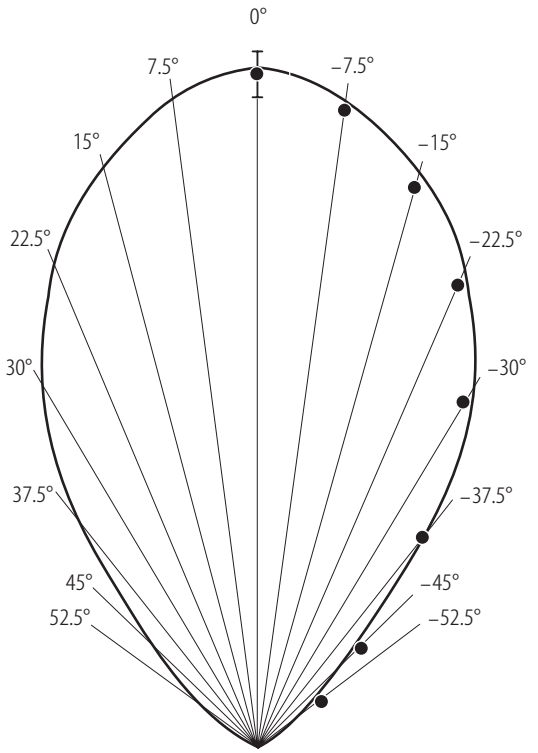

Fig. 55. Angle-resolved intensities of desorbing N_2 molecules from a N covered W(110) surface, where the peak temperature of desorption is 1560 K. The non-cosine distribution is consistent with an activation energy of adsorption of 17.4 kJ/mol. The full line is the calculated desorption flux distribution based on this activation energy; [81Cos].

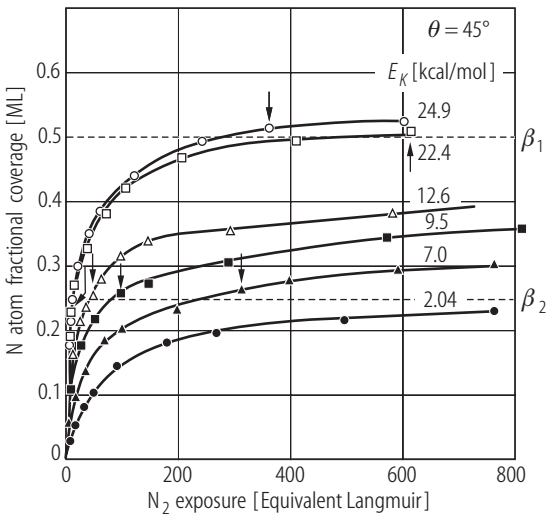

Fig. 56. Uptake curves of N coverage versus N_2 exposure on W(110) for various kinetic energies of the incident N_2 beam, with the surface temperature at 820 K. The sticking coefficient and total amount of adsorbed N increase with higher kinetic energy; [84Lee].

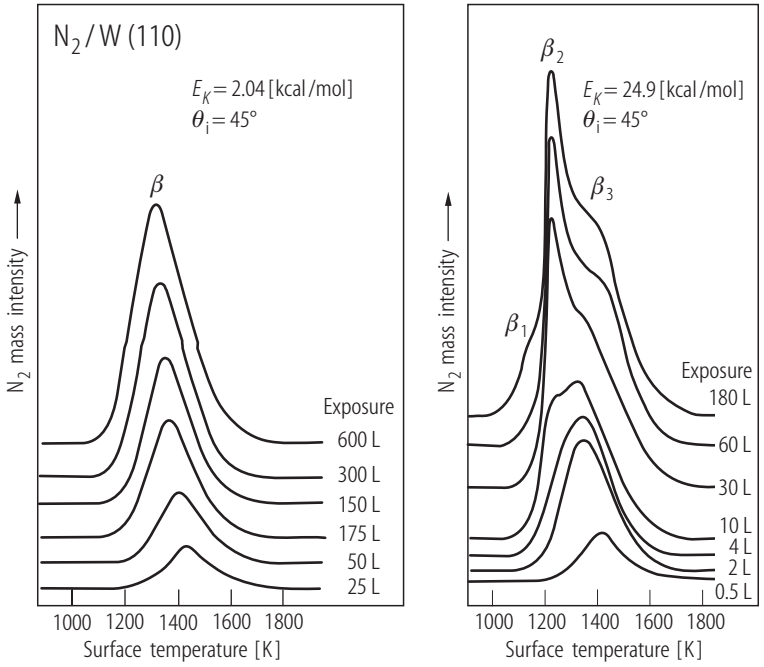

Fig. 57. Thermal desorption spectra of N_2 from a N covered W(110) surface as a function of exposure (coverage) for two different kinetic energies of the incident N_2 molecular beam, angle of incidence 45°. (a) E_k = 8.54 kJ/mol, (b) E_k = 104 kJ/mol; [84Lee]. Note the occupation of several β-states for the higher incident kinetic energy.

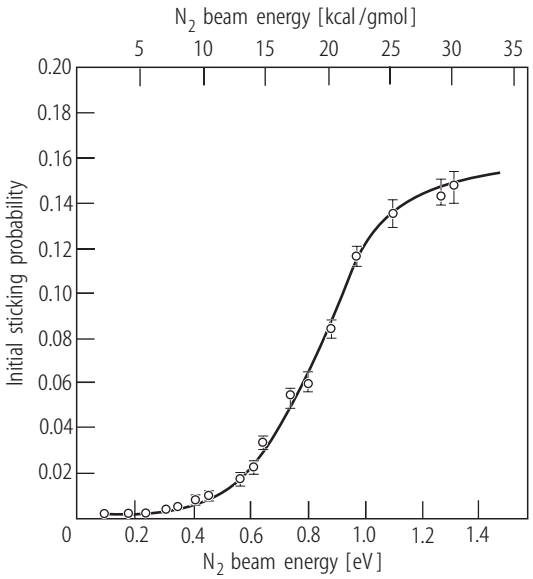

Fig. 58. Initial sticking probability of dissociative N_2 adsorption on W(110) as a function of N_2 kinetic energy at 45° incidence; [84Lee]. The sticking coefficient at thermal energies was 0.0035.

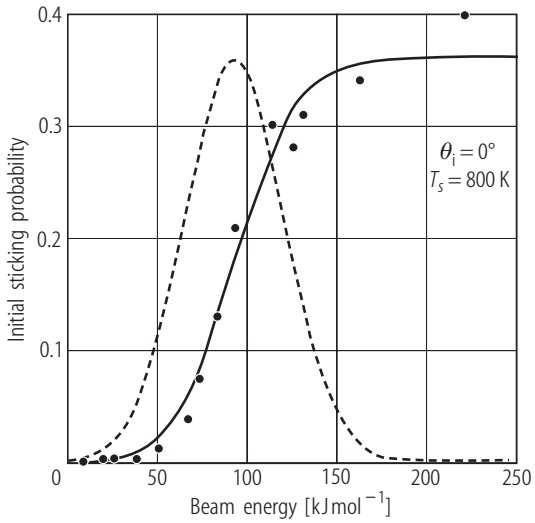

Fig. 60. Initial sticking coefficient of dissociative N_2 adsorption on W(110) versus kinetic energy of incident molecules for normal incidence and a surface temperature of 800 K. The dashed curve represents a Gaussian barrier height distribution corresponding to the probability of molecules dissociating at a given incident energy; [86Pfn].

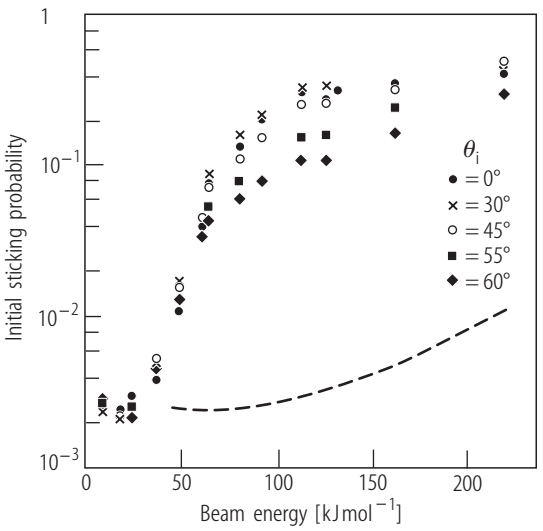

Fig. 59. Log-plot of initial sticking coefficient of dissociative N_2 adsorption on W(110) versus kinetic energy of incident molecules for angles of incidence between 0 and 60°, with the surface temperature at 800 K. The dashed line indicates the predicted behavior for 60° incidence, based on normal energy scaling of the 0° data; [86Pfn].

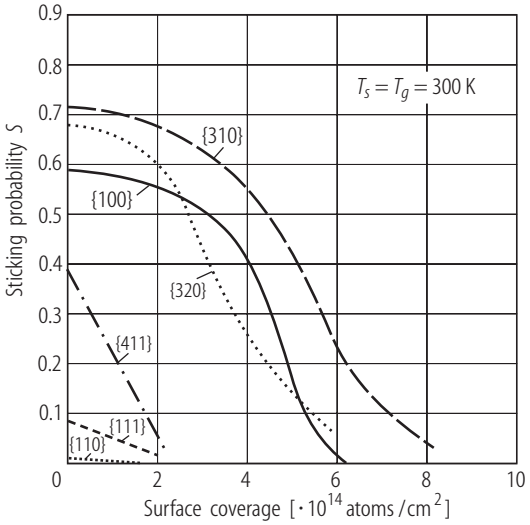

Fig. 61. Structure sensitivity of N_2 adsorption: Comparison of sticking probabilities for dissociative N_2 adsorption on various tungsten single crystal surfaces at room temperature. The lowest sticking coefficient is found for the densely packed W(110) surface while the highest is observed for the open (310) and (320) faces; [75Sin].

Adsorption of N_2 on W(100) is apparently also activated because the initial sticking coefficient decreases strongly with increasing surface temperature above 300 K [83Aln]. The experimental data could be modelled by assuming a molecular precursor state which traps N_2 molecules prior to their dissociation. The latter rate is competing with desorption from the precursor state. A difference in activation energies for desorption and adsorption into the dissociated state was found to be 18 kJ/mol [83Aln]. A study of the angular velocity distribution of N_2 molecules scattered from the W(100) surface has shown that the trapping probability into the precursor state is nearly independent of surface and beam temperatures, and thus confirmed the earlier interpretation of measured dissociative sticking coefficients [88Ret].

The situation for N_2 adsorption on Cr(110) seems to be unresolved. Although molecular N_2 states exist at low temperature [90Shi, 91Dow], one of them a π-bonded species serving as a possible precursor state to dissociation [90Shi], there are insufficient data on the rate of dissociative adsorption as a function of temperature or kinetic energy of incident molecules [84Miy], to decide on the existence of an activation barrier. The high propensity for forming a stable chromium nitride seems to enhance sticking. No detailed study of the influence of steps on the rate of dissociative adsorption is known.

Finally it is worth noting that the gas phase reaction of N_2 molecules with metal nano-clusters of varying sizes has been studied for for Mo, Nb, V and W [95Mit, 96Mit, 98Ber, 98Hol, 99Hol]. Molecular as well as dissociative adsorption on these clusters has been found.

3.7.1.8 Organization of the tables

The collected data related to physical and chemical aspects of adsorbed CO and N_2 on metal surfaces are presented in a total of 13 tables. The content of these tables is as follows:

Table 3: CO adsorption, thermodynamic properties (2D ordered structures; coverage; heat of adsorption; activation energy and pre-exponential factor of desorption; initial sticking coefficient)

Table 4: Adsorbed CO dissociation parameters (adsorbed state, coverage; temperature, pre-exponentail factor and activation energy of dissociation; desorption temperature of state)

Table 5: Crystallographic and vibrational data of adsorbed CO (frequencies; adsorption site)

Table 6: Adsorbed CO (low frequency vibrational data by EELS, TEAS [2003Gra] and IETS [2002Ho])

Table 7: Additional structural data of adsorbed CO (2D ordered structure; coverage; adsorption site; Me-C and C-O bond lengths; tilt angle of CO)

Table 8: Electronic structure of adsorbed CO (MO valence levels in eV)

Table 9: Core level spectroscopic data of adsorbed CO (C1s and O1s binding energies; chemical state of CO)

Table 10: Thermodynamic properties of adsorbed N_2 (2D ordered structures; coverage; heat of adsorption; activation energy and pre-exponential factor of desorption; initial sticking coefficient)

Table 11: Adsorbed N_2 dissociation parameters (adsorbed state, coverage; temperature, pre-exponentail factor and activation energy of dissociation; desorption temperature of state)

Table 12: Crystallographic and vibrational data of adsorbed N_2 (frequencies; adsorption site)

Table 13: Additional structural data of adsorbed N_2 (2D ordered structure; coverage; adsorption site; Me-N and N-N bond lengths)

Table 14: Electronic structure of adsorbed N_2 (MO valence levels in eV)

Table 15: Core level spectroscopic data of adsorbed N_2 (N1s binding energies)

Table 3. CO adsorption (thermodynamics)

Substrate	Structure	Coverage of adsorbate	Heat of adsorption E_{ad} [kJ/mol]	Technique	Activation energy of desorption E_d [kJ/mol]	Pre-exponential factor ν_d [s^{-1}]	Sticking coefficient $s(\theta)$	Temperature of desorption [K]	References
Ag(111)	Disordered		27.2	TDS		1×10^{13} ass.			76McE1
Ag(110)	Disordered		27.2	TDS		1×10^{13} ass.			76McE1
Al(111)		~1		Desorpt. Rate vs. $1/T$;	~20	1×10^{13} ass.		<40	80Chi, 89Jac
			22.1	Theory					83Bag
			47.3	Theory					96Ham
Al(100)				TDS	33	1×10^{14} ass.			86Pau3
Au(110)	Disordered		below 33.5			1×10^{13} ass.			87Out
Co(0001)			128 → 96	Isotherms					83Pap
	(√3×√3)R30°	1/3		TDS	103±8	1×10^{13} ass.			77Bri
	(√7×√7)R19.2°	0.59							
	(2√3×2√3)R30°	7/12							83Gre
Co(10$\bar{1}$0)	p(2×1)	0.5	145	Isotherms					82Pap
	c(2×1)	1.0	decr. to 120						
				TDS	~92	2×10^{13}			84Hab
Co(10$\bar{1}$0)	p(2×1)	≤ 0.5		TDS	110.7	3.1×10^{13}	0.89	~400 α_2	96Too
	(2×1)p2mg	1.0			105	2×10^{13}		~340 α_1	
	c(2×6)	>1.0						600 β	
Co(10$\bar{1}$2)	(3×1)								78Pri
Co(10$\bar{2}$0)	(3×1)	2/3	143	Isotherms					85Pap
Cr(110)	c(4×2)	0.25 α_1					≈0.9-0.4 coverage dependent		84Shi, 85Shi3, 86Shi
		≥ 0.3 α_2							

Substrate	Structure	Coverage of adsorbate	Heat of adsorption E_{ad} [kJ/mol]	Technique	Activation energy of desorption E_d [kJ/mol]	Pre-exponential factor ν_d [s^{-1}]	Sticking coefficient $s(\theta)$	Temperature of desorption [K]	References
Cu(100)	c(2×2)	0.5							
	c(7√2×√2) R45°	0.57							
		0-0.1	69	Isosteric heat		1×10^{13} ass		300	72Tra1
		0.1-0.5	56	LEED, $\Delta\phi$					
		0.5-0.6	53						
		0-0.6		Laser, TDS	65-40	10^{16}-10^{13}			83Bur
				TREELS		$10^{-15\pm1}$			86Dub
		0		TDS, EELS	55.27 ± 1.26	$10^{-15.3\pm0.4}$			90Pet,
		0-0.15	69.9-60.8	Isosteric heat					91Pet2
		0.15-0.35	60.8	IRAS					92Tru
		0		Opt. Refl.,			0.85 at		
		0-0.57		TDS	51		110 K		96Dvo,
							0.85-0.1		00Dvo
Cu(111)	(√3×√3)R30°	1/3		TDS, MB			0.70	148/168	99Kne2
				TDS				148/168	86Kir
			50	IRAS					79Hol
			44.2	AES, LEED,	45				77Kes
				EELS, TDS				127	99Kne2
	(1.5×1.5) R18°	0.44	50	LEED, UPS					75Con
			35.1	AES, LEED,					77Kes
				EELS					
	(1.39×1.39) hex			TDS	34			127	86Kir
		0.52		TDS			0.87	112	99Kne2
		0-0.4	53.6	MB		3×10^{15}			
		0-0.25		TDS		1×10^{15}	0.9±0.1		90Hin

Substrate	Structure	Coverage of adsorbate	Heat of adsorption E_{ad} [kJ/mol]	Technique	Activation energy of desorption E_d [kJ/mol]	Pre-exponential factor ν_d [s^{-1}]	Sticking coefficient $s(\theta)$	Temperature of desorption [K]	References
Cont'd.		0-0.3		TDS		2×10^{14}			86Kir
		>0.35		TDS	40				
		0-0.33	50	IRAS	26				79Hol
		0.33-0.52	38	IRAS					
Cu(110)		0	54.8-58.6	TDS				215	73Wac
		0.1-0.5	57-38	TDS				205-215	92Chr
		0		TDS, EELS	50.24 ± 4.18	$10^{-13.6 \pm 1.0}$		210	91Pet2
		0-0.5		TDS,	53-42	10^{13} - 2×10^{9}	0.46	205-220	85Har
		0-1		MB	52	1×10^{13} ass.	0.95±0.05	215	01Kun
		0.2-0.6		Opt. Refl.,TDS	75-50	10^{18} - 10^{12}	1-0.25	215	96Jin
		0-0.77	55	TDS				205-220	77Hor2
Fe(110)		0.38		TDS			0.8	400-405 α	79Bro,
		α			96	1×10^{13} ass.	0.85	800 β	81Yos
		β			134-201	1×10^{-2}	0.08		82Gon,
									83Wed
Fe(100)		0.5 ML C	77±4	Isosteric heat					85Vin
		0.25 ML C,O	100±5	TDS					
		α_1-states			60-105	1×10^{13} ass.			80Ben
		β			220				
Fe(100)		α_1		TDS	53.6	1×10^{13} ass.		220	87Moo1,
		α_2			75.4			306	87Moo2,
		α_3			109.7			440	89Lu
		β						820	
Fe(111)		α_1		TDS	88	1×10^{13} ass		340	84Sei,
		α_2			105			420	85Sei

Substrate	Structure	Coverage of adsorbate	Heat of adsorption E_{ad} [kJ/mol]	Technique	Activation energy of desorption E_d [kJ/mol]	Pre-exponential factor ν_d [s^{-1}]	Sticking coefficient $s(\theta)$	Temperature of desorption [K]	References
Cont'd.		β			209			(700) 820	
Fe(111)		α_0		TDS				~250	86Bar2
		α_1			91	$\sim10^{17}$		~340	89Whi
		α_2						~395	
		β			137	$\sim10^{13}$		~760	
Ir(111)	(√3×√3)R30°	1/3	146.5±0.4	Isosteric heat		2.4×10^{14} ass.	~1	150-300	76Com1
		1/3	113.0-132.7	Isosteric heat		1×10^{13} ass.	1-0.7	450-525	76Com2
		1/3		LEED/UPS		2.4×10^{14} ass.	$(1-\theta)^2$	533	78Zhd
		1/3 =	142.4	TDS		2.4×10^{14} ass.			76Küp
	(2√3×2√3)R30°	5.2×10^{14} cm^{-2}	141.5±2.1	Isosteric heat		2.4×10^{14} ass.			76Zhd
		5.2×10^{14} cm^{-2}	125.6±0.4						78Tay2
		7/12 =				2.4×10^{14} ass.			76Küp
		9.1×10^{14} cm^{-2}	133.9	TDS					76Zhd
		7.1×10^{14} cm^{-2}	139.0±2.1	Isosteric heat		2.4×10^{14} ass.	0.065	423	
		4.0×10^{14} cm^{-2}	142.8±2.1	Isosteric heat		2.4×10^{14} ass.	0.5	465	
		2.1×10^{14} cm^{-2}	154.5±2.1	Isosteric heat		2.4×10^{14} ass.	0.87	520	
		from θ=0 to θ = 0.7		TDS	175-110	2×10^{15}		380-450	97Sus1
Ir(110)	(2×2)	0.25	154.9	Isosteric heat	113.0			448	73Chr
		(0.9-1)*1/4 coverage θ		TDS/AES/ LEED	123.5	1×10^{13} ass	<1	433, 503, 613	78Nie
		$0<\theta<0.75$		Isosteric heat	146.5 – 67 θ	1×10^{13}-	1-0.8		78Tay1
	(4×2)	θ=0			154.9	1×10^{9}	1.04±0.05		
		0.75			83.7	1×10^{13}	0.8		
		variable θ		TDS	146.5±8	1×10^{9}		600	89Mar

Substrate	Structure	Coverage of adsorbate	Heat of adsorption E_{ad} [kJ/mol]	Technique	Activation energy of desorption E_d [kJ/mol]	Pre-exponential factor ν_d [s^{-1}]	Sticking coefficient $s(\theta)$	Temperature of desorption [K]	References
Cont'd.		8 kJ/mol to 142.4 kJ/mol		MB, variable beam energy			0.8 0.35		87Ste
Mo(100)		α		TDS				220-300	73Lec,
		β_1			260	1×10^{13} ass.			73Vis,
		β_2			328				80Ko2
		β_3			357				
Mo(100)		β-states		TDS	280-357 coverage dep.	1×10^{13} ass.		490 1030 1290	78Fel
Mo(100)		α_1		TDS	54	1×10^{15} ass.		150	85Zae
		α_2			96			290	
		β_1			264	1×10^{-2} and		840	
		β_2			293	2^{nd} ord. ass.		940	
		β_3			389			1250	
Mo(110)		β_1	0.28	TDS	209	1×10^{10}			77Gil
		β_2	0.21		414	1×10^{19}			
Ni(100)	c(2×2)	0.5	125.6	Isosteric heat		1×10^{13} ass.			72Tra2
		0.5		TDS	138.6	1×10^{13} ass.		450	83Koe1
	p(3√2×√2)R45°	0.67	121.4	Isosteric heat		1×10^{13} ass.			72Tra2
		0.67		TDS, IRAS	22	10^5			95Vas
	c(5√2×√2)R45°	0.6		TDS, IRAS	70	10^{13}			
		0-0.6	126-112	SIMS, isosteric heat		1×10^{13} ass.			79Bor
			40.6	TDS		1×10^{13} ass.		170 α_0	80Yat
			58.2	TDS		1×10^{13} ass.		240 α_0	

Substrate	Structure	Coverage of adsorbate	Heat of adsorption E_{ad} [kJ/mol]	Technique	Activation energy of desorption E_d [kJ/mol]	Pre-exponential factor ν_d [s^{-1}]	Sticking coefficient $s(\theta)$	Temperature of desorption [K]	References
Cont'd.			70.8	TDS		1×10^{13} ass.		290 α_0	
			86.2	TDS		1×10^{13} ass.		350 β_1	
			110.5	TDS		1×10^{13} ass.		440 β_2	
		0		TDS	109.3	1×10^{13} ass.			81Joh
		0		TDS	116.4 ± 2	6×10^{15}			78Mad
		0-sat.	123-99	Calorimetry		1×10^{15}	0.74		93Stu
		<0.1		TDS	127	1.6×10^{14}	0.91		93Tak
		0		TDS, IRAS	134 -70	$10^{17.5}$			95Vas
Ni(111)	c(4×2)	0.5		TDS	55	8×10^{9}		445	87Fro
		0.5		TDS, XPS				320	98Hel
	c(2√3×4)rect	0.62		TDS, XPS				100	
	(√3×√3)R30°	1/3		TDS	108.8	1×10^{13}		440	76Con
		1/3	98	Isosteric heat		1×10^{13}			74Chr
		1/3		TDS, XPS				370	98Hel
	(√7×√7)R19°	0.35		TDS	110	1×10^{13}			87Fro
		0.57		TDS	58	2×10^{9}			87Fro
		0.57		TDS, XPS				220	98Hel
		0-sat.	130-95	Calorimetry		3×10^{14}	0.72-0.28		93Stu
		0		TDS			0.9		88Sur
		0-0.3		TDS	125	8×10^{14}			87Fro
		>0.3-0.6		TDS	125-58	1×10^{9}			
			134	TDS					84Gij
		0		TDS			0.91		81Cam1
		0-0.4	149.5	TDS		10^{17}-10^{21}	1.05-0.2		80Iba
		0-0.5	111-84	Isosteric heat		1×10^{13}	1-0.54	440	74Chr

Substrate	Structure	Coverage of adsorbate	Heat of adsorption E_{ad} [kJ/mol]	Technique	Activation energy of desorption E_d [kJ/mol]	Pre-exponential factor ν_d [s^{-1}]	Sticking coefficient $s(\theta)$	Temperature of desorption [K]	References
Cont'd.		0.1-0.9	113-88	LITD		1×10^{13}			89Zhu
		sat.		PES Isotherms		1×10^{13}			79Rub
Ni(110)	(2×1) p2mg	1.0	101	Calorimetry		3×10^{15}	0.26		93Stu
		1.0	129.7±4	Isotherms,TDS	121.4±8.4	$6\times10^{16\pm1.4}$			92DeA
	c(4×2)	0.78±0.01	131.9±2.5	Isotherms,TDS	143.6±3.7	$9.2\times10^{17\pm0.5}$			
	c(8×2)	0.68±0.02	130.2±1.6	Isotherms,TDS	130.2±1.6	$7.6\times10^{14\pm0.2}$			
	c(2×2)	½	125.6	isosteric heat	117.2	1×10^{13} ass.			73Tay
		0-1	133-101	Calorimetry		3×10^{15}	0.75-0.26		93Stu
		0-1		TDS	127-109	$10^{14.7}$		355 α_1	90Fei
								425 α_2	
		0	bridge 133.1	EELS, isobars					87Bau
		0	top 136.1						
		10^{-3} - 0.2		EELS, TDS	108	3×10^{12}	0.9		86Fro
				TDS	83.7-96.3	10^{13} - 10^{15}		330 α_1	75Fal
				TDS	138.2	8.5×10^{15}		420 α_2	85Beh
			121	TDS				360 α_1	81Ber
			121	TDS				455 α_2	
		0.7-1.0	104.7	Isosteric heat		1×10^{13} ass.			73Mad2
		<0.7	125	Isosteric heat		1×10^{13} ass.			73Mad3
Os(0001)	(√3×√3)R30°	0.33						450 α_1	83Ven
		0.42						505 α_2	
	(2√3×2√3)R30°	0.63						526 α_3	
Os (poly)	saturation struct.			TDS	131	1×10^{13} ass.			80Fuk1

Substrate	Structure	Coverage of adsorbate	Heat of adsorption E_{ad} [kJ/mol]	Technique	Activation energy of desorption E_d [kJ/mol]	Pre-exponential factor ν_d [s^{-1}]	Sticking coefficient $s(\theta)$	Temperature of desorption [K]	References
Pd(100)		Low	150.7	Isosteric heat		1×10^{13} ass.			69Tra1
		0.45	128	Isosteric heat		1×10^{13} ass.			
		low-0.5	150-85	Isosteric heat					78Bra1
		low-0.45	161	Isosteric heat		3×10^{16}	0.6		80Beh
		0.15		TDS	154.1	2×10^{16}			
		low	168	Calorimetry		1×10^{13} ass.	0.83		97Yeo1
		0.45	115	Calorimetry		1×10^{13} ass.	0.65		
		0.8	76	Calorimetry		1×10^{13} ass.	0.35		
	$(2\sqrt{2}\times\sqrt{2})R45°$	0.5	167.5	Calorimetry		1×10^{13} ass.	0.65		
Pd(111)		0		TDS	148.6	$1\times10^{15.3}$			89Guo
		0	125.6	TDS		1×10^{13} ass			93Sza2
		0-1/3	142.4	Isosteric heat		1×10^{13} ass			70Ert
	$(\sqrt{3}\times\sqrt{3})R30°$	1/3	142.4	TDS		1×10^{13} ass	0.96		74Con1
	c(4×2)	0.5	134.0	TDS		1×10^{13} ass			
		0.55	23.4±0.8	MB					01Sta
		0-0.4		SHG			1-0.1		02Bou
Pd(110)		Low		MB	130		0.93		01Hir
				Isothermic			0.95		00Yag
				MB	126-149	1×10^{13} ass	0.5		99Jon
	(2×1)p2mg	1.0		Isosteric heat	113.0	1×10^{13} ass			74Con1
	(4×2)	0.75		Isosteric heat	150.7	1×10^{13} ass			
	c(2×2)	0.5		Isosteric heat	167.5	1×10^{13} ass			
Pt(100)-(hex)		0-1	180-85	MB			0.74-0.04		93Hop, 96Yeo
		0		LEED, EELS	115.1		0.7		83Beh

Substrate	Structure	Coverage of adsorbate	Heat of adsorption E_{ad} [kJ/mol]	Technique	Activation energy of desorption E_d [kJ/mol]	Pre-exponential factor ν_d [s^{-1}]	Sticking coefficient $s(\theta)$	Temperature of desorption [K]	References
Cont'd.		0-0.4		LEED, EELS			0.70-0.1		
	p(1×1)			Isosteric heat	134.0	1×10^{13} ass			75Kne
	c(4×2)	0.75		Isosteric heat	108.9	1×10^{13} ass			
	c(2×2)	0.5							
	β_1			TDS	98.8	1×10^{13} ass	0.24	400	77McC
	β_2				111.0	1×10^{13} ass	0.24	450	
	β_3				121.8	1×10^{13} ass	0.24	525	
	β_4				133.5	1×10^{13} ass	0.24	550	
Pt(100)-(1×1)		0		XPS, uptake			0.6		78Bro
		0-0.4		LEED,EELS			0.7		83Beh
		0.5	138.2	LEED,EELS			0.6		
		0-1	225-85	MB			0.61-0.04		96Yeo
	c(2×2)	0.5							
	c(5√2×√2)R45°	0.6							
	c(3√2×√2)R45°	0.67							
	c(4×2)	0.75							
Pt(111)	(√3×√3)R30°	1/3	138.2±8	Isosteric heat	117.2	1×10^{13} ass			74Lam1
	c(4×2)	0.5		TDS	100.5	1×10^{13} ass			76Chr
	c(4×2)	0.25 top	130±5	TDS, EELS		5×10^{14}±50%	Function		93Cud
		0.25 bridge	100±5	TDS, EELS		1×10^{13}±50%	of T and B		
		0-0.13	133−68.5 θ	TEAS		1.4×10^{14}		400	84Poe
		<0.01	134	TEAS		4.3×10^{14}		430	87Ver
		0.1-0.5	118±19	Calorimetry			0.7-0.1		97Yeo2
		0	183±8	Calorimetry			0.8		
		0.5-1	118±19-65±3	Calorimetry			0.05		

Substrate	Structure	Coverage of adsorbate	Heat of adsorption E_{ad} [kJ/mol]	Technique	Activation energy of desorption E_d [kJ/mol]	Pre-exponential factor ν_d [s^{-1}]	Sticking coefficient $s(\theta)$	Temperature of desorption [K]	References
Cont'd.		0-0.5-0.67		TDS,LEED, $\Delta\Phi$	134-41	1×10^{15} ass	0.8-0.04		77Ert
		0.1-0.5		LI-TDS	134-67				86See
				MB					96Zae
		0.1-0.5		Isosteric heat	145±15		0.8		82Ste
Pt(110)-		0		T-modulation	150.7 ± 6	3×10^{14}			88Eng
(1×2)	(1×1)	0.5-1		Isosteric heat	129.4	1×10^{13} ass	0.8	425	76Com3
		1		Isosteric heat	133	1×10^{13} ass	0.8		82Hof1
	(2×1)p1g1	1		Isosteric heat	133 ± 4	1×10^{13} ass	0.8	505	76Com3
				Isosteric heat	104	1×10^{13} ass			76McC
	(2×1)p2mg	1							
		0.2-0.5		Isosteric heat	160 ± 15		1		82Jac1
		0.1	148	MB					80Fai
		0.6	140 ± 15						
		0.78 ± 0.05		Isosteric heat	135 ± 10				
	c(8×4)	1					1	380	82Jac1
	β_1				82.9	1×10^{13} ass	0.64	350	77McC
	β_2				108.9	1×10^{13} ass	0.64	460	
	α_2			TDS	105.1	1×10^{13} ass		412	73Bon
	α_3				120.2	1×10^{13} ass		511	
	β_1				131.5	1×10^{13} ass		511	
Re(0001)		α		TPD	105-113	1×10^{13} ass.		450	77Hou,
		β						810	80Duc
									90Ros

Substrate	Structure	Coverage of adsorbate	Heat of adsorption E_{ad} [kJ/mol]	Technique	Activation energy of desorption E_d [kJ/mol]	Pre-exponential factor ν_d [s^{-1}]	Sticking coefficient $s(\theta)$	Temperature of desorption [K]	References
Re $(10\bar{1}0)$		α_1		TPD	80	1×10^{13} ass.			88Kel
		α_2			105				
		β-states			176-218				
Rh(100)		0		MBS mod	149.5±10	$10^{16.3\pm1.1}$			97Wei
		0		MBS single	135.2±8	$10^{14.5\pm0.9}$			
		0		TPD	131.0±4	$(4\pm3)\times10^{16}$	0.75		94deJ
		0		TPD	134.4	8.4×10^{12}			82Kim
		0		TPD	127.7±4	1×10^{13} ass			
				TDS	121.4	1×10^{13} ass			78Cas
		0 for 100 -	122	Reverse flash			0.86-0.58		97Med
		500 K	33	Reverse flash			0.04		
		T<170 K	94	Reverse flash			0.7		
	c(2×2)	0.5		TPD	129.8	1×10^{13} ass			78Cas
	(4√2×√2)R45°	0.75							
	c(6×2)	0.83							
Rh(111)		0 to	134±8 to	LDS		$10^{14\pm0.5}$to	0.8±0.05		88See
	(2×2) 3CO	0.75	59	LDS		10^{13}	~0		
		0		MBS mod.	161.2±6	$10^{16.5\pm0.6}$			97Wei
		0		MBS single	164.9±3	$10^{16.9\pm0.2}$			
		variable θ	$135-6.8\,\theta-160\,\theta^2$	Isosteric heat by MBS He		$1.33\times10^{14}\times\exp(0.344\theta+48.8\,\theta^2)$			91Pet1
		0		TPD	132	$10^{13.6\pm0.3}$	0.76±0.04		79Thi2
		5L		TPD	130	1×10^{13} ass			78Cas
		0		MBS			0.95-0.62	273	99Beu

Substrate	Structure	Coverage of adsorbate	Heat of adsorption E_{ad} [kJ/mol]	Technique	Activation energy of desorption E_d [kJ/mol]	Pre-exponential factor ν_d [s^{-1}]	Sticking coefficient $s(\theta)$	Temperature of desorption [K]	References
Rh(110)-(1×1)		0	132	MBS, TPD		1×10^{13} ass.	0.68±0.01		91Bow
		0-1	132-108	MBS, TPD				485, 425, 390	
		low		TPD	124	1×10^{13} ass.		495	80Bai
		low		TPD	130	1×10^{13} ass.		485	77Mar
		low		MBS mod.	174 ± 4	$1\times10^{17.8\pm0.4}$		485	97Wei
		low		MBS single	164 ± 6	$1\times10^{16.8\pm0.6}$		485	
	(1×1)	$0.2<\theta<0.33$	150-120	TPD		10^{14} - 10^{12}		490	93Bar
	c(2×2)	$0.33<\theta<0.55$	120-70	TPD		10^{12} - 10^{7}		490, 440, 390	
	(2×1)p2mg	>0.55	70-50	TPD		10^{7} - 10^{4}		490, 440, 390	
Rh(110)-(1×2)	(1×2)	$0.2<\theta<0.4$	100-60	TPD		10^{9} - 10^{5}		485	93Bar
	c(2×4)	$0.4<\theta<0.63$	60-45	TPD		10^{5} - 10^{3}		485, 400	
	(2×2)p2mg	>0.63	45-20	TPD		10^{3} - 10^{0}		485, 400	
Ru(0001)	(√3×√3)R30°			TDS	~98 ~117	1×10^{13} ass.	0.85		70Gra, 74Mad, 75Fug1, 75Fug3, 77Fug, 79Tho, 93Ove
Ru(0001)	(√3×√3)R30°			MBS at 85 K			0.92-0.58 with variable E_{kin}		99Kne1
				MBS at 273 K			0.96-0.84 with variable E_{kin}		2000Rie

Substrate	Structure	Coverage of adsorbate	Heat of adsorption E_{ad} [kJ/mol]	Technique	Activation energy of desorption E_d [kJ/mol]	Pre-exponential factor ν_d [s^{-1}]	Sticking coefficient $s(\theta)$	Temperature of desorption [K]	References
Ru(0001)	(√3×√3)R30°	0.05-0.25 0.33 >0.35	160±6 175 120-110	Isotherms and TDS	160±6 175 120-110	~2×10^{16} ~1×10^{19} ~1×10^{14}	0.7-0.55 ≈0.3 <0.25		78Pfn, 83Pfn1, 83Pfn2
Ru(0001)		 atop site Hollow site	160.3 114 91	Theory Theory					96Ham 00Kop
Ru(0001)		α_1 α_2 β		TDS	~127 ~109 ~146	1×10^{13} ass.		440 520-460 580	85Shi1
Ru$(10\bar{1}0)$				TDS	102 126	1×10^{13} ass.		403 513	77Ku
Ru$(10\bar{1}0)$	(3×1) ("2×1") (3×1) (2×1)p2mg $\begin{pmatrix} 4 & \bar{1} \\ 1 & 2 \end{pmatrix}$	0.3 0.47 0.67 1.0 1.22	157 at θ<0.5	Isosteric heat and TDS	150 ~125 100 100	 1×10^{15}	1.0 at θ<0.85		89Lau
Ru$(10\bar{1}0)$	(3×1) (4×1) $\begin{pmatrix} 4 & \bar{1} \\ 1 & 2 \end{pmatrix}$	<0.3 ~1.0 >1		TDS	140 75 ~50	~1×10^{14} ~1×10^{9} ~1×10^{6}			96Rot
Ru$(10\bar{1}1)$	$\begin{pmatrix} 1 & 1 \\ 3 & 0 \end{pmatrix}$	α β		TDS	~105 ~118	1×10^{13} ass.	0.6		76Ree

Substrate	Structure	Coverage of adsorbate	Heat of adsorption E_{ad} [kJ/mol]	Technique	Activation energy of desorption E_d [kJ/mol]	Pre-exponential factor ν_d [s^{-1}]	Sticking coefficient $s(\theta)$	Temperature of desorption [K]	References
Ru(11$\bar{2}$0)	p(1×2)	α_1		TDS	103			440-460	01Wan1,
	(1×2)-p2mg	α_2			85			400	01Wan2
		β_1			89			500	
		β_2						540	
Ru(11$\bar{2}$1)		α_1		TDS				380	03Fan
		α_2						430-450	
		β						540	
W(100)	c(2×2)	0.5					1.0		67And,
		α, β							79Wan
W(110)		α_1		Isothermal			0.72-0.95,	~150	71Koh,
		α_2		desorption			temp.	~300	73Koh
		"virgin"			40	~10^4	depend.	~375	77Leu,
		β_1			230	2.8×10^{12}		~975	83Umb
		β_2			291±13	1.2×10^{12}		~1125	
W(110)	p(2×7)	~0.2		LEED, XPS					77Ste1,
	c(4×1)	>0.3							77Ste2
	p(3×1)	~0.5							
	p(4×1)	~0.65							
	p(5×1)	~0.8							

Table 4: Adsorbed CO (dissociation parameters)

Substrate	Adsorbed State	Coverage θ	Temperature of dissociation [K]	Activation energy of dissociation [kJ/mol]	Pre-exponential factor [s^{-1}]	References
Cr(110)			~300			82Kat
	α_1	0.25	~200			84Shi
Mn/Fe(110)	α	Mn/Fe=0.06	~220			93Sie
	β					
	α		~270			
	β	Mn/Fe=0.1				
Mo(110)		"clean"		71	$10^{10.6}$	81Kel, 81Sem, 86Eri
		C		36	$10^{3.9}$	
		O		51	$10^{6.6}$	
		C,O		79	$10^{11.6}$	
		S		79	$10^{12.3}$	
		K		74	$10^{10.9}$	
Mo(100)	α	0.54-0.63	~220	58-65	10^{13} ass.	73Lec, 73Vis, 80Ko2, 81Sem
Ni(100)	defects		500	83.7		86Ste
Ni[5(111)×(1$\bar{1}$0)]		low	300			78Erl
Fe(110)		0.36	<300			79Bro
Ir(111)		>10^{-6} torr	>650			76Com2
Re(0001)	α	0.31	>400			77Hou, 83Tat, 85Tat
	β	0.026				
W(110)	"virgin"		>300	46-63	10^{13}	83Umb
	α_1		275-400			
	β_1					
	β_2					
Zr polycrystal	β		<300			80Foo

Table 5. Adsorbed CO (crystallographic and vibrational data)

Substrate	Structure	Coverage/ adsorbed state	Vibrational frequency [cm^{-1}] Me-C	C-O	Adsorption site / configuration	Technique	References
Al(111)		saturated		2137	CO perpend. to surface	EELS	89Jac
Al(100)				2135		IRAS T <40 K	88Ryb
Al(100)			440	2060		EELS	86Pau3, 87Pau
K/Al(100)		~ 1 ML K		1060			
				1250			
				1750			
				1910			
Ag(110)		at 13 K		2153			01Hah
Au(332)				2120		IRAS	97Rug
Co(0001)				2012-2048	atop	PMIRAS	96Bei
				1850-1900	bridge		
				2055-2080	defect sites		
Co $(10\bar{1}0)$	p(2×1)	<0.56		1972-2020	atop	IRAS	96Too
	(2×1)p2mg	0.5-1.0		1900-1967	2-fold bridge, tilted CO		
	c(2×6)	>1.0		1984			
Cr(110)	c(4×2)	0.25; α_1	450-475	1150-1200	"lying down" in	EELS	84Shi, 85Shi2, 85Shi3
				1330	2-fold hollow;		
	(1×1)	α_2	495	1865	perpendicular in		
				1975	atop, bridge		
Cu/Al(111)		0.5 ML Cu		1260	di-sigma bonded		93Col

Substrate	Structure	Coverage/ adsorbed state	Vibrational frequency [cm^{-1}] Me-C	C-O	Adsorption site / configuration	Technique	References
Cu(100)	c(2×2)	0.5	342.8	2089.0	atop	EELS	88Uvd
			344.5	2086	atop	IRAS	95Hir
			345.2	2079.3	atop	IRAS	
			344.56 ± 0.16		atop	IRAS	98Gra2
				2084	atop	IRAS	85Ryb
	c(7√2×√2) R45°	0.57	338.8	2093.0	atop, bent	EELS	88Uvd
		0.1 - 0.57		2076-2086	atop	IRAS	97McC
		0	334.3	2076	atop	IRAS	95Hir
		0		2065	atop	STM-IETS	99Lau
Cu(111)	(√3×√3)R30°	1/3	338.5	2076	atop	IRAS	95Hir,94Hir,
				2076	atop	IRAS	93Hir,90Hir
				2076	atop	IRAS	79Pri
				2068	atop	IRAS	85Hay2
		0	334.0	2078	atop	IRAS	95Hir
		0		2078	atop	IRAS	79Hol
	(1.4×1.4)hex,	0.52 at 7 K		1837, 2068	bridge, atop	IRAS	85Hay2
	(7×7)	0.52 at 77 K		1812, 1830,	bridge, atop		
				2068		IRAS	79Pri
		0.52		2070			
Cu(110)	(2×1)	0.5		2094	T	IRAS	82Woo
			685	2082	T	EELS	79Wen
			345		T	IRAS	94Hir
				2078	T	SFG	92Mor
		0		2073	T	STM-IETS	99Lau
		0		2089	T	IRAS	82Woo
		0-sat.		2090, 2106	T, step edges	IRAS	84Hol

Substrate	Structure	Coverage/ adsorbed state	Vibrational frequency [cm^{-1}] Me-C	C-O	Adsorption site / configuration	Technique	References
Fe(100)		Low θ, α_3		1180-1245	"lying down"	IRAS	85Ben
Fe(100)		α_1	470	2070	T	EELS	87Moo2
		α_2	530	2020	2-fold		
		α_3	395	1210	4-fold		
		β					
Fe(100)		α_3	375	1155-1170	CO	EELS	89Lu
		β	400		O (>400 K)		
			510-520		C		
Fe(111)		A		1530	Deep hollow	EELS	84Sei, 85Sei
		B	515	1805-1850	Shall. Hollow		
		C	550	2000	atop		
Fe(111)		a_1		1325-1485	Deep hollow	EELS	86Bar2
		a_2		1520-1575	Deep hollow		89Whi
		b		1735-1860	Shall. Hollow		
		c	550	1945-2015	atop		
Fe/Cu(100)		8 ML Fe		1929-1998	bridge	IRAS	99Tan
				2020-2048	atop		
Ir(100)(1×1)	c(2×2)	0.5	497	2068-1998	atop	EELS	91Kis
		low cov.		2026		IRAS	93Mar
Ir(100)(5×1)	(1×1)	0.5	485	2075-2005	atop	EELS	91Kis
	(5×1) not lifted	variable θ		5 bands 2025-2097		IRAS	93Mar
Ir(111)		Variable θ	475-490	2025-2050	atop	EELS	89Mar
				2030-2090		IRAS	96Lau
Ir(110)		Variable θ	475-490	2012-2070	atop	EELS	89Mar
		Low θ		2001	atop	IRAS	95Lyo

Substrate	Structure	Coverage/ adsorbed state	Vibrational frequency [cm^{-1}] Me-C	C-O	Adsorption site / configuration	Technique	References
Cont'd.		Saturation		2086	atop	IRAS	
Mo(100)		θ<0.2	400	1065	"lying down" or	EELS	85Zae
				1235	inclined		
		θ>0.4	400	1085			
				2100	atop		
Mo(110)			565-575		O	EELS	91Che
			400		C		
				1130	CO "lying down"		
				1345	or inclined,		
				1500	upright CO		
				1920-2055			
Mo(110)		<0.3		low-frequency comp. not seen by IRAS;	inclined CO, titrated with coadsorbed Cu;	IRAS	91He1
		>0.3		1885-1896	upright CO in		
				1927	different sites		
				1993-2040			
Ni(100)	c(2×2)	0.5	484	2065	atop	EELS	88Uvd
				2068	atop	EELS	82Bib
	(3√2×√2) R45°	0.67		2008	bridge	EELS	88Uvd
				2049	atop	EELS	
				2068,1931	atop, bridge	EELS	82Bib
	c(5√2×√2) R45°			2056, 1976	atop, bridge	IRAS	95Vas
		0.6	468	2041	2/3 atop	EELS	88Uvd
				1920	1/3 bridge	EELS	
		0 - 0.5		2045 - 2076	atop	IRAS	93Sin

Substrate	Structure	Coverage/ adsorbed state	Vibrational frequency [cm^{-1}] Me-C	C-O	Adsorption site / configuration	Technique	References
Ni(111)	(√3×√3)R30°	0.33	400	1910		EELS	79Cam, 80Erl
				1878	bridge	IRAS	88Sur
				1878	fcc, hcp hollow	IRAS, XPD	94Dav
				1900	bridge	IRAS	79Cam
	c(4×2)	0.5	400	1910, 2050	bridge, atop	EELS	80Erl
				1898	bridge	IRAS	85Ryb
				1910, 2055	bridge, atop	IRAS	88Sur
				1910	fcc, hcp hollow	IRAS, XPD	94Dav
				2055	atop	IRAS, XPD	
				1910	bridge	IRAS	79Cam
	(√7/2×√7/2)R19.1°	0.57	400	1903- 1912	bridge	IRAS	88Sur
				2055	atop	TRAS	
				1903- 1912	fcc, hcp hollow	IRAS, XPD	94Dav
				2055	atop	IRAS, XPD	
				2045, 1910	atop, bridge	IRAS	79Cam
		0 - 0.2		1817-1823	3 fold hollow	IRAS	88Sur
				1817-1823	fcc, hcp hollow	IRAS, XPD	94Dav
				1831-1857	bridge	IRAS	88Sur
				1831-1857	fcc, hcp hollow	IRAS, XPD	94Dav
		0.05		1817	3 fold hollow	IRAS	79Cam
		0	380	1815	bridge	EELS	80Erl
		saturat.	380	1912, 2033	atop, bridge	EELS	77Ber
		0 - 0.57		1920, 2050	atop, bridge	EELS	87Fro
		0 - 0.57		1830-1912, 2050	fcc hollow, atop	IRAS	97Smi
		0 - 0.2		1820	hcp hollow	IRAS	

Substrate	Structure	Coverage/ adsorbed state	Vibrational frequency [cm^{-1}] Me-C	C-O	Adsorption site / configuration	Technique	References
Ni(110)	(2×1) p2mg	1.0	410	1900	atop, short br.	EELS	90Voi
		1.0	430	1960	atop	EELS	87Bau
		>0.9	444	2016, 1904	atop, tilted	EELS	81Nis
		<0.85	430	1840, 1960	atop, bridge, ratio 2.5:1	EELS	87Bau
		0.05	436	1855, 1960	atop, bridge	EELS	81Nis
		0.2	444	1879, 1976	atop, bridge	EELS	
		low		1880, 1990	atop, bridge	EELS	81Ber
		~0.5	450, 345	1935, 2015	atop	EELS	
Ni(510)		increasing exposure	378	1594	step (bottom)	EELS, LEED	96Sve
				1876-1900	bridge (step, terrace)		
			402	2004-2012	atop (terrace)		
			459	2052	defect sites (step, terrace)		
Pd(100)	(2√2×√2) R45°	0.5	347	1952	bridge	EELS	88Uvd
		0.5	339	1904	bridge	EELS	79Beh
	(3√2×√2) R45°	0.67	315	1960	bridge	EELS	88Uvd
	(4√2×√2) R45°	0.75	338	1984	bridge	EELS	
		0.75	282	1984	bridge, tilt	EELS	
		low - 0.5		1895 - 1949	bridge	IRAS	78Bra1
		0.6		1975	bridge	IRAS	82Ort
		low-0.75	360	1890 - 1940	bridge	EELS, SIMS	85Bro
Pd(111)	(√3×√3)R30°	1/3		1849	hollow	IRAS	83Hof1
	c(4×2)	0.5		1918	bridge	IRAS	

Substrate	Structure	Coverage/ adsorbed state	Vibrational frequency [cm^{-1}] Me-C	C-O	Adsorption site / configuration	Technique	References
Cont'd.	(√3×2)rect	0.5		1920	bridge	EELS	90Tüs1
	(√3×35)rect	0.514		1910, 1957	bridge	EELS	
	(√3×11)rect	0.545		1901, 1962	bridge	EELS	
	(√3×7)rect	0.571		1962	bridge	EELS	
	c(√3×5)rect	0.6		1951	bridge	IRAS	83Hof1
	c(4√3×8)rect	0.63		1951, 2097	atop, hollow	IRAS	
	(2×2)	0.75		1951, 2097	atop, hollow	IRAS	
		$<10^{-6}$ mbar		2083, 1955	atop, bridge	SFG	98Bou
		$>10^{-6}$ mbar		2103, 1890	atop, hollow	SFG	
		domain boundaries		2093, 1940	atop, bridge	SFG	
				1890	hollow	SFG	
		0.3 L - 2.7 L		1823 - 1936	atop, hollow	EELS	00Sur
Pd(110)	(2×1)p2mg	1.0	383	2003.5	short bridge	EELS	99Kat1
	(1×1)	0.05-0.3		1882-1912	bridge	IRAS	89Rav, 90Rav1
	(4×2)	0.3-0.5		1925, 1982, 1943	bridge	IRAS	90Rav2
	(4×2)	0.5-0.6		2068, 1992, 1951,1902, 1864	bridge	IRAS	
				1959-1976			
				1903-1909	bridge		
	(4×2)	0.6-0.7		2003	bridge	IRAS	
	(2×1)p1g1	1		1890-2000	bridge	IRAS	
	c(2×2)	0-15 L at 110 K	~370	~2110	atop	IRAS	85Che1
	p(4×2)	0.9-15 L at 110 K	~370	1883-1912	bridge	IRAS	
	(2×1)p2mg	0-15 L, 300K	347-379	1972-2000	bridge	IRAS	

Substrate	Structure	Coverage/ adsorbed state	Vibrational frequency [cm^{-1}] Me-C	C-O	Adsorption site / configuration	Technique	References
Pd(510)	p(2√2×√2)R45°	0.5	354	1948	bridge (terrace)	EELS, LEED	96Sve
	c(5√2×√2)R45°	>0.5	346	1956	bridge		
		saturated		1996	bridge (terrace)		
				2125	atop (step)		
Pt(100)-(hex)		0		2083	atop	IRAS	90Hol, 95Mar
		>0		2086,2089,1873	atop, bridge	IRAS	95Mar
	p(1×1)	0.1-0.6		2030, 1950	atop, bridge	EELS	83Beh
	c(4×2)	0.75					
	c(2×2)	0.5					
Pt(100)-(1×1)		0-1		2065-2090	atop	IRAS	90Hol, 95Mar
		0-1		1867, 1910	bridge	IRAS	95Mar
		0.1-0.6		2030, 1950	atop, bridge	EELS	80Cros, 83Beh
	c(2×2)	0.5				LEED, EELS	64Tuc, 78Bro,
	c(5√2×√2)R45°	0.6					80Cros, 83Beh
	c(3√2×√2)R45°	0.67					
	c(4×2)	0.75					
Pt(111)	(√3×√3)R30°	1/3		2065	atop	EELS	83Hay
	c(4×2)	0.5	480	2100	50% atop	EELS	86Lah
			380	1850	50% bridge	EELS	
	c(4×2)	0.5	480	2100	50% atop	EELS	82Ste
			380	1850	50% bridge	EELS	
	c(4×2)	0.5	468	2081	50% atop	EELS	77Iba
			363	1855	50% bridge	EELS	
	c(4×2)	0.5	451		50% atop	IRAS	97Eng, 99Eng
			369		50% bridge	IRAS	
	c(4×2)	0.5		2104	50% atop	RAIRS	90Per

Substrate	Structure	Coverage/ adsorbed state	Vibrational frequency [cm^{-1}] Me-C	C-O	Adsorption site / configuration	Technique	References
Cont'd.				1854	50% bridge	RAIRS	
		0-0.5	473-462			IRAS	89Per, 90Ryb
		0-0.6	478-466			IRAS	89Mal
		0.17-0.58	470 and 380	2100 and 1850	atop, bridge	EELS	82Ste
		0.5	379	1855	bridge	EELS	79Hop
		0.5		2082.7 ± 1.8	atop	SFG	96Klü
		1		2093.3 ± 1.6	atop	SFG	
		0-0.6		2084.0-2094.7	atop	IRAS	88Ols
		10^{-7} up to		2095	atop	SFG	96Su
		700 torr		1845	bridge	SFG	
				2045		SFG	
Pt(110)	(1×1)	0.5-1	476	2097	atop	EELS	82Hof1
	(2×1)p1g1	1	476	2097	atop	EELS	
		1	475	2105	atop	EELS	84Bar
		0-1 at 300 K		2080-2130	atop	IRAS	87Hay
		low at 160 K	465	2105	atop	EELS	83Hof2
		1 at 160 K	465 and 380	2105 and 1855	atop, bridge	EELS	
		low at 300 K		2064.9 ± 1.6	atop	SFG	96Klü
		1 at 300 K		2093.7 ± 1.6	atop	SFG	
		1 at 300 K	472	2093.6	atop	EELS	
Rh(100)		0		1995	atop	IRAS	94deJ
	c(2×2)	0.5		2052	atop		
	(4√2×√2)R45°	0.75		2054	atop		
				2031, 1944	atop, bridge		
	c(6×2)	0.83		2074	atop	IRAS	

Substrate	Structure	Coverage/ adsorbed state	Vibrational frequency [cm^{-1}] Me-C	C-O	Adsorption site / configuration	Technique	References
Cont'd.				1880-1970	bridge		
		0.08, 300 K		2005, 1881	atop, bridge	IRAS	90Leu
		0.32, 300 K		2026, 1908	atop, bridge	IRAS	
		0.48, 300 K		2049, 1936	atop, bridge	IRAS	
		0.60, 300 K		2062, 1942	atop, bridge	IRAS	
		0.10, 90 K		2013, 1896	atop, bridge	IRAS	
		0.30, 90 K		2034, 2023, 1898	atop, bridge	IRAS	
		0.50, 90 K		2045, 1910	atop, bridge	IRAS	
		0.75, 90 K		2086, 1964	atop, bridge	IRAS	
		0 - 0.83 at 90-300 K	436	2000, 1895	atop, bridge	EELS	87Gur
Rh(111)	(√3×√3)R30°	1/3	460	2000	atop		81Koe
	(2×2)	0.25	480	1990	atop		80Dub
	(4×4)	0.5			atop		
	(2×2) 3CO	0.75	420	2070	67% atop,		
				1870	33% bridge		
		0.75		2065	atop		84Koe
				1855	bridge		
Rh(110)		0.05 - 0.50		2008	short bridge	EELS	97Wei
		0.50 - 0.71		2008 - 1968	short bridge	EELS	
		0.71 - 1		1968	short bridge	EELS	
Ru(0001)		0.1	436	2017	atop	EELS	79Thi1
		0.3	444	2017			
		0.6	428	2033			
Ru(0001)		~ 0.003		1984	CO stretch, 200 K	IRAS	80Pfn
	(√3×√3)R30°	0.33		2021			

Substrate	Structure	Coverage/ adsorbed state	Vibrational frequency [cm^{-1}] Me-C	C-O	Adsorption site / configuration	Technique	References
Cont'd.		0.67		2061			
	$(\sqrt{3}\times\sqrt{3})R30°$	0.33		2030.8	at 30 K (IRAS)		96Jak
				1941	$^{13}C^{16}O$		
				3940	overtone (2ν)		
	$(\sqrt{3}\times\sqrt{3})R30°$	0.33	452.8				98Jak2
			458.9		Fermi resonance		
Ru(0001)				1901	atop	Theory	00Kop
				1648	hollow		
Ru $(10\bar{1}0)$	(3×1)	0.33	453	2000	atop	EELS	89Lau
	(2×1)p2mg	1.0	433	2048			
	$\begin{pmatrix} 4 & \bar{1} \\ 1 & 2 \end{pmatrix}$	>1	443	1810			
				2062			
Ru$(11\bar{2}0)$	p(1×2)	0.25	691	1552	Tilted CO	EELS	01Wan1,
	(1×2)-p2mg	0.5	402-482	1930-2050	atop		01Wan2
Ru$(11\bar{2}1)$		Low	442	1335	4-fold hollow	EELS	03Fan
				1946	atop		
		Intermediate	498	1487	defect site		
				1769	bridge		
W(100)		α	363	2065	CO in atop,	EELS	77Fro
		β	548 (C)		dissociated into C		
			605 (O)		and O		
W(100)		α_1 "virgin"	360	2100	at 100 K;	EELS	85Fra
		α + β	545	2065	β state is		
			625		dissociated CO		

Substrate	Structure	Coverage/ adsorbed state	Vibrational frequency [cm^{-1}] Me-C	C-O	Adsorption site / configuration	Technique	References
W(100)					CO stretch	IRAS	93Rif
		α		2023-2099	at 90 K		
		α_1		2082-2102	at 295 K		
		α_2		2061-2070			
W(110)		0.23-0.5		1360	tilted CO		82Hou, 91Hou
		0.23-0.77		1960-2040	upright CO		

Table 6. Adsorbed CO (low frequency vibrational data by EELS, TEAS [03Gra] and IETS [02Ho])

Substrate	Structure	Coverage θ	Adsorption site	Vibrational frequency [cm^{-1}]	Mode assignment	References
Al(111)		low		34.7	ν_4 fr. Transl.	03Gra
Ag/NiAl(110)	Single atom		atop	209.7	ν_3 fr. Rotation	03Wal
Au/NiAl(110)	Single atom		atop	282.2	ν_3 fr. Rotation	03Wal
Cu(100)	c(2×2)	0.5	atop	284.7	ν_3 fr. Rotation	90Hir
			atop	287.8	ν_3 fr. Rotation	95Hir
			atop	32.2-45.1	ν_4 fr. Transl.	95Ell
			atop	287.2±0.16	ν_3 fr. Rotation	98Gra2
			atop	31.69±0.16	ν_4 fr. Transl.	
	c(7√2×√2)R45°	0.57	atop, bent	290.3	ν_3 fr. Rotation	88Uvd
		0	atop	284	ν_3 fr. Rotation	95Hir
		0	atop	292.8	ν_3 fr. Rotation	99Lau
Cu(111)	(√3×√3)R30°	1/3	atop	282.3	ν_3 fr. Rotation	95Hir,94Hir, 93Hir, 90Hir
		0	atop	294.2	ν_3 fr. Rotation	95Hir
		0	atop	32.83±0.4	ν_4 fr. Transl.	96Bra, 02Hei
Cu(110)		0	atop	293±2.5	ν_3 fr. Rotation	99Lau
	(2×1)	0.5	atop	39.5±5	ν_4 fr. Transl [110]	97Ahn
			atop	25±4	ν_4 fr. Transl [100]	
		0.07, 40K	atop	29±0.8	ν_4 fr. Transl [110]	98Bra
			atop	26±0.8	ν_4 fr. Transl [100]	
		0.07, 110K	atop	30±0.8	ν_4 fr. Transl [110]	
			atop	27±0.8	ν_4 fr. Transl [100]	
			atop	288	ν_3 fr. Rotation	94Hir
Cu(211)		single CO	atop	46.7	ν_4 fr. Transl.	99Mor
				289	ν_3 fr. Rotation	
Cu(511)			atop	24.6±0.8	ν_4 fr. Transl.	96Bra
Cu(211)				24.2±0.8	ν_4 fr. Transl.	
	Step site			25.8±0.4	ν_4 fr. Transl.	
	Defect site			20.2±0.4	ν_4 fr. Transl.	
Fe(110)	p(1×2)		atop	37	ν_4 fr. transl.	92Toe
Ir(100)(1×1)	c(2×2)	0.5	atop	425	ν_3 fr. Rotation	91Kis
				53	ν_4 fr. Transl.	
Ir(100)(5×1)	(1×1)	0.5	atop	425	ν_3 fr. Rotation	91Kis
				53	ν_4 fr. Transl.	
Ni(100)	c(2×2)	0.5	atop			
	(3√2×√2)R45°	0.67	bridge	258	ν_3 fr. Rotation	88Uvd
		0.07	atop, bridge	28.2	ν_4 fr. Transl.	87Ber
		0.5	atop	30.6	ν_4 fr. Transl.	
	c(5√2×√2)R45°	0.6	33% atop, 67% bridge	363	ν_3 fr. Rotation	88Uvd

Substrate	Structure	Coverage θ	Adsorption site	Vibrational frequency [cm^{-1}]	Mode assignment	References
Ni(111)	c(4×2)	0.5	bridge	184	ν_3 fr. Rotation	85Per
				76	ν_4 fr. Transl.	
		0.5	bridge	302	ν_3 fr. Rotation	91Ha
				95	ν_4 fr. Transl.	
Ni(110)	(2×1)p2mg	1.0	atop, bridge	384.7	ν_5 fr. Rotation	90Voi
				100	ν_6 fr. Transl.	
	c(4×2)			40	ν_4 fr. Transl.	
	c(8×2)			30	ν_4 fr. Transl.	
		0.1-0.3	atop	31.4	ν_4 fr. Transl.	97Ber
		1.0	bridge	60.4	ν_4 fr. Transl.	
Pd(100)	(3√2×√2)R45°	0.67	bridge	403	ν_3 fr. Rotation	88Uvd
	(4√2×√2)R45°	0.75	bridge	411	ν_3 fr. Rotation.	
Pd(110)	(2×1)p2mg	1.0	short bridge	201.6	ν_3 fr. Rotation	99Kat1
				427.5	ν_4 fr. Rotation	
				338.7	ν_5 fr. Rotation	
				69.4	ν_6 fr. Transl.	
			bridge	69.2	ν_4 fr. Transl.	00Kaw
Pt(110)-(1×2)	(1×1)	1	atop	420	ν_3 fr. Rotation	84Bar
	(2×1)p1g1	1	atop	420	ν_3 fr. Rotation	
				475	ν_2 fr. Rotation	
		1 at 300 K	atop	404	ν_3 fr. Rotation	96Klü
Pt(111)	c(4×2)	0.5	atop, 50%	411	ν_3 fr. Rotation	82Ste, 86Lah,
				48.5	ν_4 fr. Transl.	93Sza1
			bridge, 50%	425	ν_3 fr. Rotation	
				144	ν_4 fr. Rotation	
				360	ν_5 fr. Rotation	
				60	ν_6 fr. Transl.	
		0.03-0.05	atop	47.8	ν_4 fr. Transl.	98Gra3
		0.25	bridge	64.4	ν_4 fr. Transl.	98Gra1
			atop	55.9	ν_4 fr. Transl.	
Rh(111)	Low θ		atop	46.4	fr. Transl.	93Wit
	(√3×√3)R30°	1/3	atop	45.2	fr. Transl.	
	(2×2)-3CO	3/4	atop	46.0	fr. Transl.	01Wit
			hollow	92.8	fr. Transl.	
Ru(0001)	(√3×√3)R30°		atop	45	fr. Transl.	79Wil
Ru(0001)	(√3×√3)R30°	0.33	atop	40±8	ν_4 fr. transl.	96Gie
			atop	46.3	ν_4 fr. Transl.	97Bra
		<0.09	atop	47.5	ν_4 fr. Transl.	
W(110)		low		64	ν_4 fr. Transl.	03Gra

Table 7. Adsorbed CO (additional structural data, bond lengths and bond angles)

Substrate	Structure	Cover./ Ad-state	Adsorption site	Bond length [Å] Me-C	C-O	n-n	Me-Me	Tilt angle [deg]	Technique	References
Ag(100)	c(2×2)					4.09	2.89			76McE1
	c(4×2)					5.78				
Ag(111)	p(√3×√3)R30°	1/3				5.01	2.89		LEED	85Sch
	p(2×2)					5.78				
Au(110)	disordered						2.88		LEED	94San2
										94San3
Co(0001)	(√3×√3)R30°	0.33	atop	1.78±0.06	1.17±0.06		2.04 in 1st layer	no tilt	LEED	00Lah
Cu(100)	c(2×2)	0.5	atop	1.90±0.10	1.13±0.10	3.61	2.56		LEED	80And
		0.5	atop	1.92±0.05	1.13	3.62	2.56		NEXAFS, PED	86McC
		0.5	atop						LEED	82Bib
		0.5	atop			3.6			EELS, LEED	88Uvd
		0.5	atop		1.15±0.10				NEXAFS	83Stö
		0.5	atop	1.90±0.10	1.15±0.10	3.61	2.56		LEED	80Ton
	c(7√2×√2)R45°	0.58	atop						LEED	72Tra1
		0.57	atop						LEED	79Pri
		0.57	atop						LEED	82Bib
		0.57	atop			3.6-3.0	2.56	6-15°	EELS, LEED	88Uvd
	c(5√2×√2) R45°	0.6	atop						LEED	72Tra1
		0.6	atop			2.56	2.56		LEED	82Bib
Cu(111)	(√3×√3)R30°	1/3	T						STM	99Bar
				1.91±0.01			2.56		ARPEFS	96Mol
			T						LEED, IRAS	85Hay2
	(1.5×1.5)R18°		T						LEED	80Hol
		0.44	T	1.91±0.02			2.56		ARPEFS	96Mol

Substrate	Structure	Cover./ Ad-state	Adsorption site	Bond length [Å] Me-C	C-O	n-n	Me-Me	Tilt angle [deg]	Technique	References
Cont'd.	(1.39×1.39) hex		T						LEED	80Hol
	(1.4×1.4)hex,	0.52	T, B						LEED	80Hol
	(7×7)	0.52	B:T, 12:13						LEED	79Pri
			B:T, 12:13						LEED, IRAS	85Hay2
		0.52	B, T						STM	99Bar
Cu(110)	(2×1)	0.5	T				2.556	no tilt	LEED,ESDIAD	96Ahn
			T	1.87±0.02	1.15±0.05			no tilt	ARUPS	95Hof
			T					no tilt ±10°	XPD	86Hol
		0.25-0.5	T						LEED, TDS	85Har
		0.5	T			3.61			LEED, IRAS	82Woo
		0.5	(H)						LEED, IRAS	77Hor2
	(5/4×2)	0.8	T				2.556	±2.5°	LEED,ESDIAD	96Ahn
	c(5/4×2)	0.8	T						LEED, TDS	85Har
	c(1.3×2)	0.77	T						LEED, IRAS	82Woo
			(H)						LEED, IRAS	77Hor2
Cu(210)			atop	1.87±0.02	1.16±0.03		2.54±0.75	θ_{CO}=18±6 θ_{CuC}=6±5	PED	01Ter
Fe(100)	c(2×2)	0.25 C	dissoc. CO	2.083					LEED	78Jon
		0.25 O	4-fold hollow	2.083						
Fe(100)		α_3 β	4-fold holl. dissociated		1.43			54.7°	NEXAFS	89Dwy
Fe(100)		α_3	4-fold hollow					55°±2° 45°±10° >45°	XPD NEXAFS CDAD	89Sai 87Moo3 94Wes
Ir(100)-(1×1)	c(2×2)	0.5	atop						LEED LEED	69Gra 78Nie

Substrate	Structure	Cover./ Ad-state	Adsorption site	Bond length [Å] Me-C	C-O	n-n	Me-Me	Tilt angle [deg]	Technique	References
Cont'd.			atop						LEED	91Kis
	(1×1)		atop						LEED	93Mar
			atop						LEED	91Kis
Ir(100)-	(2×2)	0.25	atop						LEED	69Gra
(5×1)	(1×1)	<0.94							LEED	76Bro
		0.5	atop						LEED	91Kis
	(5×1) not lifted								LEED	93Mar
Ir(111)	(√3×√3)R30°	1/3							LEED	69Edm
						4.69	2.72		LEED	71Gra
			3-fold H						LEED	77Iva
			3-fold H			4.7	2.72	0 ±15°	LEED	81Sea
			3-fold H						LEED	78Com
			3-fold H						LEED	76Com1
			3-fold H			4.7	2.72		LEED	76Com2
			3-fold H						LEED	73Wei
			2-fold Br						LEED	74Doy
			3-fold H			4.7			LEED	76Hag
			2-fold Br						LEED	76Küp
			atop						EELS	89Mar
			atop						IRAS/LEED	96Lau
Ir(111)	(2√3×2√3)R30°	7/12	2 fold br.						LEED	77Iva
			2 and 3 fold			3.56	2.72		LEED	76Hag
			2 and 3 fold			3.55	2.72		LEED	81Sea
			2 and 3 fold			3.55	2.72		LEED	78Com
			2 and 3 fold			3.55	2.72		LEED	76Com1
			2 and 3 fold			3.55	2.72		LEED	76Com2
			2 and 3 fold						LEED	76Küp

Substrate	Structure	Cover./ Ad-state	Adsorption site	Bond length [Å] Me-C	C-O	n-n	Me-Me	Tilt angle [deg]	Technique	References
Cont'd.			atop						EELS	89Mar
			terminal						IRAS/LEED	96Lau
Ir(110)-	(2×2)	1							LEED	73Chr
(1×2)		1/4	4-fold H						LEED	78Tay1
										78Tay2
										78Tay3
									LEED	78Nie
	(4×2)	3/4	4 and 2 fold						LEED	78Tay1
										78Tay2
										78Tay3
Ir(110)		0.33	top						IRAS/LEED	95Lyo
(331)+(111) microfacets		0.8	top							
Mo(100)		α						no tilt	ESDIAD	80Nie
Mo(100)		θ<0.5	4-fold					40°±10°	NEXAFS	87Ful
			hollow					40°±5°	ARUPS	
Ni(100)	c(2×2)	0.5	T	1.80±0.04	1.13±0.05	3.52	2.489	no tilt	ARPEFS	81Kev
		0.5	T					no tilt	LEED	82Bib
		0.5							LEED	72Tra2
		0.5	T						LEED	78Hor1
		0.5	T						LEED	78All
		0.5	T					no tilt	LEED, EELS	88Uvd
		0.5	T	1.80±0.10	1.15±0.10	3.52	2.489	no tilt	LEED	79And2
		0.5	T	1.71±0.10	1.15±0.10	3.52	2.489		LEED	80And
		0.5	T	1.70±0.10	1.13±0.10	3.52	2.489		LEED	80Ton
		0.5	T	1.80±0.10	1.15±0.05	3.52	2.489		LEED	79Hei2
		0.5	T	1.80	1.15	3.52	2.489		XPD	79Pet

Substrate	Structure	Cover./ Ad-state	Adsorption site	Bond length [Å] Me-C	C-O	n-n	Me-Me	Tilt angle [deg]	Technique	References
Cont'd.	(3√2×√2)R45°	0.69							LEED	72Tra2
		0.67	B						LEED	82Bib
		0.67	B					tilted	LEED, EELS	88Uvd
	c(5√2×√2)R45°	0.6							LEED	72Tra2
		0.6	B, T						LEED	82Bib
		0.6	1/3 B, 2/3 T					bridge no tilt, atop tilt	LEED, EELS	88Uvd
Ni(111)	c(4×2)	0.5							LEED	82Net
		0.5	H	1.78±0.10	1.19±0.23	2.88	2.03 ass.		SEXAFS	93Bec
		0.5	fcc, hcp H			2.88			XPS	98Hel
		0.5	fcc-H	1.32±0.10		2.88	2.10±0.15		PED	94Dav
		0.5	64% hcp-H	1.29±0.05			2.10±0.15		PED	93Sch
		0.5	fcc-H	1.27±0.07		2.88	2.03 ass.		PED	94Dav
		0.5	64% hcp-H	1.29±0.07			2.03 ass.			
		0.5	fcc-H	1.32±0.07		2.88	2.04+0.12		PED	96Dav
		0.5	65% hcp-H	1.28±0.04			2.04-0.04			
		0.5	fcc-H	1.29±0.08	1.18±0.07	2.88	2.07±0.11	7+10°	PED	94Map
		0.5	2/3 hcp-H	1.34±0.07	1.15±0.07		2.07±0.11	6+10°		
	(2×2)	0.25	fcc-H	1.30±0.08		4.89	2.10±0.06		PED	96Dav
		0.25	64% hcp-H	1.26±0.04			2.10±0.06			
		0.25	atop	1.8±0.04	1.13	4.89	2.10		ARPEFS	81Kev
	(√3×√3)R30°	1/3	bridge	1.27±0.05	1.13	4.33	2.10			
		0.33	24% atop, B,76% H						LEED	76Con
		0.33				4.33			XPS	98Hel
	(√7×√7)R19°	1/3							LEED	74Chr
		0.57				3.30			LEED	76Con
			T, B			3.30			XPS	98Hel

Substrate	Structure	Cover./ Ad-state	Adsorption site	Bond length [Å] Me-C	C-O	n-n	Me-Me	Tilt angle [deg]	Technique	References
Cont'd.		0.57							LEED	82Net
	c(2√3×4)rec	0.62	Intermed.			2.77			XPS	98Hel
Ni(110)	(2×1) p2mg	1.0 at	B	1.83±0.02	1.117±0.1	2.49	2.490	θ_{CO}=23.9±0.7°	X-ray diff.	01Pet
		2.3 bar			1.21±0.03		2.492	θ_{NiC}=21.3±0.5°		
		1.0 at	B	1.84±0.02		2.49		θ_{CO}=23.5±0.7°		
		10^{-10} bar			1.19±0.03		2.492	θ_{NiC}=21.7±0.5°		
		1.0	B	1.15±0.07		2.49		θ_{CO}=20±4°	LEED	94Zha
					1.85±0.04		2.49	θ_{NiC}=20±4°		
		1.0	B	1.12±0.05		2.49		θ_{CO}=17±3°	LEED	88Han
					1.95±0.05		2.49	θ_{NiC}=27±3°		
		1.0	B, T			2.49		θ_{CO}=19°	XPD	92Kna
							2.49	θ_{NiC}=19°		
		1.0	B			2.49		θ_{CO}=19°	ARPES	93Hua
					1.94±0.02		2.49	θ_{NiC}=16±2°		
		1.0	B			2.49		θ_{CO}=17±2°	STM	95Spr
		1.0	B	1.13±0.05		2.49	2.49	θ_{CO}=21±3°	X-ray diff.	95Rob
					1.92±0.05		2.49	θ_{NiC}=27±2°		
		1.0	B	1.20±0.04		2.49		θ_{CO}=26±4°		
					1.87±0.03		2.49	θ_{NiC}=26±3°		
		1.0	B			2.49		θ_{CO}=20±5°	SEXAFS	93Pan
		1.0	B			2.49	2.49	θ_{CO}=17±2°	LEED	86Kuh
		1.0	B			2.49	2.49	θ_{CO}=17±2°	ESD	85Rie
		1.0	B			2.49	2.49	Tilted	LEED	85Beh
		1.0	B			2.49	2.49	Tilted	LEED	73Mad3
	c(4×2)	0.75	B, T			3.3	2.49	no tilt	LEED	85Beh
	c(8×2)	0.62	B, T			4.0	2.49	no tilt		
		0.3 - 0.9						θ_{CO}=(0-21)±1°	XPD	89Wes

Substrate	Structure	Cover./ Ad-state	Adsorption site	Bond length [Å] Me-C	C-O	n-n	Me-Me	Tilt angle [deg]	Technique	References
Pd(100)	(2√2×√2)R45°	0.5	B	1.93±0.07	1.15±0.10	2.745	2.74		LEED	80Beh
									LEED	78Bra1
									LEED	82Ort
									LEED	92Ber2
						3.9	2.74		LEED, EELS	88Uvd
									LEED	91And
					1.3±0.2				X-ray diffr.	96Sch
	(3√2×√2)R45°	0.67	B			2.74	2.74		LEED	92Ber2
						2.8	2.74	14-30°	LEED, EELS	88Uvd
									LEED	91And
									LEED	82Bib
	(4√2×√2)R45°	0.75	B			2.8	2.74		LEED	92Ber2
						2.8	2.74	29°	LEED, EELS	88Uvd
									LEED	91And
	c(4×2)R45°	0.5	B			3.9			LEED	69Tra1
	c(5√2×√2)R45°						2.74		LEED	82Bib
	c(7√2×√2)R45°						2.74		LEED	
Pd(111)	(√3×√3)R30°	1/3	Fcc H			4.71			LEED	70Ert
		1/3	Fcc H			4.71			LEED	83Hof1
		1/3	Fcc H			4.71			LEED	78Con
		1/3	Fcc H	1.29±0.05	1.15±0.05	4.71	2.748		LEED	87Oht
		1/3	Fcc H	1.25±0.04	1.11±0.04	4.71	2.2462		LEED	00Zas2
		1/3	Fcc, hcp H			4.71			STM	02Ros
		1/3	Fcc H	1.27±0.04	1.25±0.14	4.71	2.25	0±23°	PED	98Gie
	c(4×2)	0.5	B			3.6			LEED	83Hof1
		0.5	B			3.6			LEED	78Con
		0.5	B			3.6			LEED	84Mir
		0.5	B			3.6			STM	02Ros

Substrate	Structure	Cover./ Ad-state	Adsorption site	Bond length [Å] Me-C	C-O	n-n	Me-Me	Tilt angle [deg]	Technique	References
Cont'd.		0.5	Fcc H	1.31±0.06	1.14±0.12	3.6	2.25	0±25°	PED	98Gie
			Hcp H	1.37±0.06	1.14±0.14	3.6	2.25	0±25°		
	(√3×2)rect	0.5	B						LEED	90Tüs1
	(√3×35)rect	0.514	B							
	c(√3×17)rect	0.529	B							
	(√3×11)rect	0.545	B							
	c(√3×9)rect	0.556	B							
	(√3×7)rect	0.571	B							
	c(√3×5)rect	0.6	B							
		0.6	B						LEED	83Hof1
			B						LEED	78Con
	c(4√3×8)rect	0.63	B, H, T						LEED	83Hof1
			B, H, T						LEED	78Con
	split (2×2)	2/3	T, H						LEED	83Hof1
			T, H						LEED	78Con
	(2×2)	3/4	T, fcc H, hcp H						STM	02Ros
		3/4	T, H						LEED	83Hof1
Pd(110)	(2×1)p2mg	0.7-1.0	Short B						LEED	74Con1
		0.75	B						LEED, XPS	97Ram
		1	Short B	1.84±0.14	1.15			Alt. tilt. 6±6, 24±3	XPD	94Loc
	(2×1)	1	T	2.11±0.06	1.16±0.04	2.74	3.28	Alt. tilt. 2±5, 11±4	TLEED	93Wan
	(2×1)p1g1 or p2mg	1	B	1.97±0.03	1.15	2.74	3.28	22±5	PED	02Kit
	(2×1)p2mg	0.7-1	B			2.75	3.28	Alt. tilt	LEED,EELS	99Kat2
	(2×1)p2mg +	0.4-0.7	B					Alt. tilt		

Substrate	Structure	Cover./ Ad-state	Adsorption site	Bond length [Å] Me-C	C-O	n-n	Me-Me	Tilt angle [deg]	Technique	References
Cont'd.	(3×1)									
	(2×1)	0.3-0.4	B					upright		
	c(2×4)	0.1-0.3	B					upright		
	(2×1)p2mg		B						LEED	00Yag
	(4×2)	0.3-0.75	B						LEED	91Hu
			B						LEED,IRAS	90Rav2
			B						LEED	00Yag
		0.75							LEED,XPS	97Ram
	(2×1)p2mg								LEED	88He
	(4×2)								LEED	74Con1
	(1×1)	0.05-0.3							LEED, IRAS	90Rav1
Pt(100)-(hex)	(1×1)								LEED	81Nor
									LEED	75Kne
									LEED	81Bar2
			B and T						LEED,EELS	83Beh
									LEED	68Mor
	c(4×2)	0.75							LEED	64Tuc
									LEED	81Nor
									LEED	75Kne
									LEED	81Bar2
			B and T						LEED,EELS	83Beh
									LEED	68Mor
	c(2×2)	0.5	T, islands						LEED,EELS	83Beh
Pt(100)-(1×1)	c(2×2) or	0.2-0.5	T, islands					normal	LEED,EELS	83Beh
	(√2×√2)R45°	0.5	1/3 B, 2/3 T						LEED,IRAS	95Mar
		0.5	B						LEED,EELS	78Pir
		0.5	B						LEED	82Bib
	c(5√2×√2)R45°	0.6	2/3 B. 1/3 T						LEED,IRAS	95Mar

Substrate	Structure	Cover./ Ad-state	Adsorption site	Bond length [Å] Me-C	C-O	n-n	Me-Me	Tilt angle [deg]	Technique	References
Cont'd.	c(3√2×√2)R45°	0.67	1/2 B, 1/2 T						LEED,IRAS	95Mar
									LEED,EELS	83Beh
	c(4×2)	0.75	2/3 B, 1/3 T						LEED,IRAS	95Mar
			2/3 B, 1/3 T						LEED	78Bro
									ARUPS	82Bro
									LEED,EELS	83Beh
Pt(111)	(√3×√3)R30°	1/3	T			4.80	2.78	Normal	LEED	77Ert
			T						LEED	91Won
			T						LEED	82Ste
			T						LEED	90Ryb
	c(4×2)	0.5	1/2 T	1.85±0.025	1.15±0.05	T:5.4;4.8	2.769	Normal	LEED	87Ogl
			1/2 B	1.85±0.025	1.15±0.05	T-B:3.7		Normal	LEED	88Bla
		0.5	1/2 T	1.92±0.04	1.12±0.04		2.77	Normal	LEED	00Zas1
			1/2 B	1.40±0.04	1.19±0.04				LEED	82Ste
		0.5	1/2 T, 1/2 B						LEED	90Ryb
	(√3/2×√3/2)R15°	0.58	~½ T, ½ B					Tilt?	LEED	82Ste
	2/3(√3×3)rect	0.67	¼ T, ¾ B						LEED	98Ma
	(2×2)	1/3	0.88 T	1.85±0.10	1.15±0.10		2.77		LEED	87Ogl
	disordered		0.12 B	2.08±0.10	1.15±0.10					
	(4×4)	0.18	T						LEED	87Tüs
		0.19	T						LEED	90Ryb
	(8×8)	0.3	T							
	hexagonal	200 Torr				3.7	2.77		STM	98Jen
	(√19×√19)R23.4°	0.67				3.7	2.77		STM	94Vil
Pt(110)-(1×2)	(1×1)	0.5-1	T				2.77		LEED	76Com3
			T					25°	LEED, ARUPS	82Hof1
			T						LEED	82Fer
			T						RBS	82Jac1

Substrate	Structure	Cover./ Ad-state	Adsorption site	Bond length [Å] Me-C	C-O	n-n	Me-Me	Tilt angle [deg]	Technique	References
Cont'd.			T						LEED	72Bon1
			T						LEED	74Lam1
			T						LEED	74Lam2
			T						LEED	76Com3
	(2×1)p1g1	1	T			2.77		Zig-Zag	LEED	82Hof1
			T			2.77		26 ± 2°	ARUPS	82Bar
			T							84Bar
			1/4 B, 3/4 T					normal	EELS,ARUPS	86Fre1
			0.16 B, 0.84 T						LEED, XPS UPS	84Rie
	(2×1)p2mg	1	T			2.77		20°	RBS	82Jac1
	c(8×4)	1	T			2.77		normal	LEED,ARUPS	82Hof1
		1	T						UPS	82Fer
		>0.2 at 160 K	1/3 B, 2/3 T					15 ± 5°	ARUPS, LEED	83Hof2
		2L	T	1.9 ± 0.1	1.3 ± 0.1			10° - 24°	RHEED	95Sch
Rh(100)	c(2×2)	0.5	T						XPS, LEED	98Str
			T			3.80	2.69		EELS, LEED	97Wei
			T			3.80	2.69		XPS, LEED	96Bar
			T			3.80	2.69		LEED, IRAS	94deJ
			T			3.80	2.69	normal	LEED, EELS	87Gur
			-			3.80	2.69		LEED	82Kim
			4 fold H			3.80	2.69		LEED	78Cas
	(4√2×√2)R45°	0.75	0.7 B, 0.3 T						XPS, LEED	98Str
			2/3 B, 1/3 T						XPS, LEED	96Bar
			0.5 B, 0.5 T			3.59	2.69	tilt	LEED, IRAS	94deJ
			2/3 B, 1/3 T			2.69	2.69	normal	LEED, EELS	87Gur
									LEED	82Kim

Substrate	Structure	Cover./ Ad-state	Adsorption site	Bond length [Å] Me-C	C-O	n-n	Me-Me	Tilt angle [deg]	Technique	References
Cont'd.			T, B, H			3.17			LEED	66Tuc
	c(6×2)	0.83	0.45 B, 0.55 T						XPS, LEED	98Str
			0.55 B, 0.45 T						XPS, LEED	96Bar
			1/5 B, 4/5 T			3.23	2.69	tilt	LEED, IRAS	94deJ
	"split (2×1)"	0.83	B, H			2.69	2.69		LEED	78Cas
Rh(111)	(2×2) at <120 K	0.25	T			5.38	2.69		LEED, XPS	97Beu
			T			5.38	2.69		LEED, XPS	98Beu
	(1×1) at >120 K	0.25	T				2.69			
			T				2.69		XPS	01Sme
	(√3×√3)R30°	1/3	H			4.7	2.69		LEED	78Cas
		1/3	T			4.7	2.69		LEED	79Thi2
		1/3	T	1.95±0.1	1.07±0.1	4.7	2.69	Normal	LEED	81Koe
			T			4.7	2.69		LEED, XPS	97Beu
			T			4.7	2.69		LEED, XPS	98Beu
	(4×4)-8CO at <120 K	0.5					2.69		LEED, XPS	97Beu
							2.69		LEED, XPS	98Beu
	split (2×2)	>0.5	T, B, H			3.6	2.69		LEED	78Cas
							2.69		EELS	80Dub
	(2×2)-3CO	0.75	T, H			3.2	2.69		LEED	78Cas
		0.75				3.11	2.68		LEED	79Thi2
		0.75	2/3 T	1.94±0.1	1.15±0.1	2.85±0.1	2.68	<15°	LEED	83vHo1
			1/3 B	2.03±0.07	1.15±0.1	3.23±0.1	2.69	normal	LEED	
		0.75	1/3 T			3.1	2.69		LEED, XPS	97Beu
			1/3 H hcp			3.1	2.69		LEED, XPS	98Beu
			1/3 H fcc			3.1	2.69		LEED, XPS	01Sme
		0.75	1/3 T	1.86±0.05	1.17	3.1	2.69	normal	SXD	99Lun

Substrate	Structure	Cover./ Ad-state	Adsorption site	Bond length [Å] Me-C	C-O	n-n	Me-Me	Tilt angle [deg]	Technique	References
Cont'd.			1/3 H hcp	1.49±0.05	1.16	3.1	2.69	normal	SXD	
			1/3 H fcc	1.49±0.05	1.16	3.1	2.69	normal	SXD	
	(2×1)	0.5							STM	00Cer
	(√7×√7)R19°	3/7							STM	
	(2×2)-3CO	5-700torr							STM	
		0 to 0.75	T, B						LEED,XPS	84deL
		0 to 0.75	T, H hcp, H fcc						XPS	01Sme
Rh(110)-(1×1)	(2×1)p1g1	1	Short bridge						LEED	77Mar
	c(2×2)	0.5								
	c(2×2) split	0.3-0.5	Short bridge						LEED	94Wei
	c(2×2)	0.5	Short B							
	(3×2)	2/3	Short B							
	(4×2)	0.75	Short B							
	(5×2)	4/5	Short B							
	(2×1)p2mg	1	T					13°		
	(1×1)	0.18 at 120 K	T						LEED, XPS	93Dha
	c(2×2) streaky	0.37	T							
	c(2×2)	0.54	T							
	(2×1)p2mg	1.0 at 120 K	0.57 B, 0.43 T							
	(2×1)p2mg	1.0 at 270 K	0.80 B, 0.2 T							
Rh(110)-(1×2)	(1×2)	0.24 at 120 K	0.45 B, 0.55 T						LEED, XPS	93Dha
	(2×2) poor	0.46 at	0.54 B,							

Substrate	Structure	Cover./ Ad-state	Adsorption site	Bond length [Å] Me-C	C-O	n-n	Me-Me	Tilt angle [deg]	Technique	References
Cont'd.		120 K	0.46 T							
	c(2×4) diffuse	0.52 at 270 K	0.46 B, 0.54 T							
	c(4×2)	0.75 at 270 K	0.57 B, 0.43 T							
	(2×2)p2mg	1.0 at 270 K	0.53 B, 0.47 T							
Ru(0001)	(√3×√3)R30°	0.33	atop	2.0±0.1	1.1±0.1			no tilt	LEED	83Mic
Ru(0001)	(√3×√3)R30°	0.33	atop					12°-16°	ESDIAD	79Mad, 93Ove
				1.93±0.04	1.10±0.05			dynamic tilt, temp. depend.	LEED	96Gie
Ru(0001)	(2√3×2√3)R30° disordered	0.05-0.2	atop	2.0 ± 0.15	(1.1)			≤ 10° tilt upright	ARUPS DLEED	85Hof 89Pie
Ru(0001)			atop	1.92	1.165				Theory	00Kop
			hollow	1.58	1.199					
W(110)		0.23-0.5						~ 70°	ESDIAD	82Hou
W(111)		α (v)						no tilt at 100K	ESDIAD	76Mad

Table 8. Adsorbed CO (valence electronic structure). Electron binding energies are referenced to the Fermi-level.

Substrate	Structure	Coverage/ adsorbed state	MO valence levels [eV] 5σ	1π	4σ	Technique	Reference
Ag(110)	disordered		9.1	11.9	14.8	UPS	84Kra
Al(111)	disordered		7.9	11.0	13.7	UPS	80Chi
		monolayer	12.35	15.33	18.04	UPS	89Jac
		multilayer	12.99	15.99	18.74		
Au(110)	disordered		-	10.0	12.5	UPS	89Düc, 94San2
			9.8±0.6	9.8±0.6	12.7	UPS	
Co(0001)			8.2	6.8	10.8	UPS	79Fre, 83Pap
	(√3×√3)R30°	1/3	7.9±0.1	7.25±0.3	10.75±0.05	ARUPS normal emission	83Gre
	(2√3×2√3)R30°	7/12					
Co(10$\bar{1}$0)	(2×1)		~7.5	~7.5	11	UPS	82Pap
Cr(110)	c(4×2)	α_1	~7.5	~7.5	11.6	UPS	86Shi
		α_2	~7.5	~7.5	10.8		
Cu(100)	c(2×2)	0.5	8.5	8.5	11.8	UPS	85Hes
			8.5	8.5	11.5	UPS	77All2
			8.5	8.5	11.8	UPS	94San3
			8.8	7.5	12.0	XES	00Föh1, 00Föh2
Cu(111)	(√3×√3)R30°	0.33	8.6	8.6	11.7	UPS	86Kir
		0.33	8.5	8.5	11.6	UPS	75Con
Cu(110)	(2×1)	0.5	8.4	8.4	11.8	RPES	85Che2
						UPS	82Mar
		0.3	8.5	8.5	12.0	ARUPS	78Kan
Fe(110)			7.6	7.6	10.6	UPS	79Bro, 83Jen
	(1×2)	0.5	8.1	6.9			94Mar

Substrate	Structure	Coverage/ adsorbed state	MO valence levels [eV] 5σ	1π	4σ	Technique	Reference
Cont'd.		~ 0.1-0.5	7.5-8.3	7.5-8.3 cov. dep.	10.5-10.7	ARUPS	
Fe(100)	c(2×2)		7.1	7.1	10.5	UPS	77Rho
Fe(100)		α_1 α_2 α_3 β				UPS	88Cam
Fe(111)		atop bridge	8.54 7.37	8.93-9.21 8.72-9.65	11.45 10.81	Theory	89Ron
Ir(100)			9.2	8.6	11.7	ARUPS	80Sea
Ir(100)(5×1)	(1×1)	top	7.2	8.5	11.3	UPS	76Bro
Ir(111)	(√3×√3)R30°	1/3	9.1	8.8	11.7	ARUPS	81Sea
			7.3	8.7	11.2	UPS/XPS	78Zhd
	(2√3×2√3)R30°	7/12	8.5	9.0	11.9	ARUPS	81Sea
			9.2	8.6	11.7	ARUPS	80Sea
			7.8	8.6	11.3	UPS	76Zhd
Ir(110)			8.6	7.2	11.2	UPS	89Düc
Mn/Cu(100)	c(8×2)-Mn	0.83 ML Mn	7.4	7.4	10.7	UPS	99Grü
Ni(100)	c(2×2)	0.5	7.2	5.5	10.3	XES	00Föh1, 00Föh3
		0.5	8.3	7.8	10.8	UPS	77All1
		0.5	8.0	7.5	10.6	ARUPS	78All
		0.5	7.5	7.5	10.7	PES	94San3
		0.5	8	8	11	UPS	80Smi
		0.5	8	8	11	ARUPS	78Hor1
		0.5	7.5	7.5	10.7	UPS	71Eas

Substrate	Structure	Coverage/ adsorbed state	MO valence levels [eV] 5σ	1π	4σ	Technique	Reference
Cont'd.	(3√2×√2)R45°	0.66	8.2	7.2	10.8	UPS	83Koe1
		0.69	6.5	7.9	10.9	UPS	81Bru
Ni(111)			8.7	7.1	11.7	UPS	76Wil
	c(4×2)	0.5	8.4	7.3, 6.1	11.2	ARUPS	90Sch
	(√7/2×√7/2) R19.1°	0.57	8.5		11.2	ARUPS	
	(√7/2×√7/2) R19°	0.57	8	8	10.9	UPS	88Gum
			7.8	7.8	10.6	UPS	76Con
			8.5	8.5	11.6	UPS	86Wur
Ni(110)	(2×1)p2mg	1.0	8.4	6.7	10.5 - 11.4	ARUPS	86Kuh, 89Kuh
		1.0	8.4	6.5	11.7	UPS	82Hor
		1.0	8.0	8.0	11.0	UPS	84Rie
Os (poly)		~0.4	8.3	8.3	11.0	UPS	80Fuk1
Pd(100)	(2√2×√2) R45°	0.5	7.6	7.3	10.5	UPS	94San1
		0.5 L-20 L	7.9	7.9	10.8	UPS	80Beh
Pd(111)	(√3×√3) R30°	1/3	8.2	7.5	11.2	UPS	76Llo
	c(4×2)	0.5	7.8	7.3	10.7	UPS	84Mir
			7.8	7.8	11	UPS	95Ban
Pd(110)		1	7.9	7.9	10.8	UPS	78Weh
Pt(100)	c(4×2)	0.75	8.8	7.6	11.4	ARUPS	82Bro
Pt(111)	(4×4)		9.2	8.3	11.7	UPS	94San1
			9.2	8.4	11.9	UPS	79Nor
			9.6	8.6	12.0	UPS	
		10 L	8.6	8.6	11.7	UPS	89Mur
			8.1	9.1	11.8	UPS	81Mil
Pt(110)		0.6	9.2	7.9	11.6	YPES	89Düc
			9.2	8.2	11.7	UPS	81Bar1

Substrate	Structure	Coverage/ adsorbed state	MO valence levels [eV] 5σ	1π	4σ	Technique	Reference
Cont'd.		5 L	8.7	8.7	11.8	UPS	77Shi1
	(2×1)p1g1	1	9.25	8.2	11.7	UPS	82Bar
	c(4×2)		9.2	8.3	11.7	UPS	82Hof2
Re(0001)		α	7.9	7.9	11.0	UPS	80Fuk2
			~ 7	8.15	10.8		85Tat
			7.3-8.15	7.3-8.15	11.1		80Duc
Rh(100)			7.6		10.8	UPS	83Koe1
Rh(111)		Sat. at 300 K	8.3	7.8	11.2	UPS	78Bra2
Rh(110)-(1×1)	(2×1)p2mg	1	7.6	8.7	10.6	UPS	81Bai 80Bai
Ru(0001)		α	7.7	7.7	10.5	UPS	75Fug1
Ru(0001)			7.7	7.7	10.8		85Shi1
Ru(1,1,10)							
Ru(0001)	(√3×√3)R30°	0.33	7.55	7.4	10.5	ARUPS	85Hof
	(2√3×2√3)R30°	0.56	7.9	7.3	10.6		
Ru $(10\bar{1}0)$			7.4	7.4	10.6		75Bon1
W(100)		α	8.9	8.9		UPS	73Bak
		β	5.9 (C)				
W(100)		"virgin"	7.6	7.6	11.4	UPS	76Vor
		α	8.7	8.7			
		β	6.5	6.5			
W(100)		α_1	8.7	8.70		ARUPS	76Plu
		α_2	8.3	8.3	11.4		
W(110)		"virgin"	~7.3	~7.3	10.4		
		α	7.8	7.8	10.8		

Table 9. Adsorbed CO (core level binding energies; adsorption states; molecular/atomic species).
Electron binding energies are referenced to the Fermi-level.

Substrate	Structure	Coverage/ adsorbed state	Chemical state	Core level energies [eV]		References
				C 1s	O 1s	
Ag(110)			CO	286.4	533.9	94San2
Au(110)			CO	286.8	533.7	94San2
Co(0001)	(√3×√3)R30°		CO	285.8±0.4	531.9±0.4	83Gre, 00Cab, 00Fre
Co(10$\bar{1}$2)			CO	285.3		81Pri
Cu(100)	c(2×2)	0.5	atop	286.3	533	92Bjö
	c(7√2×√2)R45°	0.57	atop	286.3	533	90Ant
Cu(110)		Sat.			533.2	92Chr
	(2×1)	0.5	atop	286	533	86Hol
Fe(110)			CO		531.9	79Bro
			Dissociated		530.3	
			CO	285.5	531.6	98Sey
Fe(100)			CO at	285.6	532.1	78Bru
			123-150 K	284.8	532.4	80Ben
Fe(100)		α_1	CO		532.2	87Moo1
		α_2	CO		531.4	
		α_3	CO tilted		530.6	
		β	Dissociated	282.0	529.9	
Fe(111)			CO	285.4	532.0	77Tex
			Dissociated	282.8	530.0	
Fe/W(110)		α (v), <300 K	CO		531.8	97Nah
		β, >300 K	Dissociated		530.1	
Ir(111)	(2√3×2√3)R30°	7/12	CO		530	76Zhd

Substrate	Structure	Coverage/ adsorbed state	Chemical state	Core level energies [eV]		References
				C 1s	O 1s	
Mn/Fe(110)		α	CO		531.8	93Sie
		β	Dissociated		530.2	
Mo(100)		α-states	CO	286.0	532.5	85Zae
		β-states	Dissociated	284.5	530.8	
Ni(100)	c(2×2)	0.5	atop	285.8	532.2	92Bjö
		0.5	atop	285.8	531.4	98Föh, 99Föh1
	(3√2×√2)R45°	0.67	bridge	285.7	531.5	88Uvd
		0.69		285.6	531.5	81Bru
	c(5√2×√2)R45°	0.6	33% atop, 67% bridge	285.8	532.2	88Uvd
				285.5	531.3	
		7 L		285.5	531.2	83Koe2
Ni(111)	c(4×2)	0.5	fcc-hollow	285.24	530.86	98Hel
			hcp-hollow	285.24	530.86	
	(√3×√3)R30°	1/3	fcc-hollow	285.24	530.86	
	(√7×√7)R19°	0.57	bridge	285.32	531.01	
			atop	285.96	532.15	
	c(2√3×4)rect	0.62	interm. bridge	285.32	531.01	
				287	532.3	84Jug
Os (poly)		~0.4	CO	286.3	532.4	80Fuk1
Pd(100)	(2√2×√2)R45°	0.5	bridge	285.9	531.4	92Bjö, 94San1, 94San2, 94San3
					531.2	95Ped
	(3√2×√2)R45°	0.67	bridge	286.0	531.6	92Bjö, 94San1, 94San2, 94San3
	(4√2×√2)R45°	0.75	bridge	286.1	531.7	92Bjö, 94San1, 94San2, 94San3

Substrate	Structure	Coverage/ adsorbed state	Chemical state	Core level energies [eV]		References
				C 1s	O 1s	
Pd(111)		0.03	100% hollow	285.53		00Sur
		0.1	94% H, 6% bridge	285.53, 285.73		
		0.21	89% H, 11% bridge	285.53, 285.73		
		0.32	76% H, 24% bridge	285.54, 285.74		
		0.41	63% H, 37% bridge	285.55, 285.74		
		0.48	45% H, 55% bridge	285.60, 285.78		
		0.50	44% H, 56% bridge	285.59, 285.76		
Pd(110)	(4×2)	0.75, 300 K	bridge on ridge	286.3		97Ram
			bridge in grooves	286.1		
	(1×1)	low		284.8		
	(2×1)p2mg	0.75 at 135 K	bridge on ridge	286.3		
Pt(110)-(1×2)		0-1 at 300 K	atop		532.7	86Fre1
	c(8×4)	1 at 120 K	75% atop, 25% bridge		532.8, 531.0	
	(2×1)p2mg	1.0 at 80-600 K	atop	287.1	533.2	01Now
	c(8×4)	1.09 at 80-240 K	80% atop, 20% bridge	287.1	533.1, 531.2	
Pt(111)	(4×4)	0.18	atop	286.7	532.6	94Bjö
	c(4×2)	0.5	50% atop,	286.7	532.7	95Bar
			50% bridge	286.0	531.0	
	c(5×√3)	0.6	33% atop,	286.7	532.7	
			67% bridge	286.0	531.0	
Re(0001)		α, at 100 K	CO		533.6	85Tat
			CO		532.1	
	(2×2)	β, at 420 K	Dissociated		530.5	
Re(0001)		α	CO		532	80Duc, 80Fuk2
		β	Dissociated		530	
Re/Pt(111)		0.55 ML Re	CO at Pt-site	286.0	531.1	99Ram

Substrate	Structure	Coverage/ adsorbed state	Chemical state	Core level energies [eV]		References
				C 1s	O 1s	
Cont'd.				286.6	532.8	
			CO at Re-site	285.7		
Rh(100)	c(2×2)	0.5	atop	285.85		98Str
	(4√2×√2)R45°	0.75	bridge	285.45		
	c(6×2)	0.83	atop		532.4	96Bar
			bridge		531.5	
Rh(111)		low	atop	284.04		01Sme
	(√3×√3)R30°	1/3	atop	286.0	532.1	97Beu
	(2×2)	0.25	atop	286.0	532.1	
	(4×4)	0.5	atop	286.0	532.1	
	(2×2) 3CO	0.75	67% fcc hollow	285.35	530.6	
			33% atop	286.0	532.1	
		0.75	33% atop	285.99		01Sme
			33% fcc H, 33% hcp H	285.29		
		3 L	atop	286.03		
			bridge	285.42		
			hollow	285.25		
		1 L-20 L	atop	286.1	532.0	84deL
			(bridge)	285.3	530.8	
Rh(110)-(1×1)	(2×1)p2mg	1 (10 L dose)	atop	285.4	531.3	80Bai, 81Bai
			bridge		530.8	93Dha
			atop		531.9	
	(1×1)	0.18 at 120 K	atop			
	c(2×2) streaky	0.37	atop			
	c(2×2)	0.54	atop			
	(2×1)p2mg	1.0 at 120 K	57% bridge, 43% atop			

Substrate	Structure	Coverage/ adsorbed state	Chemical state	Core level energies [eV]		References
				C 1s	O 1s	
Rh(110)-			bridge		530.8	93Dha
(1×2)			atop		531.9	
	(1×2)	0.24 at 120 K	45% bridge, 55% atop			
	c(4×2)	0.75 at 270 K	57% bridge, 43% atop			
	(2×1)p2mg	1.0 at 270 K	53% bridge, 47% atop			
Ru(0001)	(√3×√3)R30°	α	CO		531.7±0.2	75Fug2, 75Fug3, 77Fug
					531.85±0.15	85Shi1
		β			530.1±0.2	
		α			532	
		β			~530.5	
Ru $(10\bar{1}0)$		$\theta \leq 0.6$	atop CO		531.7	96Rot
		$\theta > 0.6$			531.9	
		$\theta > 1$	atop		531.9	
			bridge		530.9	
Ti(0001)			dissociated	281.8±0.2	529.8±0.2	78Fuk, 80Fuk3
Ti(0001)			dissociated CO,	281.9	530.4	98Kuz
			bulk C and O phases	283.2	531.8	
				284.4		
W(poly)		α_1	CO	≈287.3	534.2	74Yat1
		α_2	CO	≈287.3	532.8	
		"virgin"	CO	≈285.4	531.5	
		β	dissociated	≈283.1	530.5	
W(100)		α_1	CO	286.2	533.0	74Yat2, 74Yat3
						76Yat1
		α	CO		533	
		"virgin", β_1	CO and dissoc.		531.7	

Substrate	Structure	Coverage/ adsorbed state	Chemical state	Core level energies [eV]		References
				C 1s	O 1s	
Cont'd.		β_2, β_3	dissociated	283.2	530.1-530.6	
W(110)		α	CO	285.8±0.5	532.0±0.4	77Umb, 83Umb
		"virgin"	CO	285.5±0.3	531.6±0.3	77Ste1
		β	dissociated	283.1±0.3	530.4±0.2	
Zn/Ru(0001)		0.16-0.57 ML Zn ~ 1 ML O	CO		535.2	93Rod
O/Zn(0001)			physisorbed CO	291.5	537.7	90Car

Table 10. Molecular N_2 adsorption (thermodynamics)

Substrate	Structure	Coverage/ adsorbed state	Heat of adsorption E_{ad} [kJ/mol]	Technique	Activation energy of desorption E_d [kJ/mol]	Pre-exponential factor ν_d [s^{-1}]	Sticking coefficient $s(\theta)$	References
Cr(110)		0.36					0.09	84Miy
		γ state		TDS	14			91Dow
					28	1×10^{13} ass.		
Fe(110)			209	TDS	234	1×10^{13} ass.	10^{-7} - 10^{-6}	77Boz2
Fe(100)	c(2×2)	β	222	TDS	243	1×10^{13} ass.	10^{-7} - 10^{-6}	77Boz1, 77Boz2
		β	218		214		10^{-7} - 10^{-6}	
Fe(111)		α	31.4	Isotherms			0.003 at 120 K	82Ert2
				TDS		$\sim2\times10^{10}$		
		γ	~24	TDS				84Gru1, 84Gru2, 85Str

Substrate	Structure	Coverage/ adsorbed state	Heat of adsorption E_{ad} [kJ/mol]	Technique	Activation energy of desorption E_d [kJ/mol]	Pre-exponential factor ν_d [s^{-1}]	Sticking coefficient $s(\theta)$	References
Fe(111)		β, θ_{max} = 0.55		MB, variable incidence energy			1×10^{-6} at 300 K, ~0.1 at high incident kinetic energy	87Ret1, 87Ret2
Fe(111)		δ			20.7	2.1×10^{13}		87Gru2
		γ	31	Isobars	24.5	1×10^{13}		
				TDS	25-28			
		γ (on α)	38	Isobars				
Ir(110)-(1×2)		0 - 1		TDS	35.5-25.1	10^{8} - 10^{11}	1	81Ibb
	p1g1(2×2)	1						
Ir(100)-(1×1)		γ, 90 K	30	TDS		1×10^{13} ass.		93Gar
Ir(100)-(5×1)		97 K	25	TDS		1×10^{13} ass.		93Gar
		130 K						
		160 K						
Mo(110)		β at 300 K		TDS	339±13	0.01	0.09	72Mah
Mo(100)	clean			TDS			0.6±0.1 at 200 K	80Ko1
	c(2×2)-C						$<1\times10^{-3}$	
Mo(111)	c(3×2)-N, facets to (433) at 850 K	β at 300 K θ_{max} = 0.35		AES			0.05	83Ega
Ni(100)	c(2×2)	0.5, γ, 120 K		TDS, LEED	25	1×10^{13} ass.	1	84Gru3
		0.1 - 0.5		TDS	44 - 25	1×10^{13} ass.	1- 0	
	c(2×2)	0.5		LEED				84Dow
Ni(111)		0	35	TDS		1×10^{13} ass.		91Yos
		at 90 K		TDS	20	1×10^{13} ass.		86Bre

Substrate	Structure	Coverage/ adsorbed state	Heat of adsorption E_{ad} [kJ/mol]	Technique	Activation energy of desorption E_d [kJ/mol]	Pre-exponential factor ν_d [s^{-1}]	Sticking coefficient $s(\theta)$	References
Ni(110)	(2×1)	0 - 0.65		TDS	42	1×10^{13} ass.	1 - 0.45	84Gru3
	fluid	0.65 - 0.75		TDS	42 - 21	1×10^{13} ass.	0.45 - 0.5	83Gru2
	c(1.4×2)	0.75 - 1.0		TDS	21	1×10^{13} ass.	0.5 - 0	84Gru3
		0 - 1	36.6-42-20	TDS		8×10^{12}		80Gol
	(2×1)	0.5		LEED				88Kuw
	fluid	0.5 - 0.67		LEED	13			
	c(1.4×2)	0.72		LEED, TDS				
	(2×1)	0.5		LEED				83Jac1
	(2/3×1/3)	0.72		LEED				
	(1×1) gas	0 - 0.3, >140K		LEED				83Gru1
	(2×1)	0.5		LEED				
	fluid	0.5 - 0.72		LEED				
	c(1.4×2)	0.72		LEED				
Pd poly		γ at 78 K		TDS	25 - 41	1×10^{13} ass.	0.67	68Kin
Pd(110)	(2×1)	γ at 120 K		TDS	25	1×10^{13} ass.		87Kuw
Pt(111)		120 K		TDS	40	1×10^{13} ass.	0.15	77Shi2
Re(0001)		γ		TDS, FIM	~40	1×10^{13}	adsorbs at 80 K	76Liu
		β					$<10^{-5}$ at 300 K	
Re(0001)		α		TDS	24±1	1×10^{11}	0.88	87Haa1
		β			260±20	1×10^{-2}	9×10^{-6}	
Re$(11\bar{2}0)$		α		TDS	21±2	1×10^{9}	0.92	87Haa1
		β			29±2	1×10^{10}		
					240±40	1×10^{-2}	4×10^{-4}	
Rh(100)				TDS, FEM	38	1×10^{13} ass.		83Hen

Substrate	Structure	Coverage/ adsorbed state	Heat of adsorption E_{ad} [kJ/mol]	Technique	Activation energy of desorption E_d [kJ/mol]	Pre-exponential factor ν_d [s^{-1}]	Sticking coefficient $s(\theta)$	References
Rh(111)				TDS, FEM	35	1×10^{13} ass.		83Hen
Rh(110)				TDS, FEM	43	1×10^{13} ass.		83Hen
Rh (poly)		γ_1 at 110 K		TDS, FEM	30	1×10^{13} ass.		83Hen
		γ_2 at 160 K		TDS, FEM	45	1×10^{13} ass.		
		γ_3 at 225 K		TDS, FEM	60	1×10^{13} ass.		
Ru(0001)		γ 75 K		TDS	24.4	1×10^{13} ass.		83Ant, 86Ant
	$(\sqrt{3}\times\sqrt{3})R30°$	95 K			31.4			
Ru(0001)	$(\sqrt{3}\times\sqrt{3})R30°$	δ	28	Isotherms		$\sim1\times10^{12}$		82Feu, 83Men
		γ	42	TDS	38-40	$\sim1\times10^{16}$	0.4 (increase to 0.65 at $\theta = 0.17$)	97Mor
		γ	59	Theory				
Ru(0001)		β					1×10^{-12} at 300 K	96Die, 97Jac
Ru(0001)	clean	β		TPD			$\sim2\times10^{-12}$ at 300 K	99Dah
							$\sim7\times10^{-10}$ at 500 K	
	Au decorated steps, $\theta_{Au} = 0.01$						$\sim2\times10^{-17}$ at 500 K	
Ru $(10\bar{1}0)$		β		TDS			1×10^{-12} at 300 K	96Die, 97Jac
Ru $(11\bar{2}1)$							1×10^{-12} at 300 K	
W(110)		γ		TDS (WFC)	~38			65Del
W(110)		β		TDS	331±13	0.05	0.004	71Tam, 75Sin
	(2×2)		0.25				~0.01 at 300 K	79Som
W(110)		γ-state (0.7)		TDS	27	1×10^{11}		76Yat2
				isothermal desorption	43	1×10^{15}	~0.7 at 100 K	90Lin

Substrate	Structure	Coverage/ adsorbed state	Heat of adsorption E_{ad} [kJ/mol]	Technique	Activation energy of desorption E_d [kJ/mol]	Pre-exponential factor ν_d [s^{-1}]	Sticking coefficient $s(\theta)$	References
W(110)		β_3	θ_{max} = 0.2				0.003 at 820 K E_i <20 kJ/mol	84Aue, 84Lee
W(110)		β					0.003 at 800 K E_i <30 kJ/mol	86Pfn
W(100)		γ (γ^+, γ^-) β		TDS (WFC)	42-46 314			65Del
W(100)		γ (γ^+, γ^-) β		TDS	39-44 308	1×10^{13} 0.23	 0.4 at 300 K	70Cla
W(100)		β					0.59±0.01 at 300 K	74Kin
	c(2×2)	δ (precursor)			≥ 18		0.60 at 90 K	83Aln
		β		TDS	335±13	0.05	0.50-0.58 at 300-405 K	66Est, 71Tam
W(111)		γ α β		TDS (WFC)	38 67 ~314			65Del
W(111)							0.08±0.01 0.09	72Kin, 74Kin

Sticking coefficients of N_2 adsorption at 300 K on various surfaces of W, such as (100), (310), (320), (411), (111) and (110), were published by [75Sin] (see Fig. 61). The heat of adsorption in the β-state is given as ~320 kJ/mol.

Table 11. Adsorbed N_2 (desorption temperatures and dissociation parameters)

Substrate	Adsorbed State	Coverage θ	Temperature of dissociation [K]	Activation energy of dissociation [kJ/mol]	Pre-exponential factor [s^{-1}]	Temperature of desorption [K]	References
Fe(110)	β			~29		920	77Boz2
Fe(100)	β			~21-46		920-1000	76Ert, 77Boz1
Fe(111)	β			~ 0		880	
Fe(111)	γ		110 (conversion to α-state)			~90	82Ert2, 85Tsa, 86Whi1
	α		145 - 160			160	
	β					850	
Re(0001)	α			14±2		~120	70Doo, 87Haa1
	β					~1100	
Re(0001)	α, 4×1 (N_2)		170<*T*<300			160	89He
	β, 2×2 (N)					900-1300	
Re $(11\bar{2}0)$	α_1			6±1		129	87Haa1, 87Haa2
	α_2					155	
Ru(0001)	δ	>0.17				88-100	82Feu
	γ	0 - 0.4				113-124	
Ru(0001)	β			39±10 (steps) 126±20 (terrace) 183 (theory) 212 (theory)			99Dah 97Rom
W(110)	γ		128-148 conversion γ to β-state	~40		150	76Yat2, 90Lin
W(110)	β		300 K	17.4 (single activation barrier)		1560	81Cos

Substrate	Adsorbed State	Coverage θ	Temperature of dissociation [K]	Activation energy of dissociation [kJ/mol]	Pre-exponential factor [s^{-1}]	Temperature of desorption [K]	References
W(110)	β_1 β_2 β_3	0.5 (max.)	820 K	~41 (estimated activation barrier)		1180* 1245* 1310-1430	84Lee
W(110)	β	low cov.	800 K	92 (maximum of activation barrier distribution)			86Pfn
W(310)				no barrier		1390-1420	81Cos

* populated at higher kinetic energy of incident N_2 [84Lee].

Table 12. Adsorbed N_2 (crystallographic and vibrational data)

Substrate	Structure	Coverage/ adsorbed state	Vibrational frequency [cm^{-1}] Me–N	Me–N_2	N–N	Adsorption site / configuration	Technique	References
Al(111)		δ at 20 K			2339 + satellites	physisorbed N_2 vertical	EELS	89Jac, 90Jac
Cr(111)		α at 100 K			1170	π-bonded N_2	EELS	88Fuk
			530			atomic N		
Fe(111)		γ					EELS	84Gru1, 85Tsa
		α_1	435		1490 ($^{15}N_2$) 1555 ($^{14}N_2$)	side-on bonded		
K/Fe(111)		α_2 (with K)	460		1370 ($^{15}N_2$)	side-on bonded		
		β	470			atomic N		
Fe(111)	T <80 K	γ			2100	terminal bonded	EELS	85Tom, 86Whi1,
	T >110 K	α_1	435		1415-1490	side-on bonded		86Whi2
K/Fe(111)		α_2 (with K)	460		1170	K-influenced		
Ir(111)		84 K	330		2210	vertical	EELS	90Cor
Ir(100)-(1×1)		θ = 0 - 1			2211-2190	vertical	IRAS	93Gar
	(√2×√2)R45°	θ = 0.5			2201	vertical	IRAS	
Ir(100)-(5×1)		θ = 0 - 1			2208	vertical	IRAS	93Gar
Ni(111)	(√3×√3)R30°	θ = 0 - 0.33			2218 - 2194	vertical	IRAS	91Yos
	(2×2)	0.5 at 83 K			2186	vertical	IRAS	89Qui
Ni(110)		100 K	335		2195	chemisorbed	EELS	89Sch
		125 K	322		2185	chemisorbed	EELS	82Hor
		90 K	339		2194	chemisorbed	EELS	88Kuw
		80 K	346		2194	chemisorbed	EELS	86Str
		115 K	339		2194	chemisorbed	EELS	82Ban

Substrate	Structure	Coverage/ adsorbed state	Vibrational frequency [cm^{-1}] Me–N	Me–N_2	N–N	Adsorption site / configuration	Technique	References
Cont'd.	c(1.4×2)	θ = 0.72			2194	chemisorbed	IRAS	87Bru
		0.1 - 0.72			2200 - 2194	chemisorbed	IRAS	86Bru
Pd(110)	(2×1)	γ sat. 120 K		242	2242	chemisorbed	EELS	87Kuw
Pt(111)		120 K			2240		IRAS	77Shi2
Ru(0001)		γ 75 K		278-291	2247-2198	chemisorbed N_2	EELS	83Ant, 87deP,
	(√3×√3)R30°	95 K		280-301	2252-2212	vertical		92Shi
Ru(0001)	(√3×√3)R30°				2209-2189		IRAS	87deP
				300	2195		EELS	
		θ_K = 0.05		305	2150			
Ru(0001)		γ saturated at 40 K		282	2192	chemisorbed N_2, atop, vertical;	EELS	92Shi
		δ			2329, 4610	physisorbed N_2	(off specular)	
		β		568		atomic N		93Shi
Ru(0001)	(√3×√3)R30°	γ at 0.33			2239	chemisorbed N_2	Theory	97Mor
Ru (10$\bar{1}$0)		δ			2329	physisorbed N_2	EELS	95Gru
	(2×3), θ=0.5	γ		282	2192	chemisorbed N_2		
		β		330		$\nu_{\parallel}$ atomic N		97Die
				484		$\nu_{\perp}$ atomic N		
W(100)		α at 105 K			1048	chemisorbed N_2	EELS	89Sel
					1209	π-bonded		
		β		520		atomic N		
		γ^-			1500	chemisorbed N_2		
		γ^+		274	2200			
W(100)		α		604	2136	chemisorbed N_2	EELS	80Ho
		β			1451	bridge-bonded N_2		
				967		atomic N		

Table 13. Adsorbed N_2 (additional structural data; bond lengths)

Substrate	Structure	Coverage θ or adsorbed state	Species	Adsorption site	Bond length [Å]		Tilt angle	Technique	References
					Me-N	N-N			
Ni(100)	(√3×√3)R30°	0.33	N_2	atop	2.25±0.01	1.10±0.07	no tilt	ARPEFS	96Mol
Fe(111)		~0.2	N_2 γ-state at 60 K		>2.5		no tilt	NEXAFS SEXAFS	89Wen, 90Wen
Fe(100)	c(2×2)	0.5	atomic N β-state	4-fold hollow	1.83			LEED	82Imb
Ru(0001)	(√3×√3)R30°	0.33 (95 K)	N_2	atop	2.00±0.05	1.10±0.04	no tilt	LEED	94Blu
Ru(0001)	(√3×√3)R30°	0.33	N_2		2.00	1.13		Theory	97Mor
Ru(0001)	(2×2)-N	0.25	atomic N	3-fold hcp	1.93			LEED	97Sch1
	(√3×√3)R30°	0.33			1.93				
O/Ru(0001)	(2×2)-O + N_2		N_2	atop		1.12±0.06	no tilt		95Ove
W(100)	(√2×√2)R45°	0.5	atomic N	4-fold hollow	2.29			LEED	82Gri

Table 14. Adsorbed N_2 (valence electronic structure). Electron binding energies are referenced to the Fermi-level.

Substrate	Structure	Coverage/ adsorbed state	MO valence levels [eV] $3\sigma_g$	$1\pi_u$	$2\sigma_u$	Molecule orientation	Technique	Reference
Al(111)		δ at 20 K	9.85	11.0	12.85	physisorbed N_2 vertical	UPS	89Jac
Cr(110)		θ<0.7 α at 90 K	8.4	7.1	12.7	molecular N_2 inclined, π-bonded	UPS	90Shi
Fe(111)		γ at ~77 K	8.6	8.3	11.8-11.2	vertical	ARUPS	87Fre
		α at 110 K	8.4	7.5	12.3	inclined		
Ir(110)-(1×2)	p1g1(2×2)	1 at 95 K	8.0	8.0	11.8	vertical	UPS	81Ibb
Ni(100)		γ at 77 K	7.6	7.6	12.4	vertical	UPS	81Bru
	c(2×2)	γ, 0.5	7.6	7.3	12.4	vertical	XES	98Ben
	c(2×2)	γ, 0.5, 90 K	8.3	8.1	12.8	vertical	UPS	84Dow
Ni(111)		γ at 70 K	9.0	9.0	13.0	vertical	UPS	86Bre
		γ at 80 K	8.6	8.6	12.2	vertical	UPS	90Rao
		γ	8.7	8.2	12.5	vertical	UPS	88Umb
Ni(110)		γ at 90 K	8.1	7.8	11.8	vertical	UPS	82Hor
		γ at 80 K	8.6	8.6	11.8	vertical	UPS	90Rao
Pd (poly)		1 at 80 K	9.2	9.2	12.8	vertical	UPS	91Rao
Pd(111)		At 90 K	8.7	10.3	11.9	random	ARUPS	82Hor
Ru(0001)	(√3×√3)R30°		7.9*	7.9	12.4	near vertical	ARUPS	85Hes, 87deP
			7.5	7.5 (10.5)	12.0			
Ru(0001)		δ	9.2	10.5	12.2	physisorbed N_2	ARUPS	92Shi
	(√3×√3)R30°	γ at 40 K	7.9	7.9	12.0	chemisorb. N_2		
W(110)		γ	7.0	7.0	11.7	chemisorbed N_2	UPS	79Fug
W(110)		γ at~120 K	7.5	7.6	11.9-12.1	chemisorbed N_2 vertical	ARUPS	80Umb, 82Umb

*Dispersion of $3\sigma_g$ level found to be <0.1 eV [85Hes].

Table 15: Adsorbed N_2 (core level binding energies; adsorption states; molecular/atomic species). Electron binding energies are referenced to the Fermi-level.

Substrate	Structure	Coverage/ adsorbed state	Core level energies [eV] N 1s	Chemical state	References
Cr(111)		α at 100 K	397.8 398.9	chemisorbed N_2 π-bonded	88Fuk
Fe(111)		γ T <85 K α β	401.2, 405.9 399 397	terminal bonded N_2 side-on bonded N_2 atomic N	84Gru1, 84Gru2
Ir(110)-(1×2)	p1g1(2×2)	1 at 95 K	399.2 404.2 satellite	vertical N_2	81Ibb
Ni(111)		δ at 20 K γ	403.6 400 shoulder 401.0 405.5 satellite	physisorbed N_2 chemisorbed N_2	86Bre
		γ	401 405.5 sattelite	chemisorbed N_2	88Umb
Ni(100)		γ	399.3 400.5 405.2 satellite	chemisorbed N_2	84Umb
	c(2×2)	γ, θ = 0.5	399.4 400.7 406 satellite	chemisorbed N_2	90Mar
		γ at 80 K	400.0 405.2 satellite	chemisorbed N_2	90Rao
		γ at 77 K	400.7 405.8 satellite	chemisorbed N_2	81Bru
Ni(110)		γ at 80 K	400.5 406.0 satellite	chemisorbed N_2	90Rao
		γ at 130 K	400.1 401.5 406.7 satellite	chemisorbed N_2	80Gol
Pd (poly)		At 80 K	401.3 405.1 satellite	chemisorbed	91Rao
Re(0001)		γ	400.0 405.4	molecular N_2	84Gru2
		β, T >160 K	396.3	atomic N	
Ru(0001)		γ	399.3 400.7 405 satellite	molecular N_2	82Umb, 84Umb
Ru(0001)		γ	400.3	molecular N_2	95Bir

Substrate	Structure	Coverage/ adsorbed state	Core level energies [eV] N 1s	Chemical state	References
			405.3		
		β	397.4	atomic N	
W(110)		γ (0.5)	399.1±0.2	molecular N_2	79Fug, 90Zha
			400.4±0.2		
			405.5±0.5	N_2 shake-up sat.	
		β	~397	atomic N	
W(110)		γ	399.3	molecular N_2	82Umb, 84Umb
			400.5		
			405.5 satellite		

3.7.1.9 References

47Cou Coulson, C., Longuet-Higgins, H.: Proc. R. Soc. (London) A **192** (1947) 16.
51Dew M. J. S. Dewar, Bull. Soc. Chim. France **18**, C79 (1951).
54Eis Eischens, R.P., Pliskin, W.A., Francis, S.A.: J. Chem. Phys. **22** (1954) 1786.
58Eis Eischens, R.P., Pliskin, W.A.: Adv. Catal. **10** (1958) 1.
59Eis Eischens, R.P.: J. Electrochem. Soc. **106** (1959) C201.
61Ehr1 Ehrlich, G.: J. Chem. Phys. **34** (1961) 29.
61Ehr2 Ehrlich, G., Hudda, F.G.: J. Chem. Phys. **35** (1961) 1421.
62Ehr1 Ehrlich, G.: J. Chem. Phys. **36** (1962) 1171.
62Ehr2 Ehrlich, G., Hudda, F.G.: J. Chem. Phys. **36** (1962) 3233.
63Kle Klein, R., Leder, L.B.: J. Chem. Phys. **38** (1963) 1866.
64Bly Blyholder, G.: J. Phys. Chem. **68** (1964) 2772.
64Kle Klein, R., Little, J.W.: Surf. Sci. **2** (1964) 167.
64Oma Omar, R.M., Dillon, J.A.: Surf. Sci. **2** (1964) 227.
64Tuc Tucker, C.W.: Surf. Sci. **2** (1964) 516.
65Del Delchar, T.A., Ehrlich, G.: J. Chem. Phys. **42** (1965) 2686.
66Est Estrup, P.J., Anderson, J.: J. Chem. Phys. **45** (1966) 2254.
66Haa Haas, T.W.: Surf. Sci. **5** (1966) 345.
66Tuc Tucker, C.W.: J. Appl. Phys. **37** (1966) 3013.
67And Anderson, J., Estrup, P.J.: J. Chem. Phys. **46** (1967) 563.
67Lew Lewis, R., Gomer, R.: Nuovo Cimento Suppl. **5** (1967) 506.
68Kin King, D.A.: Surf. Sci. **9** (1968) 375.
68Mor Morgan, A.E., Somorjai, G.A.: Surf. Sci. **12** (1968) 405.
68vOs van Oostrom, A., in: Proc. 8th Intern. Conf. on Phen. in Ionized Gases, Vienna, 1968, p. 291.
69Bly Blyholder, G., Allen, M.C.: J. Am. Chem. Soc. **91** (1969) 3158.
69Dew Dewar, M.: The Molecular Orbital Theory of Organic Chemistry, New York: McGraw Hill, 1969.
69Edm Edmonds, T., Pitkethyly, R.C.: Surf. Sci. **17** (1969) 450.
69Gra Grant, J.A.: Surf. Sci. **18** (1969) 228.
69Tra1 Tracy, J.C., Palmberg, P.W.: J. Chem. Phys. **51** (1969) 4852.
70Cla Clavenna, L.R., Schmidt, L.D.: Surf. Sci. **22** (1970) 365.
70Doo Dooley, G.J., Haas, T.W.: Surf. Sci. **19** (1970) 1.
70Ert Ertl, G., Koch, J.: Z. Naturforsch. A **25** (1970) 1906.
70For Ford, R.R.: Adv. Catal. **21** (1970) 51.
70Gra Grant, J.T., Hass, T.W.: Surf. Sci. **21** (1970) 76.
71Eas Eastman, D.E., Cashion, J.K.: Phys. Rev. Lett. **27** (1971) 1520.
71Gra Grant, J.T.: Surf. Sci. **25** (1971) 451.
71Koh Kohrt, C., Gomer, R.: Surf. Sci. **24** (1971) 77.
71Tam Tamm, P.W., Schmidt, L.D.: Surf. Sci. **26** (1971) 286.
72Bon1 Bonzel, H.P., Ku, R.: Surf. Sci. **33** (1972) 91.
72Bon2 Bonzel, H.P., Ku, R.: J. Vac. Sci. Technol. **9** (1972) 663.
72Eis Eischens, R.P.: Acc. Chem. Res. **5** (1972) 74.
72Kin King, D.A., Goymour, C.G., Yates jr., J.T.: Proc. R. Soc. (London) A **331** (1972) 361.
72Mah Mahnig, M., Schmidt, L.D.: Z. Phys. Chem. N.F. **80** (1972) 71.
72Pri Pritchard, J.: J. Vac. Sci. Technol. **9** (1972) 895.
72Tra1 Tracy, J.C.: J. Chem. Phys. **56** (1972) 2748.
72Tra2 Tracy, J.C.: J. Chem. Phys. **56** (1972) 2736.
73Bak Baker, J.M., Eastman, D.E.: J. Vac. Sci. Technol. **10** (1973) 223.
73Bon Bonzel, H.P., Ku, R.: J. Chem. Phys. **58** (1973) 4617.

73Chr Christman, K., Ertl, G.: Z. Naturforsch. A **28** (1973) 1144.
73Koh Kohrt, C., Gomer, R.: Surf. Sci. **40** (1973) 71.
73Lec Lecante, J., Riwan, R., Guillot, C.: Surf. Sci. **35** (1973) 271.
73Mad1 Madey, T.E., Yates jr., J. T., Erickson, N.E.: Chem. Phys. Lett. **19** (1973) 487.
73Mad2 Madden, H.H., Küppers, J., Ertl, G.: J. Chem. Phys. **58** (1973) 3401.
73Mad3 Madden, H.H., Ertl, G.: Surf. Sci. **35** (1973) 211.
73Tay Taylor, T.N., Estrup, P.J.: J. Vac. Sci. Technol. **10** (1973) 26.
73Vis Viswanath, Y., Schmidt, L.D.: J. Chem. Phys. **59** (1973) 4184.
73Wac Wachs, I.E., Madix, R.J.: J. Catal. **53** (1973) 208.
73Wei Weinberg, W.H.: J. Vac. Sci. Technol. **10** (1973) 89.
74Che Chesters, M.A., Hopkins, B.J., Leggett, M.R.: Surf. Sci. **43** (1974) 1.
74Chr Christman, K., Schober, O., Ertl, G.: J. Chem. Phys. **60** (1974) 4719.
74Con1 Conrad, H., Ertl, G., Koch, J., Latta, E.E.: Surf. Sci. **43** (1974) 462.
74Dal Betta, R.A.D., Piken, A.G., Shelef, M.: J. Catal. **35** (1974) 54.
74Doy Doyen, G., Ertl, G.: Surf. Sci. **43** (1974) 197.
74Ege Egelhoff, W.F.J.: Surf. Sci. **141** (1984) L324.
74Kin King, D.A., Wells, M.G.: Proc. R. Soc. (London) A **339** (1974) 245.
74Lam1 Lambert, R.M., Comrie, C.M.: Surf. Sci. **46** (1974) 61.
74Lam2 Lambert, R.M.: Surf. Sci. **49** (1974) 325.
74Mad Madey, T.E., Menzel, D.: Jpn. J. Phys. Suppl. **2**, Part 2 (1974) 229.
74Yat1 Yates jr., J.T., Madey, T.E., Erickson, N.E.: J. Vac. Sci. Technol. **11** (1974) 225.
74Yat2 Yates jr., J.T., Madey, T.E., Erickson, N.E.: Surf. Sci. **43** (1974) 257.
74Yat3 Yates jr., J.T., Erickson, N.E., Worley, S.D., Madey, T.E.: The use of XPS for studying adsorbed molecules, in: The Physical Basis for Heterogeneous Catalysis. Batelle Institute Materials Science Coll.; Drauglis, A., Jaffee, R.I. (eds.), New York: Plenum, 1974, p. 75-105.
75Bon1 Bonzel, H.P., Fischer, T.E.: Surf. Sci. **51** (1975) 213.
75Bon2 Bonzel, H.P., Helms, C.R., Kelemen, S.: Phys. Rev. Lett. **35** (1975) 1237.
75Bru Brundle, C.R.: J. Electron Spectrosc. Relat. Phenom. **7** (1975) 484.
75Con Conrad, H., Ertl, G., Küppers, J., Latta, E.E.: Solid State Commun. **17** (1975) 613.
75Dal Betta, R.A.D., Piken, A.G., Shelef, M.: J. Catal. **40** (1975) 173.
75Fal Falconer, J.L., Madix, R.J.: Surf. Sci. **48** (1975) 393.
75Fug1 Fuggle, J.C., Steinkilberg, M., Menzel, D.: Chem. Phys. **11** (1975) 307.
75Fug2 Fuggle, J.C., Madey, T.E., Steinkilberg, M., Menzel, D.: Chem. Phys. Lett. **33** (1975) 233.
75Fug3 Fuggle, J.C., Madey, T.E., Steinkilberg, M., Menzel, D.: Surf. Sci. **52** (1975) 521.
75Kne Kneringer, G., Netzer, F.P.: Surf. Sci. **49** (1975) 125.
75Lam Lambert, R.M.: Surf. Sci. **49** (1975) 325.
75Sin Singh-Boparai, S.P., Bowker, M., King, D.A.: Surf. Sci. **53** (1975) 55.
76Bro Broden, G., Rhodin, T.: Solid State Commun. **18** (1976) 105.
76Chr Christman, K., Ertl, G., Pignet, T.: Surf. Sci. **59** (1976) 365.
76Com1 Comrie, C.M., Weinberg, W.H.: J. Vac. Sci. Technol. **13** (1976) 264.
76Com2 Comrie, C.M., Weinberg, W.H.: J. Chem. Phys. **64** (1976) 250.
76Com3 Comrie, C.M., Lambert, R.M.: J. Chem. Soc. Faraday Trans. **72** (1976) 1659.
76Con Conrad, H., Ertl, G., Küppers, J., Latta, E.E.: Surf. Sci. **57** (1976) 475.
76Dem Demuth, J.E., Eastman, D.E.: Solid. State Commun. **18** (1976) 1497.
76Ert Ertl, G., Grunze, M., Weiss, M.: J. Vac. Sci. Technol. **13** (1976) 314.
76Hag Hagen, D.I., Nieuwenhuys, B.E., Rovida, G., Somorjai, G.A.: Surf. Sci. **57** (1976) 632.
76Küp Küppers, J., Plagge, A.: J. Vac. Sci. Technol. **13** (1976) 259.
76Liu Liu, R., Ehrlich, G.: J. Vac. Sci. Technol. **13** (1976) 310.
76Llo Lloyd, D.R., Quinn, C.M., Richardson, N.V.: Solid State Commun. **20** (1976) 409.
76Mad Madey, T.E., Czyzewski, J.J., Yates jr., J.T.: Surf. Sci. **57** (1976) 580.

76McC Mc Cabe, R.W., Schmidt, L.D.: Surf. Sci. **60** (1976) 85.
76McE1 McElhiney, G., Papp, H., Pritchard, J.: Surf. Sci. **54** (1976) 617.
76Plu Plummer, E.W., Waclawski, B.J., Vorburger, T.V., Kuyatt, C.E.: Prog. Surf. Sci. **7** (1976) 149.
76Ree Reed, P.D., Comrie, C.M., Lambert, R.M.: Surf. Sci. **59** (1976) 33.
76Rho Rhodin, T.N., Broden, G.: Surf. Sci. **60** (1976) 466.
76Van Vannice, M.A.: Catal. Rev. Sci. Eng. **14** (1976) 153.
76Vor Vorburger, T.V., Sandstrom, D.R., Waclawski, B.J.: J. Vac. Sci. Technol. **13** (1976) 287.
76Wil Williams, P.M., Butcher, P., Wood, J., Jakobi, K.: Phys. Rev. B **14** (1976) 3215.
76Yat1 Yates jr., J.T., Madey, T.E., Erickson, N.E., Worley, S.D.: Chem. Phys. Lett. **39** (1976) 113.
76Yat2 Yates jr., J.T., Klein, R., Madey, T.E.: Surf. Sci. **58** (1976) 469.
76Zhd Zhdan, P.H., Boreskov, G.K., Baronin, A.I., Egelhoff, W.F., Weinberg, W.H.: Chem. Phys. Lett. **44** (1976) 528.
77All1 Allyn, C.L., Gustafsson, T., Plummer, E.W.: Chem. Phys. Lett. **47** (1977) 127.
77All2 Allyn, C.L., Gustafsson, T., Plummer, E.W.: Solid State Commun. **24** (1977) 531.
77Ber Bertolini, J.C., Dalmai-Imelik, G., Rousseau, J.: C. R. Seances Acad. Sci. (Paris) Ser. C **285** (1977) 409.
77Boz1 Bozso, F., Ertl, G., Grunze, M., Weiss, M.: J. Catal. **49** (1977) 18.
77Boz2 Bozso, F., Ertl, G., Grunze, M., Weiss, M.: J. Catal. **50** (1977) 519.
77Bri Bridge, M.E., Comrie, C.M., Lambert, R.M.: Surf. Sci. **67** (1977) 393.
77Col Collins, D.M., Spicer, W.E.: Surf. Sci. **69** (1977) 85.
77Doy Doyen, G., Ertl, G.: Surf. Sci. **69** (1977) 157.
77Ert Ertl, G., Neumann, M., Streit, K.M.: Surf. Sci. **64** (1977) 393.
77Fro Froitzheim, H., Ibach, H., Lehwald, S.: Surf. Sci. **63** (1977) 56.
77Fug Fuggle, J.C., Umbach, E., Feulner, P., Menzel, D.: Surf. Sci. **64** (1977) 69.
77Gil Gillet, E., Chiarena, J.C., Gillet, M.: Surf. Sci. **66** (1977) 596.
77Hor1 Horn, K., Pritchard, J.: J. Phys. **38** C4 (1977) 164.
77Hor2 Horn, K., Hussain, M., Pritchard, J.: Surf. Sci. **63** (1977) 244.
77Hou Housley, M., Ducros, R., Piquard, G., Cassuto, A.: Surf. Sci. **68** (1977) 277.
77Iba Ibach, H.: Surf. Sci. **66** (1977) 56.
77Iva Ivanov, V.P., Boreshov, G.K., Savchenko, V.I., Egelhoff, W.F., and Weinberg, W.H.: J. Catal. **48** (1977) 269.
77Kes Kessler, J., Thieme, F.: Surf. Sci. **67** (1977) 405.
77Kis Kisliuk, P.: Surf. Sci. **64** (1977) 43.
77Ku Ku, E., Gjostein, N.A., Bonzel, H.P.: Surf. Sci. **64** (1977) 465.
77Leu Leung, C., Vass, M., Gomer, R.: Surf. Sci. **66** (1977) 67.
77Mar Marbrow, R.A., Lambert, R.M.: Surf. Sci. **67** (1977) 489.
77McC Mc Cabe, R.W., Schmidt, L.D.: Surf. Sci. **66** (1977) 101.
77Pal Palmer, R.L., Vroom, D.A.: J. Catal. **50** (1977) 244.
77Rho Rhodin, T.N., Brucker, C.F.: Solid. State Commun. **23** (1977) 275.
77Shi1 Shirley, D.A.: Phys. Scr. **16** (1977) 398.
77Shi2 Shigeishi, R.A., King, D.A.: Surf. Sci. **62** (1977) 379.
77Ste1 Steinbrüchel, C., Gomer, R.: Surf. Sci. **67** (1977) 21.
77Ste2 Steinbrüchel, C., Gomer, R.: J. Vac. Sci. Technol. **14** (1977) 484.
77Tex Textor, M., Gay, I.D., Mason, R.: Proc. R. Soc. (London) A **356** (1977) 37.
77Umb Umbach, E., Fuggle, J.C., Menzel, D.: J. Electron Spectrosc. Relat. Phenom. **10** (1977) 15.
78All Allyn, C.L., Gustafsson, T., Plummer, E.W.: Solid State Commun. **28** (1978) 85.
78Bon Bonzel, H.P., Broden, G., Pirug, G.: J. Catal. **53** (1978) 96.
78Bra1 Bradshaw, A.M., Hoffman, F.M.: Surf. Sci. **72** (1978) 513.
78Bra2 Braun, W., Neumann, M., Iwan, M., Koch, E.E.: Phys. Status Solidi (b) **90** (1978) 525.

78Bro Broden, G., Pirug, G., Bonzel, H.P.: Surf. Sci. **72** (1978) 45.
78Bru Brundle, C.R.: IBM J. Res. Dev. **22** (1978) 235.
78Cas Castner, D.G., Sexton, B.A., Somorjai, G.A.: Surf. Sci. **71** (1978) 519.
78Com Comrie, C.M., Weinberg, W.H.: J. Chem. Phys. **64** (1978) 250.
78Con Conrad, H., Ertl, G., Küppers, J.: Surf. Sci. **76** (1978) 323.
78Dwy Dwyer, D.J., Somorjai, G.A.: J. Catal. **52** (1978) 291.
78Erl Erley, W., Wagner, H.: Surf. Sci. **74** (1978) 333.
78Fel Felter, T.E., Estrup, P.J.: Surf. Sci. **76** (1978) 464.
78Fug Fuggle, J.C., Umbach, E., Menzel, D., Wandelt, K., Brundle, C.R.: Solid State Commun. **27** (1978) 65.
78Fuk Fukuda, Y., Lancaster, G.M., Honda, F., Rabalais, J.W.: J. Chem. Phys. **69** (1978) 3447.
78Gun Gunnarsson, O., Schönhammer, K.: Phys. Rev. Lett. **41** (1978) 1608.
78Hor1 Horn, K., Bradshaw, A.M., Jacobi, K.: Surf. Sci. **72** (1978) 719.
78Hor2 Horz, G.: High Temp. High Pressures **10** (1978) 283.
78Jon Jona, F., Legg, K.O., Shih, H.D., Jepsen, D.W., Marcus, P.M.: Phys. Rev. Lett. **40** (1978) 1466.
78Kan Kanski, J., Ilver, L., Nilsson, P.O.: Solid State Commun. **26** (1978) 339.
78Mad Madix, R.J., Benzinger, J.B.: Ann. Rev. Phys. Chem. **29** (1978) 285.
78Nie Nieuwenhuys, B.E., Somorjai, G.A.: Surf. Sci. **72** (1978) 8.
78Pfn Pfnür, H., Feulner, P., Engelhardt, H.A., Menzel, D.: Chem. Phys. Lett. **59** (1978) 481.
78Pir Pirug, G., Hopster, H., Ibach, H.: Ned. Tijdschr. Vacuumtechniek **16** (1978) 152.
78Plu Plummer, E.W., Salaneck, W.R., Miller, J. S.: Phys. Rev. B **18** (1978) 1673.
78Pri Prior, K.A., Schwaha, K., Lambert, R.M.: Surf. Sci. **77** (1978) 193.
78Sch Schönhammer, K., Gunnarsson, O.: Solid State Commun. **26** (1978) 399.
78Tay1 Taylor, J.L., Ibbotson, D.E., Weinberg, W.H.: J. Chem. Phys. **69** (1978) 4298.
78Tay2 Taylor, J.L., Weinberg, W.H.: Surf. Sci. **78** (1978) 259.
78Tay3 Taylor, J.L., Weinberg, W.H.: J. Vac. Sci. Technol. **15** (1978) 590.
78Weh Wehner, P.S., Kevan, S.D., Williams, R.S., Davis, R.F., Shirley, D.A.: Chem. Phys. Lett. **57** (1978) 334.
78Zhd Zhdan, P.A., Boreskov, G.K., Boronin, A.I., Schepelin, A.P., Egelhoff, W.F., Weinberg, W.H.: Surf. Sci. **71** (1978) 267.
79And1 Andersson, S.: Surf. Sci. **89** (1979) 477.
79And2 Anderson, S., Pendry, J.B.: Phys. Rev. Lett. **43** (1979) 363.
79Bat Batra, I., Hermann, K., Bradshaw, A.M., Horn, K.: Phys. Rev. B **20** (1979) 801.
79Beh Behm, R.J., Christmann, K., Ertl, G., van Hove, M.A., Thiel, P.A., Weinberg, W.H.: Surf. Sci. **88** (1979) L59.
79Bes Besocke, K., Wagner, H.: Surf. Sci. **87** (1979) 457.
79Bor Bordoli, R.S., Vickerman, J.C., Wolstenholme, J.: Surf. Sci. **85** (1979) 244.
79Bro Brodén, G., Gafner, G., Bonzel, H.P.: Surf. Sci. **84** (1979) 295.
79Cam Campuzano, J.C., Greenler, R.G.: Surf. Sci. **83** (1979) 301.
79Erl Erley, W., Ibach, H., Lehwald, S., Wagner, H.: Surf. Sci. **83** (1979) 585.
79Fre Freund, H.J., Hohlneicher, G.: Ber. Bunsenges. Phys. Chem. **83** (1979) 100.
79Fug Fuggle, J.C., Menzel, D.: Surf. Sci. **79** (1979) 1.
79Hei1 Heilmann, P., Heinz, K., Müller, K.: Surf. Sci. **83** (1979) 487.
79Hei2 Heinz, K., Lang, E., Müller, K.: Surf. Sci. **87** (1979) 595.
79Hol Hollins, P., Pritchard, J.: Surf. Sci. **89** (1979) 486.
79Hop Hopster, H., Ibach, H.: Surf. Sci. **77** (1979) 109.
79Hor1 Horn, K., Pritchard, H.: J. Phys. (Paris) **38** (1979) C4-164.
79Hor2 Horn, K., Bradshaw, A.M., Hermann, K., Batra, I.P.: Solid State Commun. **31** (1979) 257.
79Kre Krebs, H.J., Bonzel, H.P., Gafner, G.: Surf. Sci. **88** (1979) 269.

79Mad Madey, T.E.: Surf. Sci. **79** (1979) 575.
79Nor Norton, P.R., Goodale, J.W., Selkirk, E.B.: Surf. Sci. **83** (1979) 189.
79Pet Petersson, L.G., Kono, S., Hall, N.F.T., Fadley, C.S., Pendry, J.B.: Phys. Rev. Lett. **42** (1979) 1545.
79Pir Pireaux, J.J., Ghijsen, J., McGowan, J.W., Verbist, J., Caudano, R.: Surf. Sci. **80** (1979) 488.
79Pol Polizzotti, R.S., Ehrlich, G.: J. Chem. Phys. **71** (1979) 259.
79Pri Pritchard, J.: Surf. Sci. **79** (1979) 231.
79Ric Richardson, N.V., Bradshaw, A.M.: Surf. Sci. **88** (1979) 255.
79Ris Rissmann, E.F., Parry, J.M.: J. Phys. Chem. **79** (1975) 1975.
79Rub Rubloff, G.W.: Surf. Sci. **89** (1979) 566.
79Som Somerton, C., King, D.A.: Surf. Sci. **89** (1979) 391.
79Thi1 Thiel, P.A., Weinberg, W.H., Yates jr., J.T.: J. Chem. Phys. **71** (1979) 1643.
79Thi2 Thiel, P.A., Williams, E.D., Yates jr., J.T., Weinberg, W.H.: Surf. Sci. **84** (1979) 54.
79Tho Thomas, G.E., Weinberg, W.H.: J. Chem. Phys. **70** (1979) 954.
79Toy Toyoshima, I., Somorjai, G.A.: Catal. Rev. Sci. Eng. **19** (1979) 105.
79Wan Wang, C., Gomer, R.: Surf. Sci. **84** (1979) 329.
79Wen Wendelken, J.F., Ulehla, M.V.K.: J. Vac. Sci. Technol. **16** (1979) 441.
79Wil Williams, E.D., Weinberg, W.H., Sobrero, A.: J. Chem. Phys. **76** (1979) 1150.
80And Andersson, S., Pendry, J.B.: J. Phys. C **13** (1980) 2547.
80Bai Baird, R.J., Ku, R.C., Wynblatt, P.: Surf. Sci. **97** (1980) 346.
80Beh Behm, R.J., Christmann, K., Ertl, G., van Hove, M.A.: J. Chem. Phys. **73** (1980) 2984.
80Ben Benziger, J., Madix, R.J.: Surf. Sci. **94** (1980) 119.
80Car Carroll, J.J., Madey, T.E., Melmed, A.J., Sandstrom, D.R.: Surf. Sci. **96** (1980) 508.
80Chi Chiang, T.-C., Kaindl, G., Eastman, D.E.: Solid State Commun. **36** (1980) 25.
80Cros Crossley, A., King, D.A.: Surf. Sci. **95** (1980) 131.
80Dub Dubois, L.H., Somorjai, G.A.: Surf. Sci. **91** (1980) 514.
80Duc Ducros, R., Alnot, M., Ehrhardt, J.J., Housley, M., Piquard, G., Cassuto, A.: Surf. Sci. **94** (1980) 154.
80Erl Erley, W., Wagner, H., Ibach, H.: Surf. Sci. **80** (1980) 612.
80Ert Ertl, G.: Catal. Rev. Sci. Eng. **21** (1980) 201.
80Fai Fair, J., Madix, R.J.: J. Chem. Phys. **73** (1980) 3480.
80Foo Foord, J.S., Goddard, P.J., Lambert, R.M.: Surf. Sci. **94** (1980) 339.
80Fuk1 Fukuda, Y., Rabalais, J.W.: Chem. Phys. Lett. **76** (1980) 47.
80Fuk2 Fukuda, Y., Honda, F., Rabalais, J.W.: Surf. Sci. **93** (1980) 338.
80Fuk3 Fukuda, Y., Honda, F., Rabalais, J.W.: Surf. Sci. **91** (1980) 165.
80Gay Gay, R.R., Nodine, M.H., Herich, V.E., Zeiger, H.J., Solomon, E.I.: J. Am. Chem. Soc. **102** (1980) 6752.
80Gol Golze, M., Grunze, M., Driscoll, R.K.: Appl. Surf. Sci. **6** (1980) 464.
80Goo Goodman, D.W., Kelley, R.D., Madey, T.E., Yates jr., J.T.: J. Catal. **63** (1980) 226.
80Ho Ho, W., Willis, R.F., Plummer, E.W.: Surf. Sci. **95** (1980) 171.
80Hol Hollins, P., Pritchard, J.: Surf. Sci. **99** (1980) L389.
80Iba Ibach, H., Erley, W., Wagner, H.: Surf. Sci. **92** (1980) 29.
80Ko1 Ko, E.I., Madix, R.J.: Surf. Sci. **100** (1980) L449.
80Ko2 Ko, E.J., Madix, R.J.: Surf. Sci. **100** (1980) L505.
80Kre Krebs, H.J., Bonzel, H.P.: Surf. Sci. **99** (1980) 570.
80Mah Mahaffy, P.R., Dignam, M.J.: Surf. Sci. **97** (1980) 377.
80Nie Niehus, H.: Surf. Sci. **92** (1980) 88.
80Pfn Pfnür, H., Menzel, D., Hoffmann, F.M., Ortega, A., Bradshaw, A.M.: Surf. Sci. **93** (1980) 431.
80Ros Rosén, A., Grundevik, P., Morovic, T.: Surf. Sci. **95** (1980) 477.

80Sea Seabury, C.W., Rhodin, T.N., Traum, M.M., Benbow, R., Hurych, Z.: Surf. Sci. **97** (1980) 363.
80Smi Smith, R.J., Anderson, J., Lapeyre, G.J.: Phys. Rev. B **22** (1980) 632.
80Ton Tong, S.Y., Maldonado, A., Li, C.H., van Hove, M.A.: Surf. Sci. **94** (1980) 73.
80Umb Umbach, E., Schichl, A., Menzel, D.: Solid State Commun. **36** (1980) 93.
80Yat Yates jr., J.T., Goodman, D.W.: J. Chem. Phys. **73** (1980) 5371.
81Bai Baird, R.J.: J. Electron Spectrosc. Relat. Phenom. **24** (1981) 55.
81Bar1 Bare, S.R., Hofmann, P., King, D.A.: Vacuum **31** (1981) 463.
81Bar2 Barteau, M.A., Ko, E.I., Madix, R.J.: Surf. Sci. **102** (1981) 99.
81Ber Bertolini, J.C., Tardy, B.: Surf. Sci. **102** (1981) 131.
81Bru Brundle, C., Bagus, P.S., Menzel, D., Hermann, K.: Phys. Rev. B **24** (1981) 7041.
81Cam1 Campuzano, J.C., Dus, R., Greenler, R.G.: Surf. Sci. **102** (1981) 172.
81Cam2 Campbell, C.T., Ertl, G., Kuipers, H., Segner, J.: Surf. Sci. **107** (1981) 207.
81Cas Cassuto, A., King, D.A.: Surf. Sci. **102** (1981) 388.
81Cos Cosser, R.C., Bare, S.R., Francis, S.M., King, D.A.: Vacuum **31** (1981) 503.
81Dav Davies, J.A., Jackmann, T.E., Jackson, D.P., Norton, P.R.: Surf. Sci. **109** (1981) 20.
81Duc Ducros, R., Housley, M., Piquard, G., Alnot, M.: Surf. Sci. **109** (1981) 235.
81Ert Ertl, G., Huber, M., Lee, S.B., Paál, Z., Weiss, M.: Appl. Surf. Sci. **8** (1981) 373-86.
81Fre Freund, H.-J., Plummer, E.W.: Phys. Rev. B **23** (1981) 4859.
81Ibb Ibbotson, D.E., Wittrig, T.S., Weinberg, W.H.: Surf. Sci. **110** (1981) 313.
81Joh Johnson, S., Madix, R.J.: Surf. Sci. **108** (1981) 77.
81Kel Kellogg, G.L.: Surf. Sci. **111** (1981) 205.
81Kev Kevan, S.D., Davis, R.F., Rosenblatt, D.H., Tobin, J.G., Mason, M.G., Shirley, D.A., Li, C.H., Tong, S.Y.: Phys. Rev. Lett. **46** (1981) 1629.
81Koe Koestner, R.J., van Hove, M.A., Somorjai, G.A.: Surf. Sci. **107** (1981) 439.
81Kro Kroeker, R.M., Kaska, W.C., Hansma, P.K.: J. Chem. Phys. **74** (1981) 732.
81Lin Lin, T.H., Somorjai, G.A.: Surf. Sci. **107** (1981) 573.
81Mil Miller, J.N., Ling, D.T., Stefan, P.M., Weissmann, D.L., Shek, M.L., Lindau, I., Spicer, W.E.: Phys. Rev. B **24** (1981) 1917.
81Nis Nishijima, M., Masuda, S., Sakisaka, Y., Onchi, M.: Surf. Sci. **107** (1981) 31.
81Nor Norton, P.R., Davies, J.A., Creber, D.K., Sitter, C.W., Jackman, T.E.: Surf. Sci. **108** (1981) 205.
81Pri Prior, K.A., Scott, E.G., Lambert, R.M.: Chem. Phys. Lett. **80** (1981) 517.
81Sea Seabury, C.W., Jensen, E.S., Rhodin, T.N.: Solid. State Commun. **37** (1981) 383.
81Sem Semancik, S., Estrup, P.J.: Surf. Sci. **104** (1981) 26.
81Yos Yoshida, K.: Jpn. J. Appl. Phys. **20** (1981) 823.
82Ban Bandy, B.J., Canning, N.D.S., Hollins, P., Pritchard, J.: J. Chem. Soc. Chem. Commun. (1982) 58.
82Bar Bare, S.R., Griffiths, K., Hofmann, P., King, D.A., Nyberg, G.L., Richardson, N.V.: Surf. Sci. **120** (1982) 367.
82Bib Biberian, J.P., van Hove, M.A.: Surf. Sci. **118** (1982) 443.
82Bon Bonzel, H.P., Krebs, H.J.: Surf. Sci. **117** (1982) 639.
82Bro Brooks, R., Richardson, N.V., King, D.A.: Surf. Sci. **117** (1982) 434.
82Ert1 Ertl, G., Lee, S.B., Weiss, M.: Surf. Sci. **114** (1982) 527.
82Ert2 Ertl, G., Lee, S.B., Weiss, M.: Surf. Sci. **114** (1982) 515.
82Fer Ferrer, S., Bonzel, H.P.: Surf. Sci. **117** (1982) 234.
82Feu Feulner, P., Menzel, D.: Phys. Rev. B **25** (1982) 4295.
82Flo Flodström, S.A., Martinsson, C.W.B.: Appl. Surf. Sci. **10** (1982) 115.
82Gon Gonzalez, L., Miranda, R., Ferrer, S.: Surf. Sci. **119** (1982) 61.
82Gri Griffiths, K., King, D.A., Aers, G.C., Pendry, J.B.: J. Phys. C **15** (1982) 4921.

82Hei Heinz, K., Lang, E., Strauss, K., Müller, K.: Appl. Surf. Sci. **11/12** (1982) 611.
82Hof1 Hofmann, P., Bare, S.R., King, D.A.: Surf. Sci. **117** (1982) 245.
82Hof2 Hofmann, P., Bare, S.R., Richardson, N.V., King, D.A.: Solid State Commun. **42** (1982) 645.
82Hor Horn, K., DiNardo, J., Eberhardt, W., Freund, H.-J., Plummer, E.W.: Surf. Sci. **118** (1982) 465.
82Hou Houston, J.E., Madey, T.E.: Phys. Rev. B **26** (1982) 554.
82Imb Imbihl, R., Behm, R.J., Ertl, G., Moritz, W.: Surf. Sci. **123** (1982) 129.
82Jac1 Jackman, T.E., Davies, J.A., Jackson, D.P., Norton, P.R., Unertl, W.N.: J. Phys. C **15** (1982) L99.
82Jac2 Jackman, T.E., Davies, J.A., Jackson, D.P., Unertl, W.N., Norton, P.R.: Surf. Sci. **120** (1982) 389.
82Kat Kato, H., Sakisaka, Y., Miyano, T., Kamel, K., Nishijima, M., Onchi, M.: Surf. Sci. **114** (1982) 96.
82Kim Kim, Y., Peebles, H.C., White, J.M.: Surf. Sci. **114** (1982) 363.
82Liu Liu, R., Ehrlich, G.: Surf. Sci. **119** (1982) 207.
82Mar Mariani, C., Middelmann, H.-U., Iwan, M., Horn, K.: Chem. Phys. Lett. **93** (1982) 308.
82Mes Messmer, R.P., Lamson, S.H., Salahub, D.R.: Phys. Rev. B **25** (1982) 3576.
82Net Netzer, F.P., Madey, T.E.: J. Chem. Phys. **76** (1982) 710.
82Ort Ortega, A., Hoffman, F.M., Bradshaw, A.M.: Surf. Sci. **119** (1982) 79.
82Pap Papp, H.: Ber. Bunsenges. Phys. Chem. **86** (1982) 555.
82Poe Poelsema, B., Verheij, L.K., Comsa, G.: Surf. Sci. **152-153** (1985) 496.
82Poe1 Poelsema, B., deZwart, S.T., Comsa, G.: Phys. Rev. Lett. **49** (1982) 578.
82Poe2 Poelsema, B., Verheij, L.K., Comsa, G.: Phys. Rev. Lett. **49** (1982) 1731.
82Poe3 Poelsema, B., Palmer, R.L., Mechtesheimer, G., Comsa, G.: Surf. Sci. **117** (1982) 60.
82Poe4 Poelsema, B., Palmer, R.L., Comsa, G.: Surf. Sci. **123** (1982) 152.
82Spe1 Spencer, N.D., Somorjai, G.A.: J. Phys. Chem. **86** (1982) 3493.
82Spe2 Spencer, N.D., Shoonmaker, R.C., Somorjai, G.A.: J. Catal. **74** (1982) 129.
82Ste Steininger, H., Lehwald, S., Ibach, H.: Surf. Sci. **123** (1982) 264.
82Stö Stöhr, J., Jaeger, R.: Phys. Rev. B **26** (1982) 4111.
82Thi Thiel, P.A., Behm, R.J., Norton, P.R., Ertl, G.: Surf. Sci. **121** (1982) L553.
82Umb Umbach, E.: Surf. Sci. **117** (1982) 482.
82Woo Woodruff, D.P., Hayden, B.E., Prince, K., Bradshaw, A.M.: Surf. Sci. **123** (1982) 397.
83Aln Alnot, P., King, D.A.: Surf. Sci. **126** (1983) 359.
83Ant Anton, A., Avery, N., Toby, B., Weinberg, W.H.: J. Electron Spectrosc. Relat. Phenom. **29** (1983) 181.
83Bag Bagus, P.S., Nelin, C.J., Bauschlicher, C.W.: Phys. Rev. B **28** (1983) 5423.
83Beh Behm, R.J., Thiel, P.A., Norton, P.R., Ertl, G.: J. Chem. Phys. **78** (1983) 7437.
83Boz Bozso, F., Yates jr., J.T., Arias, J., Metiu, H., Martin, R.M.: J. Chem. Phys. **78** (1983) 4256.
83Bro Brown, A., Vickerman, J.C.: Surf. Sci. **124** (1983) 267.
83Bur Burgess, D., Viswanathan, R., Hussla, I., Stair, P.C., Weitz, E.: J. Chem. Phys. **79** (1983) 5200.
83Ega Egawa, C., Naito, S., Tamaru, K.: Surf. Sci. **125** (1983) 605.
83Fre Freund, H.-J., Greuter, F., Heskett, D., Plummer, E.W.: Phys. Rev. B **28** (1983) 1727.
83Gre Greuter, F., Heskett, D., Plummer, E.W., Freund, H.J.: Phys. Rev. B **27** (1983) 7117.
83Gru1 Grunze, M., Kleban, P.H., Unertl, W.N., Rys, F.S.: Phys. Rev. Lett. **51** (1983) 582.
83Gru2 Grunze, M., Unertl, W.N.: J. Vac. Sci. Technol. A **2** (1983) 896.
83Hay Hayden, B.E., Bradshaw, A.M.: Surf. Sci. **125** (1983) 787.
83Hen Hendrickx, H.A.C.M., Hoek, A., Nieuwenhuys, B.E.: Surf. Sci. **135** (1983) 81.
83Hof1 Hoffmann, F.M.: Surf. Sci. Rep. **3** (1983) 107.
83Hof2 Hofmann, P., Bare, S.R., King, D.A.: Phys. Scr. T **4** (1983) 118.

83Jac1 Jacobi, K., Rotermund, H.H.: Surf. Sci. **133** (1983) 401.
83Jac2 Jackman, T.E., Griffiths, K., Davies, J.A., Norton, P.R.: J. Chem. Phys. **79** (1983) 3529.
83Jen Jensen, E.S., Rhodin, T.N.: Phys. Rev. B **27** (1983) 3338.
83Koe1 Koel, B.E., Peebles, D.E., White, J.M.: Surf. Sci. Rep. **125** (1983) 709.
83Koe2 Koel, B.E., Peebles, D.E., White, J.M.: Surf. Sci. **125** (1983) 739.
83Men Menzel, D., Pfnür, H., Feulner, P.: Surf. Sci. **126** (1983) 374.
83Mic Michalk, G., Moritz, W., Ertl, G.: Surf. Sci. **129** (1983) 92.
83Pap Papp, H.: Surf. Sci. **129** (1983) 205.
83Pfn1 Pfnür, H., Menzel, D.: J. Chem. Phys. **79** (1983) 2400.
83Pfn2 Pfnür, H., Feulner, P., Menzel, D.: J. Chem. Phys. **79** (1983) 4613.
83Poe1 Poelsema, B., Verheij, L.K., Comsa, G.: Phys. Rev. Lett. **51** (1983) 522.
83Poe2 Poelsema, B., Palmer, R.L., DeZwart, S.T., Comsa, G.: Surf. Sci. **126** (1983) 641.
83Sch Schmeisser, D., Demuth, J.E.: J. Electron Spectrosc. Relat. Phenom. **29** (1983) 313.
83Stö Stöhr, J., Glaud, J.L., Eberhardt, W., Dufka, D., Madix, R.J., Sette, F., Kaestner, R.J., Döbler, U.: Phys. Rev. Lett. **51** (1983) 2412.
83Tat Tatarenko, S., Ducros, R., Alnot, M.: Surf. Sci. **126** (1983) 422.
83Thi Thiel, P.A., Behm, R.J., Norton, P.R., Ertl, G.: J. Chem. Phys. **78** (1983) 7448.
83Umb Umbach, E., Menzel, D.: Surf. Sci. **135** (1983) 199.
83Ven Vennemann, N., Schwarz, E.W., Neumann, M.: Surf. Sci. **126** (1983) 273.
83vHo1 van Hove, M.A., Koestner, R.J., Somorjai, G.A.: Phys. Rev. Lett. **50** (1983) 903.
83vHo2 van Hove, M.A., Koestner, R.J., Frost, J. C., Somorjai, G.A.: Surf. Sci. **129** (1983) 482.
83Wed Wedler, G., Ruhmann, R.: Appl. Surf. Sci. **14** (1983) 137.
84Ass Asscher, M., Somorjai, G.A.: Surf. Sci. **143** (1984) L389.
84Aue Auerbach, D.J., Pfnür, H.E., Rettner, C.T., Schlaegel, J.E., Lee, J., Madix, R.: J. Chem. Phys. **81** (1984) 2515.
84Bae Baetzold, R.C.: Phys. Rev. B **30** (1984) 6870.
84Bag1 Bagus, P.S., Nelin, C.J., Bauschlicher, C.W.: J. Vac. Sci. Technol. A **2** (1984) 905.
84Bag2 Bagus, P.S., Hermann, K., Bauschlicher, C.W.: J. Chem. Phys. **81** (1984) 1966.
84Ban Banholzer, W.F., Masel, R.I.: Surf. Sci. **137** (1984) 339.
84Bar Bare, S.R., Hofmann, P., King, D.A.: Surf. Sci. **144** (1984) 347.
84Bau Bauschlicher jr., C.W., Bagus, P.S.: J. Chem. Phys. **81** (1984) 5889.
84deL de Louise, L.A., White, E.J., Winograd, N.: Surf. Sci. **147** (1984) 252.
84Dow Dowben, P.A., Sakisaka, Y., Rhodin, T.N.: Surf. Sci. **147** (1984) 89.
84Gij Gijzeman, O.L.J., van Zandvoort, M.M.J., Labohm, F., Vleigenthart, J.A., Jongert, G.: J. Chem. Soc. Faraday Trans. **80** (1984) 771.
84Gru1 Grunze, M., Golze, M., Hirschwald, W., Freund, H.J., Pulm, H., Seip, U., Tsai, M.C., Ertl, G., Küppers, J.: Phys. Rev. Lett. **53** (1984) 850.
84Gru2 Grunze, M., Golze, M., Fuhler, J., Neumann, M., Schwarz, E., in: The intermediates in N2 dissociation on Re and Fe; 8th International Congress on Catalysis, Berlin, 1984, p. 133-143.
84Gru3 Grunze, M., Dowben, P.A., Jones, R.G.: Surf. Sci. **141** (1984) 455.
84Gru4 Grunze, M., Fuhler, J., Neumann, M., Brundle, C.R., Auerbach, D.J., Behm, J.: Surf. Sci. **139** (1984) 109.
84Hab Habenschaden, E., Küppers, J.: Surf. Sci. **138** (1984) L147.
84Her Hermann, K., Bagus, P.S., Bauschlicher, C.W.: J. Phys. Rev. B **30** (1984) 7313.
84Hof Hofmann, P., Bare, S.R., King, D.A.: Surf. Sci. **144** (1984) 347.
84Hol Hollins, P., Davies, K.J., Pritchard, J.: Surf. Sci. **138** (1984) 75.
84Jug Jugnet, Y., Himpsel, F.J., Avouris, P., Koch, E.E.: Phys. Rev. Lett. **53** (1984) 198.
84Koe Koel, B.E., Crowell, J.E., Mate, C.M., Somorjai, G.A.: J. Phys. Chem. **88** (1984) 1988.
84Kra Krause, S., Mariani, C., Prince, K.C., Horn, K.: Surf. Sci. **138** (1984) 305.
84Lee Lee, J., Madix, R.J., Schlaegel, J.E., Auerbach, D.J.: Surf. Sci. **143** (1984) 626.

84McC McConville, C.F., Somerton, C., Woodruff, D.P.: Surf. Sci. **139** (1984) 75.
84Mir Miranda, R., Wandelt, K., Rieger, D., Schnell, R.D.: Surf. Sci. **139** (1984) 430.
84Miy Miyano, T., Kamei, K., Sakisaka, Y., Onchi, M.: Surf. Sci. **148** (1984) L645.
84Mol Moller, J.: Z. Phys. B **55** (1984) 27.
84Poe Poelsema, B., Palmer, R.L., Comsa, G.: Surf. Sci. **136** (1984) 1.
84Rie Rieger, D., Schnell, R.D., Steinmann, W.: Surf. Sci. **143** (1984) 157.
84Rog Rogozik, J., Scheidt, H., Dose, V., Prince, K.C., Bradshaw, A.M.: Surf. Sci. Lett. **145** (1984) L481.
84Sei Seip, U., Tsai, M.C., Christmann, K., Küppers, J., Ertl, G.: Surf. Sci. **139** (1984) 29.
84Shi Shinn, N.D., Madey, T.E.: Phys. Rev. Lett. **53** (1984) 2481.
84Tom Tom, H.W.K., Mate, C.M., Zhu, X.D., Crowell, J.E., Heinz, T.F., Somorjai, G.A., Shen, Y.R.: Phys. Rev. Lett. **52** (1984) 348.
84Umb Umbach, E.: Solid State Comm. **51** (1984) 365.
85Alb Albright, T.A., Burdett, J.K., Whenghbo, M.-H.: Orbital Interactions in Chemistry; New York: Wiley, 1985.
85Beh Behm, R.J., Ertl, G., Penka, V.: Surf. Sci. **160** (1985) 387.
85Ben Benndorf, C., Kruger, B., Thieme, F.: Surf. Sci. **163** (1985) L675.
85Bro Brown, A., Vickerman, J.C.: Surf. Sci. **151** (1985) 319.
85Che1 Chesters, M.A., McDougall, G.S., Pemble, M.E., Sheppard, N.: Surf. Sci. **164** (1985) 425.
85Che2 Chen, C.T., Didio, R.A., Ford, W.K., Plummer, E.W., Eberhardt, W.: Phys. Rev. B **32** (1985) 8434.
85Die Diehl, R.D., Lindroos, M., Kearsley, A., Barnes, C.J., and King, D.A.: J. Phys. C **18** (1985) 4069.
85Ell Elliott, G., Jonsson, H., Miller, D., Weare, J.H.: J. Vac. Sci. Technol. A **3** (1985) 1665.
85Fra Franchy, R., Ibach, H.: Surf. Sci. **155** (1985) 15.
85Fre Freund, H.J., Messmer, R.P., Kao, C.M., Plummer, E.W.: Phys. Rev. B **31** (1985) 4848.
85Gre Greenler, R.G., Burch, K.D., Kretzschmar, K., Klauser, R., Bradshaw, A.M., and Hayden, B.E.: Surf. Sci. **152-153** (1985) 338.
85Har Harendt, C., Goschnick, J., Hirschwald, W.: Surf. Sci. **152/153** (1985) 453.
85Hay1 Hayden, B.E., Kretzschmar, K., Bradshaw, A.M., Greenler, R.G.: Surf. Sci. **149** (1985) 394.
85Hay2 Hayden, B.E., Kretzschmar, K., Bradshaw, A.M.: Surf. Sci. **155** (1985) 553.
85Hes Heskett, D., Plummer, E.W., DePaola, R.A., Eberhardt, W., Hofmann, F.M., Moser, H.R.: Surf. Sci. **164** (1985) 490.
85Hof Hofmann, P., Gossler, J., Zartner, A., Glanz, M., Menzel, D.: Surf. Sci. **161** (1985) 303.
85Mes Messmer, R.P.: Surf. Sci. **158** (1985) 40.
85Pap Papp, H.: Surf. Sci. **149** (1985) 460.
85Per Persson, B.N.J., Ryberg, R.: Phys. Rev. Lett. **54** (1985) 2119.
85Rie Riedl, W., Menzel, D.: Surf. Sci. **163** (1985) 39.
85Ryb Ryberg, R.: Phys. Rev. B **32** (1985) 2671.
85Sch Schmeisser, D., Greuter, F., Plummer, E.W., Freund, H.-J.: Phys. Rev. Lett. **54** (1985) 2095.
85Sei Seip, U., Bassignana, I.C., Kuppers, J., Ertl, G.: Surf. Sci. **160** (1985) 400.
85Shi1 Shincho, E., Egawa, G., Naito, S., Tamaru, K.: Surf. Sci. **149** (1985) 1.
85Shi2 Shinn, N.D., Madey, T.E.: J. Chem. Phys. **83** (1985) 5928.
85Shi3 Shinn, N.D., Madey, T.E.: J. Vac. Sci. Technol. A **3** (1985) 1673.
85Sto Stoltze, P., Norskov, J.K.: Phys. Rev. Lett. **55** (1985) 2502.
85Str Strasser, G., Grunze, M., Golze, M.: J. Vac. Sci. Technol. A **3** (1985) 1562.
85Sun Sung, S.-S., Hoffmann, R.: J. Am .Chem. Soc. **107** (1985) 578.
85Tat Tatarenko, S., Alnot, M., Ehrhardt, J.J., Ducros, R.: Surf. Sci. **152-153** (1985) 471.
85Tom Tomanek, D., Bennemann, K.H.: Phys. Rev. B **31** (1985) 2488.
85Tsa Tsai, M.C., Seip, U., Bassignana, I.C., Küppers, J., Ertl, G.: Surf. Sci. **155** (1985) 387.

85Vin Vink, T.J., Gijzeman, O.L.J., Geus, J.W.: Surf. Sci. **150** (1985) 14.
85Zae Zaera, F., Collin, E., Gland, J.L.: Chem. Phys. Lett. **121** (1985) 464.
86Ant Anton, A.B., Avery, N.R., Madey, T.E., Weinberg, W.H.: J. Chem. Phys. **85** (1986) 507.
86Bag Bagus, P.S., Hermann, K.: Phys. Rev. B **33** (1986) 2987.
86Bar1 Bare, S.R., Strongin, D.R., Somorjai, G.A.: J. Phys. Chem. **90** (1986) 4726.
86Bar2 Bartosch, C.E., Whitman, L.J., Ho, W.: J. Chem. Phys. **85** (1986) 1052.
86Beh Behm, R.J., Hösler, W., Ritter, E., Binning, G.: Phys. Rev. Lett. **56** (1986) 228.
86Bre Breitschafter, M.J., Umbach, E., Menzel, D.: Surf. Sci. **178** (1986) 725.
86Bru Brubaker, M.E., Trenary, M.: J. Chem. Phys. **85** (1986) 6100.
86Dub Dubois, L.H., Ellis, T.H., Kevan, S.D.: J. Vac. Sci. Technol. A **4** (1986) 1505.
86Eri Erickson, J.W., Estrup, P.J.: Surf. Sci. **167** (1986) 519.
86Fre1 Freyer, N., Kiskinova, M., Pirug, G., Bonzel, H.P.: Appl. Phys. A **39** (1986) 209.
86Fre2 Freund, H.J., Rogozik, J., Dose, V., Neumann, M.: Surf. Sci. **175** (1986) 651.
86Fro Froitzheim, H., Köhler, U., Lammering, H.: Phys. Rev. B **34** (1986) 2125.
86Gol Golze, M., Grunze, M., Unertl, W.: Prog. Surf. Sci. **22** (1986) 101.
86Gos Goschnick, J., Wolf, M., Grunze, M., Unertl, W.N., Block, J.H., Loboda-Cackovic, J.: Surf. Sci. **178** (1986) 831.
86Hof Hoffmann, F.M., Levinos, N.J., Perry, B.N., and Rabinowitz, P.: Phys. Rev. B **33** (1986) 4309.
86Hol Holub-Krappe, E., Prince, K.C., Horn, K., Woodruff, D.P.: Surf. Sci. **173** (1986) 176.
86Imb Imbihl, R., Cox, M.P., Ertl, G.: J. Chem. Phys. **84** (1986) 3619.
86Kir Kirstein, W., Krüger, B., Thieme, F.: Surf. Sci. **176** (1986) 505.
86Kru Kruse, N.: Surf. Sci. **178** (1986) 820.
86Kuh Kuhlenbeck, H., Neumann, M., Freund, H.J.: Surf. Sci. **173** (1986) 194.
86Lah Lahee, A.M., Toennies, J.P., Wöll, C.: Surf. Sci. **177** (1986) 371.
86McC McConville, C.F., Woodruff, D.P., Prince, K.C., Paolucci, G., Chab, V., Bradshaw, A.M.: Surf. Sci. **166** (1986) 221.
86Meh Mehandru, S.P., Anderson, A.B.: Surf. Sci. **169** (1986) L281.
86Pau1 Paul, J., Cameron, S.D., Dwyer, D.J., and Hoffmann, F.M.: Surf. Sci. **177** (1986) 121.
86Pau2 Paul, J.: Nature (London) **323** (1986) 701.
86Pau3 Paul, J., Hoffmann, F.M.: Chem. Phys. Lett. **130** (1986) 160.
86Pfn Pfnür, H., Rettner, C.T., Lee, J., Madix, R.J., Auerbach, D.J.: J. Chem. Phys. **85** (1986) 7452.
86See Seebauer, E.G., Kong, A.C.F., Schmidt, L.D.: Surf. Sci. **176** (1986) 134.
86Shi Shinn, N.D., Madey, T.E.: Phys. Rev. B **33** (1986) 1464.
86Ste Steinrück, H.P., D´Evelyn, M.P., Madix, R.J.: Surf. Sci. **172** (1986) L561.
86Str Stroscio, J.A., Persson, M., Ho, W.: Phys. Rev. B **3**3 (1986) 6758.
86Whi1 Whitman, L.J., Bartosch, C.E., Ho, W., Strasser, G., Grunze, M.: Phys. Rev. Lett. **56** (1986) 1984.
86Whi2 Whitman, L.J., Bartosch, C.E., Ho, W.: J. Chem. Phys. **85** (1986) 3688.
86Wur Wurth, W., Schneider, C., Umbach, E., Menzel, D.: Phys. Rev. B. **34** (1986) R1336.
87Bau Bauhofer, J., Hock, M., Küppers, J.: Surf. Sci. **191** (1987) 395.
87Ber Berndt, R., Toennies, J.P., Wöll, C.: J. Electron Spectrosc. Relat. Phenom. **44** (1987) 183.
87Bly Blyholder, G., Lawless, M.: Prog. Surf. Sci. **26** (1987) 181.
87Bru Brubaker, M.E., Malik, I.J., Trenary, M.: J. Vac. Sci. Technol. A **5** (1987) 427.
87deP dePaola, R.A., Hoffmann, F.M., Heskett, D., Plummer, E.W.: Phys. Rev. B **35** (1987) 4236.
87Düc Dückers, K., Prince, K.C., Bonzel, H.P., Chab, V., Horn, K.: Phys. Rev. B **36** (1987) 6292.
87Fre Freund, H.J., Bartos, B., Messmer, R.P., Grunze, M., Kuhlenbeck, H., Neumann, M.: Surf. Sci. **185** (1987) 187.
87Fro Froitzheim, H., Köhler, U.: Surf. Sci. **188** (1987) 70.
87Ful Fulmer, J.P., Zaera, F., Tysoe, W.T.: J. Chem. Phys. **87** (1987) 7265.

87Gos Goschnick, J., Grunze, M., Loboda-Cackovic, J., Block, J.H.: Surf. Sci. **189-190** (1987) 137.
87Gru1 Grunze, M., Strasser, G., Golze, M.: Appl. Phys. A **44** (1987) 19.
87Gru2 Grunze, M., Strasser, G., Golze, M., Hirschwald, W.: J. Vac. Sci. Technol. A **5** (1987) 527.
87Gur Gurney, B.A., Richter, L.J., Villarrubia, J.S., Ho, W.: J. Chem. Phys. **87** (1987) 6710.
87Haa1 Haase, G., Asscher, M.: Surf. Sci. **191** (1987) 75.
87Haa2 Haase, G., Asscher, M.: Chem. Phys. Lett. **142** (1987) 241.
87Hay Hayden, B.E., Robinson, A.W., Tucker, P.M.: Surf. Sci. **192** (1987) 163.
87Her Hermann, K., Bagus, P.S., Nelin, C.J.: Phys. Rev. B **35** (1987) 9467.
87Hrb1 Hrbek, J.: J. Vac. Sci. Technol. A **5** (1987) 864.
87Hrb2 Hrbek, J., Sham, T.K., Shek, M. L.: Surf. Sci. **191** (1987) L772.
87Joh Johnson, P.D., Hulbert, S.L.: Phys. Rev. B **35** (1987) 9427.
87Kuh Kuhlenbeck, H., Saalfeld, H.B., Neumann, M., Freund, H.J., Plummer, E.W.: Appl. Phys. A **44** (1987) 83.
87Kuw Kuwahara, Y., Jo, M., Tsuda, H., Onchi, M., Nishijima, M.: Surf. Sci. **180** (1987) 421.
87Moo1 Moon, D.W., Dwyer, D.J., Bernasek, S.L.: Surf. Sci. **163** (1987) 215.
87Moo2 Moon, D.W., Bernasek, S.L., Lu, J.P., Gland, J.L., Dwyer, D.J.: Surf. Sci. **184** (1987) 90.
87Moo3 Moon, D.W., Cameron, S., Zaera, F., Eberhardt, W., Carr, R., Bernasek, S.L., Gland, J.L., Dwyer, D.J.: Surf. Sci. **180** (1987) L123.
87Ogl Ogletree, D.F., van Hove, M.A., Somorjai, G.A.: Surf. Sci. **173** (1987) 351.
87Oht Ohtani, H., van Hove, M.A., Somorjai, G.A.: Surf. Sci. **187** (1987) 372.
87Out Outka, D.A., Madix, R.J.: Surf. Sci. **179** (1987) 351.
87Pau Paul, J., Hoffmann, F.M.: J. Chem. Phys. **86** (1987) 5188.
87Ret1 Rettner, C.T., Stein, H.: J. Chem. Phys. **87** (1987) 770.
87Ret2 Rettner, C.T., Stein, H.: Phys. Rev. Lett. **59** (1987) 2768.
87Ric Richter, L.J., Gurney, B.A., Ho, W.: J. Chem. Phys. **86** (1987) 477.
87Rit Ritter, E., Behm, R.J., Pötschke, G., Wintterlin, J.: Surf. Sci. **181** (1987) 403.
87Roo Roop, B., Costello, S.A., Mullins, D.R., White, J.M.: J. Chem. Phys. **86** (1987) 3003.
87Ste Steinrück, H.P., Madix, R.J.: Surf. Sci. **185** (1987) 36.
87Tüs Tüshaus, M., Schweizer, E., Hollins, P., Bradshaw, A.M.: J. Electron Spectrosc. Relat. Phenom. **44** (1987) 305.
87Ver Verheij, L.K., Lux, J., Anton, A.B., Poelsema, B., Comsa, G.: Surf. Sci. **182** (1987) 390.
87Wes Wesner, D.A., Coenen, F.P., Bonzel, H.P.: J. Vac. Sci. Technol. A **5** (1987) 927.
87Wur Wurth, W., Schneider, C., Treichler, R., Umbach, E., Menzel, D.: Phys. Rev. B **35** (1987) 7741.
88Ass Asscher, M., Becker, O.M., Haase, G., Kosloff, R.: Surf. Sci. **206** (1988) L880.
88Bla Blackman, G.S., Xu, M.-L., van Hove, M.A., Somorjai, G.A.: Phys. Rev. Lett. **61** (1988) 2352.
88Cam Cameron, S.D., Dwyer, D.J.: Langmuir **4** (1988) 282.
88Dow Dowben, P.A., Miller, A., Ruppender, H.J., Grunze, M.: Surf. Sci. **193** (1988) 336.
88Ega Egawa, C., Iwasawa, Y.: Surf. Sci. **195** (1988) 43.
88Ehr Ehrlich, G.: Activated Chemisorption, in: Chemistry and Physics of Solid Surfaces VII. Springer Series in Surface Science 10; Vanselow, R., Howe, R. (eds.), Berlin: Springer-Verlag, 1988, p. 1-106.
88Eng Engstrom, J.R., Weinberg, W.H.: Surf. Sci. **201** (1988) 145.
88Fer Fery, P., Moritz, W., Wolf, D.: Phys. Rev. B **38** (1988) 7275.
88Fra Frank, K.-H., Sagner, H.-J., Koch, E.E., Eberhardt, W.: Phys. Rev. B **38** (1988) 8501.
88Fuk Fukuda, Y., Nagoshi, M.: Surf. Sci. **203** (1988) L651.
88God Godbey, D.J., Somorjai, G.A.: Surf. Sci. **204** (1988) 301.
88Gum Gumhalter, B., Wandelt, K., Avouris, P.: Phys. Rev. B **37** (1988) 8048.
88Han Hannaman, D.J., Passler, M.A.: Surf. Sci. **203** (1988) 449.

88He He, J.-W., Norton, P.R.: J. Chem. Phys. **89** (1988) 1170.
88Jen Jensen, E.T., Palmer, R.E., Willis, R.F., Collins, I.R., Andrews, P.T.: Vacuum **38** (1988) 353.
88Kel Kelly, D.G., Gellman, A.J., Salmeron, M., Somorjai, G.A., Maurice, V., Huber, M., Oudar, J.: Surf. Sci. **204** (1988) 1.
88Kuw Kuwahara, Y., Fujisawa, M., Onchi, M., Nishijima, M.: Surf. Sci. **207** (1988) 17.
88Lu Lu, J.-P., Albert, M.R., Bernasek, S.L., Dwyer, D.J.: Surf. Sci. **199** (1988) L406.
88Ols Olsen, C.W., Masel, R.I.: Surf. Sci. **201** (1988) 444.
88Rao Rao, C.N.R., Rao, G.R.: Chem. Phys. Lett. **146** (1988) 557.
88Ret Rettner, C.T., Schweizer, E.K., Stein, H., Auerbach, D.J.: Phys. Rev. Lett. **61** (1988) 986.
88Reu Reutt-Robey, J.E., Doven, D.J., Chabal, Y.J., Christman, S.B.: Phys. Rev. Lett. **61** (1988) 2778.
88Ryb Ryberg, R.: Phys. Rev. B **37** (1988) 2488.
88Sch Schwartz, S.B., Schmidt, L. D.: Surf. Sci. **206** (1988) 169.
88See Seebauer, E.G., Kong, A.C.F., Schmidt, L.D.: Appl. Surf. Sci. **31** (1988) 163.
88Str Strongin, D.R., Somorjai, G.A.: J. Catal. **109** (1988) 51.
88Sur Surnev, L., Xu, Z., Yates, J.T.: Surf. Sci. **201** (1988) 1.
88Umb Umbach, E.: Appl. Phys. A **47** (1988) 25.
88Uvd Uvdal, P., Karlsson, P.-A., Nyberg, C., Andersson, S., Richardson, N.V.: Surf. Sci. **202** (1988) 167.
88Yin Yinnon, A.T., Kosloff, R., Gerber, R.B., Poelsema, B., Comsa, G.: J. Chem. Phys. **88** (1988) 3722.
88Zae Zaera, F., Fischer, D.A., Shen, S., Gland, J.L.: Surf. Sci. **194** (1988) 205.
88Zhu Zhu, X.D., Rasing, T., Shen, Y.R.: Phys. Rev. Lett. **61** (1988) 2883.
89Düc Dückers, K., Bonzel, H.P.: Surf. Sci. **213** (1989) 25.
89Dwy Dwyer, D.J., Rausenberger, B., Lu, J.P., Bernasek, S.L., Fischer, D.A., Cameron, S.D., Parker, D.H., Gland, J.L.: Surf. Sci. **224** (1989) 375.
89Ehs Ehsasi, M., Seidel, C., Ruppender, H., Drachsel, W., Block, J. H., Christmann, K.: Surf. Sci. **210** (1989) L198.
89Gri Gritsch, T., Coulman, D., Behm, R.J., Ertl, G.: Phys. Rev. Lett. **63** (1989) 1086.
89Guo Guo, X., Yates jr., J.T.: J. Chem. Phys. **90** (1989) 6761.
89He He, J.-W., Goodman, D.W.: Surf. Sci. **218** (1989) 211.
89Jac Jacobi, K., Astaldi, C., Geng, P., Bertolo, M.: Surf. Sci. **223** (1989) 569.
89Kuh Kuhlenbeck, H., Saalfeld, H.B., Buskotte, U., Neumann, M., Freund, H.-J., Plummer, E.W.: Phys. Rev. B **39** (1989) 3475.
89Lau Lauth, G., Solomun, T., Hirschwald, W., Christmann, K.: Surf. Sci. **210** (1989) 201.
89Lu Lu, J.-P., Albert, M.R., Bernasek, S.L.: Surf. Sci. **217** (1989) 55.
89Mal Malik, I.J., Trenary, M.: Surf. Sci. **214** (1989) L237.
89Mar Marinova, T.S., Chakarov, D.V.: Surf. Sci. **217** (1989) 65.
89Mem Memmel, N., Rangelov, G., Bertel, E., Dose, V., Kometer, K., Rösch, N.: Phys. Rev. Lett. **63** (1989) 1884.
89Mur Murphy, R., Plummer, E.W., Chen, C.T., Eberhardt, W., Carr, R.: Phys. Rev. B **39** (1989) 7517.
89Nil Nilsson, A., Martensson, N.: Phys. Rev. B **40** (1989) 10249.
89Per Persson, B.N.J., Ryberg, R.: Phys. Rev. B **40** (1989) 10273.
89Pie Piercy, P., Heimann, P.A., Michalk, G., Menzel, D.: Surf. Sci. **219** (1989) 189.
89Qui Quick, A., Browne, V.M., Fox, S.G., Hollins, P.: Surf. Sci. **221** (1989) 48.
89Rav Raval, R., Blyholder, G., Haq, S., King, D.A.: J. Phys. Condens. Matter 1 (1989) 165.
89Ron Rong, C., Satoko, C.: Surf. Sci. **223** (1989) 101.
89Sai Saiki, R.S., Herman, G.S., Yamada, M., Osterwalder, J., Fadley, C.S.: Phys. Rev. Lett. **63** (1989) 283.
89Sch Schenk, A., Hock, M., Küppers, J.: Surf. Sci. **217** (1989) L367.

89Sel Sellidj, A., Erskine, J.L.: Surf. Sci. **220** (1989) 253.
89Wen Wenzel, L., Arvanitis, D., Schlögl, R., Muhler, M., Norman, D., Baberschke, K., Ertl, G.: Phys. Rev. B **40** (1989) 6409.
89Wes Wesner, D.A., Coenen, F.P., Bonzel, H.P.: Phys. Rev. B **39** (1989) 10770.
89Whi Whitman, L.J., Richter, L.J., Gurney, B.A., Villarrubia, J.S., Ho, W.: J. Chem. Phys. **90** (1989) 2050.
89Zhu Zhu, X.D., Rasing, T., Shen, Y.R.: Chem. Phys. Lett. **155** (1989) 459.
90Ant Antonsson, H., Nilsson, A., Martensson, N.: J. Electron Spectrosc. Relat. Phenom. **54/55** (1990) 601.
90Bec Beckerle, J.D., Casassa, M.P., Cavanagh, R.R., Heilweil, E.J., Stephenson, J.C.: Phys. Rev. Lett. **64** (1990) 2090.
90Ben Benndorf, C., Meyer, L.: J. Vac. Sci. Technol. A **8** (1990) 2677.
90Ber Berlowitz, P.J., He, J.-W., Goodman, D.W.: Surf. Sci. **231** (1990) 315.
90Car Carley, A.F., Roberts, M.W., Yan, S.: Appl. Surf. Sci. **40** (1990) 289.
90Cor Cornish, J.C.L., Avery, N.R.: Surf. Sci. **135** (1990) 209.
90Cra Craig, J.H.J., Lozano, J.: Surf. Sci. **235** (1990) L308.
90Fei Feigerle, C.S., Desai, S.R., Overbury, S.H.: J. Chem. Phys. **93** (1990) 787.
90Har Harris, A.L., Levinos, N.J., Rothberg, L., Dubois, L.H., Dhar, L., Shane, S.F., Morin, M.: J. Electron Spectrosc. Relat. Phenom. **54/55** (1990) 5.
90He He, J.-W., Shea, W.L., Jiang, X., Goodman, D.W.: J. Vac. Sci. Technol. A **8** (1990) 2435.
90Hen Henriksen, N.E., Billing, G.D., Hansen, F.Y.: Surf. Sci. **227** (1990) 224.
90Hin Hinch, B.J., Dubois, L.H.: J. Electron Spectrosc. Relat. Phenom. **54/55** (1990) 759.
90Hir Hirschmugl, C.J., Williams, G.P., Hoffmann, F.M., Chabal, Y.J.: Phys. Rev. Lett. **65** (1990) 480.
90Hol Hollins, P.: Surf. Sci. Rep. **16** (1990) 51.
90Hrb Hrbek, J.: J. Phys. Chem. **94** (1990) 1564.
90Jac Jacobi, K., Bertolo, M.: Phys. Rev. B **42** (1990) 3733.
90Koe Koel, B.E., Smith, R.J., Berlowitz, P.J.: Surf. Sci. **231** (1990) 325.
90Kuh Kuhn, W.K., He, J.W., Goodman, D.W.: Chem. Phys. Lett. **95** (1990) 5220.
90Leu Leung, L.-W.H., He, J.-W., Goodman, D.W.: J. Chem. Phys. **93** (1990) 8328.
90Li Li, J., Schiott, B., Hoffmann, R., Proserpio, D.: J. Phys. Chem. **94** (1990) 1554.
90Lin Lin, J.C., Shamir, N., Zhao, Y.B., Gomer, R.: Surf. Sci. **231** (1990) 333.
90Mar Martensson, N., Nilsson, A.: J. Electron Spectrosc. Relat. Phenom. **52** (1990) 1.
90Per Persson, B.N.J., Tüshaus, M., Bradshaw, A.M.: J. Chem. Phys. **92** (1990) 5034.
90Pet Peterson, L.D., Kevan, S.D.: Phys. Rev. Lett **65** (1990) 2563.
90Rao Rao, G.R., Rao, C.N.R.: Appl. Surf. Sci. **45** (1990) 65.
90Rav1 Raval, R., Haq, S., Blyholder, G., King, D.A.: J. Electron Spectrosc. Relat. Phenom. **54-55** (1990) 629.
90Rav2 Raval, R., Haq, S., Harrison, M.A., Blyholder, G., King, D.A.: Chem. Phys. Lett. **167** (1990) 391.
90Rod Rodriguez, J.A., Campbell, R.A., Goodman, D.W.: J. Phys. Chem. **94** (1990) 6936.
90Ros Rosenzweig, Z., Asscher, M., Wittenzellner, C.: Surf. Sci. **240** (1990) L583.
90Ryb Ryberg, R.: J. Electron Spectrosc. Relat. Phenom. **54/55** (1990) 65.
90Sch Schneider, C., Steinrück, H.-P., Pache, T., Heimann, P.A., Coulman, D.J., Umbach, E., Menzel, D.: Vacuum **41** (1990) 730.
90Shi Shinn, N.D.: Phys. Rev. B **41** (1990) 9771.
90Tüs1 Tüshaus, M., Berndt, W., Conrad, H., Bradshaw, A.M., Persson, B.: Appl. Phys. A **51** (1990) 91.
90Tüs2 Tüshaus, M.: Ph. D. Thesis Berlin, 1990.
90Voi Voigtländer, B., Bruchmann, D., Lehwald, S., Ibach, H.: Surf. Sci. **225** (1990) 151.

90Wen Wenzel, L., Arvanitis, D., Schlögl, R., Muhler, M., Norman, D., Baberschke, K., Ertl, G.: Phys. Scr. **41** (1990) 1028.

90Wur Wurth, W.: Vacuum **40** (1990) 3.

90Yos Yoshioka, K., Kitamura, F., Takeda, M., Takahashi, M., Ito, M.: Surf. Sci. **227** (1990) 90.

90Zha Zhang, Q.-J., Lin, J.C., Shamir, N., Gomer, R.: Surf. Sci. **231** (1990) 344.

91And Andersen, J.N., Qvarford, M., Nyholdm, R., Sorensen, S.L., Wigren, C.: Phys. Rev. Lett **67** (1991) 2822.

91Bec Beckerle, J.D., Cavanagh, R.R., Casassa, M.P., Heilweil, E.J., Stephenson, J.C.: J. Chem. Phys. **95** (1991) 5403.

91Ber Bertel, E.: Appl. Phys. A **53** (1991) 356.

91Bow Bowker, M., Guo, Q., Joyner, R.: Surf. Sci. **253** (1991) 33.

91Cam Campbell, R.A., Rodriguez, J.A., Goodman, D.W.: Surf. Sci. **256** (1991) 272.

91Che Chen, J.G., Colaianni, M.L., Weinberg, W.H., Yates jr., J.T.: Chem. Phys. Lett. **177** (1991) 113.

91Com Comelli, G., Sastry, M., Paolucci, G., Prince, K.C., Olivi, L.: Phys. Rev. B **43** (1991) 14385.

91Dav Davis, R., Lindsay, R., Purcell, K.G., Thornton, G., Robinson, A.W., Morrison, T.P., Bowker, M., Pudney, P.D.A., Surman, M.: J. Phys. Condens. Matter **3** (1991) S297.

91Dow Dowben, P.A., Ruppender, H.-J., Grunze, M.: Surf. Sci. **254** (1991) L482.

91Gar Gardner, P., Martin, R., Tüshaus, M., Bradshaw, A.M.: J. Electron Spectrosc. Relat. Phenom. **54** (1991) 619.

91Ha Ha, J.S., Sibener, S.J.: Surf. Sci. **256** (1991) 281.

91He1 He, J.-W., Kuhn, W.K., Goodman, D.W.: Chem. Phys. Lett. **177** (1991) 109.

91He2 He, J.-W., Goodman, D.W.: Surf. Sci. **245** (1991) 29.

91He3 He, J.-W., Kuhn, W.K., Goodman, D.W.: J. Am. Chem. Soc. **113** (1991) 6416.

91Hou Houston, J.E.: Surf. Sci. **255** (1991) 303.

91Hu Hu, P., Morale de la Garza, L., Raval, R., King, D.A.: Surf. Sci. **249** (1991) 1.

91Kis Kisters, G., Chen, J.G., Lehwald, S., Ibach, H.: Surf. Sci. **245** (1991) 65.

91Koc Koch, R., Borbonous, M., Haase, O., Reider, K.H.: Phys. Rev. Lett. **67** (1991) 3416.

91Nil Nilsson, A., Tillborg, H., Martensson, N.: Phys. Rev. Lett. **67** (1991) 1015.

91Pet1 Peterlinz, K.A., Curtiss, T.J., Sibener, S.J.: J. Chem. Phys. **95** (1991) 6972.

91Pet2 Peterson, L.D., Kevan, S.D.: J. Chem. Phys. **94** (1991) 2281.

91Por Por, E., Haase, G., Citri, O., Kosloff, R., Asscher, M.: Chem. Phys. Lett. **186** (1991) 553.

91Ran Rangelov, G., Memmel, N., Bertel, E., Dose, V.: Surf. Sci. **251/252** (1991) 965.

91Rao Rao, C.N.R., Ranga Rao, G.: Surf. Sci. Rep. **13** (1991) 221.

91Rod1 Rodriguez, J.A., Campbell, R.A., Goodman, D.W.: Surf. Sci. **244** (1991) 211.

91Rod2 Rodriguez, J.A., Campbell, R.A., Goodman, D.W.: J. Phys. Chem. **95** (1991) 2477.

91Rod3 Rodriguez, J.A., Goodman, D.W.: J. Phys. Chem. **95** (1991) 4196.

91Rod4 Rodriguez, J.A., Campbell, R. A., Goodman, D.W.: J. Phys. Chem. **95** (1991) 5716.

91Tre Treichler, R., Wurth, W., Riedl, W., Feulner, P., Menzel, D.: Chem. Phys. **153** (1991) 259.

91Won Wong, Y.-T., Hoffmann, R.: J. Phys. Chem. **95** (1991) 859.

91Xia Xiao, X.-D., Zhu, X.D., Daum, W., Shen, Y.R.: Phys. Rev. Lett. **66** (1991) 2352.

91Yos Yoshinobu, J., Zenobi, R., Xu, J., Xu, Z., Yates jr., J.T.: J. Chem. Phys. **95** (1991) 9393.

92Avr Avrin, W.F., Merrill, R.P.: Surf. Sci. **274** (1992) 231.

92Bad Badri, A., Binet, C., Lavalley, J.C.: J. Chem. Soc. Faraday Trans. **92** (1992) 1603.

92Ber1 Bernasek, S.L., Zappone, M., Jiang, P.: Surf. Sci. **272** (1992) 53.

92Ber2 Berndt, W., Bradshaw, A.M.: Surf. Sci. **279** (1992) L165.

92Bjö Björneholm, O., Nilsson, A., Zdansky, E.O.F., Sandell, A., Hernnäs, B., Tillborg, H., Andersen, J.N., Martensson, N.: Phys. Rev. B **46** (1992) 10353.

92Bor Borguet, E., Dai, H.-L.: Chem. Phys. Lett. **194** (1992) 57.

92Cam Campbell, R.A., Rodriguez, J.A., Goodman, D.W.: Phys. Rev. B **46** (1992) 7077.

92Chr Christiansen, M., Thomsen, E.V., Onsgaard, J.: Surf. Sci. **261** (1992) 179.
92Cra Craig, J.H.J., Donlin, D.: Surf. Sci. **278** (1992) L121.
92DeA DeAngelis, M.A., Glines, A.M., Anton, A.B.: J. Chem. Phys. **96** (1992) 8582.
92Dha Dhanak, V.R., Comelli, G., Cautero, G., Paolucci, G., Kiskinova, M., Prince, K.C., Rosei, R.: Chem. Phys. Lett. **188** (1992) 237.
92Eda Edamoto, K., Shiobara, E., Anazawa, T., Hatta, M., Miyazaki, E., Kato, H., Otani, S.: J. Chem. Phys. **96** (1992) 842.
92Gau1 Gaussmann, A., Kruse, N.: Surf. Sci. **279** (1992) 319.
92Gau2 Gaussmann, A., Kruse, N.: Surf. Sci. **266** (1992) 46.
92Guo Guo, X.-C., Hopkinson, A., Bradley, J.M., King, D.A.: Surf. Sci. **278** (1992) 263.
92Kna Knauff, O., Grosche, U., Bonzel, H.P., Frizsche, V.: Mol. Phys. **76** (1992) 787.
92Kuh1 Kuhn, W.K., Szanyi, J., Goodman, D.W.: Surf. Sci. **274** (1992) L611.
92Kuh2 Kuhn, W.K., He, J.W., Goodman, D.W.: J. Vac. Sci. Technol. A **10** (1992) 2477.
92Kwa Kwasniewski, V.J., Schmidt, L.D.: Surf. Sci. **274** (1992) 329.
92Lov Love, J.G., Haq, S., King, D.A.: J. Chem. Phys. **97** (1992) 8789.
92Luo Luo, S., Tobin, R.G., Lambert, D.K., Fisher, G.B., Dimaggio, C.L.: Surf. Sci. **274** (1992) 53.
92Mor Morin, M., Levinos, N.J., Harris, A.L.: J. Chem. Phys. **96** (1992) 3950.
92Nil Nilsson, A., Björneholm, O., Zdansky, E.O.F., Tillborg, H., Martensson, N.: Chem. Phys. Lett. **197** (1992) 12.
92Rod Rodriguez, J.A., Goodman, D.W.: Science **257** (1992) 897.
92Ros Ross, P.N.: J. Vac. Sci. Technol. A **10** (1992) 2546.
92Shi Shi, H., Jacobi, K.: Surf. Sci. **278** (1992) 281.
92Stö Stöhr, J.: NEXAFS Spectroscopy; Heidelberg: Springer-Verlag, 1992.
92Toe Toennies, J.P., Woll, C., Zhang, G.: J. Chem. Phys. **96** (1992) 4023.
92Tru Truong, C.M., Rodriguesz, J.A., Goodman, D.W.: Surf. Sci. **271** (1992) L385.
92Tsu Tsuei, K.-D., Johnson, P.D.: Phys. Rev. B **45** (1992) 13827.
92Was N. Wassdahl, A. Nilsson, T. Wiell, H. Tillborg, L. C. Duda, J. H. Guo, N. Martensson, J. Nordgren, J. N. Andersen, R. Nyholm, Phys. Rev. Lett. **69**, 812 (1992).
92Win Wintterlin, J., Behm, R.J.: Scanning Tunneling Microscopy, Güntherodt I.H.J., Wiesendanger, R. (eds.), Berlin: Springer, 1992, p. 39.
92Wur Wurth, W., Feulner, P., Menzel, D.: Phys. Scr. T **41** (1992) 213.
92Xia Xiao, X.-D., Zhu, X.D., Daum, W., Shen, Y.R.: Phys. Rev. B **46** (1992) 9732.
92Zhu Zhu, L., Bao, S., Xu, C.Y., Xu, Y.B.: Surf. Sci. **260** (1992) 267.
93Bar Baraldi, A., Dhanak, V.R., Comelli, G., Prince, K.C., Rosei, R.: Surf. Sci. **293** (1993) 246.
93Bec Becker, L., Aminpirooz, S., Hillert, B., Pedio, M., Haase, J., Adams, D.L.: Phys. Rev. B **47** (1993) 9710.
93Bel Bellman, A., Morgante, A., Polli, M., Tommasini, F., Cvetko, D., Dhanak, V.R., Lausi, A., Prince, K.C., Rosei, R.: Surf. Sci. **298** (1993) 1.
93Col Colaianni, M.L., Chen, J.G., Yates jr., J.T.: J. Phys. Chem. **97** (1993) 2707.
93Cud Cudok, A., Froitzheim, H., Schulze, M.: Phys. Rev. B **47** (1993) 13682.
93Dha Dhanak, V.R., Baraldi, A., Comelli, G.: Surf. Sci. **295** (1993) 287.
93Gar Gardner, P., Martin, R., Tüshaus, M., Shamir, J., Bradshaw, A.M.: Surf. Sci. **287** (1993) 135.
93He He, J.-W., Kuhn, W.K., Goodman, D.W.: Surf. Sci. **292** (1993) 248.
93Hir Hirschmugl, C.J., Dumas, P., Chabal, Y.J., Hoffmann, F.M., Suhren, M., Williams, G.P.: J. Electron Spectrosc. Relat. Phenom. **64/65** (1993) 67.
93Hom Homann, K., Jaeger, R.M., Kuhlenbeck, H.: J. Electron Spectrosc. Relat. Phenom. **62** (1993) 273.
93Hop Hopkinson, A., Bradley, J.M., Guo, X.C., King, D.A.: Phys. Rev. Lett. **71** (1993) 1597.
93Hua Huang, Z., Hussain, Z., Huff, W.R.A., Moler, E.J., Shirley, D.A.: Phys. Rev. B **48** (1993) 1696.
93Imb Imbihl, R.: Surf. Sci. **44** (1993) 185.

93Kuh1 Kuhn, W.K., Campbell, R.A., Goodman, D.W.: J. Phys. Chem. **97** (1993) 446.

93Kuh2 Kuhn, W.K., Campbell, R.A., Goodman, D.W.: Adsorption on bimetallic surfaces, in: The Chemical Physics of Solid Surfaces. 6; King, D.A., Woodruff, D.P. (eds.), Amsterdam: Elsevier, 1993, p. 157-183.

93Mar Martin, R., Gardner, P., Nalezinski, R., Tushaus, M., Bradshaw, A.M.: J. Electron Spectrosc. Relat. Phenom. **64-65** (1993) 619.

93Mur Murray, P.W., Leibsle, F.M., Li,Y., Guo, Q., Bowker, M., Thornton, G., Dharnak, V.R., Prince, K.C., Rosei, R.: Phys. Rev. B **47** (1993) 12976.

93Ove Over, H., Moritz, W., Ertl, G.: Phys. Rev. Lett. **70** (1993) 315.

93Pan Pangher, N., Haase, J.: Surf. Sci. Lett. **293** (1993) L908.

93Rif Riffe, D.M., Sievers, A.J.: Surf. Sci. **297** (1993) 1.

93Rod Rodriguez, J.A.: Surf. Sci. **289** (1993) L584.

93Sch Schindler, K.-M., Hofmann, P., Weiß, K.-U., Dippel, R., Gardner, P., Fritzsche, V., Bradshaw, A.M., Woodruff, D.P., Davila, M.E., Asensio, M.C., Conesa, J.C., Gonzales-Elipe, A.R.: J. Electron Spectrosc. Relat. Phenom. **64/65** (1993) 75.

93Sel Sellidj, A., Koel, B.E.: Surf. Sci. **284** (1993) 139.

93Shi Shi, H., Jacobi, K., Ertl, G.: J. Chem. Phys. **99** (1993) 9248.

93Sie Sieben, B., Bonzel, H.P.: Surf. Sci. **282** (1993) 246.

93Sin Sinniah, K., Dorsett, H.E., Reutt-Robey, J.E.: J. Chem. Phys. **98** (1993) 9018.

93Stu Stuckless, J.T., Al-Sarraf, N., Wartnaby, C., King, D.A.: J. Chem. Phys. **99** (1993) 2202.

93Sza1 Szabo, A., Yates, J.T.: J. Chem. Phys. **98** (1993) 689.

93Sza2 Szanyi, J., Kuhn, W.K., Goodman, D. W.: J. Vac. Sci. Technol. A **11** (1993) 1969.

93Tak Takagi, N., Yoshinobu, J., Kawai, M.: Chem. Phys. Lett. **215** (1993) 120.

93Til Tillborg, H., Nilsson, A., Martensson, N.: J. Electron Spectrosc. Relat. Phenom. **62** (1993) 73.

93Til3 H. Tillborg, A. Nilsson, T. Wiell, N. Wassdahl, N. Martensson, J. Nordgren, Phys. Rev. B. **47**, 16464 (1993).

93Wan Wander, A., Hu, P., King, D.A.: Chem. Phys. Lett. **201** (1993) 393.

93Wit Witte, G., Range, H., Toennies, J.P., Wöll, C.: J. Electron Spectrosc. Relat. Phenom. **64/65** (1993) 715.

94Bat Batteas, J.D., Barbieri, A., Starkey, E.K.: Surf. Sci. **313** (1994) 341.

94Ber Bertino, M., Ellis, J., Hofmann, F., Toennies, J.P., Manson, J.R.: Phys. Rev. Lett. **73** (1994) 605.

94Bjö Björneholm, O., Nilsson, A., Tillborg, H., Bennich, P., Sandell, A., Hernnäs, B., Puglia, C., Martensson, N.: Surf. Sci. **315** (1994) 1994.

94Blu Bludau, H., Gierer, M., Over, H., Ertl, G.: Chem. Phys. Lett. **219** (1994) 452.

94Bor Borg, A., Hilmen, A.-M., Bergene, E.: Surf. Sci. **306** (1994) 10.

94Cam Campbell, J.H., Gonzales, L.G., Ybarra, I., Craig, J.H.J.: Surf. Sci. **306** (1994) 204.

94Dav Davila, M.E., Asensio, M.C., Woodruff, D.P., Schindler, K.M., Hofmann, P., Weiss, K.U.: Surf. Sci. **311** (1994) 337.

94deJ de Jong, A.M., Niemantsverdriet, J.W.: J. Chem. Phys. **101** (1994) 10126.

94Fro Froitzheim, H., Schulze, M.: Surf. Sci. **274** (1994) 85.

94Gro Grossmann, A., Erley, W., Ibach, H.: Surf. Sci. **313** (1994) 209.

94Her Hertel, T., Knoesel, E., Hasselbrink, E., Wolf, M., Ertl, G.: Surf. Sci. **317** (1994) L1147.

94Hir Hirschmugl, C.J., Chabal, Y.J., Hoffmann, F.M., Williams, G.P.: J. Vac. Sci. Technol. A **12** (1994) 2229.

94Kam Kampshoff, E., Hahn, E., Kern, K.: Phys. Rev. Lett. **73** (1994) 704.

94Kan Kang, H C., Weinberg, W.H.: Surf. Sci. **299-300** (1994) 755.

94Loc Locatelli, A., Brena, B., Lizzit, S., Comelli, G., Cautero, G., Paolucci, G., Rosei, R.: Phys. Rev. Lett. **73** (1994) 90.

94Map Mapledoram, L.D., Bessent, M.P., Wander, A., King, D.A.: Chem. Phys. Lett. **228** (1994) 527.

94Mar Maruyama, T., Sakisaka, Y., Kato, H., Aiura, Y., Yanashima, H.: Surf. Sci. **304** (1994) 281.
94Men Meng, B., Weinberg, W.H.: J. Chem. Phys. **100** (1994) 5280.
94San1 Sandell, A., Björneholm, O., Andersen, J.N., Nilsson, A., Zdansky, E.O.F., Hernnäs, B., Karlsson, U.O., Nyholm, R., Martensson, N.: J. Phys. Condens. Matter **6** (1994) 10659.
94San2 Sandell, A., Bennich, P., Nilsson, A., Hernnäs, B., Björneholm, O., Martensson, N.: Surf. Sci. **310** (1994) 16.
94San3 Sandell, A., Björneholm, O., Nilsson, A., Hernnäs, B., Andersen, J.N., Martensson, N.: Phys. Rev. B **49** (1994) 10136.
94She Shen, Y.R.: Surf. Sci. **299-300** (1994) 551.
94Som Somorjai, G.: Introduction to surface chemistry and catalysis; New York: John Wiley & Sons, 1994.
94Son Song, Z., Lu, R., Lou, N.: Chem. Phys. Lett. **217** (1994) 142.
94Vil Villegas, I., Weaver, M.J.: J. Chem. Phys. **101** (1994) 1648.
94Wei Weimer, J.J., Loboda-Cackovic, J., Block, J.H.: Surf. Sci. **316** (1994) 123.
94Wes Westphal, C., Fegel, F., Bansmann, J., Getzlaff, M., Schönhense, G., Stephens, J.A., McKoy, V.: Phys. Rev. B **50** (1994) 17534.
94Wie T. Wiell, H. Tillborg, A. Nilsson, N. Wassdahl, N. Martensson, J. Nordgren, Surf. Sci. **304**, L451 (1994)
94Xu Xu, C., Koel, B.E.: Surf. Sci. **304** (1994) L505.
94Zha Zhao, C., Passler, M.A.: Surf. Sci. **320** (1994) 1.
95Ban Bansmann, J., Ostertag, C., Getzlaff, M., Schönhense, G., Cherepkov, N.A., Kuznetsov, V.V., Pavlychev, A.A.: Z. Phys. D **33** (1995) 257.
95Bar Baraldi, A., Barnaba, M., Brena, B., Cocco, D., Comelli, G., Lizzit, S., Paolucci, G., Rosei, R.: J. Electron Spectrosc. Relat. Phenom. **76** (1995) 145.
95Bir Birchem, T., Muhler, M.: Surf. Sci. **334** (1995) L701.
95Ell Ellis, J., Witte, G., Toennies, J.P.: J. Chem. Phys. **102** (1995) 5059.
95Gru Gruyters, M., Jacobi, K.: Surf. Sci. **336** (1995) 314.
95Her Hertel, T., Knoesel, E., Wolf, M., Ertl, G.: Nucl. Instrum. Methods Phys. Res. Sect. B **101** (1995) 53.
95Hir Hirschmugl, C.J., Williams, G.P.: Phys. Rev. B **52** (1995) 14177.
95Hof Hofmann, P., Schindler, K.-M., Bao, S., Fritzsche, V., Bradshaw, A.M., Woodruff, D.P.: Surf. Sci. **337** (1995) 169.
95Hu Hu, P., King, D.A., Lee, M.-H., Payne, M.C.: Chem. Phys. Lett. **246** (1995) 73.
95Kno Knoesel, E., Hertel, T., Wolf, M., Ertl, G.: Chem. Phys. Lett. **240** (1995) 409.
95Lyo Lyons, K.J., Xie, J., Mitchell, W.J., Weinberg, W.H.: Surf. Sci. **325** (1995) 85.
95Mar Martin, R., Gardner, P., Bradshaw, A.M.: Surf. Sci. **342** (1995) 69.
95Mit Mitchell, S.A., Lian, L., Rayner, D.M., Hackett, P.A.: J. Chem. Phys. **103** (1995) 5539.
95Nil A. Nilsson, P. Bennich, T. Wiell, N. Wassdahl, N. Martensson, J. Nordgren, O. Björneholm, J. Stöhr. Phys. Rev. B. **51**, 10244 (1995).
95Ove Over, H., Bludau, H., Kose, R., Ertl, G.: Chem. Phys. Lett. **243** (1995) 435.
95Ped Pedocchi, L., Ji, M.R., Lizzit, S., Comelli, G., Rovida, G.: J. Electron Spectrosc. Relat. Phenom. **76** (1995) 383.
95Pic1 Pick, S.: J. Phys. Condens. Matter **7** (1995) 7729-40.
95Pic2 Pick, S.: Chem. Phys. Lett. **239** (1995) 84.
95Ram Ramsier, R.D., Lee, K.-W., Yates jr., J.T.: Surf. Sci. **322** (1995) 243.
95Rob Robinson, I.K., Ferrer, S., Torrellas, X., Alvarez, J., van Silfhout, R., Schuster, R., Kuhnke, K., Kern, K.: Europhys. Lett. **32** (1995) 37.
95Sch Schwegmann, S., Tappe, W., Korte, U.: Surf. Sci. **334** (1995) 55.
95Spr Sprunger, P., Besenbacher, F., Stensgard, I.: Surf. Sci. **324** (1995) L321.
95Sza Szabo, A., Yates, J.T.: J. Chem. Phys. **102** (1995) 563.
95Vas Vasquez, N., Muscat, A., Madix, R.J.: Surf. Sci. **339** (1995) 29.

95Wei Wei, D.H., Skelton, D.C., Kevan, S.D.: Surf. Sci. **326** (1995) 167.
95Wu Wu, K., Zhai, R., Jia, J., Lu, S., Wu, S.: J. Electron Spectrosc. Relat. Phenom. **76** (1995) 201.
95Xu Xu, C., Koel, B.E.: Surf. Sci. **327** (1995) 38.
95Yeo Yeo, Y.Y., Warnaby, C., King, D.A.: Science **268** (1995) 1737.
96Ahn Ahner, J., Mocuta, D., Ramsier, R.D., Yates, J.T.: J. Chem. Phys. **105** (1996) 6553.
96Aru Arumainayagam, C.R., Tripa, C.E., Xu, J., Yates, J.T.: Surf. Sci. **360** (1996) 121.
96Bar Baraldi, A., Gregoratti, L., Comelli, G., Dhanak, V.R., Kiskinova, M., Rosei, R.: Appl. Surf. Sci. **99** (1996) 1.
96Bei Beitel, G.A., Laskov, A., Oosterbeek, H., Kuipers, E.W.: J. Phys. Chem. **100** (1996) 12494.
96Ber Bertino, M.F., Hofmann, F., Steinhögl, W., Toennies, J.P.: J. Chem. Phys. **105** (1996) 11297.
96Bra Braun, J., Graham, A.P., Hofman, F., Silvestri, W., Toennies, J.P., Witte, G.: J. Chem. Phys. **105** (1996) 3258.
96Dav Davis, R., Woodruff, D.P., Hofmann, P., Schaff, O., Fernandez, V., Schindler, K.M., Fritzsche, V., Bradshaw, A.M.: J. Phys. Condens. Matter **8** (1996) 1367.
96Die Dietrich, H., Geng, P., Jacobi, K., Ertl, G.: J. Chem. Phys. **104** (1996) 375.
96Dvo Dvorak, J., Borguet, E., Dai, H.-L.: Surf. Sci. **369** (1996) L122.
96Eva Evans, J., Hayden, B.E., Lu, G.: Surf. Sci. **360** (1996) 61.
96Gie Gierer, M., Bludau, H., Over, H., Ertl, G.: Surf. Sci. **346** (1996) 64.
96Goy Goyhenex, C., Croci, M., Claeys, C., Henry, C.R.: Surf. Sci. **352-354** (1996) 475.
96Gra Graham, A.P., Hofmann, F., Toennies, J.P., Manson, J.R.: J. Chem. Phys. **105** (1996) 2093.
96Ham Hammer, B., Morikawa, Y., Norskov, J.K.: Phys. Rev. Lett. **76** (1996) 2141.
96Hof Hofmann, F., Toennies, J.P.: Chem. Rev. **96** (1996) 1307.
96Jak Jakob, P.: Phys. Rev. Lett. **77** (1996) 4229.
96Jin Jin, X.F., Mao, M.Y., Ko, S., Shen, Y.R.: Phys. Rev. B **54** (1996) 7701.
96Klü Klünker, C., Balden, M., Lehwald, S., Daum, W.: Surf. Sci. **360** (1996) 104.
96Lau Lauterbach, J., Boyle, R.W., Schick, M., Mitchell, W.J., Meng, B., Weinberg, W.H.: Surf. Sci. **350** (1996) 32.
96Loc Locatelli, A., Brena, B., Comelli, G., Lizzit, S., Paolucci, G., Rosei, R.: Phys. Rev. B **54** (1996) 2839.
96McC Cook, J.C., McCash, E.M.: Surf. Sci. Lett. **356** (1996) L445.
96Mit Mitchell, S.A., Rayner, D.M., Bartlett, T., Hackett, P.A.: J. Chem. Phys. **104** (1996) 4012.
96Mol Moler, E.J., Kellar, S.A., Huff, W.R.A., Hussain, Z., Chen, Y., Shirley, D.A.: Phys. Rev. B **54** (1996) 10862.
96Rai Rainer, D.R., Wu, M.C., Mahon, D.I., Goodman, D.W.: J. Vac. Sci. Technol. A **14** (1996) 1184.
96Rot Rotaris, G., Baraldi, A., Comelli, G., Kiskinova, M., Rosei, R.: Surf. Sci. **359** (1996) 1.
96Sch Schuster, R., Robinson, I.K., Kuhnke, K., Ferrer, S., Alvarez, J., Kern, K.: Phys. Rev. B **54** (1996) 17097.
96Sha Sham, T.K., Shek, M.L., Hrbek, J., van Campen, D.G.: J. Vac. Sci. Technol. B **14** (1996) 3199.
96Su Su, X., Cremer, P.S., Shen, Y.R., Somorjai, G.A.: Phys. Rev. Lett. **77** (1996) 3858.
96Sve Svensson, K., Rickardsson, I., Nyberg, C., Andersson, S.: Surf. Sci. **366** (1996) 140.
96Too Toomes, R.L., King, D.A.: Surf. Sci. **349** (1996) 1.
96Wal Wallauer, W., Fischer, R., Fauster, T.: Surf. Sci. **364** (1996) 297.
96Yeo Yeo, Y.Y., Vattuone, L., King, D.A.: J. Chem. Phys. **104** (1996) 3810.
96Zac Zacchigna, M., Astaldi, C., Prince, K.C., Sastry, M., Comicioli, C., Rosei, R., Quaresima, C., Ottaviani, C., Crotti, C., Antonini, A., Matteucci, M., Perfetti, P.: Surf. Sci. **347** (1996) 53.
96Zae Zaera, F., Liu, J., Xu, M.: J. Chem. Phys. **106** (1996) 4204.
97Ahn Ahner, J., Mocuta, D., Ramsier, R.D., Yates, J.T.: Phys. Rev. Lett. **79** (1997) 1889.
97Ber Bertino, M.F., Witte, G.: Surf. Sci. **385** (1997) L984.

97Beu Beutler, A., Lundgren, E., Nyholm, R., Andersen, J.N., Setlik, B., Heskett, D.: Surf. Sci. **371** (1997) 381.
97Bra Braun, J., Kostov, K.L., Witte, G., Wöll, C.: J. Chem. Phys. **106** (1997) 8262.
97Bur Burghaus, U., Ding, J., Weinberg, W.H.: Surf. Sci. **384** (1997) L869.
97Die Dietrich, H., Jacobi, K., Ertl, G.: J. Chem. Phys. **106** (1997) 9313.
97Eng Engström, U., Ryberg, R.: Phys. Rev. Lett. **78** (1997) 1944.
97Gie Gierer, M., Barbieri, A., van Hove, M.A., Somorjai, G.A.: Surf. Sci. **391** (1997) 176.
97Gro Groenbeck, H., Rosen, A., Andreoni, W.: Z. Phys. D **40** (1997) 206.
97Jac Jacobi, K., Dietrich, H., Ertl, G.: Appl. Surf. Sci. **121** (1997) 558.
97McC Cook, J.C., McCash, E.M.: Surf. Sci. **371** (1997) 213.
97Med Medvedev, V.K., Kulik, V.S., Chernyi, V.I., Suchorski, Y.: Vacuum **48** (1997) 341.
97Mor Mortensen, J.J., Morikawa, Y., Hammer, B., Norskov, J.K.: Z. Phys. Chem. **198** (1997) 113.
97Nah Nahm, T.-U., Gomer, R.: Surf. Sci. **384** (1997) 283.
97Nil1 A. Nilsson, M. Weinelt, T. Wiell, P. Bennich, O. Karis, N. Wassdahl, J. Stöhr, M. G. Samant, Phys. Rev. Lett. **78**, 2847 (1997).
97Nil2 A. Nilsson, N. Wassdahl, M. Weinelt, O. Karis, T. Wiell, P. Bennich, J. Hasselström, A. Föhlisch, J. Stöhr, M. G. Samant, Appl. Phys. A. Mat. Sci. Proc. **65**, 147 (1997).
97Ove Over, H., Schwegmann, S., Ertl, G., Cvetko, D., de Renzi, V., Floreano, L., Gotter, R., Morgante, A., Peloi, M., Tommasini, F., Zennaro, S.: Surf. Sci. **376** (1997) 177.
97Pic Pick, S.: J. Phys. Condens. Matter **9** (1997) 141-8.
97Ram Ramsey, M.G., Leisneberger, F.P., Netzer, F.P., Roberts, A.J., Raval, R.: Surf. Sci. **385** (1997) 207.
97Rom Romm, L., Katz, G., Kosloff, R., Asscher, M.: J. Phys. Chem. B **101** (1997) 2213.
97Rug Ruggiero, C., Hollins, P.: Surf. Sci. **377** (1997) 583.
97Sch1 Schwegmann, S., Seitsonen, A.P., Dietrich, H., Bludau, H., Over, H., Jacobi, K., Ertl, G.: Chem. Phys. Lett. **264** (1997) 680.
97Sch2 Scheuer, M., Menzel, D., Feulner, P.: Surf. Sci. **390** (1997) 23.
97Sky Skytt, P., Glans, P., Gunnelin, K., Guo, J.-H., Nordgren, J.: Phys. Rev. A **55** (1997) 134.
97Smi Smirnov, K., Raseev, G.: Surf. Sci. **384** (1997) L875.
97Sna Snabl, M., Borusik, O., Chab, V., Ondrejcek, M., Stenzel, W., Conrad, H., Bradshaw, A.M.: Surf. Sci. **385** (1997) L1016.
97Sus1 Sushchikh, M., Lauterbach, J., Weinberg, W.H.: J. Vac. Sci. Technol. A **15** (1997) 1630.
97Sus2 Sushchikh, M., Lauterbach, J., Weinberg, W.H.: Surf. Sci. **393** (1997) 135.
97Wei Wei, D.H., Skelton, D.C., Kevan, S.D.: Surf. Sci. **381** (1997) 49.
97Yeo1 Yeo, Y.Y., Vattuone, L., King, D.A.: J. Chem. Phys. **106** (1997) 1990.
97Yeo2 Yeo, Y.Y., Vattuone, L., King, D.A.: J. Chem. Phys. **106** (1997) 392.
98Ben Bennich, P., Wiell, T., Karis, O., Weinelt, M., Wassdahl, N., Nilsson, A., Nyberg, M., Pettersson, L.G.M., Stohr, J., Samant, M.: Phys. Rev. B **57** (1998) 9274.
98Ber Berces, A., Hackett, P.A., Lan, L., Mitchell, S.A., Rayner, D.M.: J. Chem. Phys. **108** (1998) 5476.
98Beu Beutler, A., Lundgren, E., Nyholm, R., Setlik, B., Heskett, D., Andersen, J.N.: Surf. Sci. **396** (1998) 117.
98Bou Bourguignon, B., Carrez, S., Dragnea, B., Dubost, H.: Surf. Sci. **418** (1998) 171.
98Bra Braun, J., Weckesser, J., Ahner, J., Mocuta, D., Yates, J.T., Wöll, C.: J. Chem. Phys. **108** (1998) 5161.
98Emu Emundts, A., Pirug, G., Werner, J., Bonzel, H.P.: Surf. Sci. **410** (1998) L727.
98Föh Föhlisch, A., Wassdahl, N., Hasselström, J., Karis, O., Menzel, D., Martensson, N., Nilsson, A.: Phys. Rev. Lett. **81** (1998) 1730.
98Gie Gießel, T., Schaff, O., Hirschmugl, C.J., Fernandez, V., Schindler, K.-M., Theobald, A., Bao, S., Lindsay, R., Berndt, W., Bradshaw, A.M., Baddeley, C., Lee, A.F., Lambert, R.M., Woodruff, D.P.: Surf. Sci. **406** (1998) 90.

98Gra1 Graham, A.P.: J. Chem. Phys. **109** (1998) 9583.
98Gra2 Graham, A.P., Hofmann, F., Toennies, J.P., Williams, G.P., Hirschmugl, C.J., Ellis, J.: J. Chem. Phys. **108** (1998) 7825.
98Gra3 Graham, A.P.: Europhys. Lett. **42** (1998) 449.
98Hel Held, G., Schuler, J., Sklarek, W., Steinrück, H.-P.: Surf. Sci. **398** (1998) 154.
98Hol Holmgrem, L., Andersson, M., Rosen, A.: J. Chem. Phys. **109** (1998) 3232.
98Jak1 Jakob, P., Persson, B.N.J.: J. Chem. Phys. **109** (1998) 8641.
98Jak2 Jakob, P.: J. Chem. Phys. **108** (1998) 5035.
98Jen Jensen, J.A., Rider, K.B., Salmeron, M., Somorjai, G.A.: Phys. Rev. Lett. **80** (1998) 1228.
98Jon Jones, I.Z., Bennett, R.A., Bowker, M.: Surf. Sci. **402-404** (1998) 595.
98Kuz Kuznetsov, M.V., Frickel, D.P., Shalaeva, E.V., Medvedeva, N.I.: J. Electron Spectrosc. Relat. Phenom. **96** (1998) 29.
98Ma Ma, J., Xiao, X., DiNardo, N.J., Loy, M.M.T.: Phys. Rev. B **58** (1998) 4977.
98Mav Mavrikakis, M., Hammer, B., Norskov, J.K.: Phys. Rev. Lett. **81** (1998) 2819.
98Mor1 Mortensen, J.J., Hammer, B., Norskov, J.K.: Surf. Sci. **414** (1998) 315-29.
98Mor2 Mortensen, J.J., Hammer, B., Norskov, J.K.: Phys. Rev. Lett. **80** (1998) 4333.
98Pic Pick, S.: Phys. Rev. B **57** (1998) 1942.
98Rom Romm, L., Zeiri, Y., Asscher, M.: J. Chem. Phys. **108** (1998) 8605.
98Sey Seyller, T., Rurnschopf, K., Borgmann, D., Wedler, G.: Surf. Rev. Lett. **5** (1998) 569.
98Sha1 Sharma, R.K., Brown, W.A., King, D.A.: Chem. Phys. Lett. **291** (1998) 1.
98Sha2 Sharma, R.K., Brown, W.A., King, D.A.: Surf. Sci. **414** (1998) 68.
98Str Strisland, F., Ramstad, A., Ramsvik, T., Borg, A.: Surf. Sci. **415** (1998) L1020.
98Ven Venvik, H.J., Borg, A., Berg, C.: Surf. Sci. **397** (1998) 322.
98Wei M. Weinelt, N. Wassdahl, T. Wiell, O. Karis, J. Hasselström, P. Bennich, A. Nilsson, J. Stöhr, M. G. Samant, Phys. Rev. B. **58** 7351 (1998).
98Wie T. Wiell, J. Klepeis, P. Bennich, O. Björneholm, N. Wassdahl, A. Nilsson, Phys. Rev. B. **58**, 1655 (1998).
98Wol Wolter, K., Seiferth, O., Kuhlenbeck, H., Bäumer, M., Freund, H.J.: Surf. Sci. **399** (1998) 190.
98Yos Yoshitake, M., Yoshihara, K.: Vacuum **51** (1998) 369.
99Bar Bartels, L., Meyer, G., Rieder, K.-H.: Surf. Sci. **432** (1999) L621.
99Beu Beutl, M., Lesnik , J., Rendulic, K.D.: Surf. Sci. **429** (1999) 71.
99Car Carrez, S., Dragnea, B., Zheng, W.Q., Dubost, H., Bourguignon, B.: Surf. Sci. **440** (1999) 151.
99Dah Dahl, S., Logadottir, A., Egeberg, R.C., Larsen, J.H., Chorkendorff, I., Törnqvist, E., Norskov, J.N.: Phys. Rev. Lett. **83** (1999) 1814.
99Del Delbecq, F., Sautet, P.: Chem. Phys. Lett. **302** (1999) 91.
99Eng Engström, U., Ryberg, R.: J. Chem. Phys. **112** (1999) 1959.
99Föh1 Föhlisch, A., Hasselström, J., Karis, O., Menzel, D., Martensson, N., Nilsson, A.: J. Electron Spectrosc. Relat. Phenom. **101** (1999) 303.
99Föh2 Föhlisch, A., Hasselström, J., Karis, O., Mårtensson, N., Nilsson, A., Heske, C., Väterlein, P., Stichler, M., Keller, C., Wurth, W., Menzel, D.: Chem. Phys. Lett. **315** (1999) 194.
99Grü Grüne, M., Boishin, G., Linden, R.-J., Wandelt, K.: Surf. Sci. **433-435** (1999) 221.
99Has J. Hasselström, A. Föhlisch, O. Karis, N. Wassdahl, M. Weinelt, A. Nilsson, M. Nyberg, L. G. M. Pettersson, J. Stöhr, J. Chem. Phys. **110**, 4880 (1999).
99Hol Holmgren, L., Rosen, A.: J. Chem. Phys. **110** (1999) 2629.
99Jon Jones, I. Z., Bennett, R.A., Bowker, M.: Surf. Sci. **439** (1999) 235.
99Kat1 Kato, H., Yoshinobu, J., Kawai, M.: Surf. Sci. **427-428** (1999) 69.
99Kat2 Kato, H., Kawai, M., Joshinobu, J.: Phys. Rev. Lett. **82** (1999) 1899.
99Kne1 Kneitz, S., Gemeinhardt, J., Koschel, H., Held, G., Steinrück, H.P.: Surf. Sci. **433-435** (1999) 27.

99Kne2 Kneitz, S., Gemeinhardt, J., Steinrück, H.-P.: Surf. Sci. **440** (1999) 307.
99Lau Lauhon, L.J., Ho, W.: Phys. Rev. B. **60** (1999) R8525.
99Lee Lee, H.J., Ho, W.: Science **286** (1999) 1719.
99Lun Lundgren, E., Torrelles, X., Alvarez, J., Ferrer, S., Over, H.: Phys. Rev. B **59** (1999) 5876.
99Mor Moresco, F., Meyer, G., Rieder, K.H.: Mod. Phys. Lett. B 13 (1999) 709.
99Öst Österlund, L., Pedersen, M.O., Stensgaard, I., Laegsgaard, E., Besenbacher, F.: Phys. Rev. Lett. **83** (1999) 4812.
99Ram Ramstad, A., Strisland, F., Raaen, S., Borg, A., Berg, C.: Surf. Sci. **440** (1999) 290.
99Sta2 M. Staufer, U. Birkenheuer, T. Belling, F. Nörtemann, N. Rösch, M. Stichler, C. Keller, W. Wurth, D. Menzel, L. G. M. Pettersson, A. Föhlisch, A. Nilsson, J. Chem. Phys. **111**, 4704 (1999).
99Tan Tanabe, T., Suzuki, Y., Wadayama, T., Hatta, A.: Surf. Sci. **427-428** (1999) 414.
99Tri L. Triguero, Y. Luo, L. G. M. Pettersson, H. Agren, P. Väterlein, M. Weinelt, A. Föhlisch, J. Hasselström, O. Karis, A. Nilsson, Phys. Rev. B **59**, 5189 (1999).
99Vel Velic, D., Knoesel, E., Wolf, M.: Surf. Sci. **424** (1999) 1.
99Wol Wolf, M., Hotzel, A., Knoesel, E., Velic, D.: Phys. Rev. B **59** (1999) 5926.
00Bec Becker, T., Kunat, M., Boas, C., Burghaus, U., Wöll, C.: J. Chem. Phys. **113** (2000) 6334.
00Cab Cabeza, G.F., Légaré, P., Castellani, N.J.: Surf. Sci. **465** (2000) 286.
00Cer Cernota, P., Rider, K., Yoon, H.A., Salmeron, M., Somorjai, G.: Surf. Sci. **445** (2000) 249.
00Dvo Dvorak, J., Dai, H.-L.: J. Chem. Phys. **112** (2000) 923.
00Föh1 Föhlisch, A., Nyberg, M., Bennich, P., Triguero, L., Hasselström, J., Karis, O., Pettersson, L.G.M., Nilsson, A.: J. Chem. Phys. **112** (2000) 1946.
00Föh2 Föhlisch, A., Hasselström, J., Bennich, P., Wassdahl, N., Karis, O., Nilsson, A., Triguero, L., Nyberg, M., Pettersson, L.G.M.: Phys. Rev. B **61** (2000) 16229.
00Föh3 Föhlisch, A., Nyberg, M., Hasselström, J., Karis, O., Pettersson, L.G.M., Nilsson, A.: Phys. Rev. Lett. **85** (2000) 3309.
00Fre Freund, H.J.: Private communication, 2000 .
00Fun Funk, S., Bonn, M., Denzler, D.N., Hess, C., Wolf, M., Ertl, G.: J. Chem. Phys. **112** (2000) 9888.
00Hes1 Hess, C., Bonn, M., Funk, S., Wolf, M.: Chem. Phys. Lett. **325** (2000) 139.
00Hes2 Hess, C., Wolf, M., Bonn, M.: Phys. Rev. Lett. **85** (2000) 4341.
00Jac Jacobi, K.: Phys. Status Solidi (a) **177** (2000) 37.
00Kar O. Karis, J. Hasselström, N. Wassdahl, M. Weinelt, A. Nilsson, M. Nyberg, L. G. M. Pettersson, J. Stöhr, M. G. Samant, J. Chem. Phys. **112**, 8146 (2000).
00Kaw Kawai, M., Kato, H.: Surf. Rev. Lett. **7** (2000) 619.
00Kop Koper, M.T.M., Santen, R.A. v., Wasileski, S.A., Weaver, M.J.: J. Chem. Phys. **113** (2000) 4392.
00Lah Lahtinen, J., Vaari, J., Kauraala, K., Soares, E.A., van Hove, M.A.: Surf. Sci. **448** (2000) 269.
00Lee Lee, H.J., Ho, W.: Phys. Rev. B **61** (2000) 16347.
00Nil A. Nilsson, J. Hasselström, A. Föhlisch, O. Karis, L. G. M. Pettersson, M. Nyberg, L. Triguero, J. El. Spec. Relat. Phenom. **110**, 15 (2000).
00Nyb M. Nyberg, O. Karis, N. Wassdahl, M. Weinelt, A. Nilsson, L. G. M. Pettersson, J. Chem. Phys. **112**, 5429 (2000).
00Rie Riedmüller, B., Ciobica, I.M., Papageorgopoulos, D.C., Berenbak, B., Santen, R.A. v., Kleyn, A.W.: Surf. Sci. **465** (2000) 347.
00Sau Sautet, P., Rose, M.K., Dunphy, J.C., Behler, S., Salmeron, M.: Surf. Sci. **453** (2000) 25.
00Sti M. Stichler, C. Keller, C. Heske, M. Staufer, U. Birkenheuer, N. Rösch, W. Wurth, D. Menzel., Surf. Sci. **448**, 164 (2000).
00Sur Surnev, S., Sock, M., Ramsey, M.G., Netzer, F.P., Wiklund, M., Borg, M., Andersen, J.N.: Surf. Sci. **470** (2000) 171.

00Tri L. Triguero, A. Föhlisch, P. Väterlein, J. Hasselström, M. Weinelt, L. G. M. Pettersson, Y. Luo, H. Ågren, and A. Nilsson, J. Am. Chem. Soc. **122**, 12310 (2000).

00Yag Yagi-Watanabe, K., Fukutani, H.: J. Chem. Phys. **112** (2000) 7652.

00Zas1 Zasada, I., van Hove, M.A.: Surf. Rev. Lett. **7** (2000) 15.

00Zas2 Zasada, I., van Hove, M.A.: Surf. Sci. **457** (2000) L421.

00Zep Zeppenfeld, P., David, R., Ramseyer, C., Hoang, P.N.M., Girardet, C.: Surf. Sci. **444** (2000) 163.

01Bon Bonzel, H.P.: Introduction to physical and chemical properties of adlayer/substrate systems, in: Physics of Covered Solid Surfaces. Landolt-Börnstein III/42 A1. Bonzel, H.P. (ed.), Berlin: Springer-Verlag, 2001, p. 1-66.

01Den Denecke, R., Martensson, N.: Surface core level shifts of metals, in: Physics of Covered Solid Surfaces. Landolt-Börnstein III/42 A4. Bonzel, H.P. (ed.), Berlin: Springer-Verlag, 2004.

01Hah Hahn, J.R., Ho, W.: Phys. Rev. Lett. **87** (2001) 166102.

01Hir Hirsimäki, M., Valden, M.: J. Chem. Phys. **114** (2001) 2345.

01Jac1 Jacobi, K.: Electron work function of metals and semiconductors, in: Physics of Covered Solid Surfaces. Landolt-Börnstein III/42 A1. Bonzel, H.P. (ed.), Berlin: Springer-Verlag, 2001.

01Kun Kunat, M., Boas, C., Becker, T., Burghaus, U., Wöll, C.: Surf. Sci. **474** (2001) 114.

01Mic D. Michael, P. Mingos, J. Organomet. Chem. **635**, 1 (2001).

01Now Nowicki, M., Emundts, A., Pirug, G., Bonzel, H.P.: Surf. Sci. **478** (2001) 180.

01Pet Peters, K.F., Walker, C.J., Steadman, P., Robach, O., Isern, H., Ferrer, S.: Phys. Rev. Lett. **86** (2001) 5325.

01Ric Richmond, G.L.: Annu. Rev. Phys. Chem. **52** (2001) 357.

01See Seebauer, E.G., Jung, M.Y.L.: Surface diffusion on metals, semiconductors and insulators, in: Physics of Covered Solid Surfaces. Landolt-Börnstein III/42 A1. Bonzel, H.P. (ed.), Berlin: Springer-Verlag, 2001, .

01Sme Smedh, M., Beutler, A., Ramsvik, T., Nyholm, R., Borg, M., Andersen, J., Duschek, R., Sock, M., Netzer, F.P., Ramsey, M.G.: Surf. Sci. **491** (2001) 99.

01Sta Stacchiola, D., Wu, G., Kaltchev, M., Tysoe, W.T.: J. Chem. Phys. **115** (2001) 3315.

01Ter Terborg, R., Polcik, M., Toomes, R.L., Baumgärtel, P., Hoeft, J.T., Bradshaw, A.M., Woodruff, D.P.: Surf. Sci. **473** (2001) 203.

01Tho Thostrup, P., Christoffersen, E., Lorensen, H.T., Jacobsen, K.W., Besenbacher, F., Norskov, J.K.: Phys. Rev. Lett. **87** (2001) 126102.

01Wan1 Wang, J., Wang, Y., Jacobi, K.: Surf. Sci. **482-485** (2001) 153.

01Wan2 Wang, J., Wang, Y., Jacobi, K.: Surf. Sci. **488** (2001) 83.

01Wit Witte, G.: J. Chem. Phys. **115** (2001) 2757.

02Bou Bourguignon, B., Zheng, W.Q., Carrez, S., Fournier, F., Gaillard, M.L., Dubost, H.: Surf. Sci. **515** (2002) 567.

02Eng Engelhardt, M.P., Fuhrmann, T., Held, G., Denecke, R., Steinrück, H.P.: Surf. Sci. **512** (2002) 107.

02Hei Heinrich, A.J., Lutz, C.P., Gupta, J.A., Eigler, D.M.: Science **298** (2002) 1381.

02Ho Ho, W.: J. Chem. Phys. **117** (2002) 11033.

02Kat Kato, H.S., Okuyama, H., Yoshinobu, J., Kawai, M.: Surf. Sci. **513** (2002) 239.

02Kit Kittel, M., Terborg, R., Polcik, M., Bradshaw, A.M., Toomes, R.L., Woodruff, D.P., Rotenberg, E.: Surf. Sci. **511** (2002) 34.

02Oga H. Ogasawara, B. Brena, D. Nordlund, M. Nyberg, A. Pelmenschikov, L. G. M. Pettersson, A. Nilsson, Phys. Rev. Lett, **89**, 276102 (2002).

02Ros Rose, M.K., Mitsui, T., Dunphy, J., Borg, A., Ogletree, D.F., Salmeron, M., Sautet, P.: Surf. Sci. **512** (2002) 48.

02Unt Unterhalt, H., Rupprechter, G., Freund, H.-J.: J. Phys. Chem. B **106** (2002) 356.

02Yud Yudanov, I.V., Sahnoun, R., Neyman, K.M., and Rosch, N.: J. Chem. Phys. **117** (2002) 9887.

03Fan Fan, C.Y., Bonzel, H.P., Jacobi, K.: J. Chem. Phys. **118** (2003) 9773.

03Gra Graham, A.P.: Surf. Sci. Rep. **49** (2003) 115.

03Öst H. Öström, L. Triguero, M. Nyberg, H. Ogasawara, L. G. M. Pettersson, A. Nilsson, Phys. Rev. Lett. 91, **46102** (2003)

03Wal Wallis, T.M., Nilius, N., Ho, W.: J. Chem. Phys. **119** (2003) 2296.

04Föh1 A. Föhlisch, F. Hennies, W. Wurth, N. Witkowski, M. Nagasono, M. N. Piancastelli, L. Moskaleva, K. Neyman, N. Rösch, Phys. Rev. B **69**, 153408 (2004).

04Föh2 A. Föhlisch, W. Wurth, M. Stichler, C. Keller, A. Nilsson, Journal of Chemical Physics, **121,** 9606 (2004)

04Öst H. Öström, A. Föhlisch, M. Nyberg, M. Weinelt, C. Heske, L. G. M. Pettersson, A. Nilsson, Surf. Sci. **559** 85 (2004).